

**Pieter C.B. Luyt
(28012942)**

**A leak tight design methodology for large diameter flanges based
on non-linear modelling and analysis**

**A study done in fulfilment of the degree of MEng (Mech.)
at the
Department of Mechanical and Aeronautical Engineering,
University of Pretoria**



**Supervisor:
Prof. Nico J. Theron**

**Co-Supervisor:
Mr Francesco Pietra**

November 2015



Title: A leak tight design methodology for large diameter flanges based on non-linear modelling and analysis

Author: Mr Pieter C. B. Luyt

Institute: Department of Mechanical and Aeronautical Engineering, University of Pretoria

Supervisor: Prof. Nico J. Theron

Co-supervisor: Mr Francesco Pietra

Year: 2015

ABSTRACT

There is currently a need for large diameter flanges for the supply of water in South Africa. These large diameter pipe flanges are required to accommodate pipes with nominal bores of up to 4 m and should successfully withstand internal pressures of up to 8 MPa. No current relevant standard / code contains prescribed design values for flanges which either operate at such high pressures or have such large diameters. Due to this an alternative method of design, by means of non-linear finite element modelling, is proposed. Three types of integral flange designs are considered, namely: flat face, raised face, and a modified raised face with an O-ring groove. The effects of creep-relaxation, flange rotation, and the bolting sequence are considered.

For each of these designs a finite element model was created and compared to a small scale experiment which included strain and contact pressure measurements. The proposed non-linear finite element models were capable of accurately predicting the strains in the flanges as well as the contact pressures between the faces of the flange and the surfaces of the packing material. Finally, a comparison between the ASME design method and the proposed non-linear finite element modelling design method was done for the large diameter flanges. It was found that the ASME design code did not have the ability to accurately predict the stresses in the flanges. It was also found that by using the maximum equivalent Von Mises stress as failure criteria for the flanges and fasteners, and contact pressure for the sealing ability, circular bolted flange connections which are lighter, safer, and leak tight could be designed by means of the proposed non-linear finite element models.

Keywords: flat face flange; raised face flange; raised face flange with an O-ring groove; flange rotation; creep-relaxation; contact pressure



ACKNOWLEDGEMENTS

I would like to extend a word of thanks to everyone that supported and contributed towards this work. In particular I am grateful to those listed below:

- **Study leaders:** A special thanks to my supervisor, Prof. Nico J. Theron for consistent support and advice. Mr Francesco Pietra, my co-supervisor, for providing unparalleled assistance with ANSYS and general guidance.
- **Staff within the department of Mechanical and Aeronautical Engineering at the University of Pretoria:** Thank you to Prof. Schalk Kok who gave up much of his time to provide additional guidance and support; to Mr George Breytenbach and Mr Herman Booysen who were always ready to provide assistance during the experimental phase.
- **Rand Water:** For making this project possible through funding.
- **My father:** A special thank you to Prof. Riaan Luyt for his assistance and encouragement throughout this project.
- My sincerest gratitude to my parents, and friends (in particular Ms. Elize Cilliers, Mr Chris Church, and Mr Roelof Schoeman) for their unconditional support and encouragement.



TABLE OF CONTENTS

CHAPTER 1: INTRODUCTION AND BACKGROUND TO PROBLEM.....	1
1.1. Background to problem	1
1.2. Categories of circular bolted flange joints	1
1.3. Overview of circular bolted flange joints	2
1.4. Research objectives	3
1.5. Scope of the research	5
1.6. Layout of thesis	5
CHAPTER 2: LITERATURE REVIEW	7
2.1. Current design practices and standards	7
2.2. Taylor-Forge Method.....	7
2.2.1. Early development and preceding design methods	7
2.2.2. Implementation of the Taylor-Forge method	10
2.2.3. Application of the Taylor-Forge method to the design of large diameter flanges	16
2.2.4. Comparison of the predicted stress values by means of ASME to finite element analysis	18
2.2.5. Advantages and disadvantages of the Taylor-Forge methods	21
2.3. Finite element modelling and analysis techniques	22
2.3.1. Simplification of the geometry of a circular bolted flange joint	22
2.3.2. Loads and boundary conditions	23
2.3.2.1. Application of bolt pre-tension.....	24
2.3.2.2. Bolt tightening sequence and torque increments.....	28
2.3.2.3. Application of pressure due to internal fluid	28
2.4. Factors which influence leak tightness	29
2.4.1. Creep-relaxation of gaskets	29
2.4.2. Flange rotation.....	34
2.5. Validation of finite element analysis results by means of experimentation.....	35
CHAPTER 3: INITIAL FINITE ELEMENT MODELLING AND ANALYSIS	37
3.1. Overview for the initial finite element modelling and analysis.....	37
3.2. Purpose and goals of the initial finite element modelling and analysis.....	37
3.3. Relevant mechanical properties of the various components	37
3.3.1. Mechanical properties of the flanges and fasteners.....	37
3.3.2. Relevant mechanical properties of the O-ring.....	38
3.3.2.1. Experimental setup for the determining the relevant mechanical properties of the O-ring	38
3.3.2.2. Accounting for the stiffness of the experimental setup	39
3.3.2.3. Load-compression experiment for the O-ring	40
3.3.2.4. Analysis and characterisation of the relevant material properties of the O-ring	41
3.3.3. Relevant mechanical properties of the gasket	45
3.3.3.1. Load-closure and creep test of the compressed non-asbestos gasket insert	46
3.4. Modelling of the flange geometry	56
3.4.1. Dimensions of the components	56
3.4.2. Simplifying assumptions	56
3.4.3. Assumptions for the contact interfaces	56
3.4.3.1. Contact between the gasket and flange faces	57
3.4.3.2. Contact between the O-ring and flanges	65
3.4.3.3. Assumed contact interfaces for the initial finite element modelling and analysis	67
3.4.4. Assumptions for the boundary conditions	68
3.4.5. Assumptions made for the loads	68



5.3.3.	Calculation of the root area of the bolts	110
5.3.4.	Calculation of the total bolt load	111
5.3.5.	Calculation of the assumed principal forces and their moments.....	111
5.3.6.	Ratios and shape factors.....	112
5.3.7.	Stress formula factors.....	113
5.3.8.	Stress calculations.....	113
5.4.	Finite element modelling for the large diameter flanges	114
5.4.1.	Relevant material models for the large diameter flanges.....	114
5.4.2.	Geometry.....	115
5.4.3.	Contact interfaces.....	115
5.4.4.	Loads and boundary conditions	115
5.4.5.	Assumption for the failure criteria.....	117
5.4.6.	Results from the finite element analysis of the large diameter flat face flange.....	117
5.4.6.1.	Results for the finite element analysis of the large diameter flat face flange.....	118
5.4.6.2.	Comparison of the results for the flat face flange as calculated by ASME to the finite element analysis.....	119
5.4.7.	Results for the large diameter raised face flange.....	120
5.4.7.1.	Results from the finite element analysis of the large diameter flat face flange.....	120
5.4.7.2.	Comparison of the results for the raised face flange as calculated by ASME to the finite element analysis	122
5.4.8.	Results for the large diameter raised face flange with an O-ring groove	122
5.5.	Optimisation of large diameter flanges	125
5.5.1.	Parameterisation of the large diameter finite element models.....	125
5.5.1.1.	Assumption for the relationship between the bolt diameter and bolt hole size, and bolt diameter and washer face diameter	126
5.5.1.2.	Assumed upper and lower bounds for the flange dimensions and bolt loads	127
5.5.1.3.	Results for the parameter correlation.....	128
5.5.2.	Response surface generation and optimisation	132
5.5.2.1.	Objective and constraint functions	132
5.5.2.2.	Results from the optimisation of the flat and raised face flanges	133
5.5.2.3.	Results from the optimisation of the raised face flange with an O-ring groove	133
5.6.	Conclusion of the application of the non-linear finite element models to the design of large diameter flanges.....	139
CHAPTER 6: RECOMMENDATIONS FOR FUTURE WORK AND CONCLUSION.....		140
6.1.	Recommendations for future work	140
6.1.1.	Material modelling	140
6.1.2.	Friction.....	140
6.1.3.	Bolt tightening techniques	140
6.1.4.	Determination and implementation of external loads and moments	141
6.1.5.	Large scale experimentation	141
6.2.	Conclusion.....	141
REFERENECEES.....		143
APPENDIX A: DIN 2505 METHOD		146
APPENDIX B: FLANGE AND MODIFIED BOLT DIMENSIONS.....		149
B.1.	Dimensions of the flat face flange	149
B.2.	Dimensions of the raised face flange	149
B.1.	Dimensions of the raised face flange with an O-ring groove.....	150
B.1.	Dimensions of the modified M16 bolt	150
APPENDIX C: RESULTS FOR THE INITIAL FINITE ELEMENT MODELLING AND ANALYSIS.....		151
C.1.	Results for the finite element analysis and modelling of the flat face flange.....	151



C.2. Results for the finite element analysis and modelling of the raised face flange.....	154
C.3. Results for the finite element analysis and modelling of the modified raised face flange with an O-ring groove	157
APPENDIX D: RESULTS FOR THE INITIAL FINITE ELEMENT MODELLING AND ANALYSIS.....	159
D.1. Design of flat face flange by means of ASME VIII, Division 1	159
D.2. Design of raised face flange by means of ASME VIII, Division 1	160
APPENDIX E: MANUFACTURED AND INSTRUMENTED FLANGES	161
E.1. Instrumented flat face flange	161
E.2. Instrumented raised face flange	163
E.3. Instrumented modified raised face flange with an O-ring groove	166
APPENDIX F: RESPONSE SURFACE GENERATION AND OPTIMISATION IN ANSYS	169

LIST OF FIGURES

Figure 1-1: The different types of connections considered: (a) flat face (b) and raised face flanges with ring gaskets; and a (c) raised face flange modified to contain an O-ring.....	2
Figure 1-2: General attachment of (a) plate and (b) welded-neck flanges.....	3
Figure 1-3: Pressure and nominal bore ranges for the current usage of flat face, raised face, and O-ring flanges by Rand Water	4
Figure 1-4: Suggested flange table expansion with reference to the applicable circular bolted flange design	4
Figure 2-1: Subcomponents of a circular bolted flange connection	7
Figure 2-2: Flange fixed along its radial cross section [11].....	8
Figure 2-3: Simply supported plate under concentric loading [11].....	9
Figure 2-4: Free body diagram for the seating bolt load in accordance with the Taylor-Forge method	12
Figure 2-5: Free body diagram for the operating bolt load in accordance with the Taylor-Forge method	12
Figure 2-6: Principal moments and forces which are applicable during the seating of the gasket according to the Taylor-Forge method	13
Figure 2-7: Principal moments and forces which are applicable during operation according to the Taylor-Forge method	14
Figure 2-8: Stress distribution in the (a) axial, (b) radial, and (c) tangential direction during the seating conditions for a NPS 24 flange [18].....	19
Figure 2-9: Ratio of flange stresses in the (a) axial, (b) radial and (c) tangential direction calculated by the ASME formula and the finite element analysis [18].....	20
Figure 2-10: Geometry, loads, and boundary conditions generally applied for the finite element modelling and analysis of a circular bolted flange joint	22
Figure 2-11: Simplification of geometry from (a) full model to an (b) axisymmetric model to a (c) simplified axisymmetric model.....	23
Figure 2-12: Primary loads which applicable to the seating and operating conditions	24
Figure 2-13: Application of the pre-tension element: (a) splitting of the surface of the bolt, elements before adjustments, elements after adjustment	25
Figure 2-14: Different methods for modelling fasteners: (a) solid bolt, (b) coupled bolt, (c) spider, (d) n-bolt, (e) hybrid, and (f) rigid body element.....	27
Figure 2-15: A simplified model of a circular bolted flange showing the application of the internal pressure and pressure end thrust	28
Figure 2-16: Visco-elastic-plastic element [28].....	29
Figure 2-17: Typical gasket compression curve [28].....	30
Figure 2-18: Typical PTFE gasket stress-deformation [30].....	31
Figure 2-19: A typical rheological model and compression curve of a soft rubber gasket as shown by Alkelani <i>et al.</i> [27]	32
Figure 2-20: Effect of flange rotation: (a) before, (b) after, and (c) the relationship between the fluid pressure and contact pressure.....	34
Figure 2-21: Variation of the flange rotation as a function of both internal pressure and bolt pretension [20].....	35
Figure 2-22: The (a) experimental setup and (b) strain gauge locations of Sawa <i>et al.</i> [33]	36
Figure 2-23: The experimental setup of Bouzid <i>et al.</i> [30]	36
Figure 3-1: Test setup used for the material characterisation of the packing materials	38
Figure 3-2: Mounting of the laser displacement meter.....	39
Figure 3-3: Input force as a function of time used for determining the machine stiffness.....	39
Figure 3-4: The closure of the system as a function of force	40
Figure 3-5: Experimental load-closure results for the O-ring	41
Figure 3-6: Corrected and uncorrected mean load-closure curves for the O-ring	42
Figure 3-7: Comparison of the load-closure curves for varying coefficients of friction.....	43



Figure 3-8: Boundary conditions and contact interface for the tuning of the material model for the O-ring 43

Figure 3-9: Finite element analysis approximation of the experimental load closure curve 44

Figure 3-10: Deformation of the O-ring, with the assumed third order Ogden material model, for (a) 600 N, (b) 1 200 N, (c) 1 800 N, (d) 2 400 N, (e) 3 000 N, and (f) 3 500 N..... 45

Figure 3-11: Experimental load-closure results and the mean thereof for applied pressures of (a) 5 MPa, (b) 10 MPa, and (c) 15 MPa 48

Figure 3-12: Corrected and uncorrected mean load-closure curves for the applied pressure of (a) 5 MPa, (b) 10 MPa, and (c) 15 MPa..... 49

Figure 3-13: Boundary conditions and contact interface for the tuning of the material model for the gasket insert 50

Figure 3-14: Approximated and mean corrected experimental load-closure curves for applied pressures of (a) 5 MPa, (b) 10 MPa, and (c) 15 MPa 51

Figure 3-15: Experimental and finite element approximated creep results 53

Figure 3-16: Comparison of the experimental results, the results calculated by the finite element analysis, and the model proposed by Alkelani *et al.* [27] 54

Figure 3-17: Load-closure curves for various coefficients of friction 55

Figure 3-18: Closure due to creep for various coefficients of friction 56

Figure 3-19: Free-body diagrams for the calculation method suggested by Drago [38]..... 57

Figure 3-20: Difference in contact stress as function of the internal pressure and nominal bore when the coefficient of friction was $\mu=0.2$ and $\mu=1$ 60

Figure 3-21: Calculated distribution of the contact stress, for a coefficient of friction of: (a) $\mu=0.1$, (b) $\mu=0.3$, (c) $\mu=0.5$, (d) $\mu=0.7$, (e) $\mu=0.9$, between the flat face flange and gasket insert immediately after seating 61

Figure 3-22: Variation in the contact pressure as a function of the coefficient of friction for the flat face flange after the bolts were tightened 62

Figure 3-23: Variation in the contact pressure as a function of the coefficient of friction for the flat face flange after a period of 10 minutes 62

Figure 3-24: Variation in the contact pressure as a function of the coefficient of friction for the raised face flange after the bolts were tightened 63

Figure 3-25: Calculation of the distribution of the contact stress, for a coefficient of friction of: (a) $\mu=0.1$, (b) $\mu=0.3$, (c) $\mu=0.5$, (d) $\mu=0.7$, (e) $\mu=0.9$, between the raised face flange and gasket insert immediately after seating 64

Figure 3-26: Variation in the contact pressure as a function of the coefficient of friction for the raised face flange after a period of 10 minutes 65

Figure 3-27: Comparison of the maximum contact pressure between the gasket insert and flat face and raised face flange for various coefficients of friction 65

Figure 3-28: Contact pressure between the O-ring and flange face for (a) the underformed O-ring, and for the following coefficients of friction: (b) $\mu=0.1$, (c) $\mu=0.3$, (d) $\mu=0.5$, (e) $\mu=0.7$, (f) $\mu=0.9$ 66

Figure 3-29: Deformation of the O-ring for different coefficient of friction values during seating..... 67

Figure 3-30: Positions of Locations 1 to 4 on the flange ring and hub 69

Figure 3-31: Difference in the calculated strain values, at the various strain gauge positions, as a function of the number of bolt tightening increments 69

Figure 3-32: (a) Locations of where pressure distributions were compared, (b) reduction in contact pressures at the locations, (c, d, e, f) stress distributions at Locations 1, 2, 3, and 4 71

Figure 3-33: (a, b) Application of zero displacement normal to the surface of the flange in the tangential direction, (c) application of bolt pretension, and (d) zero displacement in the axial direction 72

Figure 3-34: Contact interfaces between: (a) gasket and top flange, (b) gasket and bottom flange, (c) nut and bolt, (d) bolt and top flange, and (e) nut and bottom flange for the flat and raised face flanges 73

Figure 3-35: Contact interface between: (a) O-ring and top flange, (b) O-ring and bottom flange, (c) nut and bolt, (d) bolt and top flange, and (e) nut and bottom flange for the raised face flange with an O-ring groove 73

Figure 3-36: The predicted contact stress between the gasket insert and the flat face flange right after bolt tightening for the (a) front and (b) isometric views 74



Figure 3-37: The predicted contact stress between the gasket inset and the flat face flange after a period of 10 minutes for the (a) front and (b) isometric views 75

Figure 3-38: The predicted contact stress between the gasket insert and the raised face flange right after bolt tightening for the (a) front and (b) isometric views 75

Figure 3-39: The predicted contact stress between the gasket inset and the raised face flange after a period of 10 minutes for the (a) front and (b) isometric views 76

Figure 4-1: Experimental setup for the flat face flange 79

Figure 4-2: Experimental setup for the raised face flange 79

Figure 4-3: Experimental setup for the raised face flange which has been modified to contain an O-ring groove 80

Figure 4-4: Modifications to the standard M16 bolt 80

Figure 4-5: General locations of all the strain gauges which were instrumented on the flange..... 81

Figure 4-6: Position of the uniaxial strain gauges relative to the washer face on the modified M16 bolt 81

Figure 4-7: Location of the 90° rosettes on the ring of the flange 82

Figure 4-8: Position of the 45°rosettes relative to the ring-hub interface of the flange 82

Figure 4-9: TekScan sensor model 5051-10 000 and how it was positioned in the flange assembly . 83

Figure 4-10: Bolt tightening sequence for the experimental setup..... 84

Figure 4-11: (a) Top view, (b) isometric view, (c) front view, and (d) back view of the measured pressure distribution, for the flat face flange, immediately after the bolts had been tightened 86

Figure 4-12: (a) Top view, (b) isometric view, (c) front view, and (d) back view of the measured pressure distribution, for the flat face flange, 10 minutes after the bolts had been tightened..... 86

Figure 4-13: (a) Top view, (b) isometric view, (c) front view, and (d) back view of the measured pressure distribution, for the raised face flange, immediately after the bolts had been tightened 88

Figure 4-14: (a) Top view, (b) isometric view, (c) front view, and (d) back view of the measured pressure distribution, for the raised face flange, 10 minutes after the bolts had been tightened..... 89

Figure 4-15: Comparison of the measured strains to the calculated strains from the finite element analysis for the flat face flange immediately after the bolts had been tightened..... 90

Figure 4-16: Comparison of the measured strains to the calculated strains from the finite element analysis of the flat face flange after a 10 minute period..... 91

Figure 4-17: Comparison of the reduction in the measured strains to the reduction in the calculated strains from the finite element analysis of the flat face flange..... 92

Figure 4-18: Comparison of the reduction in the measured strains to the reduction in the predicted strains from the second finite element analysis of the flat face flange 93

Figure 4-19: (a) Top view, (b) isometric view, (c) front view, and (d) back view of the calculated reduction in contact stress between the gasket insert and the flat face flange..... 94

Figure 4-20: (a) Top view, (b) isometric view, (c) front view, and (d) back view of the measured reduction in the contact pressure between the flat face flange and gasket insert 95

Figure 4-21: (a) Top view, (b) isometric view, (c) front view, and (d) back view of the calculated contact pressure between the gasket insert and the flat face flange based on the modified finite element model and analysis..... 96

Figure 4-22: (a) Top view, (b) isometric view, (c) front view, and (d) back view of the percentage difference in the contact pressure as a function of the number of bolt tightening increments and time between the bolt tightening increments for the flat face flange 97

Figure 4-23: Comparison of the measured strains to the calculated strains from the finite element analysis for the raised face flange immediately after the bolts had been tightened..... 98

Figure 4-24: Comparison of the measured strains to the calculated strains from the finite element analysis of the raised face flange after a 10 minute period..... 99

Figure 4-25: Comparison of the reduction in the measured strains to the reduction in the calculated strains from the finite element analysis of the raised face flange..... 99

Figure 4-26: Comparison of the reduction in the measured strains to the reduction in the predicted strains from the second finite element analysis of the raised face flange 100

Figure 4-27: (a) Top view, (b) isometric view, (c) front view, and (d) back view of the calculated contact stress between the gasket inset and the raised flange after a period of 10 minutes 101



Figure 4-28: (a) Top view, (b) isometric view, (c) front view, and (d) back view of the measured reduction in the contact pressure between the raised face flange and gasket insert 102

Figure 4-29: (a) Top view, (b) isometric view, (c) front view, and (d) back view of the percentage difference in the contact pressure as a function of the number of bolt tightening increments and time between the bolt tightening increments for the raised face flange 104

Figure 4-30: Comparison of the measured strains to the calculated strains for the finite element analysis of the raised face flange with an O-ring groove 105

Figure 5-1: Principal dimensions of a circular bolted flange connection 109

Figure 5-2: Cross-sectional dimensions of the three investigated O-ring grooves 115

Figure 5-3: Application of the boundary conditions to the non-linear finite element models of (a) the flat and raised face flanges, and (b) the raised face flange with an O-ring groove..... 116

Figure 5-4: Application of the loads to the non-linear finite element models of (a) the flat and raised face flanges, and (b) the raised face flange with an O-ring groove 116

Figure 5-5: Contact pressure between the surface of the gasket and the flat face flange for the (a) seating and (b) operating conditions 118

Figure 5-6: (a, b) Axial, (c, d) radial, and (e, f) tangential stress for the seating and operating conditions of the large diameter flat face flange 119

Figure 5-7: Contact pressure between the surface of the gasket and the raised face flange for the (a) seating and (b) operating conditions 120

Figure 5-8: (a, b) Axial, (c,d) radial, and (e,f) tangential stress for the seating and operating conditions of the large diameter raised face flange 121

Figure 5-9: Flange dimension which were parameterised 125

Figure 5-10: Data and fitted data for the hole diameter as a function of the bolt diameter 127

Figure 5-11: Data and fitted data for the washer face diameter as a function of the bolt diameter ... 127

Figure 5-12: Parameter correlation between the dimensions of the raised face flange with an O-ring groove and the (a) maximum contact pressure, and (b) flange equivalent Von Mises stress 128

Figure 5-13: Parameter correlation between the dimensions of the flat face flange and the (a) maximum contact pressure, (b) flange equivalent Von Mises stress and (c) flange rotation 130

Figure 5-14: Parameter correlation between the dimensions of the raised face flange and the (a) maximum contact pressure, (b) flange equivalent Von Mises stress and (c) flange rotation..... 131

Figure 5-15: Comparison of the axial, radial, and tangential stresses calculated by the finite element analysis with the predicted values by ASME for the eight flat face flange candidates 135

Figure 5-16: Comparison of the axial, radial, and tangential stresses calculated by the finite element analysis with the predicted values by ASME for the eight raised face flange candidates 137

Figure A-1: Analysis of the forces and moments by means of the DIN 2505 method [46] 146

Figure C-1: Strains in the tangential direction on the ring and hub of the flat face flange before creep relaxation 151

Figure C-2: Strains in the radial direction on the ring of the flat face flange before creep-relaxation 151

Figure C-3: Strains in the transposed axial direction on the hub of the flat face flange before creep relaxation 152

Figure C-4: Strains in the tangential direction on the ring and hub of the flat face flange after creep-relaxation 152

Figure C-5: Strains in the radial direction on the ring of the flat face flange after creep-relaxation... 153

Figure C-6: Strains in the transposed axial direction on the hub of the flat face flange after creep relaxation 153

Figure C-7: Strains in the tangential direction on the ring and hub of the raised flange before creep relaxation 154

Figure C-8: Strains in the radial and tangential direction on the ring and hub of the raised face flange before creep-relaxation..... 154

Figure C-9: Strains in the transposed axial direction on the hub of the raised face flange before creep relaxation 155

Figure C-10: Strains in the tangential direction on the ring and hub of the raised face flange after creep-relaxation 155

Figure C-11: Strains in the radial direction on the ring and hub of the raised face flange after creep-relaxation 156



Figure C-12: Strains in the transposed axial direction on the ring and hub of the raised face flange after creep-relaxation..... 156

Figure C-13: Strains in the tangential direction on the ring and hub of the raised face flange which has been modified to contain an O-ring 157

Figure C-14: Strains in the radial and tangential direction on the ring and hub of the raised face flange which has been modified to contain an O-ring 157

Figure C-15: Strains in the transposed axial direction on the hub of the raised face flange which has been modified to contain an O-ring 158

Figure E-1: Photograph of the instrumented flat face flange..... 161

Figure E-2: Photograph of the position of the 90° rosette which is in-line with the bolt on the ring of the flat face flange 161

Figure E-3: Photograph of the position of the 90° rosette in-between the bolts on the hub of the flat face flange 162

Figure E-4: Position, with the perpendicular distance from the edge of the flange, of the 90° rosette in-between the bolts on the ring of the flat face flange..... 162

Figure E-5: Position, with the perpendicular distance from the edge of the bolt hole, of the 90° rosette in-between the bolts on the ring of the flat face flange..... 163

Figure E-6: Photograph of the instrumented raised face flange..... 163

Figure E-7: Photograph of the position of the 90° rosette which is in-line with the bolt on the ring of the raised face flange 164

Figure E-8: Photograph of the position of the 90° rosette in-between the bolts on the hub of the raised face flange 164

Figure E-9: Position, with the perpendicular distance from the edge of the flange, of the 90° rosette in-between the bolts on the ring of the raised face flange..... 165

Figure E-10: Position, with the perpendicular distance from the edge of the bolt hole, of the 90° rosette in-between the bolts on the ring of the raised face flange..... 165

Figure E-11: Photograph of the instrumented raised face flange with an O-ring groove..... 166

Figure E-12: Photograph of the position of the 90° rosette which is in-line with the bolt on the ring of the raised face flange with an O-ring groove..... 166

Figure E-13: Photograph of the position of the 90° rosette in-between the bolts on the hub of the raised face flange with an O-ring groove 167

Figure E-14: Position, with the perpendicular distance from the edge of the flange, of the 90° rosette in-between the bolts on the ring of the raised face flange with an O-ring groove 167

Figure E-15: Position, with the perpendicular distance from the edge of the bolt hole, of the 90° rosette in-between the bolts on the ring of the raised face flange with an O-ring groove 168

Figure F-1: Example of a 2D response surface approximation by means of a standard second order polynomial..... 169

Figure F-2: Example of a 2D response surface approximation by means of Kriging..... 169

Figure F-3: Example of a 2D response surface approximation by means of non-parametric regression 170



LIST OF TABLES

Table 3-1: Relevant mechanical properties of EN 24, untempered, steel [34].....	37
Table 3-2: Relevant mechanical properties for the fasteners.....	38
Table 3-3: Dimensions of the O-ring used.....	41
Table 3-4: Relevant material parameters for the third order Ogden material model of the O-ring	44
Table 3-5: Dimensions of the gasket insert used	46
Table 3-6: Calculation of the necessary load for the creep tests	47
Table 3-7: Root mean square error and the maximum error of the ANSYS approximation of the load-closure curves	52
Table 3-8: Relevant material parameters for Prony shear relaxation	52
Table 3-9: Relevant material parameters for the Neo-Hookean model	52
Table 3-10: Root mean square error and the maximum error of the ANSYS approximation of the creep curves at the various pressures	53
Table 3-11: Root mean square error and the maximum error of the approximation of the creep curves at the various pressures by means of Alkelani <i>et al.</i> [27] 's model	54
Table 3-12: Values assumed for the nominal bore, inner diameter, and outer diameter of the flange for the calculation method suggested by Drago [38]	59
Table 3-13: Values assumed for the coefficient of friction, gasket thickness, internal pressure and tensile strength for the calculation method suggested by Drago [38].....	59
Table 3-14: Contact table for the finite element analysis of the experimental setup	67
Table 3-15: Number of nodes and elements for the various flange configurations.....	72
Table 3-16: Summary of the strains from the finite element analysis for the flat face flange	74
Table 4-1: Bridge configuration, gauge factor, bridge factor, and sampling frequency used for the measurement of the trains.....	83
Table 4-2: Summary of the strain gauge results, for the experimental setup of the flat face, flange immediately after the bolts had been tightened	85
Table 4-3: Summary of the strain gauge results, for the experimental setup of the flat face flange, 10 minutes after the bolts had been tightened	85
Table 4-4: Summary of the strain gauge results, for the experimental setup of the raised face, flange immediately after the bolts had been tightened	87
Table 4-5: Summary of the strain gauge results, for the experimental setup of the raised face flange, 10 minutes after the bolts had been tightened	87
Table 4-6: Summary of the results for the experimental setup of the raised face flange with an O-ring groove after tightening.....	89
Table 4-7: Summary of the results of the comparison between the reduction in the measured and calculated strains for the flat face flange	92
Table 4-8: Comparison of the strain results calculated by the initial and modified finite element analysis to the measured strain results for the flat face flange	93
Table 4-9: Summary of the results of the comparison between the measured and calculated strain for the raised face flange	100
Table 4-10: Summary of the results of the comparison between the measured and calculated strain for the raised face flange	101
Table 4-11: Summary of the results of the comparison between the measured and calculated strains for the raised face flange with an O-ring groove	104
Table 5-1: Shape factors for the design of the large diameter flat face flange	112
Table 5-2: Initial values for the dimension of the flat and raised face flanges	114
Table 5-3: Predicted axial stress, radial stress, and tangential stress for the design of the large diameter flat and raised face flanges in accordance with ASME VIII, Division 1,	114
Table 5-4: Assumed failure criteria for the design of large diameter flanges.....	117
Table 5-5: Results from the finite element analysis of the flat face flange.....	118
Table 5-6: Comparison of the results from the finite element analysis to the failure criteria for the flat face flange	118
Table 5-7: Comparison of the maximum axial, radial, and tangential stresses calculated by the finite element analysis and predicted by ASME VIII, Division 1 for the flat face flange.....	120
Table 5-8: Results from the finite element analysis of the flat face flange.....	121
Table 5-9: Comparison of the results from the finite element analysis to the failure criteria for the raised face flange	122



Table 5-10: Comparison of the maximum axial, radial, and tangential stresses calculated by the finite element analysis and predicted by ASME VIII, Division 1 for the raised face flange.....	122
Table 5-11: Maximum equivalent Von Mises stress, for the seating and operating conditions, when either the small, medium and large O-ring is used.....	123
Table 5-12: Contact pressure distributions, during operation, for the large, medium, and small O-rings	124
Table 5-13: Number of bolts, hole diameter, and washer face diameter for the respective nominal bolt sizes.....	126
Table 5-14: Parameter ranges for the optimisation of the flat face flange, raised face flange, and raised ace with an O-ring groove flange	128
Table 5-15: Objectives and constraints functions for the optimisation	132
Table 5-16: Dimension of the candidate flat face designs	134
Table 5-17: Results from the optimisation of the flat face flange	134
Table 5-18: Dimension of the candidate raised face designs	136
Table 5-19: Results from the optimisation of the raised face flange	136
Table 5-20: Dimensions of the candidate raised face flanges designs with O-ring grooves	138
Table 5-21: Results from the optimisation of the raised face flange with an O-ring groove	138



LIST OF SYMBOLS

Standard symbols

A_m	Required cross-sectional area of bolts	[m ²]
a	Radial distance from the inner diameter of the flange to the bolt PCD.	[m]
B	Total bolt load	[N]
B_0	Initial bolt load	[N]
B_f	Flange width	[m]
C	Viscous damping coefficient	[N.s.m ⁻¹].
b	Gasket seating width.	[m]
d	Effective diameter of the bolt	[m]
d	Inside diameter of the shell	[m]
d_b	Bolt hole diameter.	[m]
d_{min}	Minimum meridional distance	[m]
d'_L	Bolt hole reduction	[m]
d_0	Outside diameter of the flange	[m]
d_2	Inside diameter of the flange	[m]
E	Modulus of elasticity	[Pa]
e_a	Wall analysis thickness	[m]
F	Applied force	[N]
F	Shear force which acts on the shell of the flange	[N]
f	Nominal design stress	[Pa]
f_a	Allowable atmospheric bolt stress	[Pa]
f_b	Allowable operational bolt stress	[Pa]
G	Diameter of gasket load reaction	[m]
G	Total compressive force	[N]



G	Outside diameter of the flange specified by the user	[m]
G_O	Equilibrium position on bolting-up	[m]
H	Thickness of flange	[m]
H_D	Total design bolt load for bolting-up condition	[N]
H_G	Gasket load at operating condition	[N]
H_p	Force required to ensure a leak tight joint	[N]
H_T	Hydrostatic end force on area of flange face inside of the gasket	[N]
H_y	Minimum design seating stress	[Pa]
h_D	Length of the supporting line segment	[m]
h_O	Radial offset between force H_D and bolt centre line	[m]
h_f	Thickness of the flange ring	[m]
h_G	Radial offset between force H_G and bolt centre line	[m]
h_T	Radial offset between force H_T and bolt centre line	[m]
K	Stiffness coefficient of a linear spring element	[N.m ⁻¹]
M	Moment which acts on the shell of the flange	[N.m]
M'	Limit value of the moment acting on the shell	[N.m]
M_{atm}	Total flange moment for the bolting-up condition	[N.m]
m	Gasket factor suggested by the author	-
N	Moment at the middle surface of the flange ring	[N.m]
n	Number of bolts	-
P	Load due to pressure acting on the flange	[N]
P'	Pressure end load	[N]
P_b	Primary bending stress	[Pa]
P_L	Local primary membrane stress	[Pa]
P_m	General primary membrane stress	[Pa]



P_R	End load.	[N]
P_O	Bolt pre-tension	[N]
p	Operating pressure as specified by the designer	[Pa]
Q_b	Secondary bending stress	[Pa]
Q_m	Secondary membrane stress	[Pa]
R	Mid surface radius of curvature	[m]
R'	Mean radius of the shell	[m]
R_a	Root area of bolts	[m ²]
R_i	Inner radius of flange	[m]
R_o	Outer radius of flange	[m]
$R_{p1.0-T}$	1% offset of yield strength at a predefined temperature	[Pa]
$R_{p0.2-T}$	0.2% offset of yield strength at a predefined temperature	[Pa]
r	Radius of shell	[m]
S_a	Allowable bolt stress at the ambient temperature	[Pa]
S_b	Allowable bolt stress at the operating temperature	[Pa]
S_{fo}	Allowable flange stress at the ambient temperature	[Pa]
S_{fa}	Allowable flange stress at the operating temperature	[Pa]
S_{FO}	Design stress	[Pa]
S_H	Axial bending stress in the hub adjacent to the flange	[Pa]
$S_{R\cdot}$	Extreme fibre stress radial to the flange at its inner edge	[Pa]
S_T	Extreme fibre stress circumferential to the flange at its inner edge	[Pa]
S_{TB}	Circumferential bending stress	[Pa]
T	Temperature	[K]
t	Time	[s]
t_f	Thickness of flange	[m]



ν	Poisson's ratio	
W	Total bolt load	[N]
W_{m1}	Required operating bolt load	[N]
W_{m2}	Required seating bolt load	[N]
γ	Minimum design seating stress suggested by the author for the type of gasket selected by the designer	[Pa]
Z	Section modulus	[m ³]

Greek symbols

Δ	Displacement	[m]
$\dot{\Delta}$	Rate of displacement	[m.s ⁻¹]
δ	Distance between flange faces	[m]
ϵ	Strain. The subscript indicated the direction	-
σ_b	Bending stress in flange ring	[Pa]
σ_p	Stress at a specified pressure	[Pa]
σ_t	Stress at a specified temperature	[Pa]
σ_y	Yield stress	[Pa]



CHAPTER 1: INTRODUCTION AND BACKGROUND TO PROBLEM

1.1. Background to problem

There is currently a need for large diameter circular bolted flange connections for low and high pressure water pipelines in South Africa, and more specifically within the Gauteng province. The reason for this need may be found by considering how large urban areas, generally, develop. Large urban areas are commonly located near a significant body of water in order to sustain a population. However, Johannesburg (which is at the heart of the Gauteng province), developed as a result of the gold rush at the turn of the 20th century despite not being near a large body of water.

Apart from a few streams and dams the city has a shortage of water; in fact, it is the world's largest city not on a navigable body of water [1]. Therefore, almost all of the city's water demands must be met by an intricate pipe network which connects it to large distant dams. These pipe networks are often tasked with the role of rivers in that it has to continuously supply the city of Johannesburg, and its interwoven suburbs, with large quantities of water. The population of Johannesburg has increased by more than a million people from 2001 to 2011 [2]. The urban population has, therefore, increased significantly, and with it the demand for water. A need for larger diameter pipes which operate at higher pressures therefore exists, and along with it the need for larger diameter circular bolted flange connections.

The combined size and pressure requirements, for the circular bolted flange connections, are in excess of those which are currently being prescribed by the relevant standards. As a result of this, the primary objective of the research is to provide an acceptable finite element method for the expansion of existing flange tables for circular bolted flange connections.

1.2. Categories of circular bolted flange joints

Circular bolted flange connection designs are categorised as either being standard, non-standard, or special [3]. Tables with prescribed values exist for both the standard and non-standard categories. Tables with prescribed values are included in, but not limited to, the following design standards / codes: the European EN 1092-1: Steel flanges; and the American codes ANSI B16.5: Pipe flanges and flanged fittings, and ASME B16.47: Large diameter steel flanges.

The values presented in the, aforementioned, tables were calculated using fixed design methods. These fixed design methods are based on a number of tried and tested methodologies which have been proposed by a great number of research papers. These tried and tested methodologies have been adopted by many standards / codes and form part of their design-by-rule approach (which is discussed in greater detail in Chapter 2).

Special flanges are designed for instances where the pipes (or pressure vessels) are so large that neither the prescribed values for standard nor non-standard flanges may be considered [3]. Existing flange tables with prescribed values do not exist for special flanges. Instead the relevant codes and standards suggest design methods for special flanges [4] [5]. These design methods are split into one of two approaches, namely: a design-by-rule, and a design-by-analysis approach. It is also important to note that the methodologies used for the design of special flanges, have been implemented in the creation of the flange tables for the standard and non-standard flanges. It is here that the question may arise as to why the table cannot simply be extended for larger diameters or higher test pressures based on, the already implemented, design methodologies for special flanges. The answer will be considered and explained in much greater detail in Chapter 2, however, the simple answer is that it has been found that the true behaviour of the circular bolted flange connections begin to deviate significantly from the predicted behaviour (based on the design methodologies) at large diameters and / or high test pressures. This deviation results in a number of undesired consequences which include: an underestimate of the stresses and subsequent leakage of the circular bolted flange connection; or an over design of the joint [6].

1.3. Overview of circular bolted flange joints

A large number of circular bolted flange connections exist [3]. The application of a particular circular bolted flange connection design depends on the load to which it is subjected, as well as the temperatures at which it is required to operate. In this investigation, however, only three types of circular bolted flange connections were considered. The three types which were considered are: two flat face flanges containing a gasket insert (Figure 1-1.a.); a gasket insert which has been placed between two raised face flanges (Figure 1-1.b.); and two raised face flanges of which one has been modified to contain a groove for an O-ring (Figure 1-1.c.).

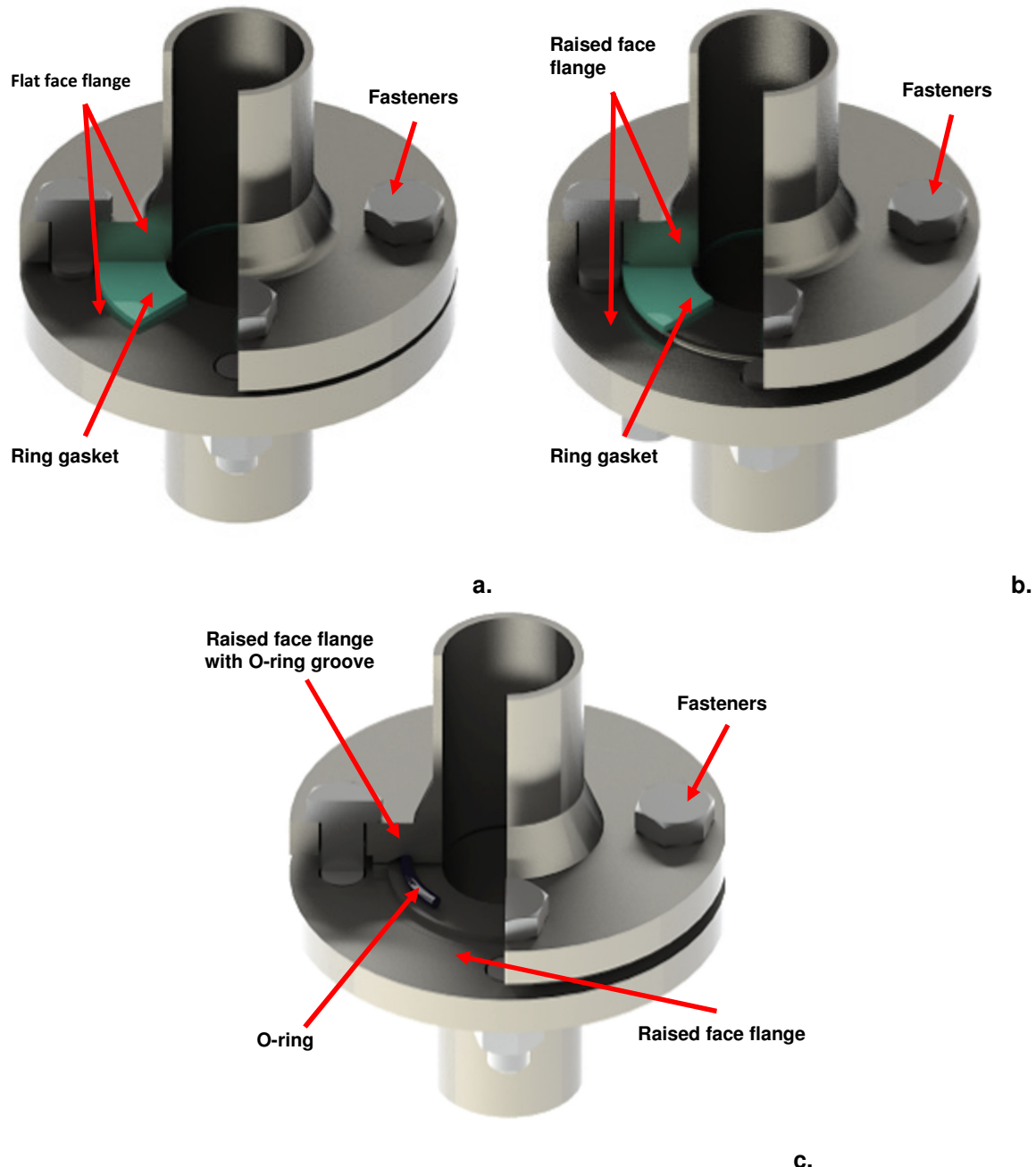


Figure 1-1: The different types of connections considered: (a) flat face (b) and raised face flanges with ring gaskets; and a (c) raised face flange modified to contain an O-ring

The three aforementioned designs may exist, and are used by Rand Water, as either circular bolted plate flange connections or as circular bolted welded-neck flange connections. Apart from the geometrical difference the plate flange and the welded-neck flange differ in the way they are attached

to pipe sections. A plate flange is attached to a pipe section by means of welding, as shown in Figure 1-2 a. The inner diameter of the plate flange is large enough so that it is able to slide over the pipe section. The weld-neck flange, on the other hand, is attached to the pipe section by means of a butt joint which connects the section of pipe to the neck of the flange (Figure 1-2 b). It is important to note that various welding methods exist for both the plate and welded-neck flange. Plate flanges and welded-neck flanges can either have a flat face, a raised face, or be modified to contain a groove for an O-ring as was shown in Figure 1-1. For this investigation only welded neck flanges (with the connection as shown in Figure 1-2 b) were considered. Weld design and the effects which it may have on the circular bolted flange connection were not considered in this investigation.

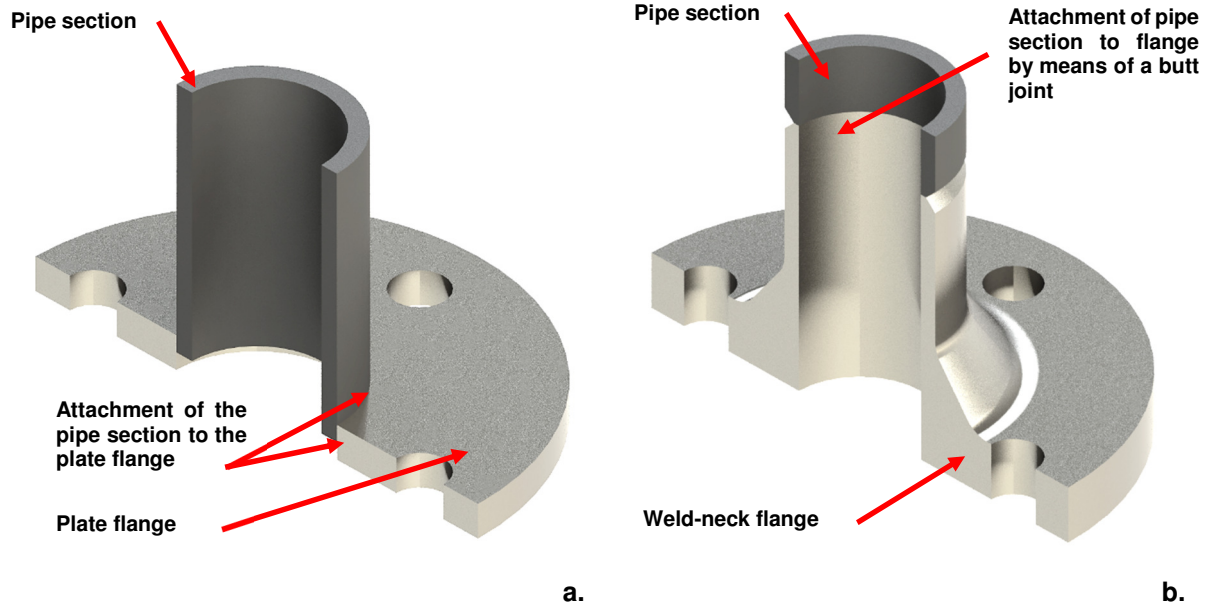


Figure 1-2: General attachment of (a) plate and (b) welded-neck flanges

1.4. Research objectives

Rand Water, which is a utility primarily responsible for the supply of water in Gauteng, have expressed a need for the expansion of their flange tables.

Rand Water's flange tables are subdivided into four pressure categories, namely: 1 500 kPa, 3 500 kPa, 5 000 kPa and 7 000-8 000 kPa. Their current flange table allows for nominal pipe diameters of up to 3 m for 1 500 kPa, and up to 2 m for the pressures of 3 500 kPa, 5 000 kPa, and 7 000-8 000 kPa. The specific circular bolted flange design used is dependent on both the required nominal bore diameter and the test pressure. Figure 1-3 shows Rand Water's current usage of flat face flanges, raised face flanges, and raised face flanges with O-ring grooves with regards to the relevant nominal bore sizes and test pressures.

From Figure 1-3 it may be observed that flat face flanges are generally used for low pressures, whereas raised face flanges which contain O-ring grooves are used for high pressures. Based on this, and the need which was expressed by Rand Water the main research objectives were:

1. A suitable design methodology, based on non-linear finite element modelling and analysis, needed to be suggested for the accurate expansion of the existing Rand Water flange table.
2. The circular bolted flange design needed to be limited to welded-neck flanges with the following face designs: flat, raised and raised with an O-ring groove.
3. The design methodology needed to take cognisance of the fact that the flange table needed to be expanded for circular bolted flange joints which are able to accommodate pipes with nominal bores of up to 4 m for the following specific test pressures: 1 500 kPa, 3 500 kPa, 5 000 kPa, 7 000 kPa,

and 8 500 kPa. The flange table, therefore, needed to be expanded as follows (and as shown in Figure 1-4):

- 3.1. Flat face flange design for test pressures up to 1 500 kPa for nominal bore diameters of 3 m to 4 m.
- 3.2. Raised face flange design for test pressures ranging from 1 500 kPa to 3 500 for nominal bore diameters of 2 m to 4 m.
- 3.3. Finally, raised face flanges with O-ring grooves for test pressures of 3 500 kPa to 8 000 kPa for nominal bore diameters of 2 m to 4 m

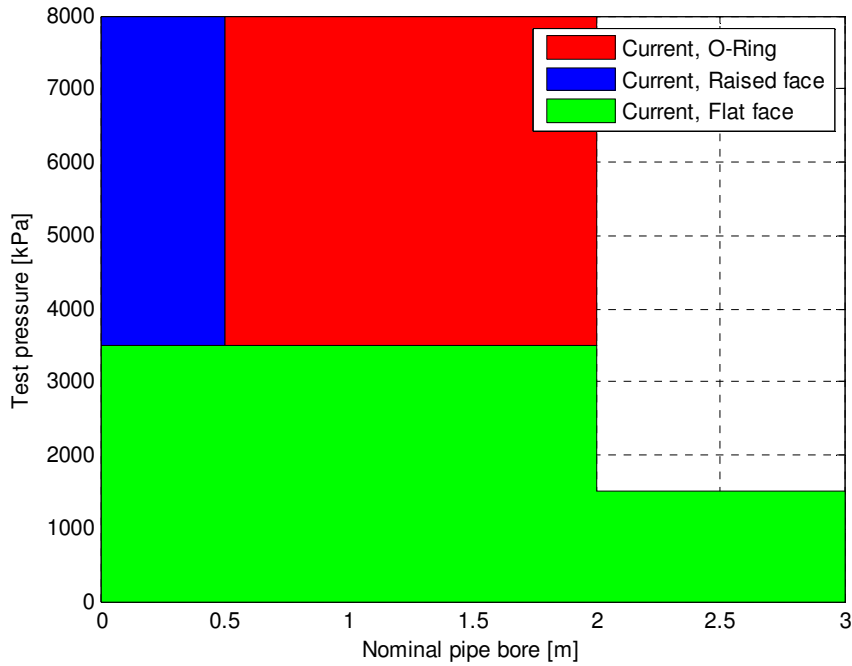


Figure 1-3: Pressure and nominal bore ranges for the current usage of flat face, raised face, and O-ring flanges by Rand Water

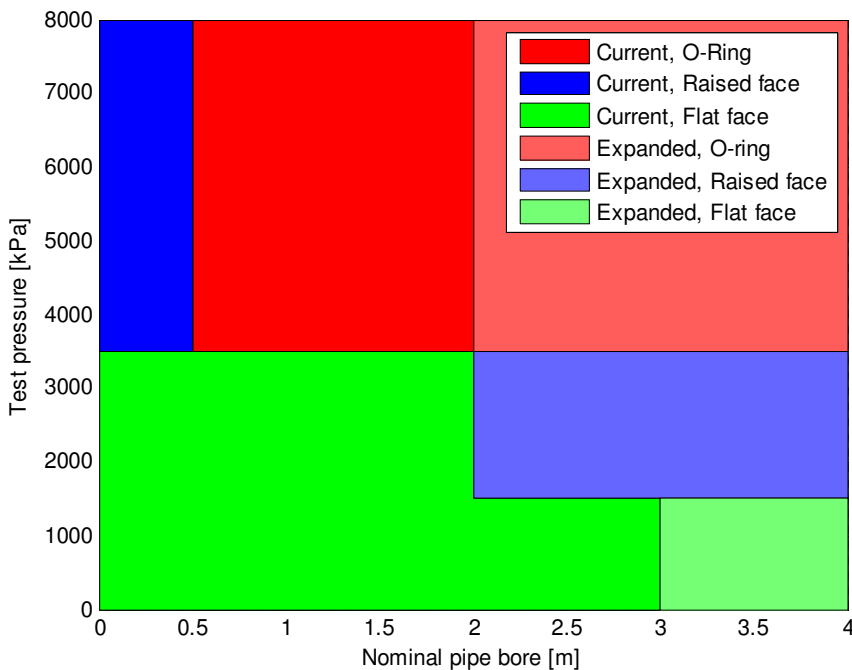


Figure 1-4: Suggested flange table expansion with reference to the applicable circular bolted flange design

1.5. Scope of the research

The purpose of this research was to provide an acceptable design methodology for the expansion of Rand Water's existing flange tables. It is for this reason that only three types of flange face designs (flat, raised, and raised with an O-ring groove) were considered for welded-neck flanges. This research was, therefore, not concerned with any other type of existing flange connection design. In addition to this, methods of joining the circular bolted flanges to the pipes were not considered. Therefore, all welding procedures and specifications were omitted.

This research, although making design suggestions, is predominantly concerned with the theoretical modelling and analysis of the specific bolted flange connections. Although small-scale experiments were done to validate the theoretical results obtained, no large scale testing was done nor considered.

Sealing forms an integral part of circular bolted flange connections, since a flange will be regarded to have failed if there is significant leakage. As a result of this, a large amount of emphasis was placed on the behaviour of the relevant gaskets and O-rings for the aforementioned circular bolted flange designs. As with flanges a large number of gasket and O-ring designs exist. For this investigation only a non-asbestos compressed fibre gasket and a standard nitrile O-ring were considered. A simplified material characterisation was done for both the compressed non-asbestos gasket and the O-ring. An in-depth, and highly accurate material characterisation of the two packing materials, however, did not form part of the scope of the investigation.

Since the primary function of the circular bolted flange connections, in this instance, was to connect pipes for the supply of water it was assumed that the flange connections will not be subjected to high temperatures or large temperature fluctuations. In addition to this it was also assumed that the flange connections will only be tasked with connecting pipes which serve as the medium of transportation for liquid water.

As part of the suggested design methodology, optimisation was considered. This did not form part of the formal scope, however, optimisation was done for illustrative purposes. An optimised, as opposed to an optimal, solution was therefore the desired outcome.

Finally, it is well known that external bending moments, external forces, and cyclic loads have a significant impact on the behaviour and performance of flanges. However, since no such data, for the specific use by Rand Water, was available the effect of external bending moments, external forces and cyclic loads have been omitted from this investigation.

1.6. Layout of thesis

This thesis is aimed at providing a methodology for the design of large diameter flanges which operate at pressures up to, and including, 8 000 kPa. However, before achieving the primary goal of suggesting a methodology, which may be used by Rand Water to expand their current flange tables, a number of secondary goals needed to be achieved. This thesis is, therefore, subdivided into six chapters (including this one), namely: 'Introduction and background to problem'; 'Literature Review'; 'Initial finite element modelling and analysis'; 'Experimental setup and results'; 'Application of method to large diameter flanges'; and 'Recommendations for future work and conclusion'.

A broad overview of the design-by-rule approach is given in the first part of the 'Literature review'. After this, specific emphasises is placed on the development, current implementation and shortcomings / advantages of the American ASME VIII design-by-rule approach, which is based on the Taylor-Forge methodology. In addition to this, special attention is given to the factors which influence leak tightness. These factors include: the creep-relaxation behaviour of gaskets, the influence which flange rotation has on the sealing ability, and the effect which bolt tightening techniques have on the desired contact stress between the gasket surface and flange faces. It is also known that thermal effects play a role in the sealing ability of flanges, this is, however, not considered in this investigation based on the assumption that the thermal expansion which results from the variation in temperature is negligible.

The final part of the literature review focuses on the finite element modelling and analysis techniques which are currently being used in the analysis of circular bolted flange connections. The important



aspects of the finite element modelling and analysis which were concentrated on were: the simplification of the geometry of a circular bolted flange connection; the loads and boundary conditions which need to be applied to the model; and the assigned contact interfaces between the various components.

One of the goals of this research was to develop an acceptable finite element model. This development is focused on in the third chapter. The first step in developing an acceptable finite element model was to accurately determine the relevant material properties of the flanges; fasteners; and packing materials. Therefore, although the focus of this chapter was on the initial finite element modelling and analysis, it included material characterisation. The material characterisation was divided into three steps for each of the two packing materials considered (namely the compressed non-asbestos gasket and the nitrile O-ring). The three steps of the material characterisation were: the experimental setup, the experimental results, and the tuning of the material model in the finite element modelling and analysis software package.

In order to draw a conclusion as to whether or not the initial finite element model and analyses was acceptable a number of experiments were completed. Chapter 4, therefore, focuses on four primary aspects of the experimentation, namely: the experimental values which needed to be determined in order to validate the finite element model and analysis, the experimental setup, the experimental procedure, and the experimental results. The final part of Chapter 4 compares the results obtained from the initial finite element analysis to the results obtained from the experimentation.

Chapter 5 focused on designing and optimising the large diameter flanges for the relevant pressures. The large diameter flanges were designed by making use of ASME VIII, Division I's design-by-rule approach and the finite element model created in Chapter 3 and validated in Chapter 4. The design values obtained from ASME VIII, Division I's design-by-rule were used as an initial guess. These values were placed in the finite element model. As stated previously it is known that the true behaviour of the circular bolted flange connections begin to deviate significantly from the predicted behaviour (based on the design methodologies) at large diameters and / or high test pressures. This may have a number of undesired consequences, which include an underestimate of the stresses in the flange which will lead to subsequent leakage, and / or an over design of the circular bolted flange connection. The purpose of the validated finite element model, therefore, was to ensure a leak tight design as well as to provide a platform from which the flange design may be optimised.

The final chapter, Chapter 6, is divided into two subsections. The first subsection focuses on future developments which could be made from this initial research. It explores possibilities for improved material modelling, the effects of friction between the surfaces of the packing materials and flange faces, the effect of external loads and moments, and the validation of the finite element models with large diameter flanges. The second subsection is a summarised conclusion of the principal findings of this report.

CHAPTER 2: LITERATURE REVIEW

2.1. Current design practices and standards

The viewpoint of many standards, and in particular pressure vessel design standards, is to follow the design-by-rule approach. This viewpoint, regarding design, generally involves fairly simple calculations, based on standardised design stresses and the adherence to specific rules which are outlined in the relevant standards [7].

The basic idea of design-by-rule is that once all the initial dimensions are fixed the designer simply applies the prescribed rules. The advantages of implementing a design-by-rule approach is, therefore, that it is simple enough to apply without an in depth understanding of all the contributing mechanisms. It is also, generally, a method which has been successfully implemented for a large variety of applications by a great number of experienced people over a long period of time [7].

The two predominant design methodologies which form the basis of the design-by-rule approach in various standards / codes are the Taylor-Forge design method, and the design method proposed in the German DIN 2505 standard. The Taylor-Forge design method forms the basis of: ASME VIII, Division 1 and Division 2; EN 13445-1, Chapter 11; and PD 5500. The method proposed in the German DIN 2505 standard, on the other hand, forms the basis of EN 1591-1, and EN 13445-1, Appendix G. In this investigation the method proposed by the German DIN 2505 standard is not formally considered; a brief description thereof is, however, given in Appendix A. A discussion of the Taylor-Forge method's development, implementation, and advantages / shortcomings is given below.

2.2. Taylor-Forge Method

The method of flange design as it was described by Waters, Rossheim, Westrom & Williams [8] is applicable to circular bolted flange connections which are under pressure and which are free to deflect under the action of a bolt load. This method of flange design is commonly referred to as the Taylor-Forge method after it was adopted by the Taylor-Forge and Pipe Works Company in Chicago, Illinois, during the 1950s [9].

When referring to a circular bolted flange connection, from a calculation point of view, it is often subdivided into the shell, hub and ring components. These subcomponents of the circular bolted flange connection are shown in Figure 2-1.

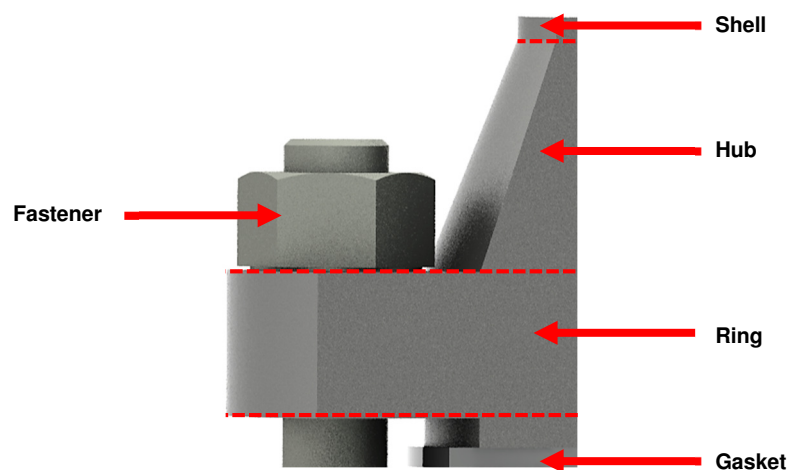


Figure 2-1: Subcomponents of a circular bolted flange connection

2.2.1. Early development and preceding design methods

The earliest known, method which was suggested for the design of circular bolted flanges was the 'locomotive method' by Risteen in 1905 [3]. An additional method was developed by Crocker & Stanford where it was assumed that the flange behaved in the same manner as a beam [3]. The equations used

in determining the stresses of both the loose rings and the integral flanges were based upon the flat-plate theory [10]. This approach is illustrated in Figure 2-2, where it was assumed that the flange is clamped along the radial cross section. For this method the concept of a moment arm, which is obtained from the bending due to the external moment and lumping together all of the bolt loads, was used. The maximum bending stress for a beam could then be calculated, from the elementary beam formula. Using the variable designations, shown in Figure 2-2, the section modulus and maximum bending stress are determined from Equations 2.1. and 2.2. respectively.

$$Z = \frac{(B_f - d_b)t_f^2}{3} \quad (2.1.)$$

where:

- B_f Width of the flange [m]
- d_b Diameter of bolt hole [m]
- t_f Thickness of flange [m]
- Z Section modulus [m³]

$$\sigma_b = 0.95 \left(\frac{W \cdot a}{(B_f - d_b)t_f^2} \right) \quad (2.2.)$$

where:

- W Total bolt load [N]
- σ_b Bending stress in flange ring [Pa]

According to Hustons & Josephs [11] this was only an approximation since the curvature of the flange ring and the effect of the pipe wall have been ignored. This method has been found to give acceptable results for instances where plate flanges have been welded to thin pipes.

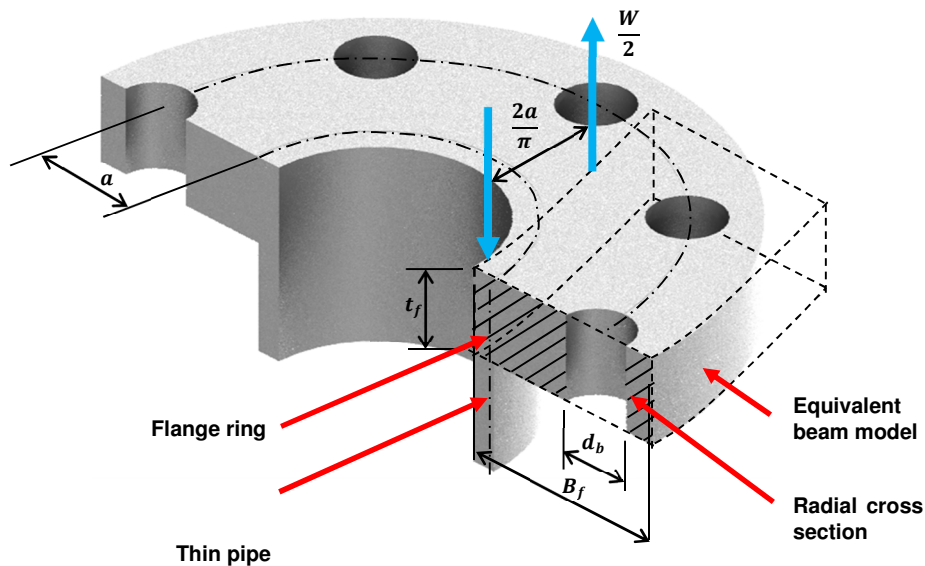


Figure 2-2: Flange fixed along its radial cross section [11]

The methods suggested by Risteen, and Crocker & Stanford [10] were later compared by Den Hertog [12]. Den Hertog compared the two methods by means of vector algebra and found them to be equivalent – although the derivations were different [3].

Waters & Taylor [12] improved upon this previous method by combining the theory of a beam on an elastic foundation and the theory for a flat plate. They were able to refine prior research by taking both radial and circumferential stresses into account. Radial stresses are of importance in flanges which are integral with thick pipes, and which can resist the angle of tilt a lot better. The refinement was achieved by considering a strip which was cut out of a cylinder and treated as a beam on an elastic foundation while the flange was regarded as a flat plate with a central hole. According to Hustons & Josephs [11] the slopes and deflections at the end of the cylinder were expressed in terms of the unknown moments and shear forces. The displacements were then equated to the slopes and deflection which were determined for the plate. This allowed the simultaneous solution of equations since there was enough equations for the unknown reactions and displacements. For the method suggested by Waters & Taylor [12] the flange design was based on the assumption that the bending moment acts on a meridian plane at the root of the hub. It was further assumed that the cylindrical surface does not alter its original curvature and that the expansion of the hub as a result of internal pressure may be neglected.

The solution for the flange problem, based on plate theory, assumed that the flange was circular with a central hole and was either loaded at the edge or was uniformly loaded over the entire surface. When it was assumed that the circular plate was loaded and supported in the same manner as shown in Figure 2-3, the maximum tangential stress will be developed at the inside corners of the plate.

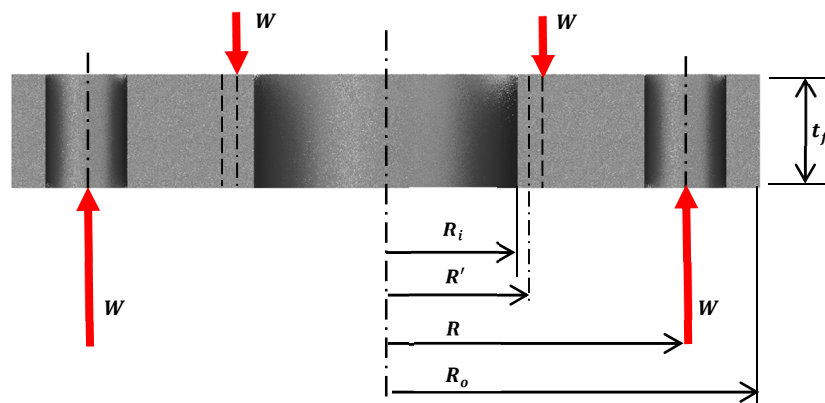


Figure 2-3: Simply supported plate under concentric loading [11]

Thus according to Waters & Taylor [12] the corner stress became:

$$\sigma_h = \frac{W(R - R')}{(R_o - R_i)t^2} \left[\frac{1.242R_o^2 \log_e \left(\frac{R_o}{R_i} \right)}{R_o^2 - R_i^2} + 0.335 \right] \quad (2.3.)$$

where:

- R Bolt pitch circle [m]
- R_i Inside radius of flange [m]
- R_o Outside radius of flange of flange [m]
- R' Section modulus [m³]

One of the drawbacks highlighted by Hustons & Josephs [11] is that the maximum circumferential stress for a plate with a small hole is twice as large as a solid plate. The implication of this becomes important in cases where the plate is not made of fracture tough material. However, this improvement, made by Waters & Taylor [12], allowed for the calculation of the radial, tangential and axial stresses, and provided a platform for further development [10].

From the late 1930s to the late 1940's Waters *et al.* [8] improved upon the work of Waters & Taylor [12] and suggested new methods for the design of bolted flange connections. These methods became commonly known as the Taylor-Forge method.

Another set of design methods, also developed during the 1950s, based on the work of Waters *et al.* [8], was suggested by Lake & Boyd. According to Nash [13] two British standards were published between 1950 and 1970. The first of these standards was the British BS 1500, which was based on the Lake & Boyd method, and which was published in the 1950s. The second was the British BS 1515 standard which, unlike the BS 1500, was based upon the Taylor-Forge method. The BS 1515 was published in 1969. The difference between the two standards, as was summarised by Nash [13], is that the BS 1515 allowed for a higher level of allowable stress with more advanced rules compared to the BS 1500. During the 1970s, however, it was decided to combine the BS 1500 and the BS 1510 into a single design code which became known as the British BS 5500 standard. The first edition of the BS 5500 was published in 1976 and continued to be used until the early 2000s. During the period 1970-2000 there was, however, an effort to draft an international standard. The international standard, then known as the ISO DIS 2694, was not widely accepted and was abandoned. In May 2002 the first issue of the European EN 13445 standard was published. As a result of this, and according to CEN rules, the British Standards Institute (BIS) was forced to withdraw the BS 5500 standard. Once in use it was found that the, then, new, European standard was not as comprehensive as the BS 5500. It was, thus, decided that the British pressure vessel standard should continue to be available. In order to do this a new document with the designation of PD 5500, which had equal the content, validity, and application as the BS 5500 standard, was published [13].

As previously mentioned, the Taylor-Forge method was widely used in the United States of America and as a result of its success became the basis of the flange design for the ASME VIII code. The ASME VIII code has been continuously updated since its first publication, however, it continues to make use of the Taylor-Forge method which has been amended.

2.2.2. Implementation of the Taylor-Forge method

The implementation of the Taylor-Forge method, shown below, was taken from Taylor-Forge, Modern Flange Design, Bulletin 502 [14], and from Moss & Basic [15].

When applying the Taylor-Forge method, the first step is to determine the size and number of bolts which will be required in order to effectively seat the gasket and ensure a leak-tight joint during operation [9]. In order to determine the size and the amount of bolts, which will be required the following values need to be, firstly, decided upon:

1. Operating pressure.
2. Ambient and operating temperature.
3. Flange material.
4. Bolting material.
5. Type and size of gasket.

Based on the material properties of the bolts and flanges, as well as on the design and operating temperatures, the allowable stresses may be calculated as follows from Equations 2.4. and 2.5.

$$S_b, S_{fo} = \left(\frac{\gamma_{0.2-T}}{1.5} \right) \quad (2.4.)$$

where:

- S_b Allowable stress at the operating temperature of the bolt [Pa]
- S_{fo} Allowable stress at the operating temperature of the flange [Pa]
- $\gamma_{0.2-T}$ Yield strength of the bolt / flange at the operating temperature [Pa]

$$S_a, S_{fa} = \left(\frac{\gamma_{m-20}}{2.4} \right) \quad (2.5.)$$

where:

- S_a Allowable stress at the ambient temperature of the bolt [Pa]
 S_{fa} Allowable stress at the ambient temperature of the flange [Pa]
 γ_{m-20} Yield strength of the bolt / flange at the ambient temperature [Pa]

Based on the type of gasket selected the Taylor-Forge method prescribes two factors, namely, m and y . The y factor is a value for the gasket design seating stress, whereas the m factor is a so called 'gasket-factor'.

From this information the total required cross sectional area of the bolts; the required operating bolt load; and the required bolt seating load may be determined. The relationship between the size of the bolts, the number of bolts, and the total required cross sectional area of the bolts is given by Equation 2.6.

$$n = \frac{A_m}{R_a} \quad (2.6.)$$

where:

- A_m Total required cross sectional area of bolts [m²]
 n Number of bolts
 R_a Total root area of bolts [m²]

From this the total required cross sectional area of the bolts is taken as the larger of:

$$A_m = \max\left(\frac{W_{m2}}{S_a}; \frac{W_{m1}}{S_b}\right) \quad (2.7.)$$

where:

- W_{m1} Required operating bolt load [N]
 W_{m2} Required seating bolt load [N]

The required seating bolt load may be calculated using Equation 2.8. and simply the load required to compress the gasket to its required seating stress.

$$W_{m2} = b\pi Gy \quad (2.8.)$$

where:

- b Gasket seating width [m]
 G Diameter at gasket load reaction [m]
 y Gasket design seating stress [Pa]

Shown in Figure 2-4 is a diagram of the application of the total bolt load and the reaction thereof from the contact interface between the flange face and the gasket surface. A free-body diagram for the operating bolt load in accordance with the Taylor-Forge method is shown in Figure 2-5. The calculations which relate to Figure 2-5 are shown in Equations 2.9. to 2.11.

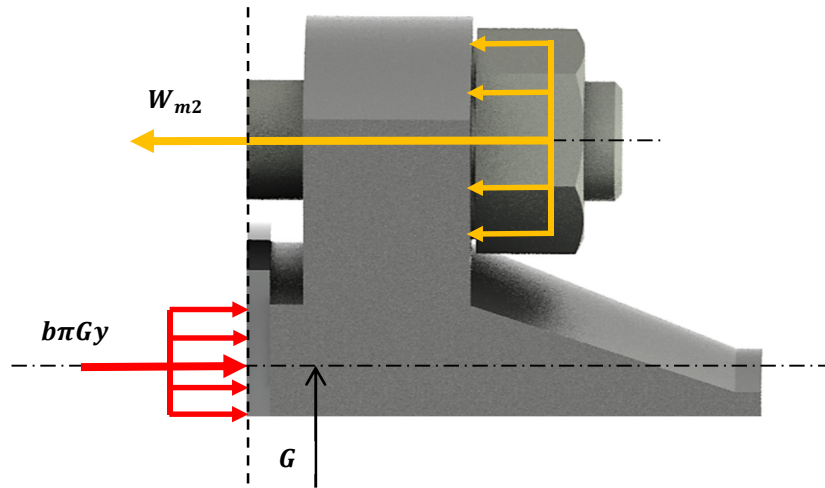


Figure 2-4: Free body diagram for the seating bolt load in accordance with the Taylor-Forge method

The total required operating bolt load is equal to the sum of the hydrostatic end force (Equation 2.9.), and the total joint-contact surface compression load (Equations 2.10.)

$$H = \frac{G^2 \pi P}{4} \quad (2.9.)$$

where:

P Operating pressure [Pa].

$$H_p = 2b\pi GmP \quad (2.10.)$$

where:

m Gasket factor.

therefore:

$$W_{m1} = H + H_p \quad (2.11.)$$

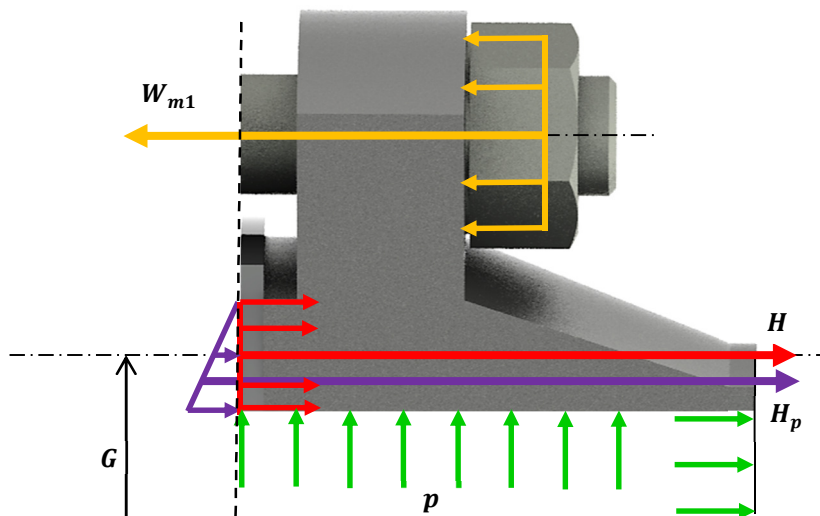


Figure 2-5: Free body diagram for the operating bolt load in accordance with the Taylor-Forge method

Once the size and the number of bolts has been determined for the design the total design bolt load may be calculated from Equation 2.12.:

$$W = \frac{(A_m + A_b)S_a}{2} \quad (2.12.)$$

where:

- A_b Actual bolt area [m²]
 W Total design bolt load [N]

The next step in the Taylor-Forge method is the calculation of the assumed principal forces and their associated moments. During the seating of the gasket the only principal force which acts on the flange is the gasket load. The forces and moments which act on the system may, therefore, be defined as follows (with the variable designation as shown in Figure 2-6). The seating gasket load is equal to the total design bolt load.

$$H_G = W \quad (2.13.)$$

where:

- H_G Seating gasket load [N]

The seating moment is taken as the product of the seating gasket load and the average of the bolt pitch circle diameter and the diameter of at the gasket load reaction.

$$M'_o = h_g \cdot H_G \quad (2.14.)$$

where:

- M_o Seating moment [N.m]

and:

$$h_g = \frac{C - G}{2} \quad (2.15.)$$

where:

- C Bolt PCD [m]

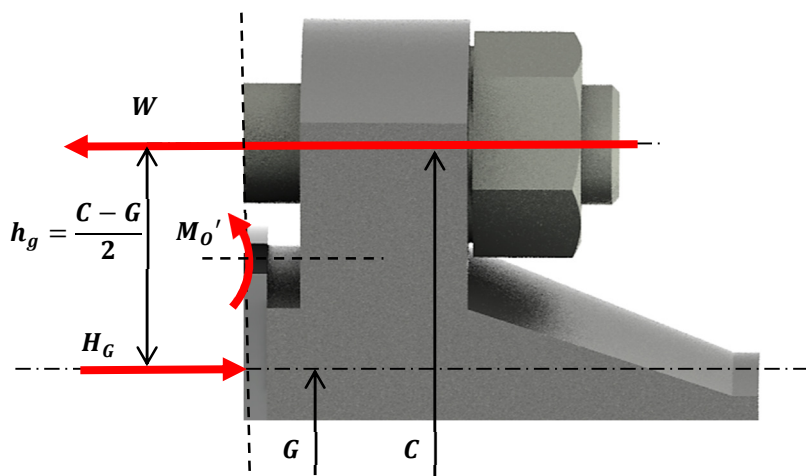


Figure 2-6: Principal moments and forces which are applicable during the seating of the gasket according to the Taylor-Forge method

During operation, however, the circular bolted flange will be subjected to three principal forces and their applicable moments. The three principal forces are: the hydrostatic end force on the area inside of the flange (designated by green in Figure 2-7); the operating gasket load (designated by red in Figure 2-7); and the total joint contact surface compression load (designated by blue in Figure 2-7).

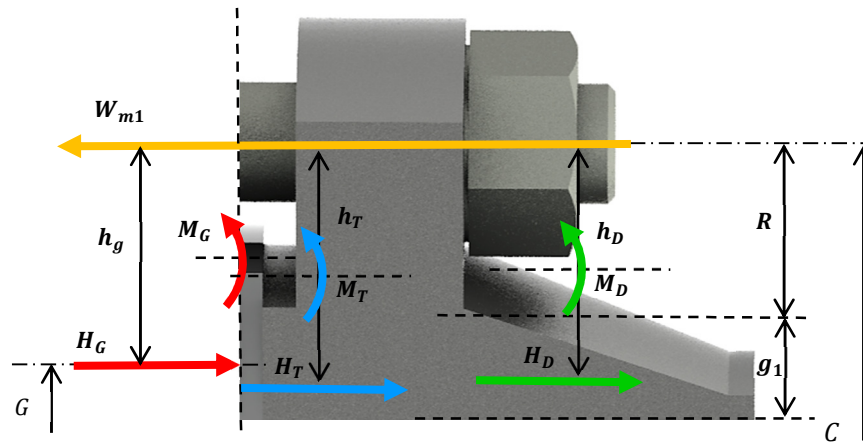


Figure 2-7: Principal moments and forces which are applicable during operation according to the Taylor-Forge method

The three principal loads, namely: the hydrostatic end force on the area inside of the flange; the operating gasket load; and the total joint contact surface compression load are calculated by means of Equations 2.16., 2.17., and 2.18., respectively.

$$H_D = \frac{\pi B^2 P}{4} \quad (2.16.)$$

where:

- B Flange inner diameter [m]
- H_D Hydrostatic end force on the area inside the flange [Pa]

$$H_G = W_{m1} - H \quad (2.17.)$$

$$H_T = H - H_D \quad (2.18.)$$

The associated moments are:

$$M_D = H_D h_D \quad (2.19.)$$

where:

- M_D Moment resulting from the hydrostatic end force on the inside are of the flange [N.m]

and:

$$h_D = R + 0.5g_1 \quad (2.20.)$$

where:

- g_1 Hub thickness at the thin end [m]
- h_D Lever arm for the hydrostatic end force on the inside area of the flange [m]
- R Distance from the bolt PCD to the thick end of the hub [m]

$$M_G = H_G h_g \quad (2.21.)$$

where:

M_G Moment resulting from the operating gasket load [N.m]

and:

$$h_g = \frac{C - G}{2} \quad (2.22.)$$

$$M_T = H_T h_T \quad (2.23.)$$

where:

M_T Moment resulting from the total joint contact surface compression load [N.m]

and:

$$h_T = \frac{R + g_1 + h_G}{2} \quad (2.24.)$$

Once the principal loads and moments had been determined the shape factors may be determined. The shape factors include the following variables: K , T , Z , Y , U , V , F , and f . These factors may be read off from a series of plots. These shape factors are given as functions of the following two ratios:

$$\frac{g_1}{g_0} \quad (2.25.)$$

and,

$$\frac{h}{h_0} \quad (2.26.)$$

where:

$$h_0 = \sqrt{B g_0} \quad (2.27.)$$

The values obtained for the shape factors may then be used to calculate the stress formula factors. The following seven stress factors will be calculated (given in Equation 2.28. to 2.34.):

$$\alpha = te + 1 \quad (2.28.)$$

where:

$$e = \frac{F}{h_0} \quad (2.29.)$$

and,

t Thickness of the flange [mm]

R Distance from the bolt PCD to the thick end of the hub [m]

$$\beta = \frac{4}{3} te + 1 \quad (2.30.)$$

$$\gamma = \frac{\alpha}{T} \quad (2.31.)$$

$$\delta = \frac{t^3}{d} \quad (2.32.)$$

$$\lambda = \gamma + \delta \quad (2.33.)$$

$$m_o = \frac{M_o}{B} \quad (2.34.)$$

$$m_G = \frac{M'_o}{B} \quad (2.35.)$$

The final step in the Taylor-Forge method is the calculation of the operating and seating stresses in the axial, radial, and tangential direction. For the operating axial, radial, and tangential stress Equation 2.36. to 2.41. are applicable:

$$S_H = \frac{f m_o}{\lambda g_1^2} \quad (2.36.)$$

$$S_R = \frac{\beta m_o}{\lambda t^2} \quad (2.37.)$$

$$S_T = \frac{m_o Y}{t^2} - Z S_H \quad (2.38.)$$

For the seating axial, radial, and tangential stress Equation 2.39. to 2.41. are applicable:

$$S_H = \frac{f m_G}{\lambda g_1^2} \quad (2.39.)$$

$$S_R = \frac{\beta m_G}{\lambda t^2} \quad (2.40.)$$

$$S_T = \frac{m_G Y}{t^2} - Z S_R \quad (2.41.)$$

2.2.3. Application of the Taylor-Forge method to the design of large diameter flanges

One of the principal publications, regarding the design of large diameter flanges, was produced by Murray & Stuart in 1961 [6]. In this publication they investigated the behaviour of large taper hub flange connections and compared it to the research done by Waters & Taylor [12], and subsequent publications by Waters *et al.* [8] and Lake & Boyd [16].

In a citation of the work done by Wesstrom & Bergh [17], Murray & Stuart [6] state that there has been no encounter of a sudden failure of flange joints. As a result of this it may be assumed that the usual criteria of failure which is excessive stresses or the establishment of plastic mechanisms do not apply to flanges. However, a flange joint will be considered to have failed if it leaks. As cited by Murray & Stuart [6], Wesstrom & Bergh [17] found that flanges tend to leak when they have either large diameters or are exposed to excessive pressures.

When designing flanges emphasis may be placed on either the design of the gasket or the design of the flange. If emphasis is placed on the design of the gasket it is implied that large rotations will be considered and plastic conditions are allowed to prevail. However, if the flange is designed in order to minimise the rotation then the focus of the design will be the flange and not the gasket; and the gasket will not be expected to operate at its limit. According to Murray & Stuart [6] this change of emphasis from the gasket design to the flange design is vital when there is either an excessive increase in the diameter of the flange or of the pressure it is subjected to. They draw this conclusion based on the

discrepancies they observed between their experimental results and the analytical methods which stem from the research done by Waters & Taylor [12].

In the research done by Waters *et al.* [8] only elastic behaviour was considered, therefore, all of the plastic effects were ignored. The method which was suggested by Waters *et al.* [8] also results in high calculated bolt stresses (which does not necessarily occur in reality). With regards to this, Murray & Stuart [6] argued that the only limit on the bolt stresses should be yield. Lake & Boyd [16], however, found that although many flanges had yielded they were still able to give good service for prolonged periods. As a result of this the Lake & Boyd method designed for yielding to occur. Murray & Stuart [6] gives a brief recap of the Lake & Boyd method by stating that the method was centred on the conventional ring type flange (plate flange), and suggested that a tapered hub flange (integral flange) can be treated in a similar fashion. It is known that the ring type flange has high discontinuity stresses at the connection between the cylinder and the flange ring. In their publication Murray & Stuart [6] state that stresses in the flange ring are low, which means that there is local redistribution. Because of this the stresses suggested in the Lake & Boyd method, therefore do not really exist. Thus, the maximum stress occurs at the hub to shell junction. In addition to this the Lake & Boyd method considered it appropriate to simplify the system by considering an infinitely long cylinder with a mean thickness instead of the tapered hub. In Murray & Stuart [6]'s opinion this simplifying assumption is likely to cause an over-estimate of the stresses since the purpose of the tapered hub, which has been disregarded, is to blend the deflection of the flange ring to those of the cylinder.

Murray & Stuart [6] stated that the most exact solution, up to that point which did not yet include the DIN 2505 method, could be obtained from the research of Waters *et al.* [9]. Because of this statement they consider and later showed that the Taylor-Forge method underestimates the stresses in large tape hub flanges.

In their research Murray & Stuart [6] considered a very similar situation to the one on which this research is focused, namely a 15 ft (~4.6 m) taper hub flange. The flanges were also considered for test pressures of 165 lb/in², 230 lb/in², and 315 lb/in² (~1 140 kPa, ~1 585 kPa, and ~2 171 kPa). In addition to this the flange had a raised face and made use of silicone rubber O-rings. They conducted both a theoretical investigation and a physical experiment.

In their theoretical analysis it was assumed that all three components of the flange (namely: the ring, the hub, and the shell) all had an equal mean diameter. It was also assumed that the external bending moment which acts on the flange ring consists of the pressure end load and the interface load. In addition to this the flange was also assumed to be subjected to an internal pressure. They analysed each of the three components individually, and then combined them so that the conditions for compatibility and equilibrium were satisfied at each of the joints. This resulted in eight linear equations which could be solved simultaneously in order to obtain the stresses, the deflections, and the rotation of the flange.

The physical experiment consisted of a hydraulic proof test which was carried out on the, aforementioned, flange layout (i.e. a raised face integral flange with silicone rubber O-rings). The flange, and relevant fasteners were instrumented with strain gauges. For the hydraulic proof tests, which were done the flanges were bolted together according to the Taylor-Forge specification. The flange was instrumented with 48 strain gauges which were placed to measure both in the axial and tangential directions. They were positioned in two lines which were disposed at 90° to one another –with respect to the centre line of the pressure vessel. In addition to this, four bolts were also instrumented with strain gauges. These strain gauges were instrumented in such a way so as to eliminate the bending stresses in the bolts. In addition to the use of strain gauges the rotations of the flanges were obtained from a telescope, mirror pair, and scale. The instrumentation of the flange allowed for the following information to be obtained:

1. The axial and tangential stresses on the outer surface of the vessel under consideration.
2. The bolt stresses as a function of the pressure.

3. The value of the interface load which is the difference between the bolt load and the pressure end load.
4. The flange rotation as a function of the pressure.

According to Murray & Stuart [6] the following flange behaviour was expected: the distance from the gasket reaction force to the bolt circle is assumed to be positive since the interface load will be inside the bolt circle. This reduction in the interface load, may or may not result in a reduction of the load with pressure since this is dependent on the initial bolt load and the geometry of the raised face. However, in their investigation they neglected the moment due to the interface load and only considered the membrane tension which is half of the product of the mean radius, the distance from centre of the thick end of the taper to the bolt circle, and the internal pressure. They continue to state that had a full-face joint been used, as is the case with a flat face integral flange, large reactions would have been obtained between the outer edges of the flange rings because of rotation. They also states that it would have been very likely that this reaction would have increased as the internal pressure increased. This means that the neglected moment due to the interface load may have had an appreciable influence on the behaviour of the flange. Thus, the conclusion which may be drawn is this: when the outer edges of the flange ring are not in contact (such as for a raised face integral flange) the interface load will not have an appreciable influence on the behaviour of the flange.

Murray & Stuart [6] compared the experimental results to the predicted results of the Lake & Boyd method and the Taylor-Forge method. Because the Lake & Boyd method was never intended for the design of large diameter flanges a large discrepancy between the experimental results and the predicted results were obtained. This large discrepancy may be attributed to the large bending stress which occurs in the simplified model of the Lake & Boyd method. In reality this does not occur due to the 'bending function' of the tapered hub. In addition to this it was found that there was a close agreement between the experimental and theoretical results for the raised face flange, and that the rotations were, as previously thought, unaffected by the interface load. Thus a theoretical analysis may be carried out by only considering the pressure end load and the bolt load which is required to maintain equilibrium. Conversely, it was found that for a full face joint the interface load had an effect, and will need to be included in a theoretical analysis.

2.2.4. Comparison of the predicted stress values by means of ASME to finite element analysis

Nagata & Sawa [18] compared flange stresses predicted by the ASME design code to those calculated by finite element modelling and analysis. In this research, Class 150 raised face flanges which varied in size from NPS 2 to NPS 24 were used. The gasket material was assumed to be spirally wound, and the flanges needed to be able to connect to Schedule 40 piping. With regards to this research three sets of results were considered. The first set of results shown are the stress distributions in the axial, radial, and tangential directions (Figure 2-8). The second set of results compared the maximum axial, radial and tangential stresses as predicted by ASME to those calculated by the finite element analysis. The final set of results are plots of the ratio of the stress values predicted by ASME to those calculated by the finite element analysis for both the seating and operating conditions.

Figure 2-8 (a) shows the stress distribution in the axial direction during the seating. From these results it may be observed that the inside surface of the hub of the flange has axial compression, whilst the outside angled surface of the hub is in axial tension. In addition to this, the area near the bolt hole towards the hub is also in axial compression. The maximum stress lies at the interface of the hub and ring of the flange. These conditions are true for both the seating and operating conditions. In the radial direction, for the seating condition, the maximum stress lies at the interface between the flange hub and ring - Figure 2-8 (b). The minimum stress lies near the outer edge of the raised face of the flange. Only two clearly distinct stress distributions form, namely: the radial tension at the interface between the hub and ring of the flange; and the radial compression at the outer edge of the raised face. The final set of stress distribution results which were considered are the tangential stresses in the flange. The maximum stress was located at the interface between the shell and hub of the flange, whilst the minimum stress was located near the outer diameter of the raised face flange, as shown in Figure 2-8 (c). The maximum

stress decreases towards the inner surface of the flange. These results for the various stress distributions are important since it will be used later in the investigation for validation purposes.

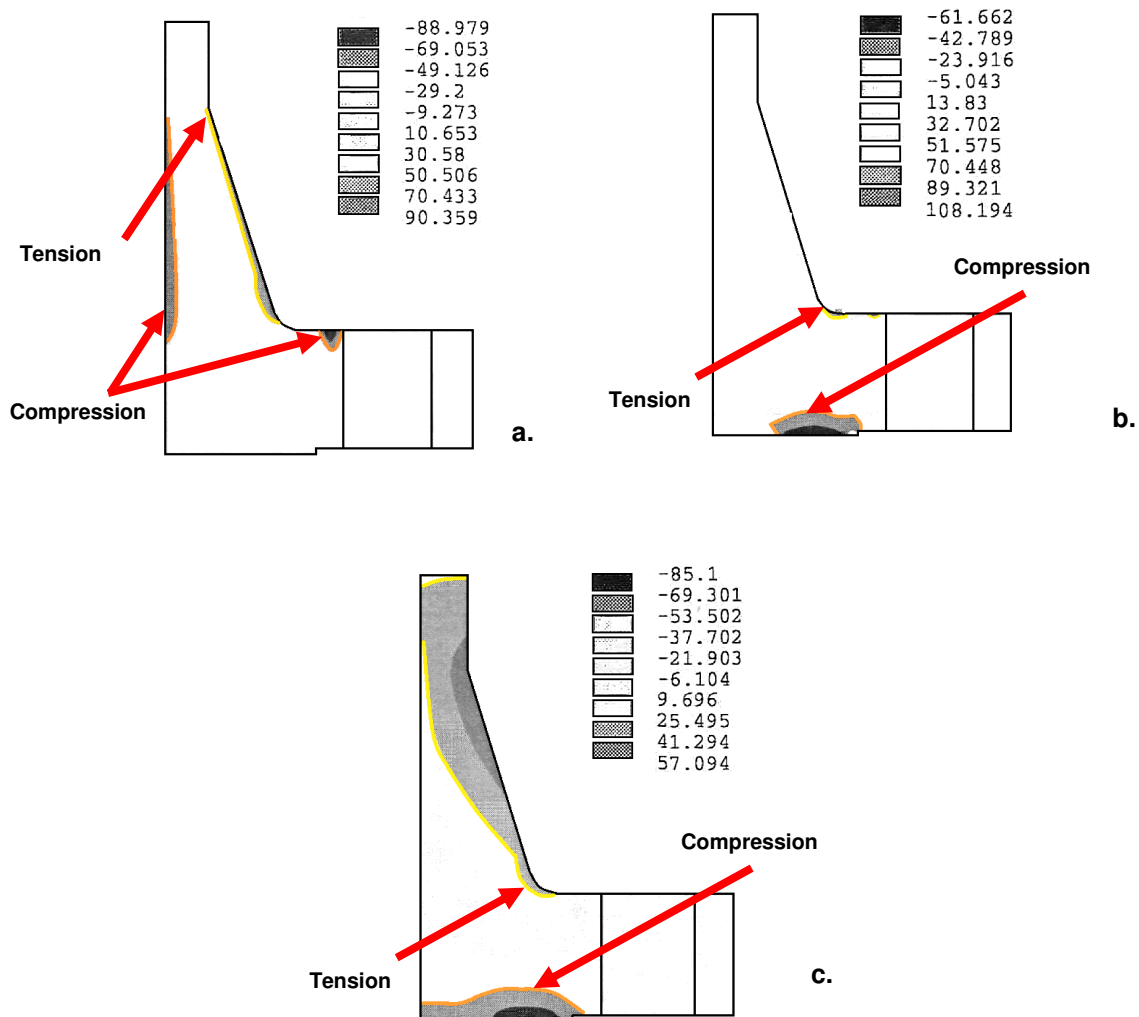


Figure 2-8: Stress distribution in the (a) axial, (b) radial, and (c) tangential direction during the seating conditions for a NPS 24 flange [18]

Nagata & Sawa [18] found, for both the seating and operating conditions, that the stresses in the radial direction were predicted by ASME to be the highest. The lowest predicted stresses, from ASME, were in the tangential direction. For a NPS 10 flange, for the seating and operating conditions, the maximum tangential and radial stresses were predicted to be ~85% and ~35%, respectively, of the maximum radial stress. For a NPS 24 flange, however, the maximum tangential and radial stresses were predicted to be ~75% and ~30%, respectively, of the maximum radial stress. It was, therefore, shown that an increase in flange size resulted in a larger difference between the predicted stresses by ASME.

From the results of Nagata & Sawa [18] 's finite element analysis, however, it was shown that the highest calculated stresses were in the axial direction with the lowest being in the radial direction. This was true for both the seating and operating conditions. Unlike the predicted results by ASME, the difference in calculated stress values did not increase as the size of the flange increased. The tangential stress remained above ~75% of the maximum axial stress, whereas the radial stress never exceeded ~65%.

The axial stress values, from the ASME stress formula, as calculated by Nagata & Sawa [18] are ~1.5 times greater than those calculated by the finite element analysis for a NPS 24 flange - Figure 2-9 (a). This difference, in the axial stress value increases as the nominal bore size of the flange decreases. A similar trend is observed for the tangential stress. The lowest difference, between the predicted values

based on ASME and the calculated values from the finite element analysis, is obtained at the largest flange nominal bore size. The difference increases as the flange nominal bore size is reduced. From Figure 2-9 (c) it may also be observed that the calculated tangential values from the finite element analysis exceed those predicted by ASME for nominal bore sizes greater than 8 inches since the ratio is smaller than 1. Although the predicted values, by ASME, are an underestimation, according to Nagata & Sawa [18], it remains acceptable. A much more erratic curve may be observed when considering the ratio of calculated and predicted values for the stresses in the radial direction. The value for the ratio does not seem to decrease or increase as the nominal bore size increases. The ratio varies between ~ 3.3 and ~ 7.6 . This according to Nagata & Sawa [18] is an overestimation and the stress evaluation in the radial direction, by the code, seems to be inadequate or overly conservative. Finally, in all three instances, shown in Figure 2-9, the curves for both the seating and operating conditions follow the same trend in that a higher ratio is predicted for the pressurised condition than for the seating condition. This implies that the ASME code is more conservative for the operating condition when pressure is applied.

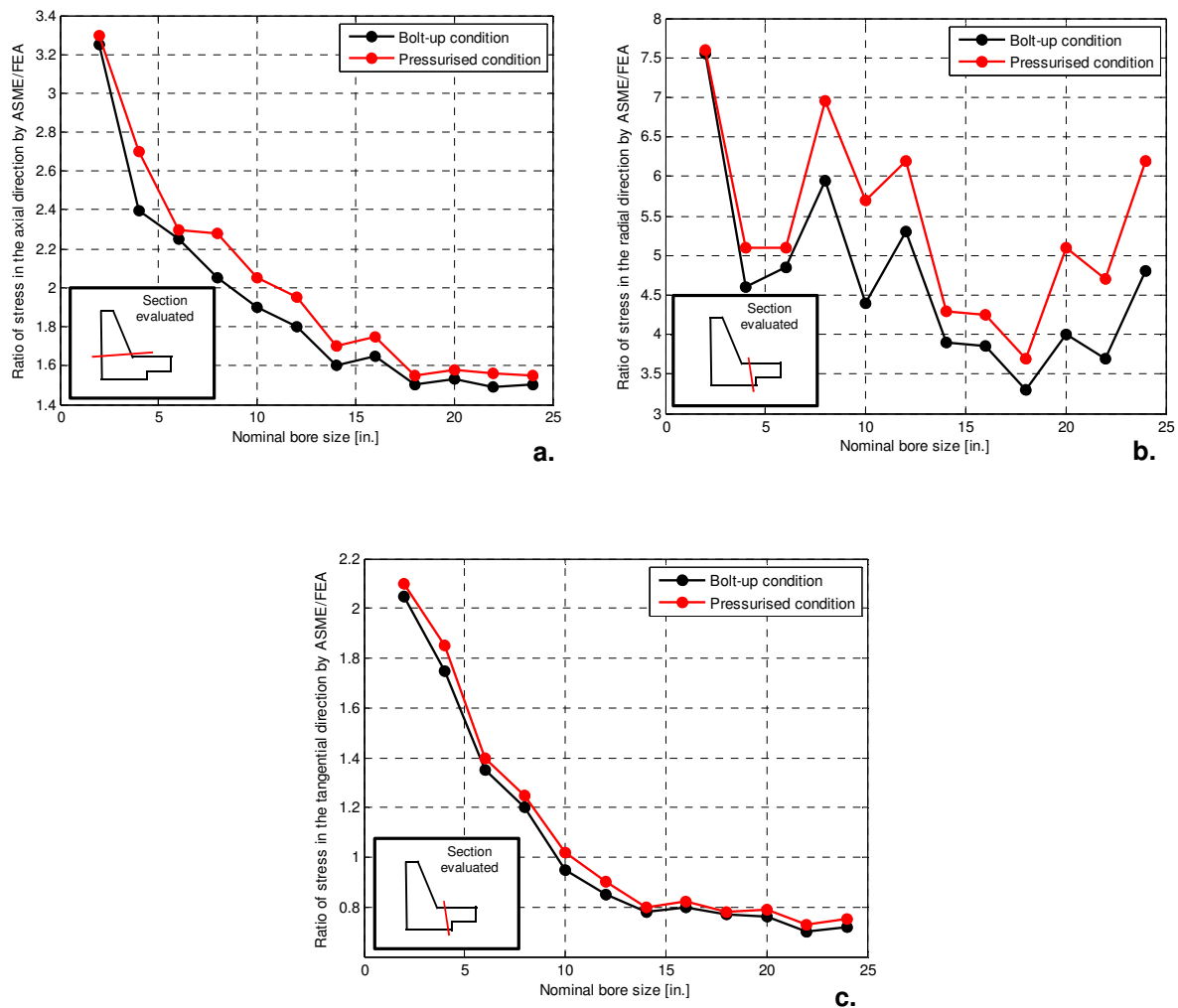


Figure 2-9: Ratio of flange stresses in the (a) axial, (b) radial and (c) tangential direction calculated by the ASME formula and the finite element analysis [18]

In their opinion the evaluation of the stress in the radial direction may be eliminated from the ASME code. Rather than basing the failure criteria on the maximum stresses in the axial, radial, and tangential directions they suggest using stress intensity (Tresca criterion).

2.2.5. Advantages and disadvantages of the Taylor-Forge methods

The principal drawback of the design-by-rule approach is that it becomes severely limited when the complexity of the problem or design extends beyond the prescribed values. The second concern of using the design-by-rule approach, according to Strathclyde [7], is that there is generally a lack of consistency in the design criteria which is prescribed by the standards. According to him, some sections are based on elastic analysis with some limitation on the maximum stress; whereas other sections are based on limit load concepts with generally unknown factors of safety. Because some criteria are unknown it becomes incredibly difficult, and in some instances virtually impossible, to extend the code to designs / problems which have very slight variations, such as dimensions or loads, beyond the scope of the standard.

For the design of large diameter flanges Murray & Stuart [6] note a number of drawbacks which the Taylor-Forge method has. They found that for all of the flanges analysed the maximum stress predicted by the Taylor-Forge method is less than those predicted by the results of their investigation. When the diameter of the flange is small, less than 5 ft. (~1.5 m) the difference between the values from the Taylor-Forge method and the investigation are small. However, once the diameter of the flange increases above this value the difference becomes significant. This difference, according to the authors, may be attributed to the empirical aspects which have been introduced into the Taylor-Forge method. They also found that for all their experiments the rotations of the flange at design pressures was between 9.9 and 26.5 minutes of the arc (where one arc minute is equal to $\frac{\pi}{10\ 800}$ radians). They also observed that the largest value of rotation was found to exist at the largest diameter flange. It may, therefore, be concluded that as the flange size increases so the amount of rotation increases. In addition to this they emphasise the aforementioned aspect of leakage. They state the leakage becomes a very real problem for large diameter flanges which operate at high pressures. In 1961 they suggested a number of correction factors in order to account for this. They, however, still believe that a well-defined and implemented computer model and analysis will give better results.

Kirshna *et al.* [20] states that leakage is a persisting problem when flanges are designed by means of codes such as the ASME VIII, PD 5550 or EN 13445-1, Chap. 11. It is important to note that all of these standards are based upon the Taylor-Forge method. Kirshna *et al.* [20] continues by stating the complexities associated with bolted flange joints, which make use of gaskets, arise primarily from the nonlinear behaviour of the gaskets combined with the associated permanent deformation. Another factor which contributes to the complexity of analysing bolted joints with gaskets is the flange rotation and contact stresses. These are caused by the bolt pretension, and increase when the joint becomes subjected to the internal pressure. Standards, such as the ASME VIII code, have attempted to correct this problem by adding a rigidity constraint 'J' which is based upon fixed rotation. A similar procedure was suggested by Murray & Stuart [6]. Although this assists in accounting for the fixed rotation it is not ideal as the rotation of the flange is not a single unique value. Flange rotation results in variable compression across the face of the gasket from the inner radius to the outer radius. This variation also results in varying contact stresses along the radius. In the study done by Kirshna *et al.* [20] it was stated that the rigidity factor 'J' for an integral flange is equivalent to a flange rotation limit factor of 0.3° for an integral flange. Kirshna *et al.* [20], however, found that leakage in flanged joints may occur even if the flange rotation is well below the value of 0.3°. This proves that the problem of leakage cannot simply be corrected by adding a rigidity constant.

From the aforementioned investigations a number of conclusion may be drawn. Firstly, that both the Lake & Boyd methodology and the Taylor-Forge methodology (on which the American ASME VIII code, the British PD 5550 and the European EN 13445-1, Chap. 11 standard are based) are not wholly suitable for the design of large diameter flanges which operate at high pressures. The reason it is not suitable is because circular bolted flange joints have been found to leak. This leakage is caused by excessive rotation which results in a reduction of the contact stresses tasked with sealing the joint [20]. It was found that as the flange diameter increases so the rotation increases implying that leakage is more likely to occur at larger diameter flanges than at smaller ones [6].

2.3. Finite element modelling and analysis techniques

There exists a large number of published articles which relate to the finite element modelling and analysis of circular bolted flange connections. Each of these articles model circular bolted flange connections in a similar way. The geometry, applied loads, and boundary conditions which are generally applied are shown in Figure 2-10. The circular bolted flange joint is considered to be axisymmetric and has the following loads applied to it: the bolt pre-tension; the internal pressure; and the end-thrust load [18] [20] [21].

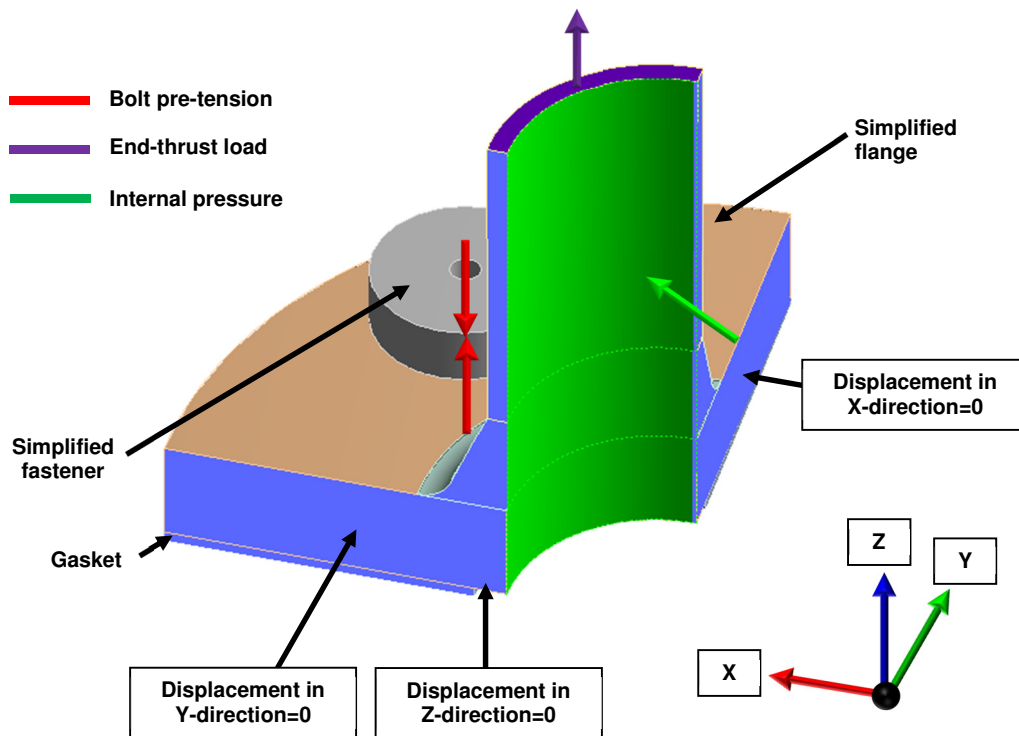


Figure 2-10: Geometry, loads, and boundary conditions generally applied for the finite element modelling and analysis of a circular bolted flange joint

The simplification of the geometry; the boundary conditions, and the manner in which each of the, aforementioned loads are applied is explained in greater detail in the sub-sections to follow.

2.3.1. Simplification of the geometry of a circular bolted flange joint

The geometric shape of a circular bolted flange connection is generally considered to be axisymmetric [18] [20] [21]. This means that the geometric characteristics are cylindrically symmetrical about an axis. For example a flange with ten evenly spaced bolts may be represented with a 36° segment. Similarly a flange with four equally spaced bolts may be represented by a 90° segment (Figure 2-11) [20].

The geometry of a circular bolted flange joint may be further simplified by regarding the flange to be symmetrical on both sides of the gasket. As a result of this, for example, the 90° segment may be further simplified as shown in Figure 2-11 (c) [18].

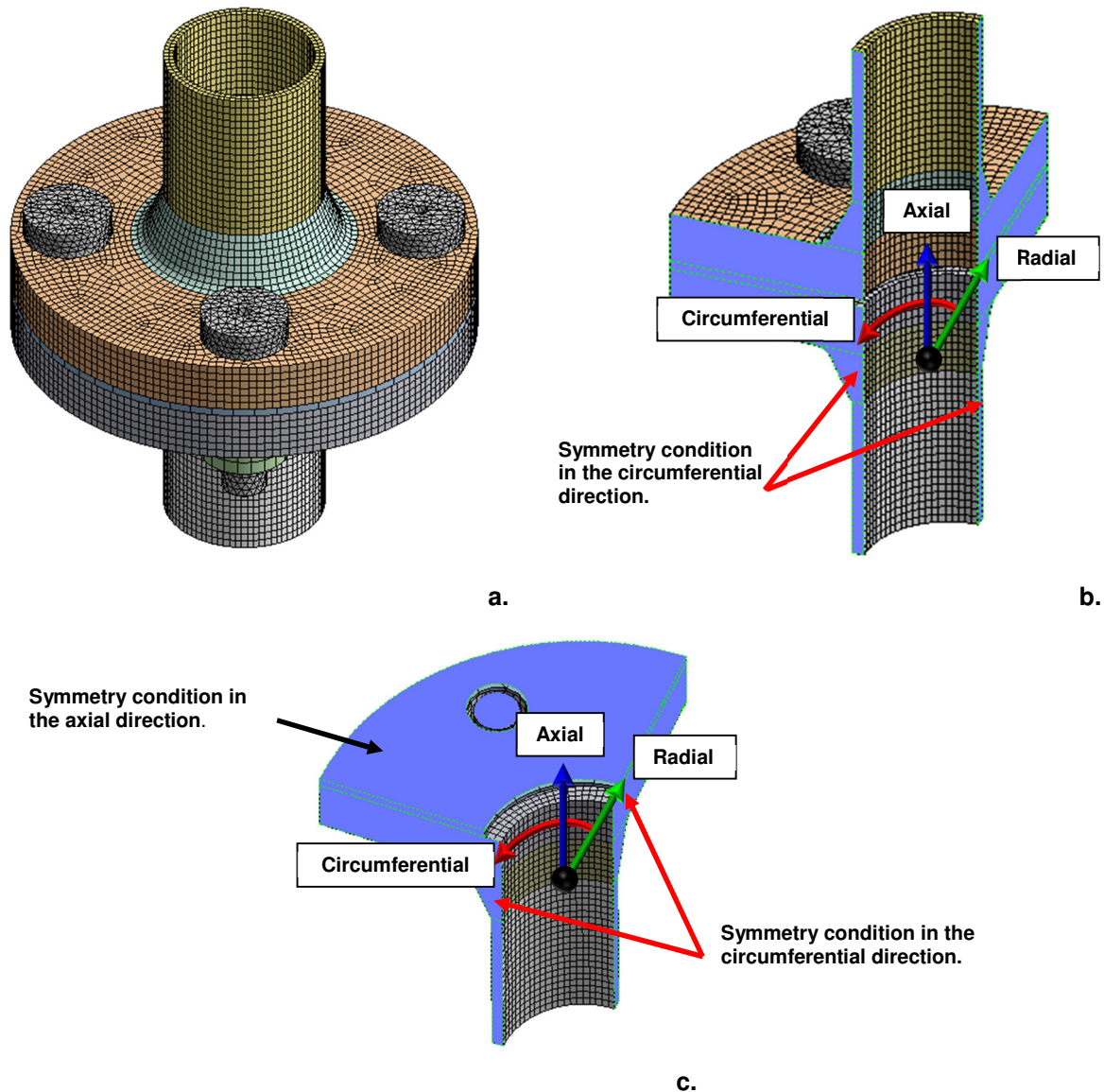


Figure 2-11: Simplification of geometry from (a) full model to an (b) axisymmetric model to a (c) simplified axisymmetric model

2.3.2. Loads and boundary conditions

Circular bolted flange connections exist in one of two conditions, namely: the seating condition or the operating condition [3] [18].

The seating condition is the initial assembly and tightening of the bolts. As a result of this the only load which is considered, during this condition, is the one caused by the pre-tensioning of the bolts. It is assumed, for the seating condition, that no fluid is yet present in the pipe and both the external bending moments and axial forces do not yet have an effect. During the seating condition the gasket material is deformed in order to obtain uniform contact between the surface of the flange and the surface of the gasket.

The operating condition, as the name implies, is when the circular bolted flange joint is in operation. In this instance the joint may be subjected to the following primary loads: the internal pressure which is caused by the fluid in the pipeline; an external bending moment; an external axial force; and the bolt pre-tension which was applied during the seating condition of the bolt (Figure 2-12). In addition to the aforementioned primary loads the circular bolted flange joints may also be subjected to loads which are induced by environmental conditions or material behaviour. Examples of loads which may arise from

environmental conditions are stresses which may be induced by thermal expansion and contraction. Material behaviour, on the other hand, will include phenomenon such as creep-relaxation of the gasket.

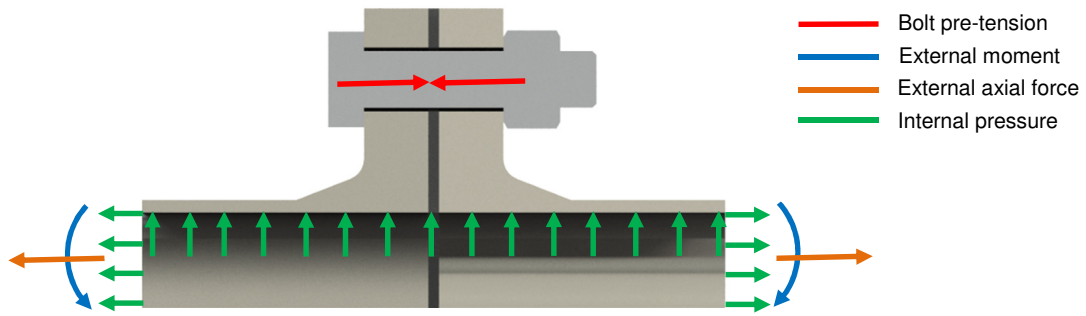


Figure 2-12: Primary loads which applicable to the seating and operating conditions

In this investigation, however, only the effects of the bolt pre-tension and internal pressure are considered. The effects of the environmental conditions, cyclic loading, and external loads and moments may form part of future work.

2.3.2.1. Application of bolt pre-tension

There exists a number of ways in which to model the fasteners and the bolt pre-tension. Each of these ways aim to accurately predict the behaviour of the fasteners while reducing the computational time and the memory usage. Six different types of bolt models are considered, namely: the solid bolt model; the coupled bolt model; the spider bolt model; the no-bolt bolt model; the hybrid bolt model; and the rigid body element bolt model [22] [23]. All of the literature pertaining to the discussion of these six bolt models were taken from the work of Kim *et al.* [22] and Montgomery [23].

The first model is the solid model, shown in Figure 2-14 (a), and , according to Kim *et al.* [22], is the most realistic. In their work they also suggested that the solid bolt be modelled with three dimensional brick elements which are defined by eight nodes, each of which has three degrees of freedom. In addition to these elements the model needs surface-to-surface contact elements and target segment elements between the following interfaces:

1. The bolt head and the upper flange.
2. The nut and the lower flange.
3. Between the upper and lower flanges.

The reason the surface-to-surface contact elements and target segment elements are used is because, from a modelling and analysis point of view, the surfaces which are in contact should be able to separate (as is the case in real life when the applied load exceeds the pre-tension). The two aforementioned elements allow for this behaviour, and, therefore, contribute towards a dependable model.

For the solid bolt model the bolt pre-tension may be applied by means of one of two methods, namely: a virtual thermal deformation or by means of pre-tension elements within the meshed part. For the method involving virtual deformation the thermal expansion coefficient is assumed to be unit and the temperature difference, ΔT , is calculated by means of the following equation:

$$\Delta T = \frac{4P_0}{\pi d^2 E} \quad (2.42.)$$

Where:

- d Effective diameter of the bolt [m]
- E The elastic modulus of the material [Pa]
- P_0 Bolt pre-tension [N]

The pre-set temperature also assists in creating the thermal shrinkage effect which the bolts may typically exhibit.

Utilising pre-tension elements within the meshed part, according to ANSYS [24], involves the following: The bolt is split to create two coincident surfaces. A pre-tension element consists of three nodes. The coincident nodes on the sectioned mid-surface of the bolt constitutes two of the nodes. The third node is a common pre-tension node. For example, as shown in Figure 2-13, a pre-tension element may consist out of the coincident node pair I and J, with a common pre-tension node K. Surfaces A and B are connected by multiple pre-tension elements, one for each coincident pair of nodes. The purpose of the pre-tension node, K, is to control and monitor the total tension loads.

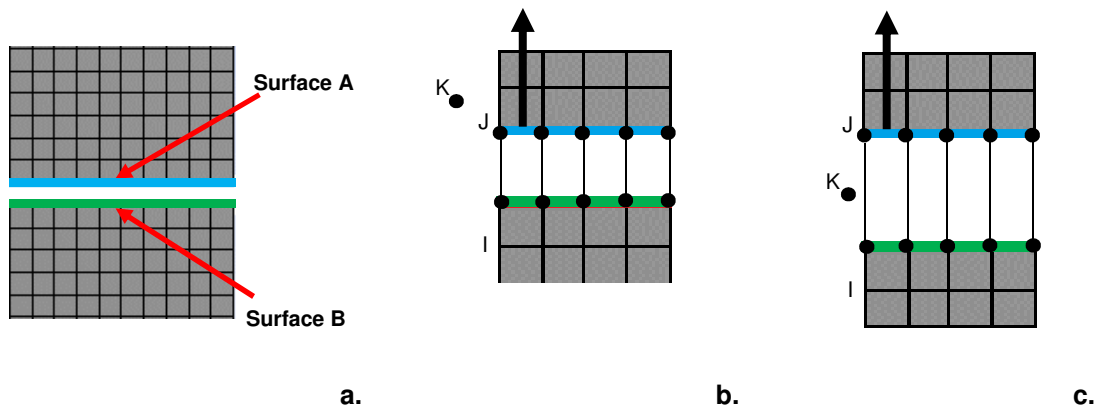


Figure 2-13: Application of the pre-tension element: (a) splitting of the surface of the bolt, (b) elements before adjustments, (c) elements after adjustment

According to Kim *et al.* [22] and Montgomery [23] this model has a number of advantages, namely: It is simple to implement, because a computer aided drawing (CAD) containing bolts may simply be imported into the finite element modelling and analysis software from where either a thermal load or pre-tension elements can be added in order to simulate the pretension effect. In addition to this, tensile, bending and thermal loads may be transferred. Finally, a full stress distribution in the head, nut, and stud may be calculated. Despite the numerous advantages, this method also has a number of drawbacks as discussed by Kim *et al.* [22] and Montgomery [23]. The first is that a large amount of elements are required, when one compares it to the other models. This large amount of elements will lead to a longer run time and push up the memory requirement. Another disadvantage is that extra effort is required to calculate the stud cross-sectional stresses; and in addition to the solid elements, contact elements will also be required.

The second model to be considered is the coupled bolt model - Figure 2-14 (b). The coupled bolt model is much simpler than the solid bolt model. A beam element is used to approximate the stud of the bolt. The nodes of the head of the bolt, in turn, are connected to the stud of the bolt by coupling their degrees of freedom. Coupling the degrees of freedom means, in this instance, to combine the independent degrees of freedom together so that the combined set contains only a prime degree of freedom – which will be applicable to all of the degrees of freedom in the coupled set. The coupling is done so that the associated nodes are forced to have the same displacement in the specified nodal coordinate direction. This allows the structure with the bolted joints to experience the pre-tension effect. The beam element is a uniaxial element with tension, compression, torsion and bending capabilities. The pre-tension effect may be implemented by directly applying an initial strain ϵ_0 to the stud and following Equation 2.43.:

$$\epsilon_0 = \frac{4P_0}{\pi d^2 E} \quad (2.43.)$$

It is also highlighted by Kim *et al.* [22] that there are no contact elements between the bolt and flanges in this model. Both Kim *et al.* [22] and Montgomery [23] agree that this specific bolt model has the following advantages: One of the biggest advantages with this method is that the number of elements

used, when compared to the solid bolt model, is very low. It will therefore solve faster and be less resource intensive. It is also advantageous since the results are easily extracted. The main drawback with this method, however, is that bending loads are not transferred.

The third model which will be considered is the spider bolt model. The spider bolt model is composed of three-dimensional beam elements, in a web-like-fashion for the stud, the head, and the nut. In this bolt model the connections between the flange and the nut and the flange and the bolts are made by means of beam elements. This allows for various loads to be transferred. In addition to this the stiffness of the head and the nut may also be considered.

For this model, however, the physical properties need to be set exactly in order to assess the head and nut stiffness. This is done by assuming that the volume of the beam elements for the head or nut is equal to that of the actual head or nut [22]. This model is very similar to the coupled bolt model and has similar advantages, namely: that the results may be easily extracted; fewer elements than most of the other models; and tensile loads are transferred through the coupled nodes. The big drawback with this model is that a large amount of extra effort is required for the modelling of the head and nut stiffness.

The fourth model which is considered is the no bolt model. In this model the pressure corresponding to the clamping force is applied to the washer face in order to mimic the effect of pre-tension. When the no bolt model is chosen the following two assumptions are made: firstly, that the joint will not separate, and secondly that the bolt stiffness is not required for the analysis [23]. This implies that the bolt load transfer will not be accounted for since there is no stiffness present, and as a result the pass or fail criteria will be based on the contact pressure and the gap instead of on the bolts load. The two biggest advantages with this model are: since the model contains no bolts it has the lowest number of elements; and, due to the absence of the bolt, this model is incredibly simple to implement. However, due to its simplicity this model has a number of drawbacks. This model cannot account for the bolts stiffness, or the change in the bolt load due to the application of a constant clamping force.

The fifth model is the hybrid model and, as the name implies, is a combination of a number of the aforementioned methods. The head and nut are modelled with solid elements whereas the stud element is modelled by means of a beam element. The purpose of the beam element is to exhibit the tensile behaviour of the bolt. Montgomery [23] suggests that the tensile behaviour of the bolt can be accurately captured by locating the starting point of the beam element half of the diameter from the top flange edge, and the end point half of the diameter from the bottom flange edge. The beam element should be attached to the solid by means of coupled nodes – where they are coupled in the bolt's axial direction. The purpose of modelling the head and nut with solid elements is to incorporate the thermal and bending load effects of the bolt. The main advantage of this model is that it is very accurate – second only to the full bolt model. The full stress distribution in the head and nut may also be calculated. The drawback, however, is that although the tensile, bending and thermal loads may be transferred through the beam element there is no visual stress distribution through the stud section.

The sixth, and final, model which is considered is the rigid body element bolt model. In this model the rigid body elements are used to represent the head and the nut, while a beam element represents the stud. This model is similar to the spider bolt in the sense that the rigid body elements are used rather than line elements. The advantages of this method are: easy to extract results; the tensile, bending and thermal loads may be transferred through the beam elements; and fewer elements than all the previous methods, other than the no bolt model – therefore faster and a less computationally intensive analysis.

The solid bolt model had the ability to most accurately predict the physical behaviour of the structure when compared to the other methods. In addition to this the results from the static analysis, completed by Kim *et.al.* [22], showed that the spider bolt model and the coupled model can save up to 62% and 49%, respectively of the computational time, and 21% and 19% of the memory usage compared to the solid bolt model.

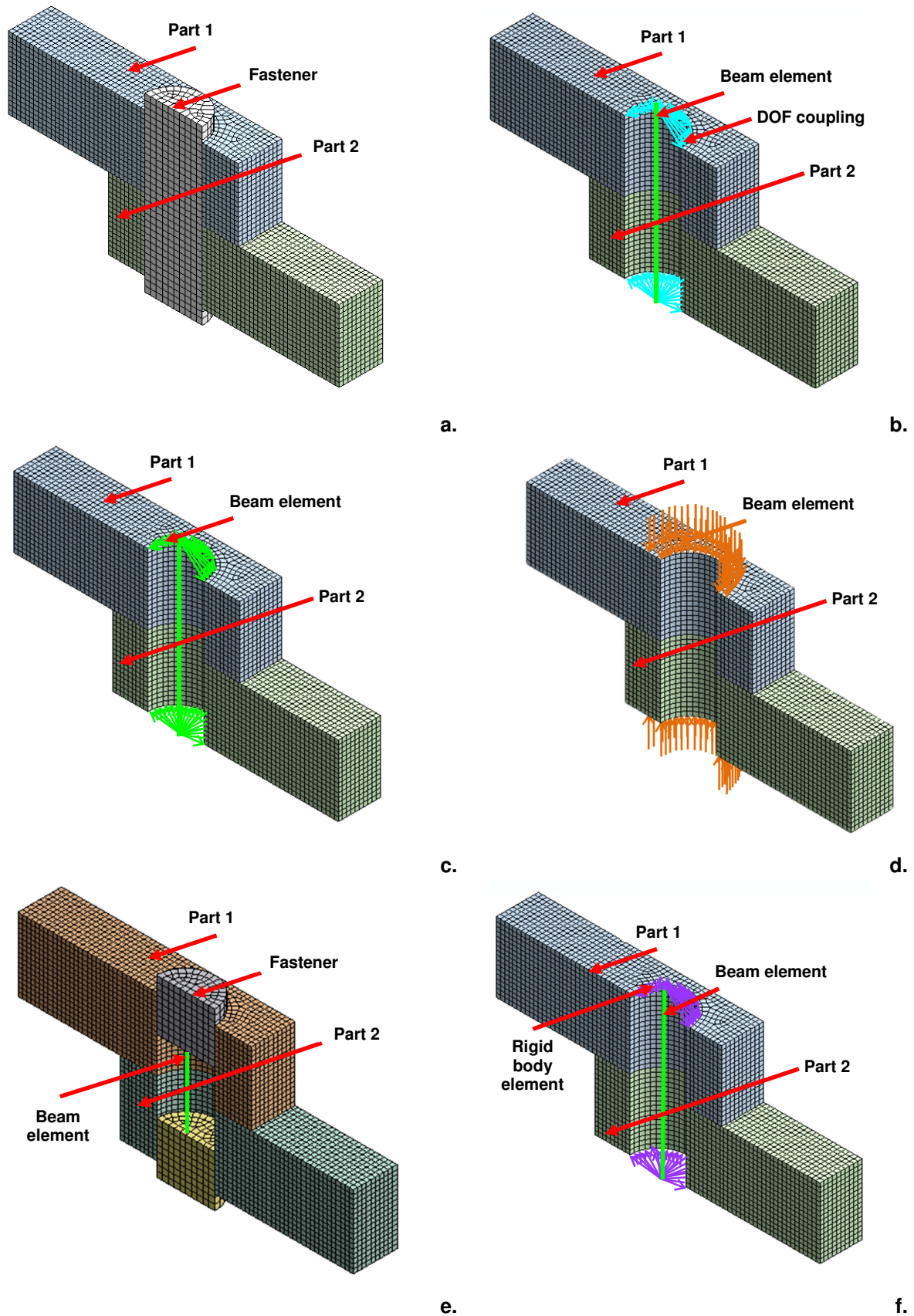


Figure 2-14: Different methods for modelling fasteners: (a) solid bolt, (b) coupled bolt, (c) spider, (d) no bolt, (e) hybrid, and (f) rigid body element

2.3.2.2. Bolt tightening sequence and torque increments

When modelling the bolts it is important to mimic that which is happening in real life. Thus the correct tightening sequence, which is the order in which the bolts are fastened, as well as the application of the torque increments, need to be followed. According to ASME [25] a cross pattern should be followed for the tightening sequence. The bolts are tightened in this manner in order to counter the elastic interaction that occurs when tightening the bolts. Elastic interaction (or bolt cross talk) is the compression caused by the tightening of a bolt. Most of the compression occurs on the gasket, but some additional compression may occur on the flange. When individual bolts are tightened additional gasket compression occurs which reduces the pre-tension of previously tightened bolts. This is countered by following the bolt tightening sequence. In addition to the tightening sequence the prescribed application of the torque increments also need to be accounted for. This is again prescribed by the ASME [25] and is explained below:

1. The first step is to 'hand tighten'. The bolts should be typically tightened up to between 15 N.m and 30 N.m.
2. Round 1: Tighten to between 20% and 30% of the target torque.
3. Round 2: Tighten to between 50% and 70% of the target torque.
4. Round 3: Tighten to 100% of the target torque.
5. Round 4: Continue tightening the bolts, but on a rotational clockwise pattern until no further nut rotation occurs at the Round 3 target torque value.
6. Time permitting wait a minimum of 4 hr and repeat Round 4. This will restore the short-term creep relaxation/embedment losses.

2.3.2.3. Application of pressure due to internal fluid

As previously mentioned a circular bolted flange joint exists in one of two conditions, either in the seating or operating conditions. During the operating condition the circular bolted flange joint is subjected to the internal pressure which is caused by the fluid travelling through the pipe – and subsequently through the flanged joint.

The internal pressure acts perpendicularly to the inside surfaces of the flange ring, hub, and shell. The internal pressure also attempts to pull the flange face apart along the axial direction [26]. As a result of this the pressure end thrust is included on the perpendicular surface of the shell in the axial direction, as shown in Figure 2-15.

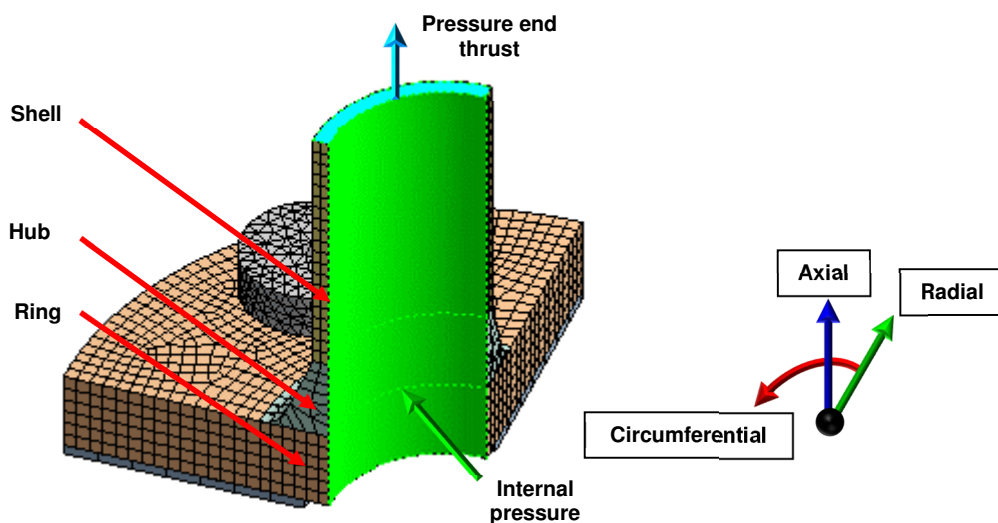


Figure 2-15: A simplified model of a circular bolted flange showing the application of the internal pressure and pressure end thrust

2.4. Factors which influence leak tightness

The purpose of a gasket in circular bolted flange connection is to create a seal between two flange pieces. According to Alkelani *et al.* [27], in theory, one does not require a gasket when two perfectly flat, smooth, and rigid flange piece are connected. It is, however, rare to attain these conditions. Gaskets have, therefore, become a necessity to ensure a leak-tight design for circular bolted flange connections. When designing or analysing a circular bolted flange connection which makes use of a gasket one needs to account for the following effects: gasket creep relaxation; flange rotation; environmental effects, and external loads and bending moments.

2.4.1. Creep-relaxation of gaskets

Creep-relaxation is the combined effect of creep and stress relaxation. Creep, with regards to the gasket, is the reduction in thickness of the material under a constant load. Stress relaxation, on the other hand, is the reduction in contact pressure for a constant displacement. The effect which gasket creep has on the contact pressure between the surface of the gasket and the face of the flange was investigated by Kauer & Strohmeier [28], Bazergui [29] and Bouzid *et al.* [30], amongst others. All of the aforementioned research indicated that the creep-relaxation had a significant effect on the contact pressure between the gasket and flange face, and subsequently could result in leakage.

The axial bolt force which is responsible for tightening a gasket reduces due to the creep-relaxation behaviour of a gasket, and specifically due to the creep of a non-asbestos gasket [31]. This reduction in the axial bolt forces results in a reduction of contact pressure between the surface of the gasket and the flange face and may result in subsequent leakage. Within the last 10 years a number of research papers have focused on the effect which the creep property has on the reduction of the axial bolt force, and the reduction in the contact pressure between the gasket and the flange faces [31] [28] [30] [27] [29]. Different methods and types of gaskets were used by each of the aforementioned references.

Yamaguchi *et al.* [31] investigated the creep-relaxation behaviour of bolted flange connections by making use of a viscoelastic model and a non-asbestos gasket. In this investigation a finite element model was created in which the gasket material was modelled as a viscoelastic. In addition to this a physical experiment was created and comprised of a Class 600, blind type, raised face flange and a non-asbestos gasket (No. 6502 that was made by Nippon Valqua Corporation). During the experiment the reduction in the axial bolt stress was measured after bolt tightening for a period of 100 hours. In the experimental setup the axial force in the bolts were determined by means of strain gauges. A linear variable differential transformer was used to determine the reduction in the thickness of the gasket. This experiment was replicated by a finite element model and analysis. Yamaguchi *et al.* [31] states that the finite element model proposed has the ability to predict the distribution of the contact stress between the gasket and flange in the axial, radial, and circumferential direction. These results were, however, not directly validated by means of an experiment. Instead the total amount of creep and stress relaxation between the finite element model and the experimentation, which was used to obtain the material properties, were compared.

Research done by Kauer & Strohmeier [28] links to that of Yamaguchi *et al.* [31]. Kauer & Strohmeier [28] also investigated the possibility of modelling the gasket material as a non-linear viscoelastic material. Kauer & Strohmeier [28] argued that a good approach to simulating non-metal gasket materials are to assume elastic plastic elements (shown in Figure 2-16).

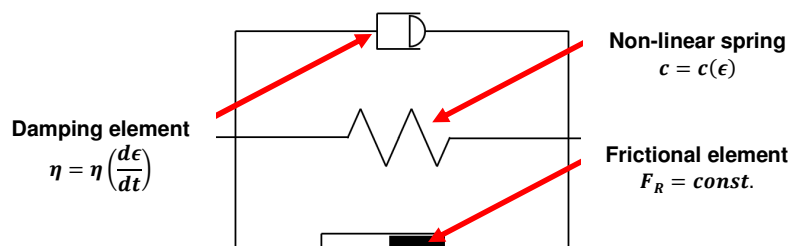


Figure 2-16: Visco-elastic-plastic element [28]

This element comprises of a damping element, non-linear spring and a frictional element. The purpose of the damping element is to account for the creep-relaxation behaviour of the gasket, whilst a non-linear spring is used to mimic the initial gasket closure due to bolt tightening. In their work, the authors, presented an example of a typical gasket compression curve, which is shown in Figure 2-17. A stabilised seating curve, indicated by the blue dotted line, was created from the gasket compression curve by neglecting the creep and relaxation during gasket seating. They argued that this curve could be simulated as a non-linear spring where $c = c(\epsilon)$.

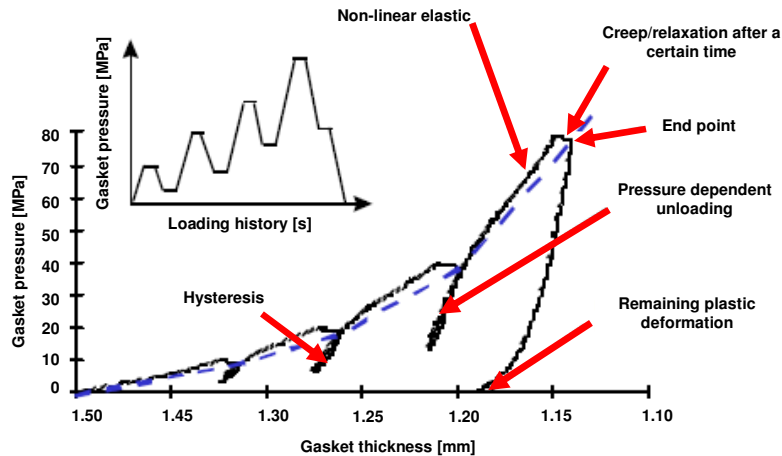


Figure 2-17: Typical gasket compression curve [28]

The visco-elastic-plastic model was implemented by Kauer & Strohmeier [28] in a finite element model and analysis of an ExPTFE gasket and a PTFE gasket. In this finite element model and analysis the reduction in contact pressure due to creep-relaxation was calculated. These values were then compared to the experimentally obtained values for the reduction in contact stress (due to creep-relaxation). They found that for the finite element analysis of the ExPTFE gasket the pressure reduced by 16.8 MPa when the bolt was fastened to 70% of its yield strength and 6 MPa when it was fastened to 40% of its yield strength. The experimentally obtained values for the pressure reduction of the ExPTFE gasket was 18 MPa and 5 MPa when the bolts were fastened to 70% and 40% of its yield strength, respectively. Similar results were obtained for the comparison of the finite element analysis results of the PTFE gasket to the experimental ones.

The statement made by Kauer & Strohmeier [28] that creep and relaxation may be neglected during the mounting/seating conditions is highlighted and will be elaborated upon in this investigation. It will be shown in this investigation that the effect which creep-relaxation has on the contact pressure during bolting-up may have a more significant effect than initially anticipated. It will also be shown that both the time between the bolt tightening increments as well as the number of increments has an effect on the influence which creep-relaxation has on the contact pressure.

Bouزيد *et al.* [30] investigated the effect which gasket creep-relaxation has on the leakage tightness of bolted flange joints. The research comprised of an analytical evaluation of the effect of gasket creep-relaxation; an experimental validation of the analytical evaluations, and a finite element analysis. They modelled the effect of creep by applying a fixed displacement. A fixed displacement was applied in order to avoid specifying a constant bolt load. In this instance a constant bolt load was not desired since the bolt load is expected to decrease with time due to the effect of creep-relaxation. The fixed displacement was applied to an equivalent bolt ring. The fixed displacement was determined by initially applying the full bolt load and recording the displacement. Shown in Figure 2-18 is a typical stress-displacement curve of a PTFE-based-type gasket.

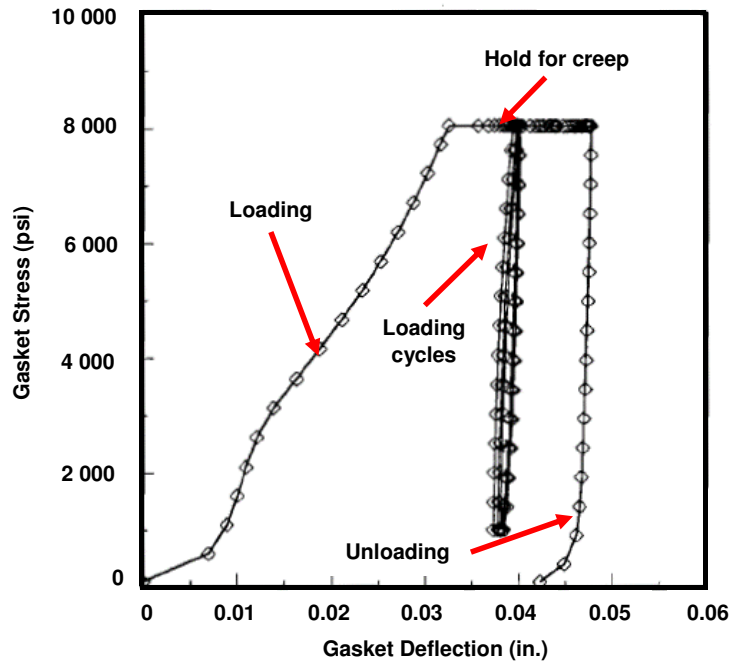


Figure 2-18: Typical PTFE gasket stress-deformation [30]

From the curve (shown in Figure 2-18), they assumed that the beginning of relaxation could be obtained from the fairly straight line from the unloading part of the curve. The creep equation which was used by them was suggested by Bazergui [29] and is shown below:

$$e_c = a + b \cdot \ln(t) \quad (2.44.)$$

Where:

- a, b Coefficient as a function of the stress level
- e_c Gasket pure creep deflection [mm]
- t Time [s]

The finite element analysis made use of an axisymmetrical model which had been further simplified by assuming an axis of symmetry along the mid-plane of the gasket material. The model was constrained against displacement in the axial direction along this line of symmetry. The expected internal pressure was applied to the inner surface of the flange and a hydrostatic end force was applied to the top surface of the unconstrained flange. The gasket material was modelled with interface elements in ANSYS. The results of the finite element analysis was then verified by an experimental procedure which will be discussed below.

Bouzid *et al.* [30] states that there was a good agreement between the analytical evaluation; the experimental validation, and the finite element analysis. Accounting for the effect of gasket creep-relaxation by means of this method, however, has one major drawback. Gasket creep-relaxation is a time dependent behaviour. This method, however, does not model creep-relaxation as such. Instead it models the change in displacement which results from the gasket creep-relaxation. The implication of this drawback is that, unless the entire stress-deformation curve of the gasket is experimentally determined beforehand, no predictions regarding the stress-relaxation can be made from the finite element analysis.

In the research done by Alkelani *et al.* [27] a viscoelastic model was proposed to take into account the effects which creep-relaxation had on a soft gasket at room temperature. A soft rubber gasket, which was considered to be red rubber, was modelled with three mechanical elements. The three mechanical

elements are shown in the rheological model in Figure 2-19 (a). The first element is an elastic spring which has a stiffness coefficient denoted by K_1 . The second element is a pure viscous dashpot with a viscous damping coefficient of C_1 . The third element, which is placed in series with the first two, is viscoelastic in nature and contains a spring and a dashpot in parallel. The spring and dashpot, of the viscoelastic element, has a stiffness and viscous damping coefficient of K_2 and C_2 , respectively.

When a sufficient load is applied to the gasket the three, aforementioned elements, deform in different ways. The spring, which has a stiffness coefficient of K_1 will be compressed by Δ_1 . Once the load is removed the spring element will return to original state since it is completely elastic. The viscous element (which is the spring and dashpot in parallel), on the other hand, exhibits time-dependent behaviour. When a load is applied the viscous element will be compressed by Δ_3 . When the element is, however, unloaded the viscous element will not immediately return to its original state, as is the case with the spring element. It will rather return to its original state after a period of time. It may, therefore, be said to be a time dependent fully recoverable element. The third element, which is regarded as being accountable for the long term gasket creep, is the dashpot which is in series with the spring and viscous elements. When this dashpot (which has a viscous damping coefficient of C_1) is compressed it will deform by an amount of Δ_2 . It will, however, not recover, and is therefore a time-dependent unrecoverable element.

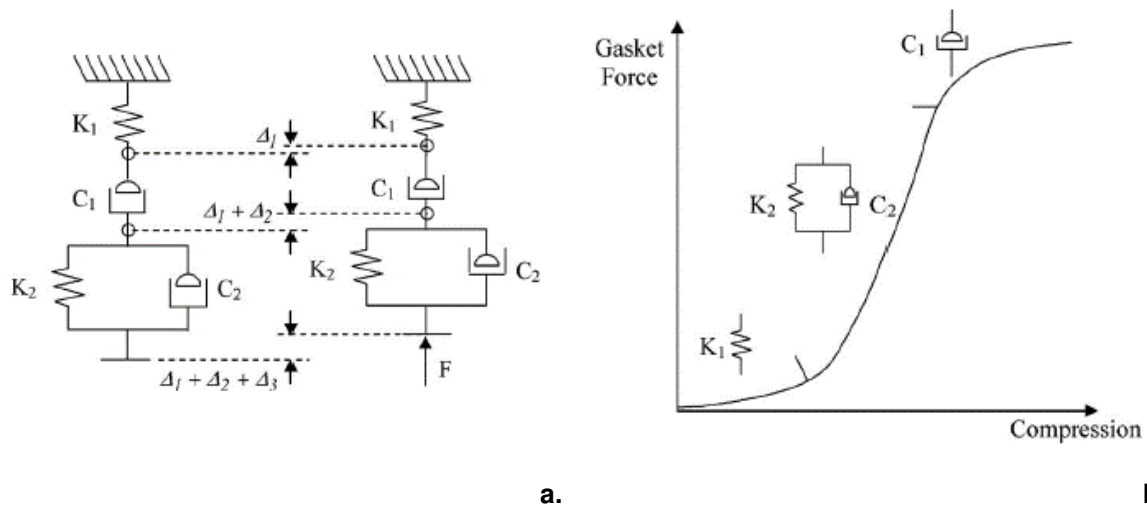


Figure 2-19: (a) A typical rheological model and (b) compression curve of a soft rubber gasket as shown by Alkelani *et al.* [27]

An estimate of the amount by which the gasket compresses and the amount by which the clamp load reduces at time t was done. When a constant compression is considered the force, F , was calculated from Equation 2.45.:

$$F = K_1 \Delta_1 = C_1 \dot{\Delta}_2 = K_2 \Delta_3 + C_2 \dot{\Delta}_3 \quad (2.45.)$$

Where:

- F Applied force [N]
- C_1 Viscous damping coefficient for the dashpot element [N.s.m⁻¹]
- C_2 Viscous damping coefficient for the viscous element [N.s.m⁻¹]
- K_1 Stiffness coefficient for the spring element [N.m]
- K_2 Stiffness coefficient for the viscous element [N.m]
- Δ_1 Displacement of the spring element [m]
- Δ_3 Displacement of the spring in the viscous element [m]

$\dot{\Delta}_2$ Rate of displacement of the dashpot element [m.s⁻¹]

$\dot{\Delta}_3$ Rate of displacement of the viscous element [m.s⁻¹]

When both constant spring rates and damping coefficients were assumed Equation 2.46. to 2.48.were used to calculate Δ_1 to Δ_3 , respectively:

$$\Delta_1 = \frac{F}{K_1} \quad (2.46.)$$

$$\Delta_2 = \frac{t}{C_1} F \quad (2.47.)$$

$$\Delta_3 = \frac{F}{K_2} - \frac{e^{-\left(\frac{K_2}{C_2}\right)t} F}{K_2} \quad (2.48.)$$

From this the total deflection was calculated from Equation 2.49.

$$\delta_g(t) = \left[\left(\frac{K_1 + K_2}{K_1 K_2} \right) + \frac{t}{C_1} - \frac{1}{K_2} e^{-\left(\frac{K_2}{C_2}\right)t} \right] F(t) \quad (2.49.)$$

From this the equivalent gasket stiffness, K_g , may be written as:

$$K_g(t) = \frac{1}{\left[\left(\frac{K_1 + K_2}{K_1 K_2} \right) + \frac{t}{C_1} - \frac{1}{K_2} e^{-\left(\frac{K_2}{C_2}\right)t} \right]} \quad (2.50.)$$

For the entire circular bolted flange connection it was assumed that the flange and the bolts will only operate within their respective linear elastic regions, therefore, they may be represented by spring elements. It was, additionally, assumed that gasket creep-relaxation occurs as soon as the bolt is tightened. It was also assumed that once the bolt is tightened that the change in the force applied to the gasket is the same in both the bolt and flange members, thus:

$$\Delta F_g = \Delta F_c = \Delta F_b \quad (2.51.)$$

Where:

ΔF_b Change in force in the bolt [N]

ΔF_c Change in force in the joint members [N]

ΔF_g Change in force in the gasket [N]

Equation 2.51 may be written as follows:

$$K_g \Delta \delta_g(t) = K_b \Delta \delta_b \quad (2.52.)$$

Where:

K_b Stiffness of the bolt [N.m⁻¹]

K_g Stiffness of the gasket [N.m⁻¹]

$\Delta \delta_b$ Change in the bolt elongation [m]

$\Delta \delta_g(t)$ Change in the gasket thickness as a function of time [m]

The change in the bolt elongation is equal to the summation of the changes in thickness of the gasket and joint, therefore:

$$\Delta\delta_c + \Delta\delta_g = \Delta\delta_b \quad (2.53.)$$

Where:

$\Delta\delta_c$ Change in the joint thickness [m]

For a soft gasket material is assumed that the change in the gasket thickness is far greater than the change in thickness of the joint. Therefore:

$$\Delta\delta_g \cong \Delta\delta_b \quad (2.54.)$$

From this the clamping force, $F(t)$, at time t may be shown to be:

$$F(t) = K_b \delta_b(t) = K_b \left[\delta_b(0) - \delta_g(0) - \frac{F(t)}{K_g(t)} \right] \quad (2.55.)$$

Where:

K_b Bolt pretension [N]

$\delta_b(0)$ Initial bolt elongation right after tightening [m]

$\delta_g(0)$ Gasket compression at initial tightening [m]

Alkelani *et al.* [27] compared the predicted results of the theoretical model, for both creep and stress relaxation, to those obtained from experimental work. They found that for both instances, for gasket thickness's of 1/16 in., 1/8 in., and 3/16 in. that the experimental and theoretical results differed by less than 5%.

2.4.2. Flange rotation

Another factor which has an adverse effect on the contact stress between the surface of the gasket and the face of the flange is flange rotation. According to Krishna *et al.* [20] flange rotation results in variable compression across the surface of the gasket which is in contact with the flange faces. As a result of this variation in compression the contact stress also vary along the radius. This variation in contact stresses may result in the flanges prying open and allowing fluid to enter between the flange face and gasket surfaces which could lead to leakage (shown in Figure 2-20).

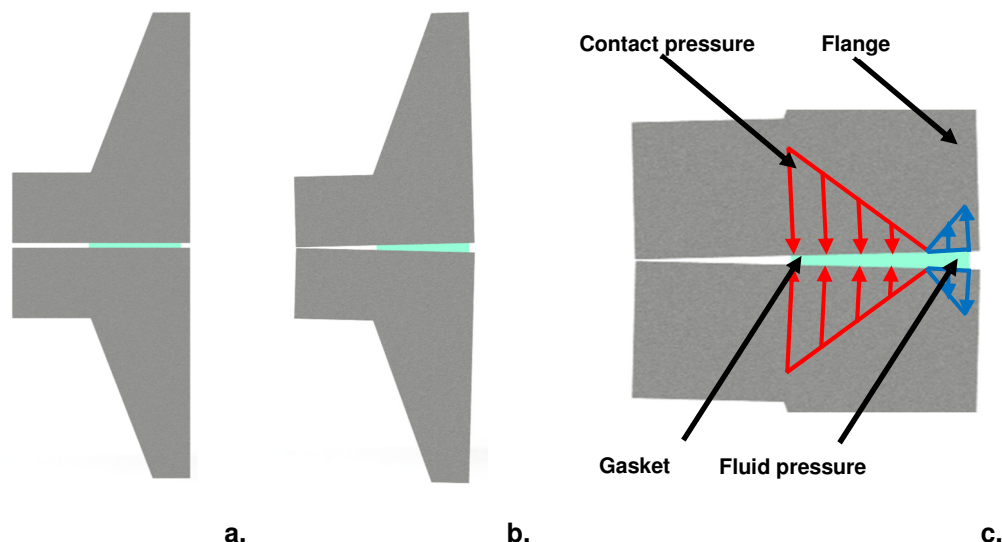


Figure 2-20: Effect of flange rotation: (a) before, (b) after, and (c) the relationship between the fluid pressure and contact pressure

From the results presented by Krishna *et al.* [20] it was observed that flange rotation was a function of both the internal pressure as well as the magnitude of the bolt pretension which was applied. From the results shown in Figure 2-21 it may be observed that an increase in both the internal pressure and bolt pre-tension results in an increase in the rotation of the flange.

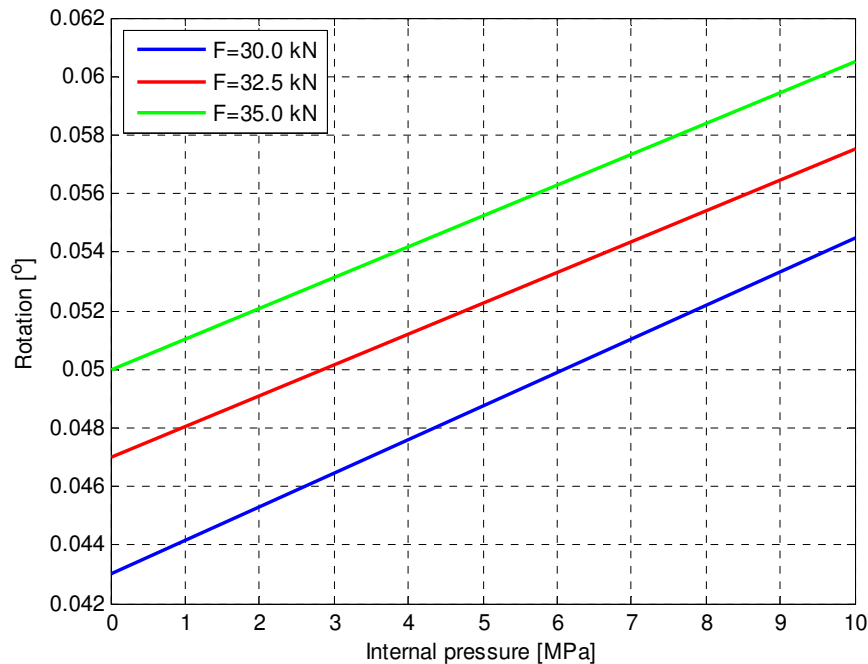


Figure 2-21: Variation of the flange rotation as a function of both internal pressure and bolt pretension [20]

2.5. Validation of finite element analysis results by means of experimentation

There exists a large number of publications relating to the topic of validating finite element analysis or theoretical developments by means of experimentation. These validations have been for instances where there are external loads and bending moments, as well as when there are thermal effects [26] [32]. However the focus of this investigation, as previously stated, is slightly simpler and will be limited to the validation of the finite element models and analysis during bolting-up. As a result of this the focus will be on the work done by Sawa *et al.* [33] and Bouzid *et al.* [30]. Both Sawa *et al.* [33] and Bouzid *et al.* [30] validated the predicted strains on the hub and ring of the flange by means of strain gauges. These strain gauges were located both in-line with the bolts as well as in-between the bolts.

Sawa *et al.* [33] did a stress analysis of pipe flange connections where the distribution of contact stresses, the load factor, the stress produced on the hub of the pipes, and the effective gasket seating width and moment arm were all analysed. Part of the analysis was to validate the theoretical development by means of an experimental setup. This experimental setup is shown in Figure 2-22. In the experiment the flange hub was instrumented with uniaxial strain gauges. As shown in Figure 2-22 the strain gauges were attached to the hub on the line A-A and in the middle of the bolt pitch B-B. In addition to instrumenting the hub with strain gauges Sawa *et al.* [33] also instrumented the bolt with strain gauges placed 180° apart, along the circumference of the bolt. The bolts were modified to contain strain gauges. A 20 mm section of the shank had its diameter reduced from 16 mm to 14 mm. The experimental setup served two purposes. Firstly to determine the stresses in the bolts and hub of the flange during gasket seating and secondly to measure the stresses in the hub during operating conditions. The operating conditions were induced by sealing both sides of the flange and pressurising the cavity.

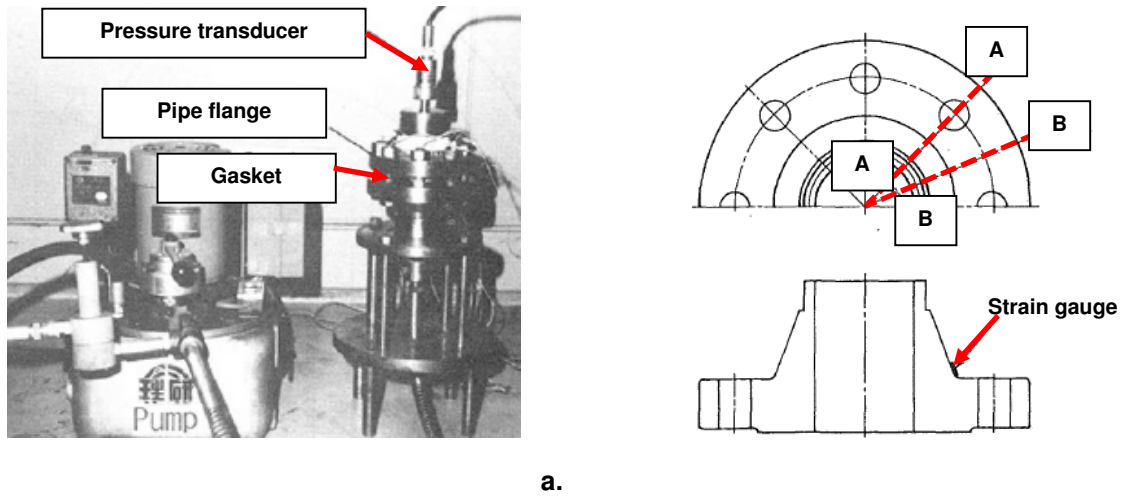


Figure 2-22: The (a) experimental setup and (b) strain gauge locations of Sawa *et al.* [33]

The previously discussed investigation done by Bouzid *et al.* [30] validated the theoretically calculated values by means of the experimental setup shown in Figure 2-23. The experimental setup measured the bolt loads, gasket displacement, and flange rotation. The bolts were modified and were instrumented with strain gauges. This allowed for the determination of the bolt loads. The displacement of the gasket and the rotation of the flange was determined by four linear variable displacement transformers which were positioned in diametrically opposed pairs. In addition to these components two platens, an upper and a lower one, were used to control the surface roughness and accommodate an O-ring for leakage measurement

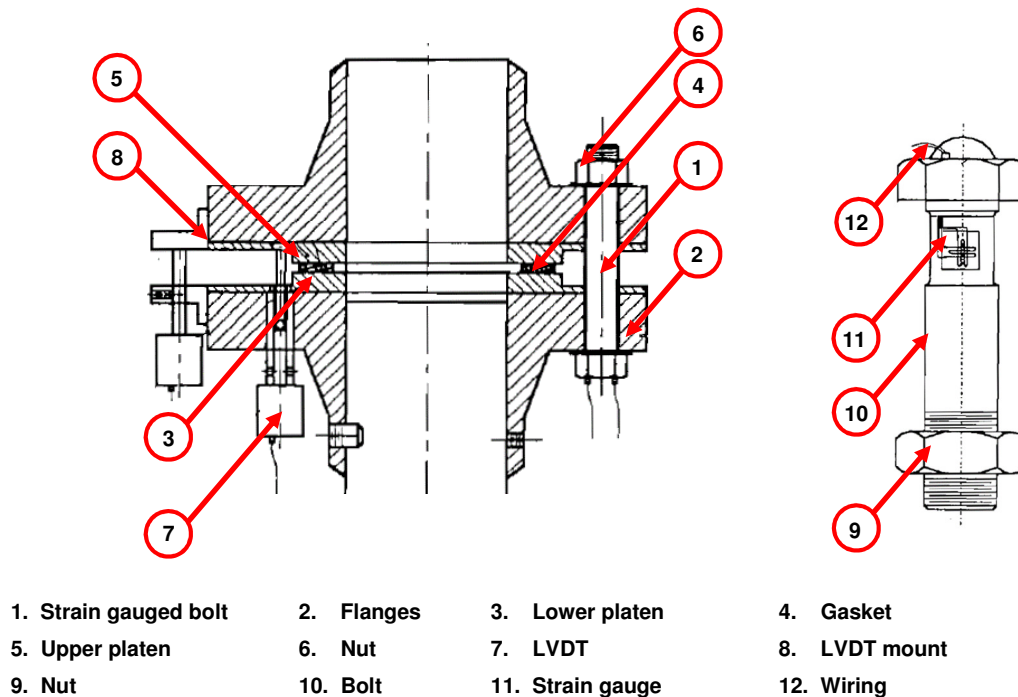


Figure 2-23: The experimental setup of Bouzid *et al.* [30]

CHAPTER 3: INITIAL FINITE ELEMENT MODELLING AND ANALYSIS

3.1. Overview for the initial finite element modelling and analysis

The design methodologies, as proposed by the various codes / standards' design-by-rule approach, have a large number of shortcomings. The biggest drawback, however, is the codes / standards' inability to accurately predict stresses in circular bolted flange connections which have large diameters and / or are subjected to large internal pressures. This has two adverse outcomes, namely: an inaccurate prediction of the contact stress between the flange face and packing material and, secondly, an over designed connection. A finite element model which addresses these shortcomings is, therefore, required.

3.2. Purpose and goals of the initial finite element modelling and analysis

The purpose of the initial finite element modelling and analyses was to suggest acceptable finite element models of the relevant circular bolted flange connections. These models needed to account for, amongst other factors:

1. Creep-relaxation behaviour of the non-asbestos compressed fibre gasket.
2. The effect of bolt tightening methods.
3. Flange rotation.

In addition to this, the finite element model and analysis also needed to provide a basis from which to design and optimise the large diameter flanges for the expansion of Rand Water's table. The finite element models, therefore, needed to have the ability to accurately predict both the stresses in the flanges as well as the contact pressures between the flange faces and packing materials. In short, the models needed to compensate for the shortcomings of the design methodologies proposed by the various codes / standards' design-by-rule approach.

3.3. Relevant mechanical properties of the various components

The different types of flanges were manufactured from the same material. Two different packings were used, namely: a compressed non-asbestos gasket insert and a nitrile O-ring. The fasteners used in the flange assembly were Class 8.8 bolts.

Unlike the flanges and fasteners, the packing materials were highly non-linear. The scope of this investigation did not include full material characterisation. However, the importance of the effect which the packing materials have on the flange assembly, was highlighted in Chapter 2. It is for this reason that a simplified material characterisation of the gasket insert and O-ring was done. It is important to note that a number of simplifying assumptions were made, however, the results were later validated in Chapter 4 when the results of the finite element analysis (which made use of the determined material properties) were compared to the experimental results.

3.3.1. Mechanical properties of the flanges and fasteners

The material, for both the flanges and fasteners, was assumed to be linear isotropic. It is also known, and will be discussed in Chapter 4, that the three types of flanges were manufactured from EN 24, untempered, steel (as prescribed by BS 970-1955). It was, therefore, assumed that the flange material had the following relevant mechanical properties [34]:

Table 3-1: Relevant mechanical properties of EN 24, untempered, steel [34]

Parameter	Symbol	Value	Unit
Modulus of elasticity (Young's modulus)	E	207	GPa
Density	ρ	7 840	kg/m ³
Poisson's ratio	ν	0.3	-

The bolts used in the experimentation, and modelled in the finite element package, were Class 8.8 bolts (which is low carbon boron steel which has been quenched and tempered). The material properties, which were assumed to be applicable to the fasteners, are shown in Table 3-2.

Table 3-2: Relevant mechanical properties for the fasteners

Parameter	Symbol	Value	Unit
Modulus of elasticity (Young's modulus)	E	210	GPa
Density	ρ	7 840	kg/m ³
Poisson's ratio	ν	0.3	-

3.3.2. Relevant mechanical properties of the O-ring

To accurately model the circular bolted flange connection which makes use of an O-ring, a suitable material model needed to be defined. Due to the complexity of the geometry of the O-ring, with regards to material characterisation, a number of simplifying assumptions were made.

Firstly, it is known that stress-strain curves are generally used to predict the relevant material coefficients for a particular non-linear model. However, in this instance, due to the complexity of the geometry of the O-ring, it was decided to characterise the packing material as follows: A load-closure curve was obtained by performing a simple compression test. A simplified 2D axisymmetric finite element model of the experimental setup was created and a suitable material model was selected for the O-ring. The loads applied to the O-ring in the finite element analysis were chosen to match those of the compression test. The material coefficients were manually tuned so that the load-closure curve from the finite element analysis matched the one from the compression test.

3.3.2.1. Experimental setup for the determining the relevant mechanical properties of the O-ring

The compression test of the O-ring was done on a 630 kN Schenck servo-hydraulic test machine. The test setup was as shown in Figure 3-1. The O-ring samples were placed between two 225 mm diameter, 40 mm thick, EN 24 untempered steel discs. A third EN 24 untempered steel disc, with a 100 mm diameter, was placed between the top head of the 630 kN Schenck servo-hydraulic test machine and the top large diameter disc. This was done to, simply, create the required gap for the laser displacement meter once the entire system was closed.



Figure 3-1: Test setup used for the material characterisation of the packing materials

The change in displacement was measured by means of a laser displacement sensor, which was mounted to the 630 kN Schenck servo-hydraulic test machine as shown in Figure 3-2.

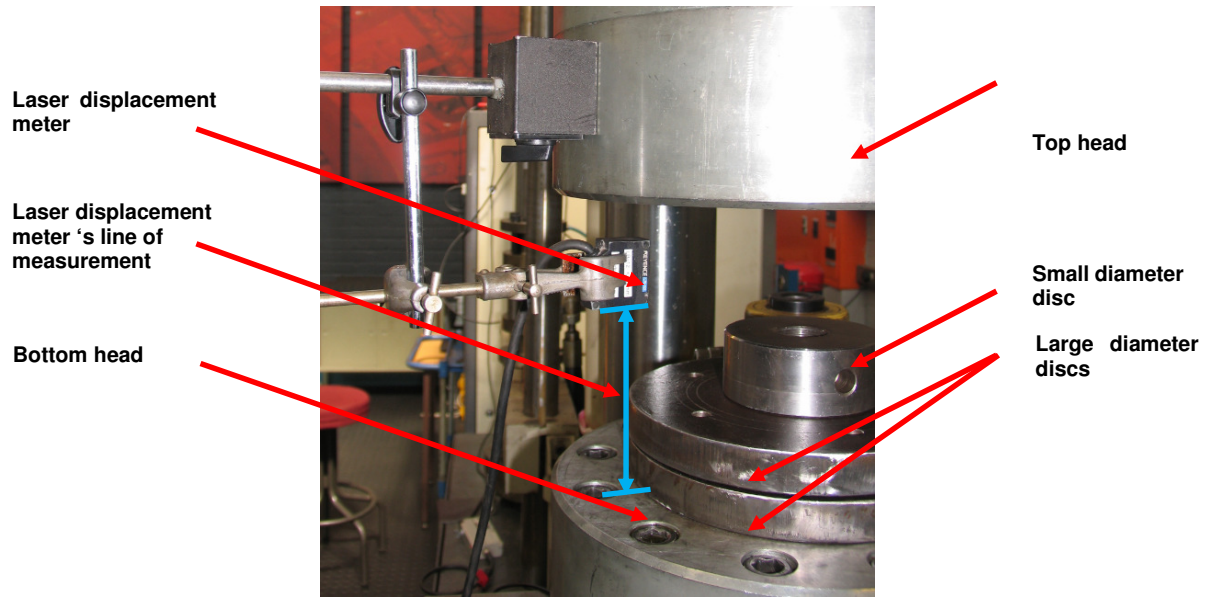


Figure 3-2: Mounting of the laser displacement meter

3.3.2.2. Accounting for the stiffness of the experimental setup

Before any compression tests were done (on either the O-ring or the gasket insert, Sections 3.3.2.3. and 3.3.3.1, respectively) the stiffness of the experimental setup was determined. This was done by measuring the change in displacement as a function of the applied force.

The stiffness of the experimental setup was determined by applying different known forces. The applied force was varied from 62.85 kN to 375.20 kN. The force was applied as shown in Figure 3-3.

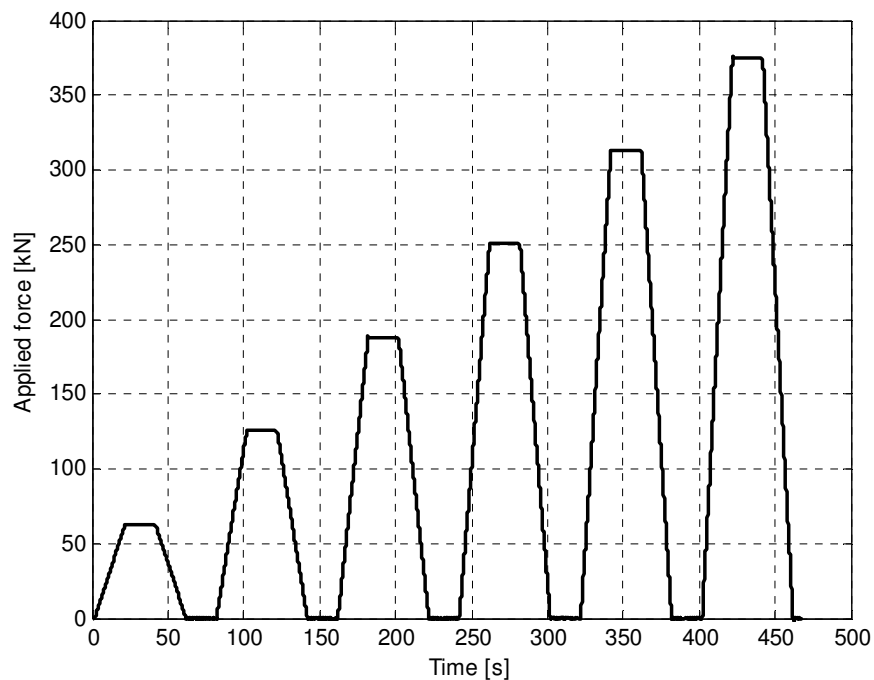


Figure 3-3: Input force as a function of time used for determining the machine stiffness

The force was initially ramped up from 0 kN to 62.85 kN in a time of 20 seconds. It was then held at this force for 20 seconds, before lowering the force again from 62.85 kN to 0 kN in a time of 20 seconds. A similar process was followed for the following force magnitudes: 125.40 kN, 186.10 kN, 250.60 kN, 312.70 kN, and 375.20 kN.

The loading and unloading procedure, as shown in Figure 3-3, was repeated three times, and the mean thereof was taken. These results are shown in Figure 3-4. The average curve shown in Figure 3-4 was calculated from the experimental data as follows: the mean applied force was calculated at specific closure values. A polynomial curve fit was then applied to these mean values.

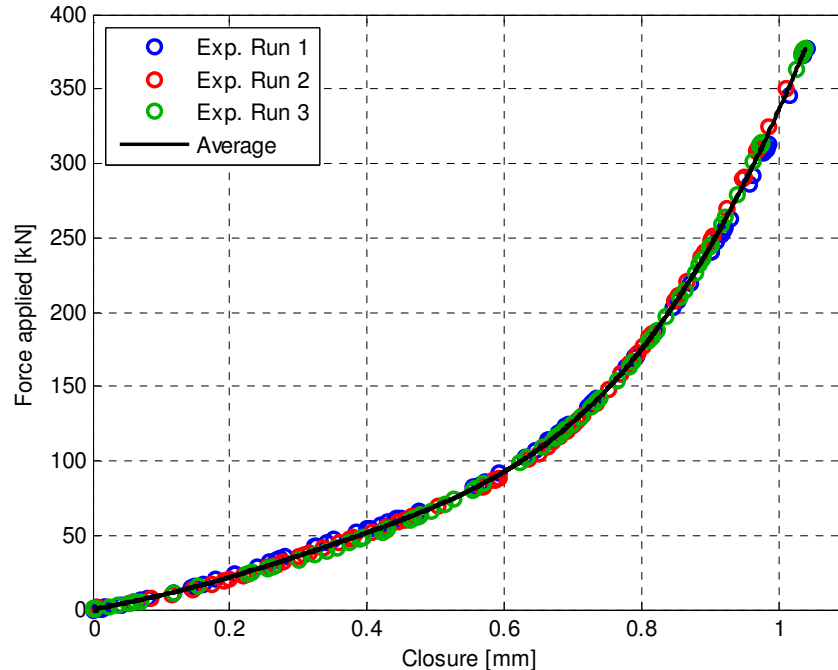


Figure 3-4: The closure of the system as a function of force

This curve was important since it was used to correct the load-closure curves for both the O-ring material and the gasket insert. The correction was done as follows: once the material had been compressed the system closure was subtracted from the measured closure to give the true material closure.

The use of a 630 kN machine for the material characterisation of an O-ring may be brought into question since the load required to compress the gasket is only $\sim 0.6\%$ of the full scale value. Two defences may be made for this. Firstly, the load cell reading remains accurate even when low loads are applied. The displacement transducer of the machine, however, does not. It is for this reason that a laser displacement meter, suitable for measuring small displacements, was included. Secondly, very accurate material characterisations of the packing materials did not form part of the primary scope of this project. The purpose of the material characterisation, as briefly stated before, was simply to obtain suitable 'ballpark figures' which could be used for the validation of the finite element models. It will be shown in Chapter 4 that this requirement was met.

3.3.2.3. Load-compression experiment for the O-ring

The experimental setup which is shown in Figure 3-1 and Figure 3-2 was used to obtain the relevant mechanical properties for the O-ring. Six compression tests were completed in order to determine the load-closure behaviour of the O-rings, which were later used in the circular bolted flange connection experiments. Each of the compression tests were done with new, unused O-rings.

The O-ring used in both the finite element analysis and in the experimental setup had dimensions as shown in Table 3-3.

Table 3-3: Dimensions of the O-ring used

Parameter	Symbol	Value	Unit
Diameter of O-ring section	d_r	5	mm
Centre to centre distance of O-ring	D_r	77	mm

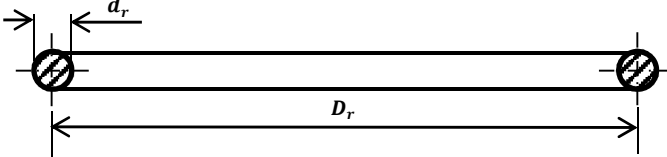


Figure 3-5 shows the results for the six compression experiments as well as the mean thereof. As before, the mean applied force was calculated at various closures, before a polynomial curve fit was applied. From these results it may be seen that the O-ring has a mean total closure of 1.22 mm when a load of 3 500 N is applied.

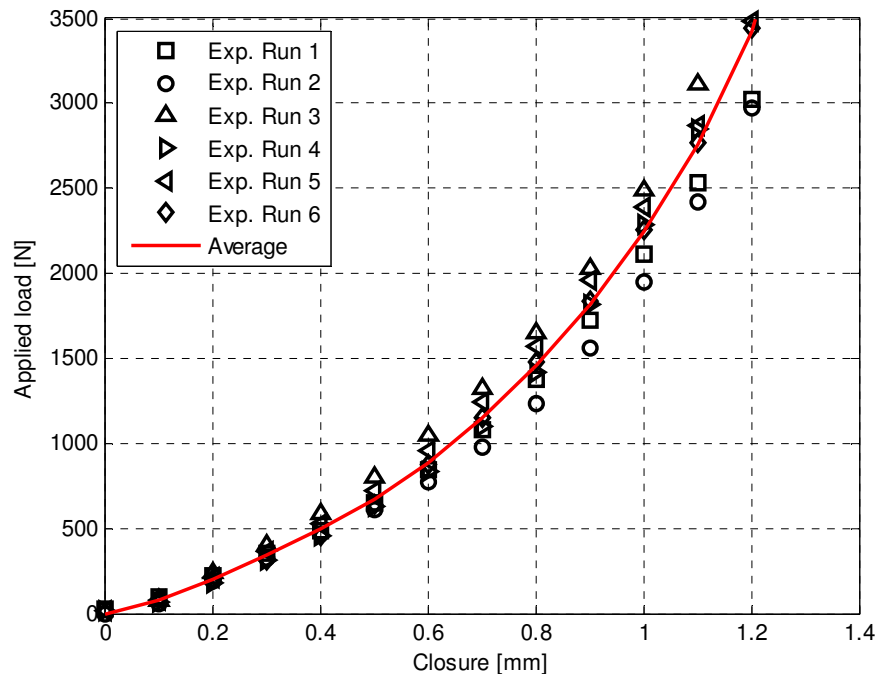


Figure 3-5: Experimental load-closure results for the O-ring

3.3.2.4. Analysis and characterisation of the relevant material properties of the O-ring

The analysis and characterisation of the relevant properties of the O-ring was divided into two parts. The first part was to correct for the stiffness of the experimental setup. The second part dealt with the tuning of the applicable material model in the finite element modelling and analysis software.

As shown, and discussed in Section 3.3.2.2., the experimental setup also deforms when loads are applied. It was, therefore, essential to take this deformation into account when characterising the relevant mechanical properties of the O-ring from the load-closure data. This was done by subtracting the measured closure value of the O-ring at a specific load with the experimental system's closure at the corresponding load. Figure 3-6 shows the graph of both the corrected and uncorrected mean load-closure curves for the O-ring. The difference between the corrected and uncorrected curves is 3.5% at 3 500 N and 1.7% at 500 N.

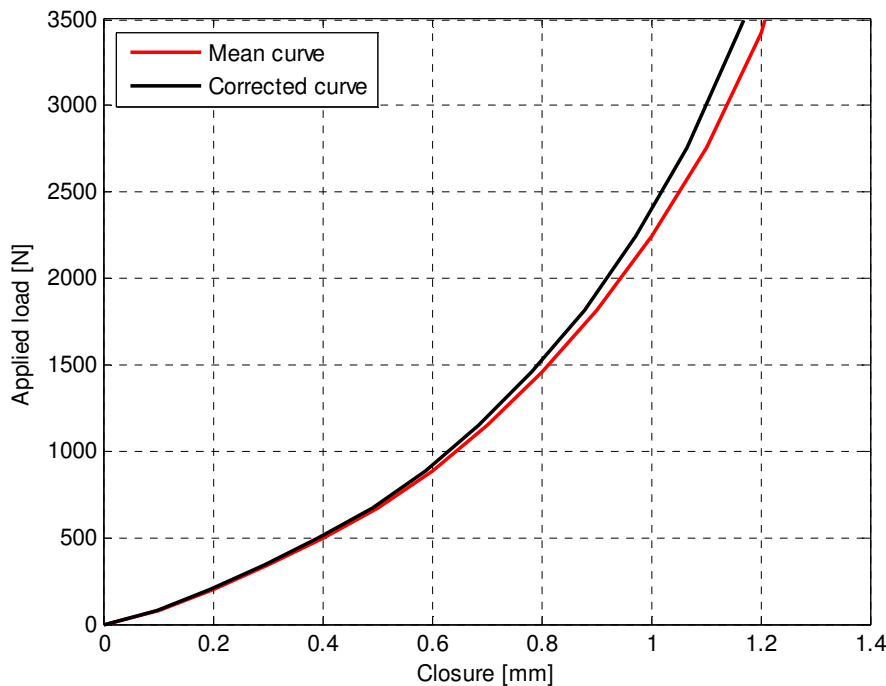


Figure 3-6: Corrected and uncorrected mean load-closure curves for the O-ring

The final step in characterising the O-ring was to select a material model and tune the material model in the finite element and analysis software so as to match the experimental results given in Figure 3-6.

Based on the knowledge that the O-ring is an elastomer, it was initially assumed that its behaviour could be modelled with any of the hyperelastic material models. The models include, but are not limited to the following: Mooney-Rivlin, Yeoh, Ogden, Neo-Hookean, Bergstrom-Boyce, and Arruda-Boyce. For this investigation a third order Ogden material model was selected as is suggested by both MSC software [35] and ANSYS [36]. There may be a more suitable non-linear model amongst the aforementioned models. Determining the most suitable model, however, did not form part of the investigation.

The material model, third order Ogden, was tuned in ANSYS 16.2 finite element modelling and analysis software. A two-dimensional model was created and contained three bodies (as shown in Figure 3-8). Body 1 and Body 3 were assumed to be made out of EN 24, untempered, steel, and were modelled as a linear isotropic material with the material properties given in Table 3-1. The O-ring is presented as Body 2, and its behaviour was modelled with a third order Ogden hyperelastic model.

The contact between the O-ring and the EN 24 plate was assumed to be frictional with a coefficient of friction of 0.9. The coefficient of friction between the O-ring and the flange face was not experimentally determined. However, a brief investigation was done to determine the effect which the coefficient of friction would have on the directional displacement of Body 2. The material parameters as given in Table 3-4 were used and the coefficient of friction was varied from 0.1 to 0.9. This investigation was done with the model, loads and boundary conditions as described and shown in Figure 3-8.

Shown in Figure 3-7 is a plot of the load-closure curves for the various coefficients of friction. The largest percentage difference between the minimum and maximum coefficients was 1.2%, at 3 500 N for a coefficients of friction of 0.1 and 0.9. For the material characterisation, this percentage difference was assumed to be negligible and a value of 0.9 was selected. A coefficient of friction of 0.9 was selected based on research done by Green & English [37], where they analysed the behaviour of elastomeric O-ring seals in compression by using the finite element method.

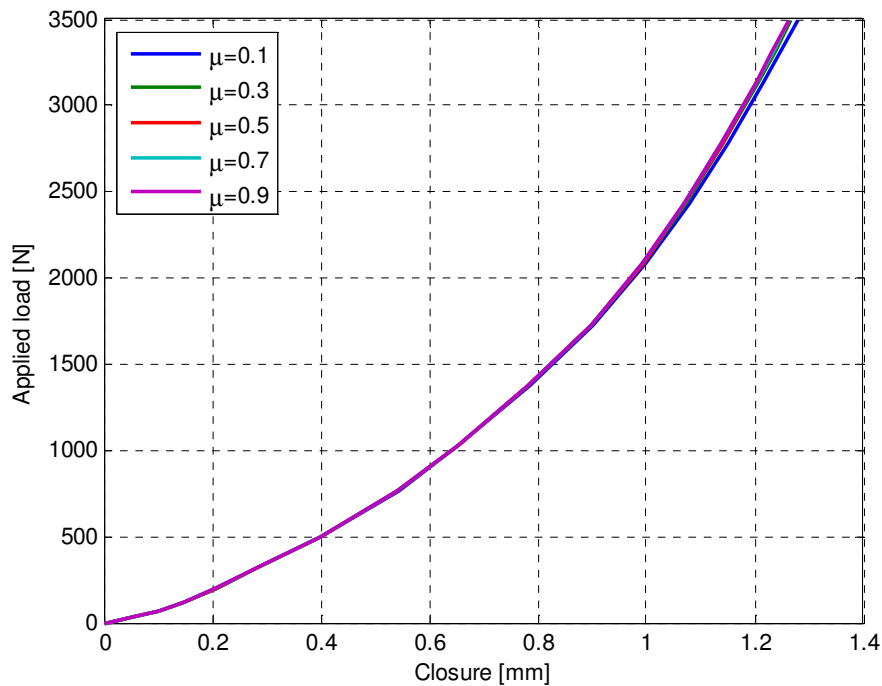


Figure 3-7: Comparison of the load-closure curves for varying coefficients of friction

For the tuning of the material model in the finite element modelling and analysis software the following loads and boundary conditions were applicable: Body 3's bottom surface was constrained against displacement in the y-direction. An equally distributed force was applied along the length of the top surface of Body 1. Body 1 and Body 3 had a height and radius of 15 mm and 120 mm respectively. Body 2 had the same dimensions as given in Table 3-3.

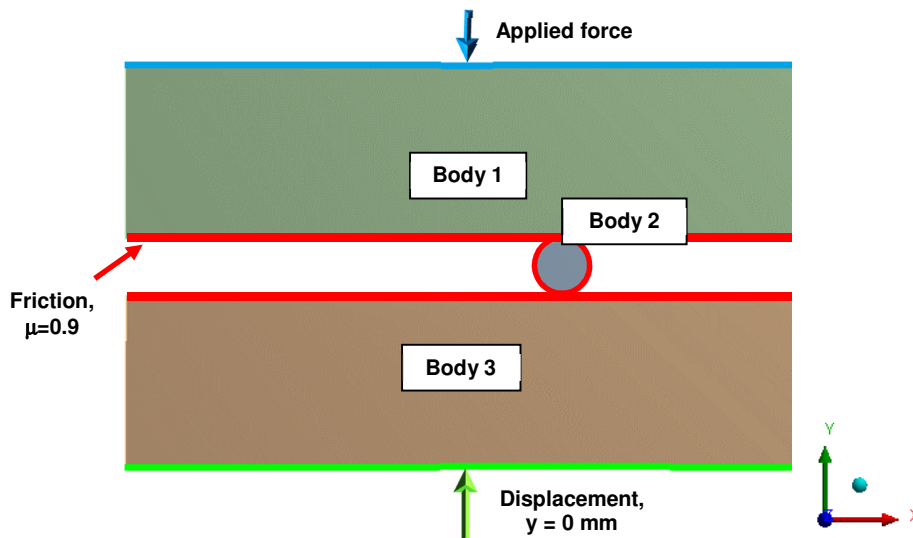


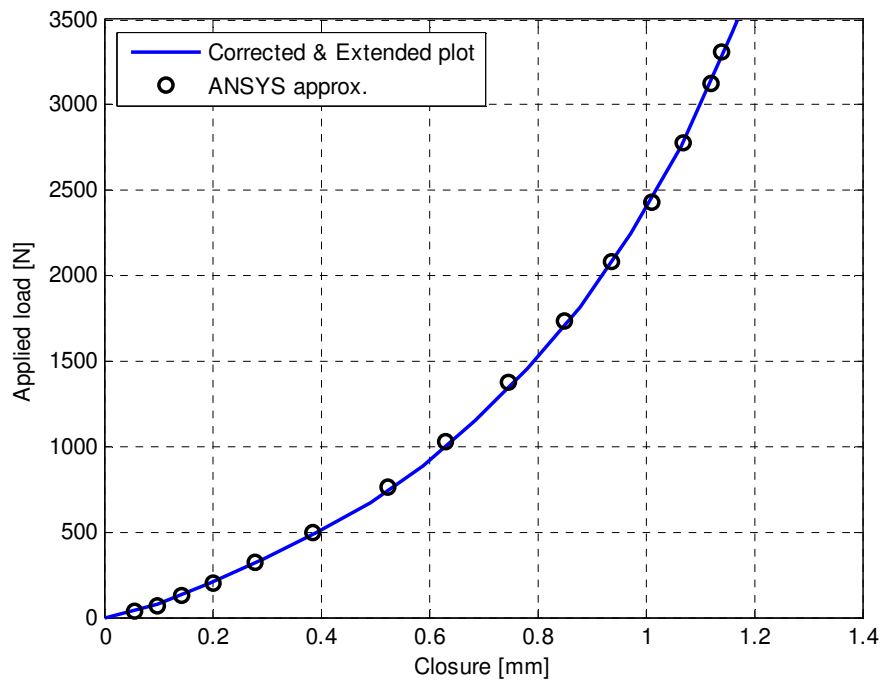
Figure 3-8: Boundary conditions and contact interface for the tuning of the material model for the O-ring

An axisymmetric 2D analysis was performed on this model. This was done to mimic the actual compression experiment which was performed. For the axisymmetric 2D analysis a total force of 3 500 N was applied so as to match the maximum load applied in the compression experiment. The material was manually tuned in the finite element modelling and analysis software until a suitable fit was found. It is important to note that this process may be optimised to find an ideal fit for the characterisation of the material with a third order Ogden material model. Shown in Table 3-4 are the relevant parameters which were used for the fit of the third order Ogden material model.

Table 3-4: Relevant material parameters for the third order Ogden material model of the O-ring

Parameter	Symbol	Value	Unit
Material shear modulus 1	μ_1	1.28	MPa
Material constant 1	A_1	5.6	-
Material shear modulus 2	μ_2	0.05	MPa
Material constant 2	A_2	0.15	-
Material shear modulus 3	μ_3	0.725	MPa
Material constant 3	A_3	0.1	-
Incompressibility parameter 1	D_1	0	-
Incompressibility parameter 2	D_2	0	-
Incompressibility parameter 3	D_3	0	-

Figure 3-9 shows a plot of the mean corrected experimental load-closure curve as well as the predicted load-closure curve based on values from the finite element modelling and analysis software.

**Figure 3-9: Finite element analysis approximation of the experimental load closure curve**

The approximation of the experimental results, by means of the finite element modelling and analysis software, had a root mean square error of 21.8 N and a maximum error of 29.6 N. For the purpose of this investigation this approximation was deemed suitable, and it will be shown in Chapter 4 that an acceptable comparison was obtained between the finite element analysis and the experimental setup of a circular bolted flange connection which made use of an O-ring.

Figure 3-10 shows the deformation of the O-ring, which had the material properties as defined in Table 3.4 for the various loads during the compression test. From these results it may be observed that the O-ring is initially, at a low compression load, easily deformed. However, as the compression load is increased so the stiffness of the O-ring increases and it deforms less. Its closure increased by 36% when the load was increased from 600 N to 1 200 N, however the closure only increased by 13% when the load was increased from 2 400 N to 3 000 N.

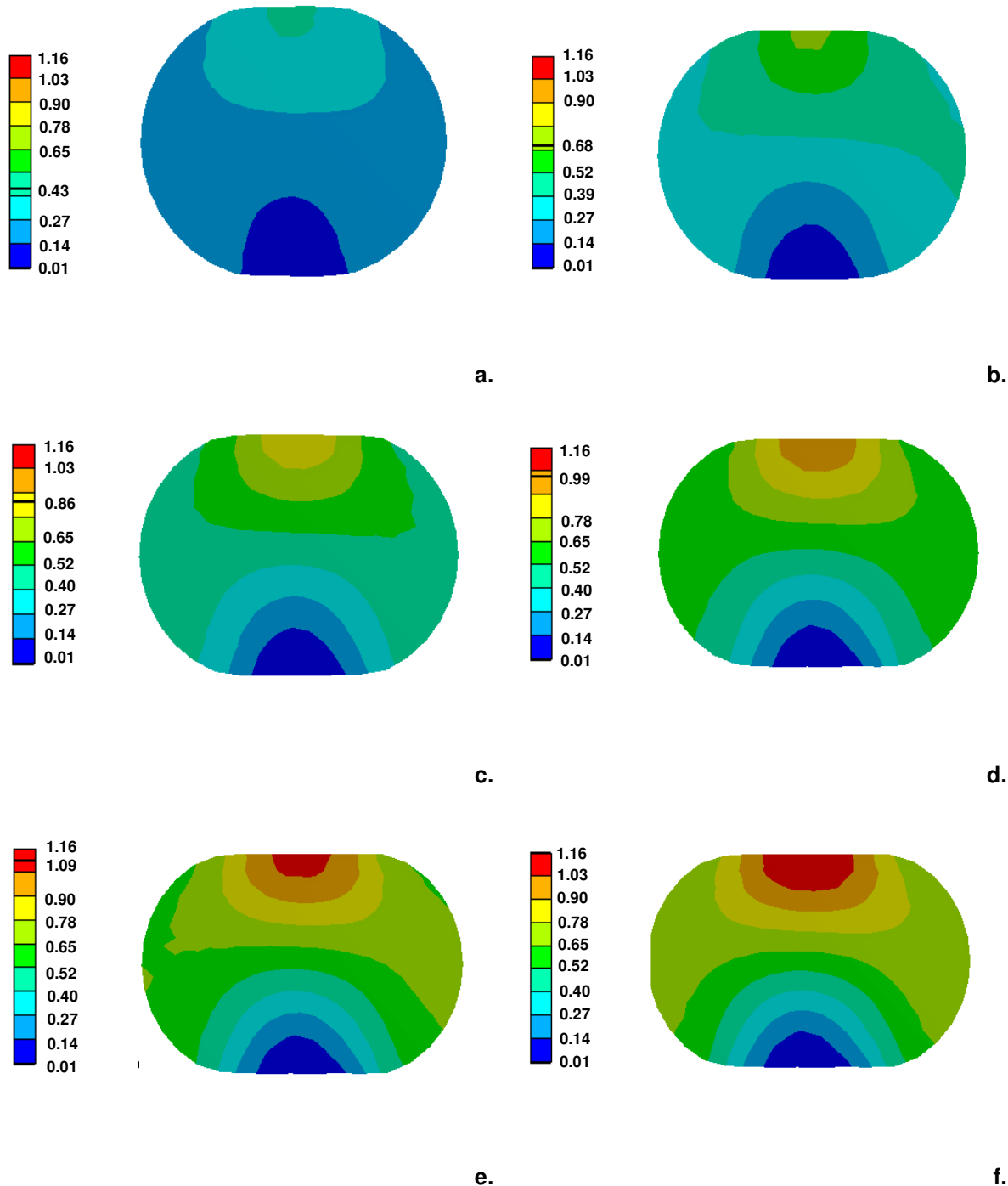


Figure 3-10: Deformation of the O-ring, with the assumed third order Ogden material model, for (a) 600 N, (b) 1 200 N, (c) 1 800 N, (d) 2 400 N, (e) 3 000 N, and (f) 3 500 N

3.3.3. Relevant mechanical properties of the gasket

The most commonly used gasket material model when considering circular bolted flange connections is the so-called 'gasket' model in ANSYS. This model makes use of interface elements. The pre-condition for its use is a pressure-closure curve. This material model has potentially two major drawbacks when applying it to a soft gasket material such as a non-asbestos compressed fibre gasket insert. The first drawback is that it is unable to accurately predict the contact stress distribution between the gasket and the flange faces. The second drawback is that its suitability for predicting long term gasket creep is questionable.

The ANSYS 'gasket' model's ability to accurately predict long term gasket creep-relaxation is questionable, in this instance, because the creep-relaxation, although a time dependent phenomenon,

is not modelled as such. The gasket creep-relaxation behaviour is rather modelled as part of the unloading curve. This implies that the gasket creep-relaxation behaviour may only be predicted up to the same time where a pressure-closure experiment was done.

It is known that the gasket exhibits creep-relaxation behaviour. To accurately present this behaviour it was decided to model the gasket insert as a non-linear viscoelastic material. In order to apply this model successfully, the material's behaviour over time needed to be determined. This could be done in one of two ways: either the material could be subjected to a constant load and the change in displacement be measured (creep test); or the material could be placed under a constant displacement and the reduction in the stress be measured (stress relaxation).

3.3.3.1. Load-closure and creep test of the compressed non-asbestos gasket insert

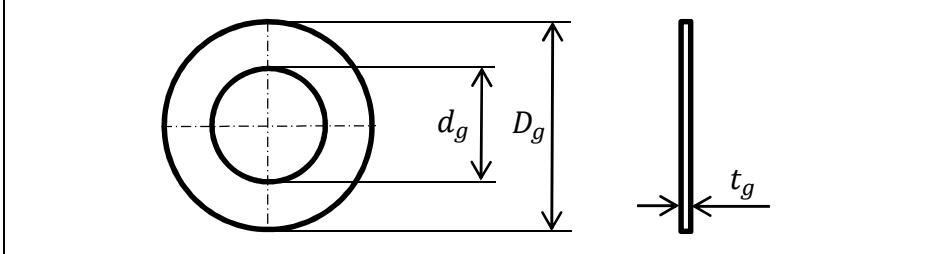
It was decided to characterise the material by means of creep tests. Nine creep tests, in total, were performed. The first three creep tests were performed at a pressure which is expected to resemble the final (i.e. after all the bolts had been tightened) contact pressure between the gasket insert and the flange faces in the experiment. The next three creep tests were performed at a pressure which was 50% higher than the initial three tests. Tests number seven, eight and nine were, conversely, performed at a pressure which was 50% lower than that of the initial three tests.

The material was tested at a 50% higher and lower pressure to determine the suitability of the material model when the loads applied by the bolts were either increased or decreased. It was, initially, desired that once the finite element model was tuned for the expected contact pressure results it would have the ability to predict the creep behaviour of the gasket at higher and lower contact pressures with the same accuracy as the expected contact pressure.

The gasket insert was tested on the same experimental setup which was used for the compression test of the O-ring (Figure 3-1). However, unlike the O-ring, the entire gasket insert was not tested. The gasket was divided into 24 equal sections of which three were tested simultaneously. In other words, only one eighth (three equal sections) of the gasket material was tested at a time. Three sections were used to minimise the effect which the stiffness of the experimental setup had on the measured load-closure curves, and to ensure that the EN-24 steel discs were correctly balanced during the test procedure. The gasket insert dimensions were as summarised in Table 3-5:

Table 3-5: Dimensions of the gasket insert used

Parameter	Symbol	Value	Unit
Inner diameter of gasket	d_g	60	mm
Outer diameter of gasket	D_g	110	mm
Thickness of gasket	t_g	5	mm



The following procedure was followed when the creep tests were performed: The gasket samples were loaded to the relevant values, as shown in Table 3-6. The loads were applied rapidly to minimise the possibility of any creep-relaxation behaviour before the actual creep test started. Once the desired maximum load was reached, it was maintained for 4 000 seconds. During the 4 000 seconds the laser displacement meter measured the change in displacement.

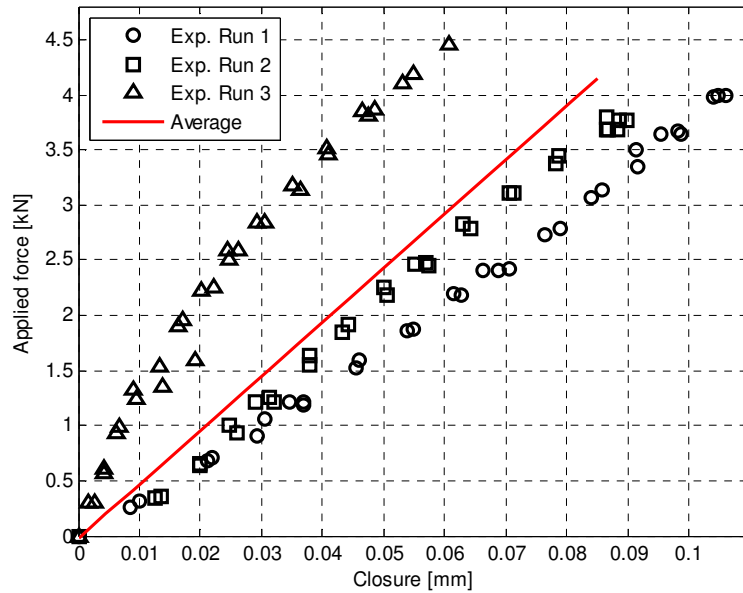
Table 3-6: Calculation of the necessary load for the creep tests

Parameter	Symbol	Value	Unit
Inner diameter of gasket	d_g	60	mm
Outer diameter of gasket	D_g	110	mm
Single contact surface area of entire gasket insert	A_g	6 676	mm ²
Single contact surface area of tested gasket insert	A_g'	835	mm ²
First applied pressure	P_1	5	MPa
Second applied pressure	P_2	10	MPa
Third applied pressure	P_3	15	MPa
First required load	F_1	4 173	N
Second required load	F_2	8 345	N
Third required load	F_3	12 518	N

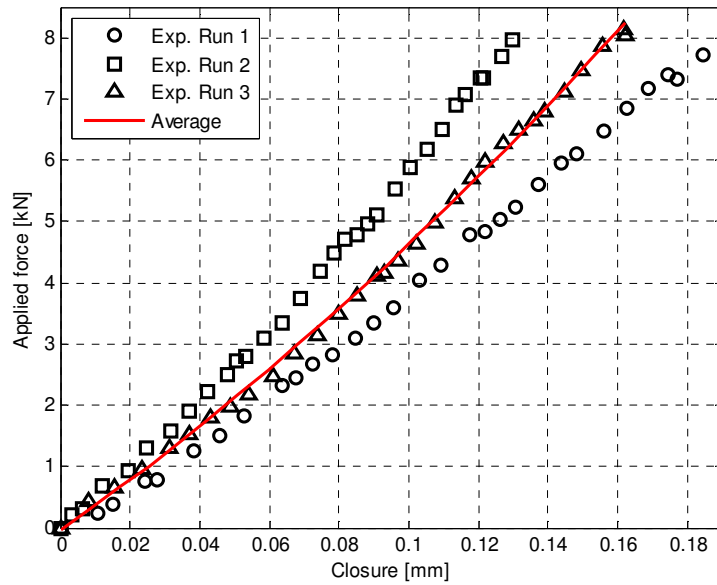
The first set of results which were considered, from this experiment, were the load-closure values of the gasket samples during the compression stage. The second set of results which were focused on was the creep results at: 5 MPa, 10 MPa, and 15 MPa applied pressure. The experiment was repeated three times at each of the applied pressures. It was decided to use the initial loading phase data of the creep test to characterise the load-closure behaviour of the gasket insert. Figure 3-11 shows the initial load-closure curves for the three experimental runs at each of the three pressures. It also shows the mean load-closure curves for each of the applied pressures. A polynomial curve fit was applied to the mean closure values at the specific applied pressure.

The experimentally obtained load-closure curves vary from one run to another. This variation may be attributed to two factors. Firstly the material of the gasket insert was not entirely homogenous and, therefore, the stiffness of the material is not uniform throughout. The second factor is that different gaskets, of the same material, were used. Although the gaskets are made from the same material they are not exactly the same and do not exhibit the exact same stiffness' when a compression test is done. The accuracy of the results obtained from the creep test may be increased by increasing the number of experimental tests done. However, for this investigation, since the material characterisation did not form part of the primary objectives, the three experimental tests completed at each of the three applied pressures were deemed to be acceptable.

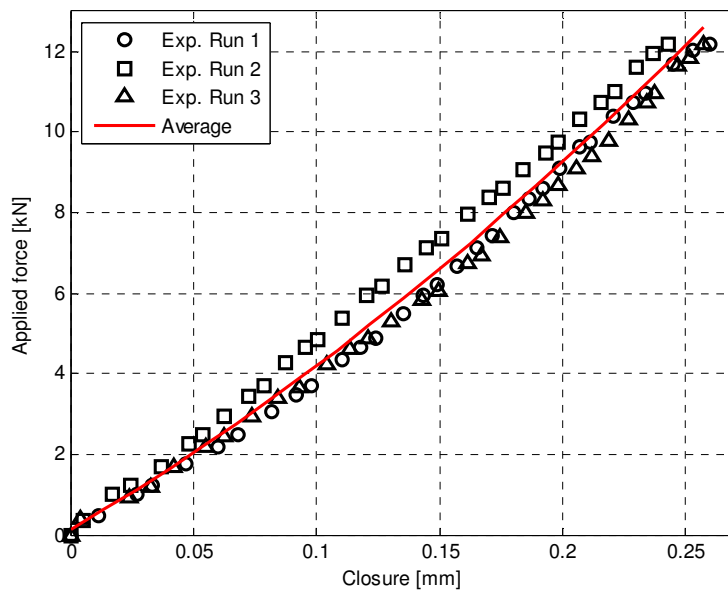
As with the material characterisation of the O-ring, the stiffness of the experimental setup needed to be accounted for. This was done in the same way as described previously – i.e. the true closure was obtained by subtracting the closure of the experimental setup, at a specific load, from the total measured closure. The results for both the uncorrected and corrected mean curves, during the loading stage of the creep tests, are shown in Figure 3-12. The correction in this instance, for the machine stiffness, resulted in ~50% difference between the mean corrected and uncorrected curves for all three instances. This reduction is much larger when compared to the results of the O-ring compression test. The reason for this large difference is that the compression loads applied to the gasket material was significantly larger and, subsequently, the deformation of the experimental setup much higher.



a.

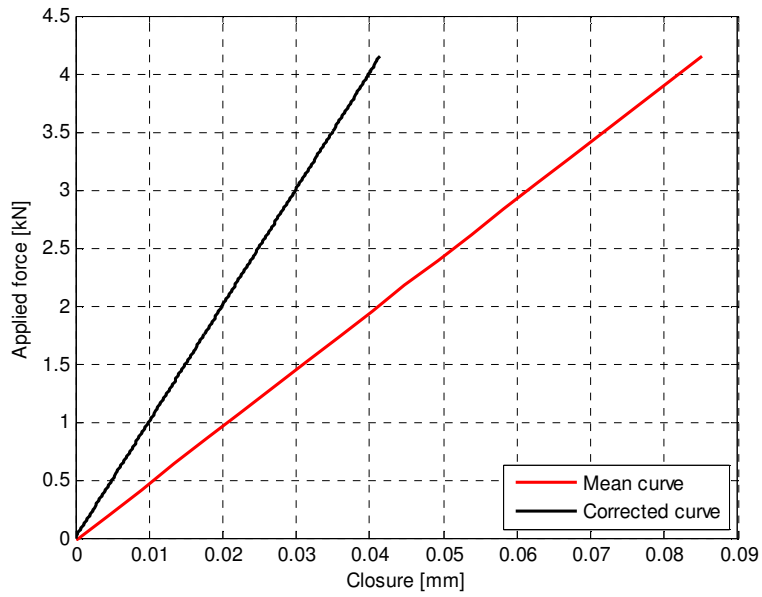


b.

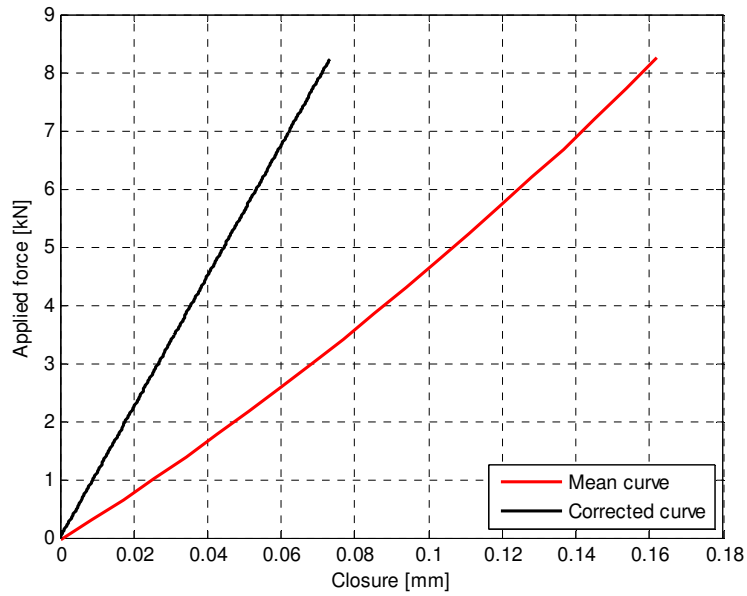


c.

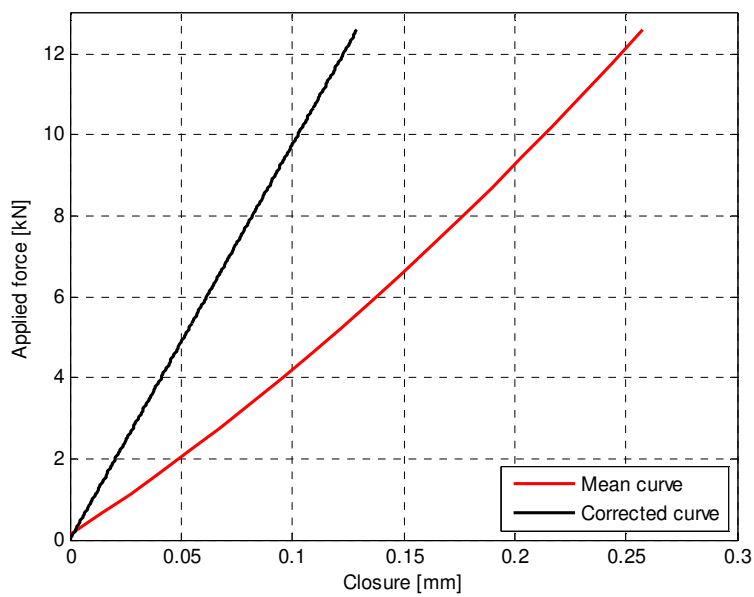
Figure 3-11: Experimental load-closure results and the mean thereof for applied pressures of (a) 5 MPa, (b) 10 MPa, and (c) 15 MPa



a.



b.



c.

Figure 3-12: Corrected and uncorrected mean load-closure curves for the applied pressure of (a) 5 MPa, (b) 10 MPa, and (c) 15 MPa

The material was tuned in ANSYS 16.2. A two-dimensional model was created and contained three bodies (Figure 3-13). Body 1 and Body 2 was assumed to be made out of EN 24 untempered steel, and was, therefore, modelled as a linear isotropic material with the same relevant material properties as given in Table 3-1. Body 2, however, was assumed to be the gasket insert material. The gasket insert material was assumed to be a non-linear viscoelastic material and its behaviour was modelled with Prony shear relaxation and Neo-Hookean models.

The contact between the gasket insert material and the EN 24 plates was assumed to be a frictional contact with a coefficient of friction of 0.3. The coefficient of friction between the gasket insert and the EN 24 steel plate was not experimentally determined. The assumption of a value of coefficient of friction of 0.3 will, however, be explained at the end of this section.

Body 3's bottom surface was constrained against displacement in the y-direction. An equally distributed force was applied along the length of the top surface of Body 1. Body 1 and Body 3 had a height and length of 20 mm and a radius of 120 mm respectively. Body 2 had the same dimensions as was given in Table 3-5.

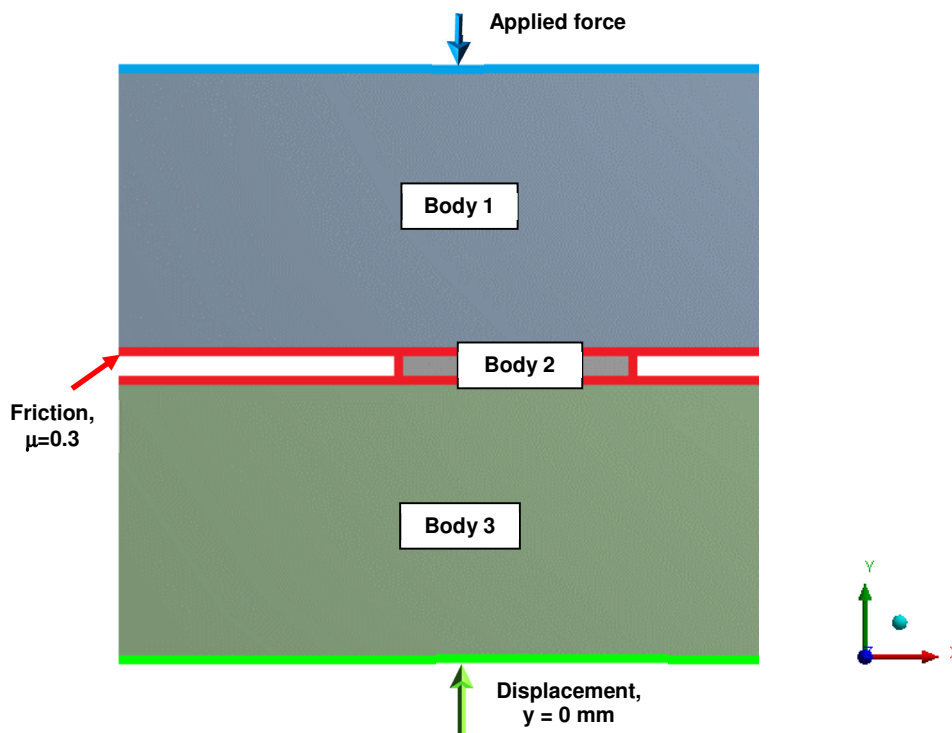
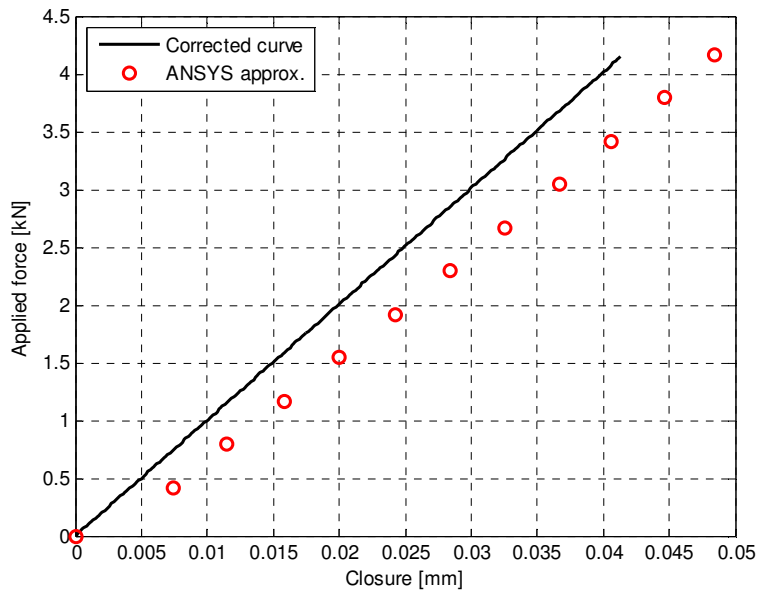


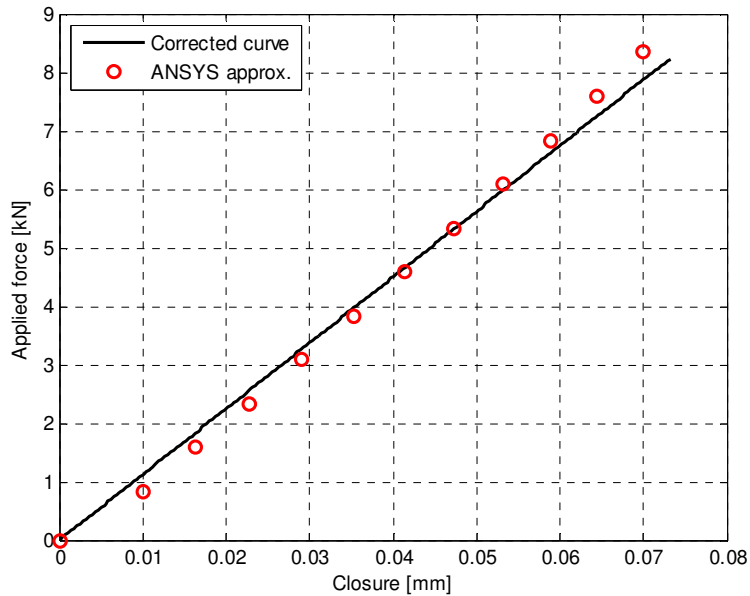
Figure 3-13: Boundary conditions and contact interface for the tuning of the material model for the gasket insert

Figure 3-14 shows the results for the tuned approximation of the corrected curves which are shown in Figure 3-12. As discussed above, the model was only tuned for the expected pressure values. This model was then applied to the instances where the applied pressure was 50% higher and lower. This was done to investigate the suitability of the tuned material model when a higher or lower pressure is applied.

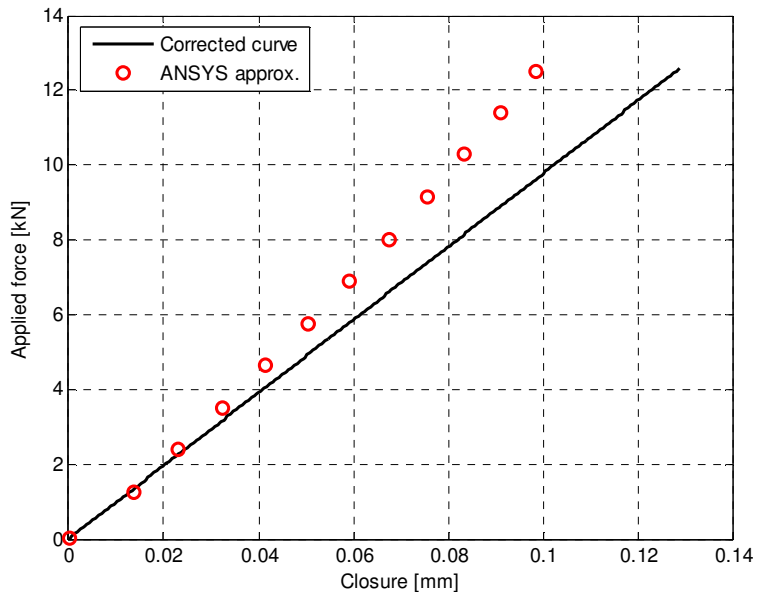
As before all the values were tuned manually. An automated optimisation analysis may have been done to improve the material characterisation. For this investigation, however, an optimal curve fit for the material characterisation was not deemed to be essential.



a.



b.



c.

Figure 3-14: Approximated and mean corrected experimental load-closure curves for applied pressures of (a) 5 MPa, (b) 10 MPa, and (c) 15 MPa



As with the material characterisation and parameter tuning of the O-ring, an axisymmetric 2D analysis was performed on the aforementioned model (shown in Figure 3-13). For the axisymmetric 2D analysis the load was varied to correspond to values given in Table 3-6 for contact pressures of 5 MPa, 10 MPa, and 15 MPa.

Given in Table 3-7 are the mean square errors as well as the mean maximum errors for the approximation of the experimental results by the finite element modelling and analysis software. The approximated curves are shown in Figure 3-14.

Table 3-7: Root mean square error and the maximum error of the ANSYS approximation of the load-closure curves

Applied pressure [MPa]	Root mean square error [kN]	Maximum mean error [kN]
5	0.47	0.07
10	0.24	0.50
15	1.46	2.98

As stated before the non-asbestos, compressed fibre gasket insert was modelled as a non-linear viscoelastic material. This was done by selecting both a Neo-Hookean model and Prony shear relaxation. The relevant material coefficients for both these models are given in Table 3-8 and Table 3-9.

Table 3-8: Relevant material parameters for Prony shear relaxation

Parameter	Symbol	Value	Unit
Relative modulus 1	α_1^K	0.45	MPa
Relaxation time 1	t_1	55	s
Relative modulus 2	α_2^K	0.07	MPa
Relaxation time 2	t_2	1 500	s
Relative modulus 3	α_3^K	0.07	MPa
Relaxation time 3	t_3	2 000	s

Table 3-9: Relevant material parameters for the Neo-Hookean model

Parameter	Symbol	Value	Unit
Initial shear modulus	μ	22.5	MPa
Incompressibility parameter	D_1	0	s

The predicted creep curves, from the finite element modelling and analysis software are shown in Figure 3-15. Also shown in Figure 3-15, are the experimentally obtained creep curves. The root mean square errors, and the mean maximum errors are given in Table 3-10.

From the results given in Figure 3-15 and Table 3-10, it may be observed that the best fit is for the pressure at which the material was tuned, namely at 10 MPa. The material model predicts higher creep values for both the instances where 50% lower and higher pressures were used. It may, therefore, be concluded that the pressure value at which the material model is tuned has its highest accuracy at that value, and does not necessarily have the desired accuracy at higher or lower pressures.

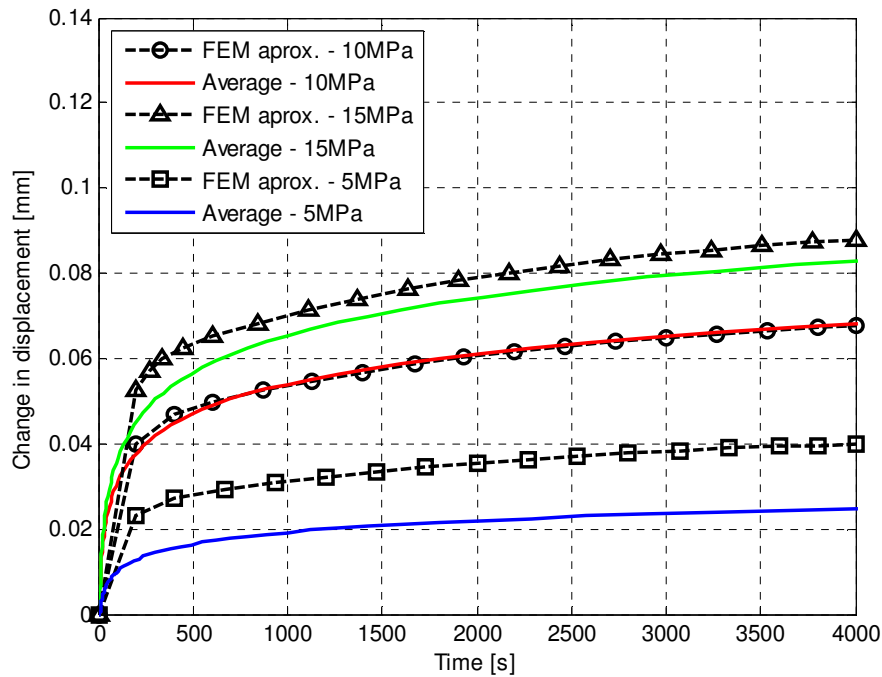


Figure 3-15: Experimental and finite element approximated creep results

Table 3-10: Root mean square error and the maximum error of the ANSYS approximation of the creep curves at the various pressures

Applied pressure [MPa]	Root mean square error [$\times 10^{-3}$ mm]	Maximum mean error [$\times 10^{-3}$ mm]
5	13.00	22.77
10	1.86	9.40
15	4.28	10.78

As discussed above, the creep values predicted by the finite element model and analysis are slightly larger at the lower and higher pressures. However, in this particular case the values are deemed acceptable, and it will be shown in Chapter 4 that an acceptable comparison is obtained between the predicted values of the FEM and the experimental results. The results of Figure 3-15, however, highlight the fact that one needs to be careful at which load the material is calibrated and then used. In addition to this, as briefly, mentioned before, the assumed or determined coefficient of friction between the gasket surface and the flange face is another factor which may greatly influence the accuracy of the values obtained after a material model has been tuned.

An additional investigation was done with regards to the creep-relaxation behaviour of the gaskets. As was discussed in Chapter 2, Alkelani *et al.* [27] proposed a model to predict the creep-relaxation behaviour in soft gaskets. Their model was implemented by following the procedure given in Chapter 2. This was done to determine whether or not the model is also applicable to non-asbestos, compressed fibre gaskets with aramid and nitrile binder (such as the one use for this investigation). As before the model was calibrated for the instance where a distributed pressure of 10 MPa is applied to the surface of the gasket material. Once the model was calibrated only the pressure values were changed (i.e. 50% higher and lower). The results of the model were then compared to those shown in Figure 3-15. The results of the comparison were plotted and are shown in Figure 3-16. In addition to this the root mean square error as well as the mean maximum errors are given in Table 3-11.

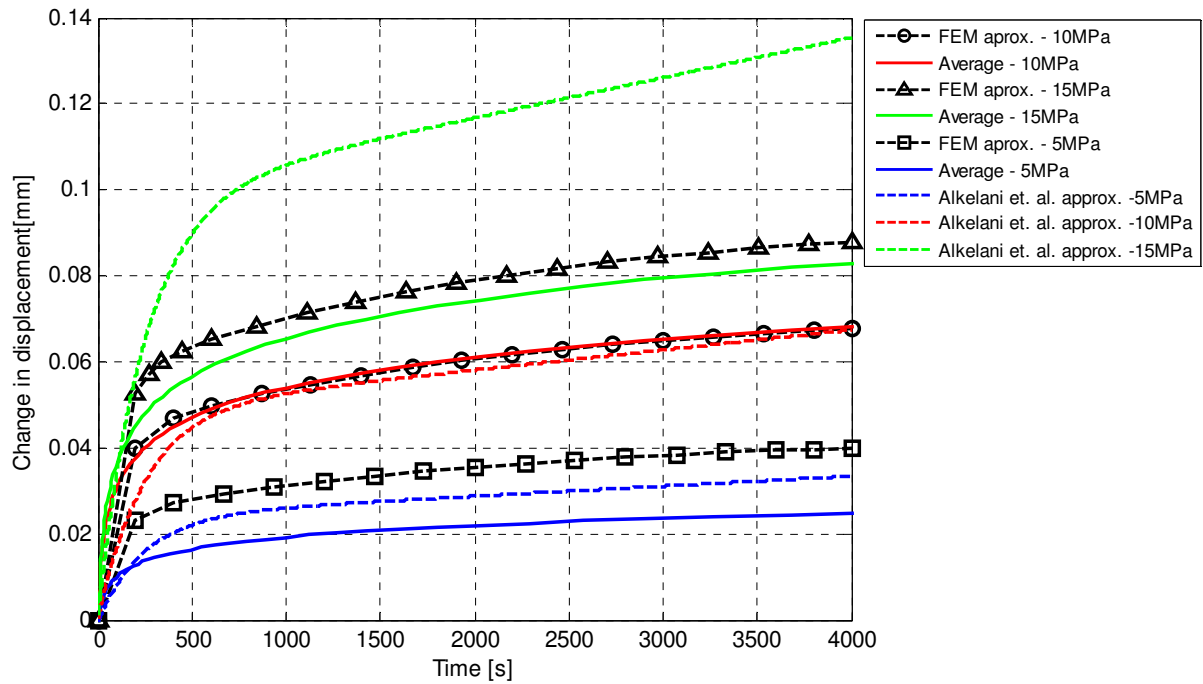


Figure 3-16: Comparison of the experimental results, the results calculated by the finite element analysis, and the model proposed by Alkelani *et al.* [27]

As with the non-linear viscoelastic model, used in the finite element analysis, it may be observed that the best fit, from the model proposed by Alkelani *et al.* [27], is for the pressure at which the material was tuned, namely 10 MPa. The material model also predicts higher creep values for both the instances where 50% lower and higher pressures were used. For the approximation of the curve at 10 MPa, the non-linear viscoelastic results from the finite element analysis has a lower root mean square error, when compared to the experimental results, than the model proposed by Alkelani *et al.* [27]. For 5 MPa a better approximation is, however, achieved, by the model proposed by Alkelani *et al.* [27]. For the instance where the pressure was increased by 50% a root mean square error of 91.78×10^{-3} mm was obtained. As with the non-linear viscoelastic model care needs to be taken when using the material model at higher pressures than was calibrated at.

Based on these preliminary results, from a very limited investigation, it seems as though the model proposed by Alkelani *et al.* [27] may have the potential to predict the creep-relaxation behaviour, of not only soft rubbery gasket materials, but also compressed fibre gaskets such as the one used in this investigation.

Table 3-11: Root mean square error and the maximum error of the approximation of the creep curves at the various pressures by means of Alkelani *et al.* [27] ‘s model

Applied pressure [MPa]	Root mean square error [$\times 10^{-3}$ mm]	Maximum mean error [$\times 10^{-3}$ mm]
5	31.99	38.55
10	16.67	20.74
15	91.78	111.02

The coefficient of friction of 0.3 between the gasket insert and the face of the flange was not experimentally determined. However, a brief investigation into the effect, which the value of the coefficient of friction has on the material characterisation, was done.

The same 2D axisymmetric model, as described above, was used for the investigation. Bodies 1 to 3 were constrained in the same way as before and a load of 66 760 N was applied (which is equal to a pressure of 10 MPa). The only value which was varied was that of the coefficient of friction. The coefficient of friction was varied from 0.1 to 0.9. The results for both the load-closure curves, at each of the aforementioned coefficients of friction, as well as for the creep were obtained. The results are shown in Figure 3-17 and Figure 3-18, respectively.

From the load-closure results it may be observed that the closure equalled 0.184 mm when a load of 66 760 N was applied and the coefficient of friction was 0.1. This is 87 % more than the closure at the same load and a coefficient of friction of 0.9. It may also be observed that the closure value decreases as the coefficient of friction increases. The difference in the closure values between the instance when the coefficient of friction was 0.1 and 0.3, was 69%, whereas the difference in closure was 13% when the coefficients of friction were of 0.7 and 0.9. The difference in closure values, therefore, decrease as the coefficient of friction increased. From these results it may be argued that the coefficient of friction between the gasket surface and that of the flat disc plays a significant role in the characterisation of the material.

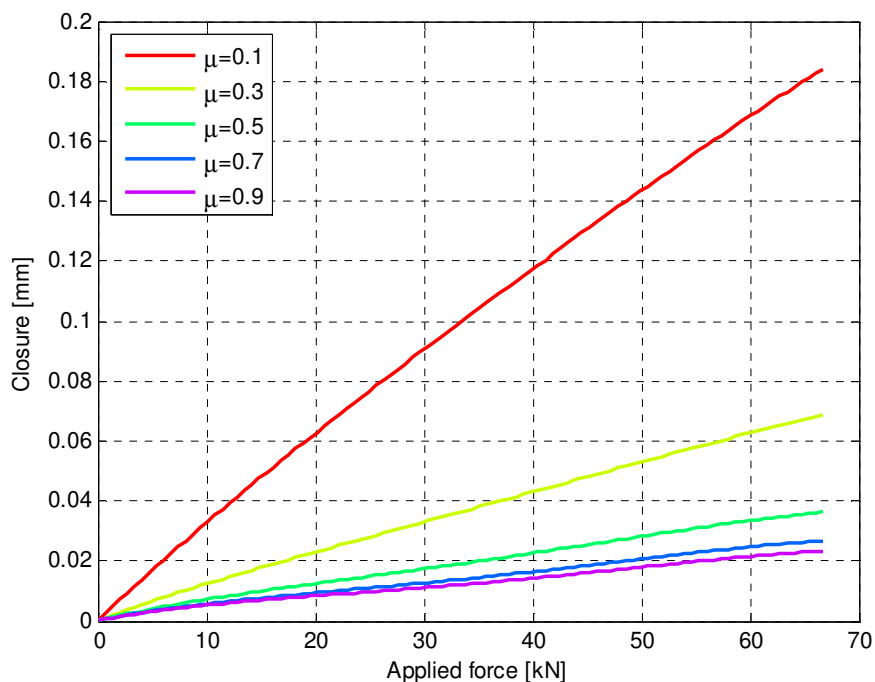


Figure 3-17: Load-closure curves for various coefficients of friction

From Figure 3-18 a similar trend may be observed when compared to that of the compression test. The highest amount of creep occurs when the coefficient of friction is the lowest. As the coefficient of friction increases so the amount of creep decreases. When the coefficient of friction increases from 0.1 to 0.3, the amount of closure due to creep decreases by 60%. However, when the value for the coefficient of friction increases from 0.3 to 0.5, the amount of closure due to creep decreases by 40%. A similar trend exists for the reduction in the amount of closure for an increase in the value of the coefficient of friction for 0.5 to 0.7, and 0.7 to 0.9.

From the results shown in Figure 3-17 and Figure 3-18 it may be concluded that the value of the coefficient of friction has a significant influence on both the load-closure response of the material and the amount of closure due to creep during the material characterisation. Based on this it is suggested that the coefficient of friction be carefully determined when characterising the gasket material.

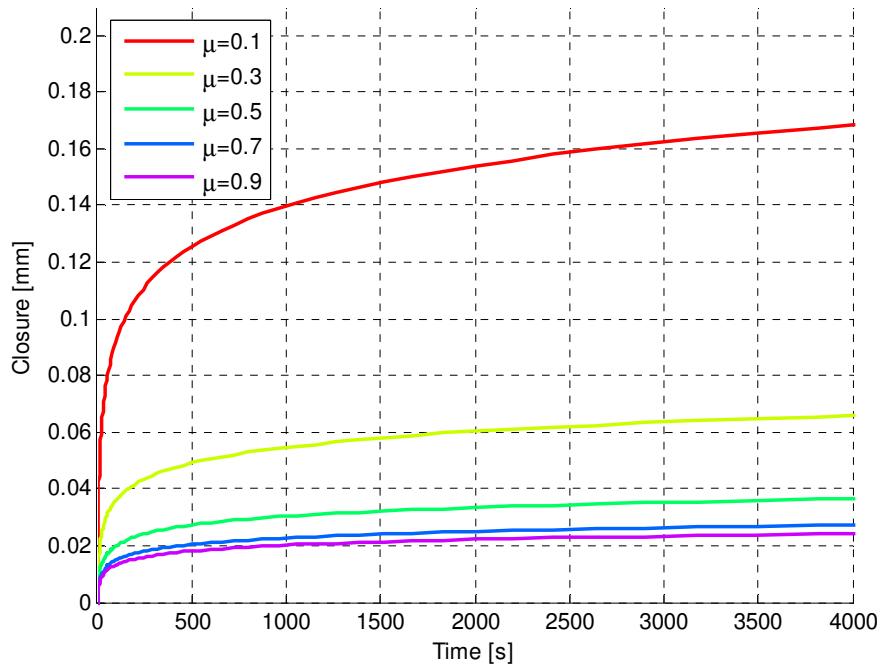


Figure 3-18: Closure due to creep for various coefficients of friction

3.4. Modelling of the flange geometry

The geometry, in this instance, was dependent on three primary factors, namely: the dimensions of the various components, the way in which the various components are assembled, and any simplifications which were made to the model.

3.4.1. Dimensions of the components

Firstly, the purpose of the initial modelling and analysis was to construct a suitable finite element model which could be experimentally validated. Therefore a standard, EN 1092-1 PN 10 DIN 50, flange was selected for the experimental setup. The relevant dimensions are given in Appendix B. It is important to note that the flange dimensions which are used in this chapter are exactly the same as those presented in Chapter 4, which deals with the experimental setup. As with the various flange pairs, the packing material (i.e. the gasket insert and the O-ring) had exactly the same dimensions as those given in Table 3-3 and Table 3-5.

3.4.2. Simplifying assumptions

The model was only simplified in three ways when compared to the experimental setup. The first simplification was with regards to the fasteners. It was assumed that the edges of the fasteners may be approximated as round instead of a hexagon. This assumption was made in order to reduce the complexity, and subsequent number of elements / nodes, on the fasteners. A reduction in the number of elements / nodes resulted in a decrease in the solving time since the analysis was less computationally expensive. The second simplifying assumption, was that the circular bolted flange connection could be approximated by an asymmetrical model. As discussed in Chapter 2, an axisymmetric model in this case is a section of the entire circular bolted flange connection. The final simplifying assumption, was that the top and bottom caps could be neglected. This changed how the boundary conditions are applied and a full discussion of this is given in Section 3.4.4.

3.4.3. Assumptions for the contact interfaces

When modelling a circular bolted flange connection, as previously described, there are five contact interfaces. The five contact interfaces are between: the bolt head and top flange; the nut and the bottom flange; the bolt and the nut; the face of the top flange and the gasket / O-ring; and the face of the bottom flange and the gasket O-ring. A brief discussion of the contact interfaces are given below.

3.4.3.1. Contact between the gasket and flange faces

The correct contact interfaces between the gasket and flange faces, from Chapter 2, are known to be frictional. In Section 3.3 it was shown that the friction coefficient assigned to the interface between the gasket and flat disc has an impact on the results for the material characterisation. In order to determine to what extent the coefficient of friction influences the contact pressure between the surface of a gasket and the face of a flange a basic calculation was done. The calculation was based on a method suggested by Drago [38], and both the flange sizes and internal pressures were varied. By varying the internal pressures and flange sizes a conclusion may be drawn as to where (with regards to flange size and internal pressure) the coefficient of friction will have the greatest effect. Drago [38] made the following assumptions for this simplified calculation:

1. The flanges are assumed to be stiff, with no bending and deflection while the bolts are being tightened.
2. Non-linear effects associated with the gasket are ignored. These include creep and stress relaxation of the gasket material.
3. The gasket material is assumed to be homogeneous.
4. The flange faces are smooth and does not have a gramophone finish.
5. There are no temperature effects on the fasteners, bolts, or gaskets.

The forces which are produced by the internal pressure and clamp load are balanced when a flange connection is on the verge of opening and blowing out the gasket [38]. For the calculations, below, the diagrams shown in Figure 3-19 are applicable.

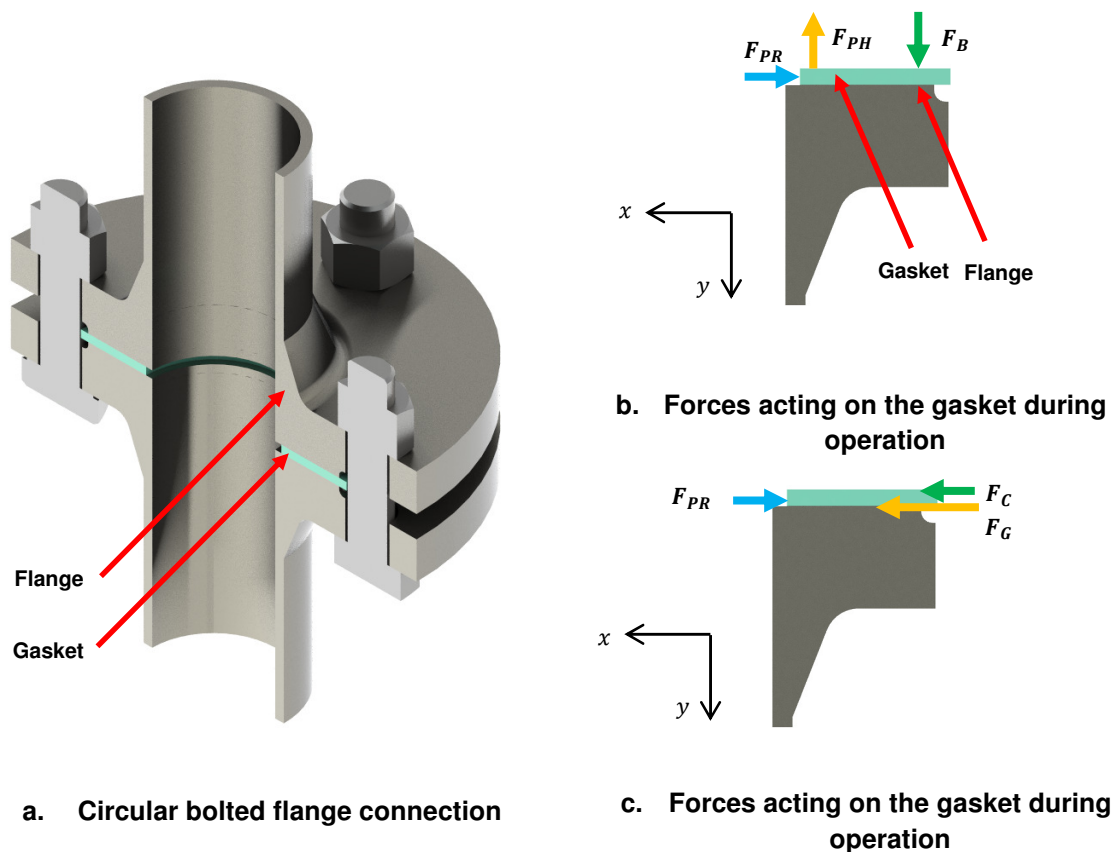


Figure 3-19: Free-body diagrams for the calculation method suggested by Drago [38]

$$F_G + F_C - F_{PR} = 0 \quad (3.1)$$

where:

$$F_G = \sigma_{GS} \left(\frac{2(D-d)}{2} \right) \cdot t = \sigma_{GS}(t(D-d)) \quad (3.2.)$$

where:

D Outer diameter of gasket [m]

d Inner diameter of gasket [m]

F_G Forced caused by the gasket's tensile strength [Pa]

t Thickness of gasket [m]

σ_g Compressive stress developed by the bolts on the gasket area [Pa]

σ_{gs} Tensile strength of the gasket [Pa]

$$F_C = \mu(F_B - F_{PH}) \quad (3.3.)$$

where:

F_B Force on the gasket due to the bolt pre-tension [N]

F_C Net radial force retaining the gasket in the connection [N]

F_{PH} Hydrostatic end force [N]

μ Coefficient of friction between the gasket and the flange surface

and:

$$F_B = \frac{\sigma_G \pi (D^2 - d^2)}{4} \quad (3.4.)$$

$$F_{PH} = \frac{P \pi d^2}{4} \quad (3.5.)$$

$$F_{PR} = P \pi d t \quad (3.6.)$$

Where:

P Internal pressure [Pa].

When Equations 3.5., and 3.6. are substituted in Equation 3.1 and re-written in terms of the contact stress between the gasket and the flange faces the following may be obtained:

$$\sigma_g = \frac{P \cdot (\mu \pi d^2 + 4 \pi d t) - 4 t \sigma_{gs} (D - d)}{\pi \mu (D^2 - d^2)} \quad (3.7.)$$

The values shown in Table 3-12 and Table 3-13 were assumed for this calculation. The nominal bore sizes with its relevant inner and outer gasket diameters are shown in Table 3-12. The coefficients of friction, internal pressures, thickness of the gasket, and tensile strength of the gasket are shown in Table 3-13. The coefficient of friction was increased in increments of 0.2 whilst the internal pressure was increased in increments of 2 MPa.

Table 3-12: Values assumed for the nominal bore, inner diameter, and outer diameter of the flange for the calculation method suggested by Drago [38]

Nominal bore [mm]	Inner diameter of gasket, d [mm]	Outer diameter of gasket, D [mm]
25	34	71
50	61	107
80	89	142
100	115	168
200	220	273
500	508	594
800	813	917
1 000	1 016	1 124
1 500	1 658	1 820
2 000	2 182	2 420
2 200	2 384	2 620
2 600	2 594	2 820
2 800	3 014	3 220
3 000	3 228	3 420
3 500	3 520	3 780
4 000	4 050	4 320

Table 3-13: Values assumed for the coefficient of friction, gasket thickness, internal pressure and tensile strength for the calculation method suggested by Drago [38]

Coefficient of friction, μ		Thickness of gasket, t [mm]	Internal pressure, P [MPa]		Tensile strength of gasket, σ_{gs} [MPa]
Lower limit	Upper limit		Lower limit	Upper limit	
0.2	1	3	2	8	12

The values shown in Table 3-12 and Table 3-13 were substituted in Equation 3.7. This gave the contact pressure between the flange face and gasket as a function of the gasket dimensions, the internal applied pressure, the thickness of the gasket and the tensile strength of the gasket. From the results it was observed that for differing values of the coefficient of friction at a specific pressure, gasket size, and internal pressure the biggest difference was between the values when $\mu=0.2$ and $\mu=1$. As a result of this the maximum contact pressure values at each of these coefficients of friction were subtracted from one another. This was done since this will give the biggest possible difference. These differences were plotted as a function of the internal pressure and nominal bore size. These results are shown in Figure 3-20.

From Figure 3-20 it may be observed that the biggest difference, as a result of the coefficient of friction, is 2.9 MPa. This value was obtained for a nominal bore of 200 mm at an internal pressure of 8 MPa. From the results it may also be observed that the difference increases as the pressure increases and the nominal bore size decreases (from a nominal bore of 200 mm). The effect of friction is, therefore, not negligible when considering the contact pressure between the gasket and the flange face.

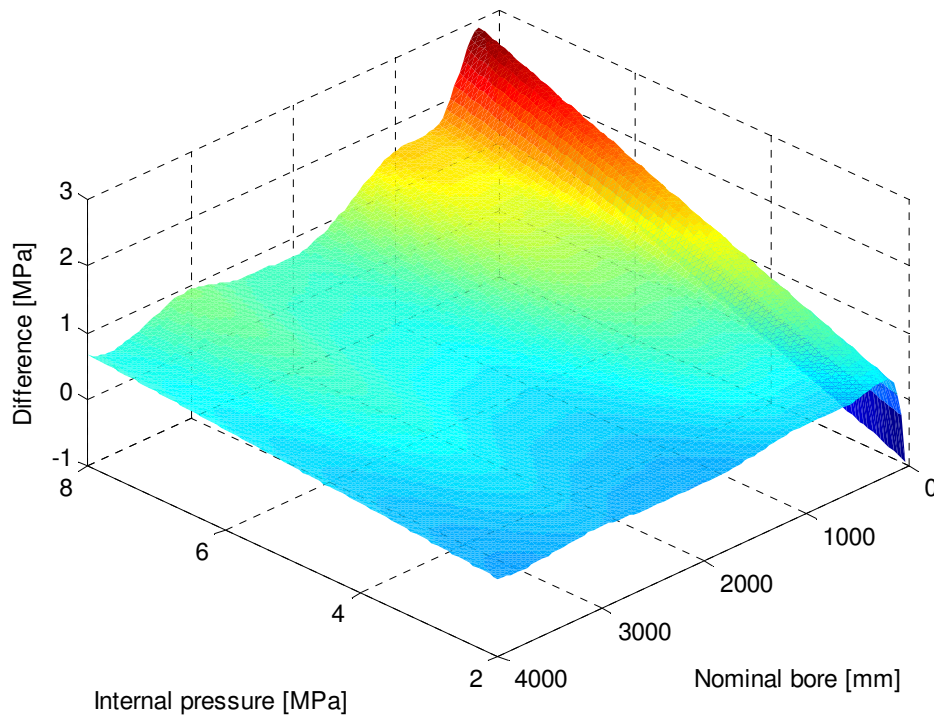


Figure 3-20: Difference in contact stress as function of the internal pressure and nominal bore when the coefficient of friction was $\mu=0.2$ and $\mu=1$

An additional investigation into the effect of friction was done by means of a simple finite element analysis. The final finite element model, as will be described at the end of this chapter, was used for this investigation. The boundary conditions and loads applied as described in Sections 3.4.4. and 3.4.5. were used. The only value which changed was that of the coefficient of friction. The effect which the value of the coefficient of friction has on the contact pressure between the faces of the flange and the gasket insert was investigated. This value was increased from 0.1 to 0.9 .

This investigation was done for both the flat face flange, and for the raised face flange. The first set of results shown is for the flat face flange immediately after seating. From Figure 3-21 and Figure 3-22 it may be observed that the value of the coefficient of friction between the gasket surface and the flange face may not be regarded as negligible for the seating condition. The maximum contact pressure, between the investigated values, was at a coefficient of friction of 0.3. The maximum contact pressure decreases as the value of the coefficient of friction is increased from 0.3 to 0.9 (Figure 3-22). A similar effect was observed in Section 3.3. when the effect of friction between the gasket surface and metal discs were investigated as part of the material characterisation.

Shown in Figure 3-21 are top views of a section of the gasket's contact pressure for the various coefficients of friction. The bolt is in-line where $y=0$ mm. This gives a good idea of the pressure distribution. As the coefficient of friction decreases from 0.9 to 0.3, the variation in the contact pressure, between the inside and outside diameter of the gasket insert, forms a sharper peak and the contact pressure is less distributed. A possible reason for this may be that for low coefficients of friction the material is able to easily deform along the contact plane – i.e the gasket becomes thinner and wider. This in turn results in a sharp peak along the central diameter of the gasket insert. The material near the inner and outer diameter of the gasket are however, still able to deform along the contact plane, hence the sharp reduction in contact pressure. For higher coefficients of friction the material becomes severely constrained, resulting in a small difference between the contact pressures at the inner and outer diameters of the gasket and the contact pressure located near the middle.

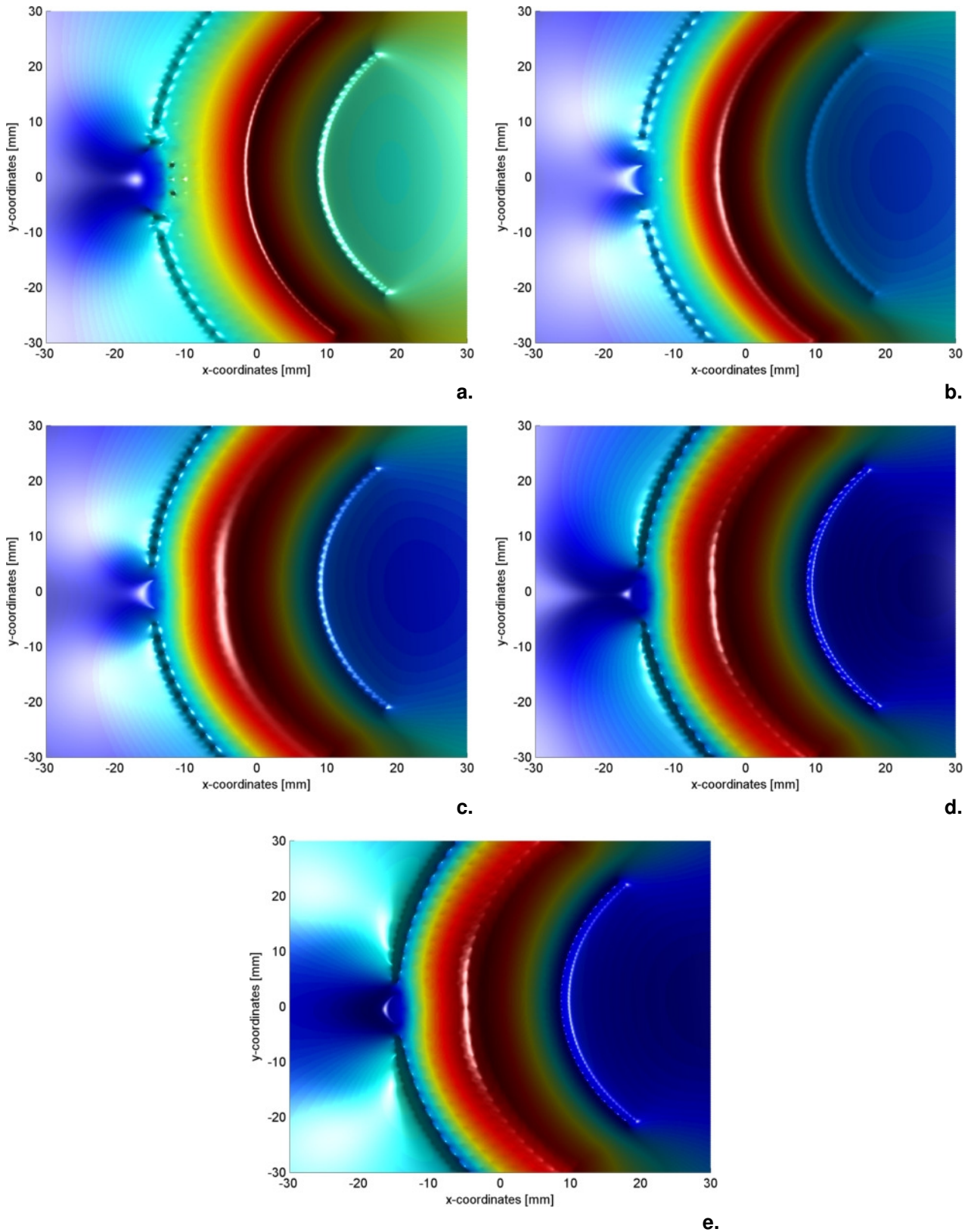


Figure 3-21: Calculated distribution of the contact stress, for a coefficient of friction of: (a) $\mu=0.1$, (b) $\mu=0.3$, (c) $\mu=0.5$, (d) $\mu=0.7$, (e) $\mu=0.9$, between the flat face flange and gasket insert immediately after seating

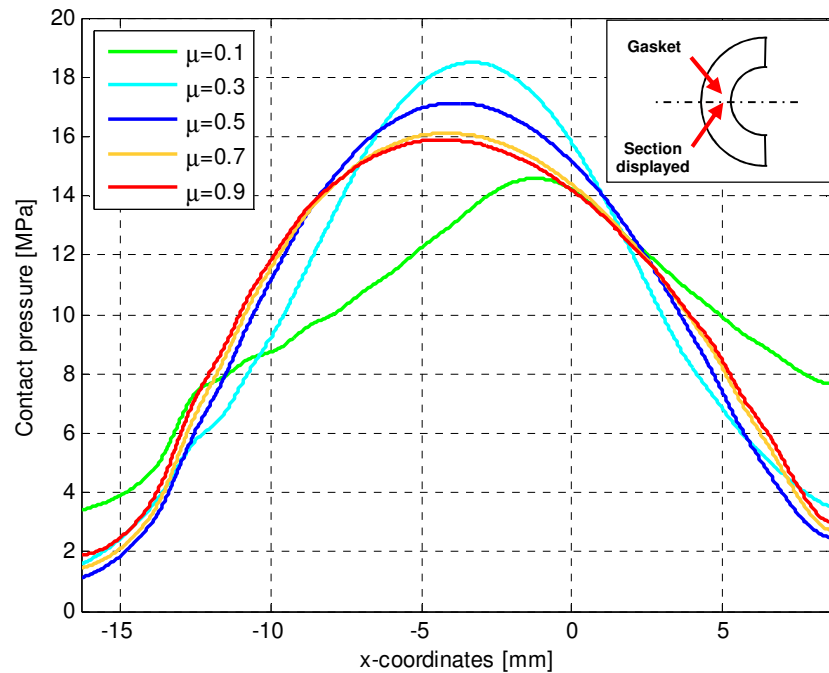


Figure 3-22: Variation in the contact pressure as a function of the coefficient of friction for the flat face flange after the bolts were tightened

The contact pressure was also determined after a period of 10 minutes. This allowed for creep-relaxation to influence the contact pressure between the gasket surface and the flange face. These results are given in Figure 3-23. From the results, it may be observed that the effect which differing coefficients of friction have on the maximum value, after a 10 minute period, was much less pronounced. The maximum value for the contact stress, after a period of 10 minutes, was 14.38 MPa for a coefficient of friction of 0.3. For the instance where the contact pressure was determined immediately after the bolts had been tightened the maximum value for the contact pressure at a coefficient of friction of 0.3 differed by 2.6 MPa when compared to the maximum contact pressure for a coefficient of friction of 0.9. After creep relaxation, however, this difference, between the maximum contact pressure at a coefficient of friction of 0.9 and 0.3, reduced to 0.8 MPa.

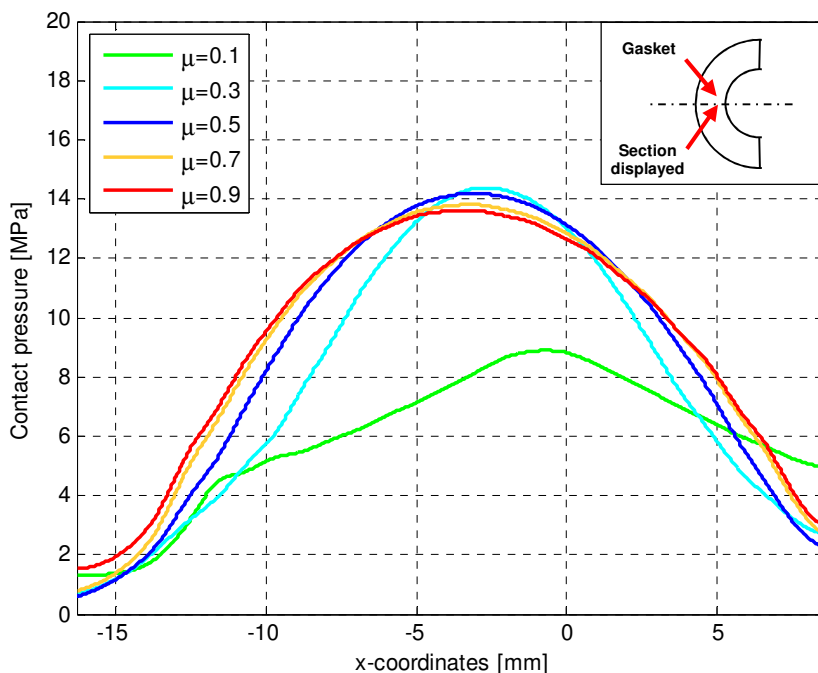


Figure 3-23: Variation in the contact pressure as a function of the coefficient of friction for the flat face flange after a period of 10 minutes

A similar analysis as before was done for the raised face flange where the coefficient of friction between the flange face and gasket was varied between 0.1 and 0.9. The results for the contact pressure between the gasket and raised face flange, immediately after seating, are shown in Figure 3-24 and Figure 3-25. Similar results were obtained for the raised face flange immediately after seating. The only difference, when compared to the results of the flat face flange, were the magnitudes of the contact pressures for the various coefficients of frictions. As shown in Figure 3-23, the flat face flange had a maximum value of 18.47 MPa for a friction of coefficient of 0.3, whilst the raised face flange had a maximum value of 22.87 MPa (Figure 3-24).

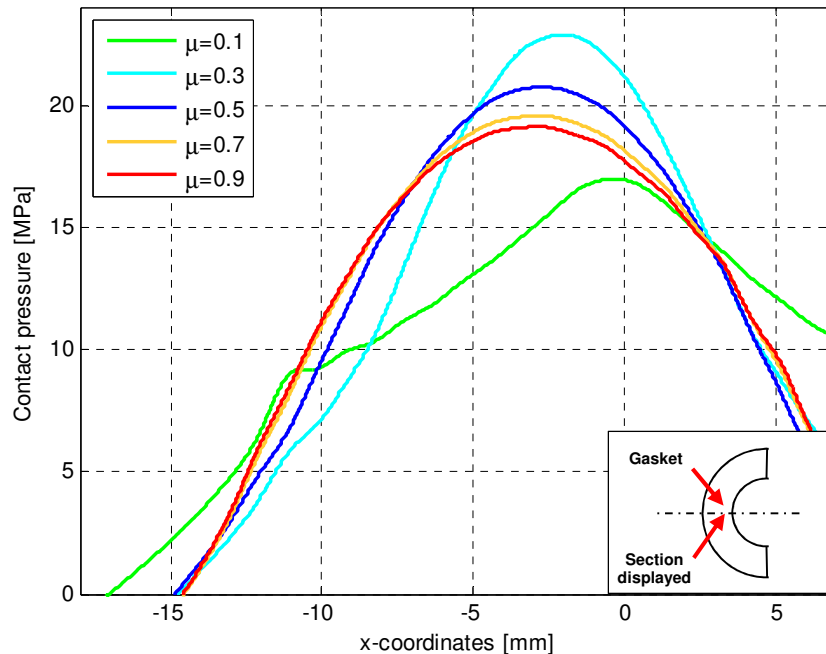


Figure 3-24: Variation in the contact pressure as a function of the coefficient of friction for the raised face flange after the bolts were tightened

In addition to determining the contact pressures, as a function of the coefficient of friction, immediately after seating they were also determined for a period of 10 minutes after the bolts had been fastened. For this instance the maximum contact pressure between the gasket and the raised face flange was 16.21 MPa for a coefficient of friction of 0.5 (Figure 3-26). When the results shown in Figure 3-26 are compared to those in Figure 3-24 it may be seen that the effect which the coefficient of friction has, after the bolts had been tightened and left for a period of time, was far less pronounced – as was the case with the flat face flange. The difference in the maximum contact pressures, for a coefficient of 0.3 and 0.9, was 4.4 MPa immediately after the bolts had been fastened. This difference reduced to 0.6 MPa after a period of 10 minutes.

The final part of the investigation compared the maximum values obtained for the various coefficients of friction for the flat face flange and for the raised face flange. These results are shown in Figure 3-27. It can be seen that the highest contact pressure value is obtained at a coefficient of friction of 0.3. This is true for both the raised face flange as well as for the flat face flange. The maximum contact pressure decreases as the value of the coefficient of friction increases from 0.3 to 0.9. The lowest contact pressure in both instances is obtained at very low values of the coefficient of friction – below 0.3.

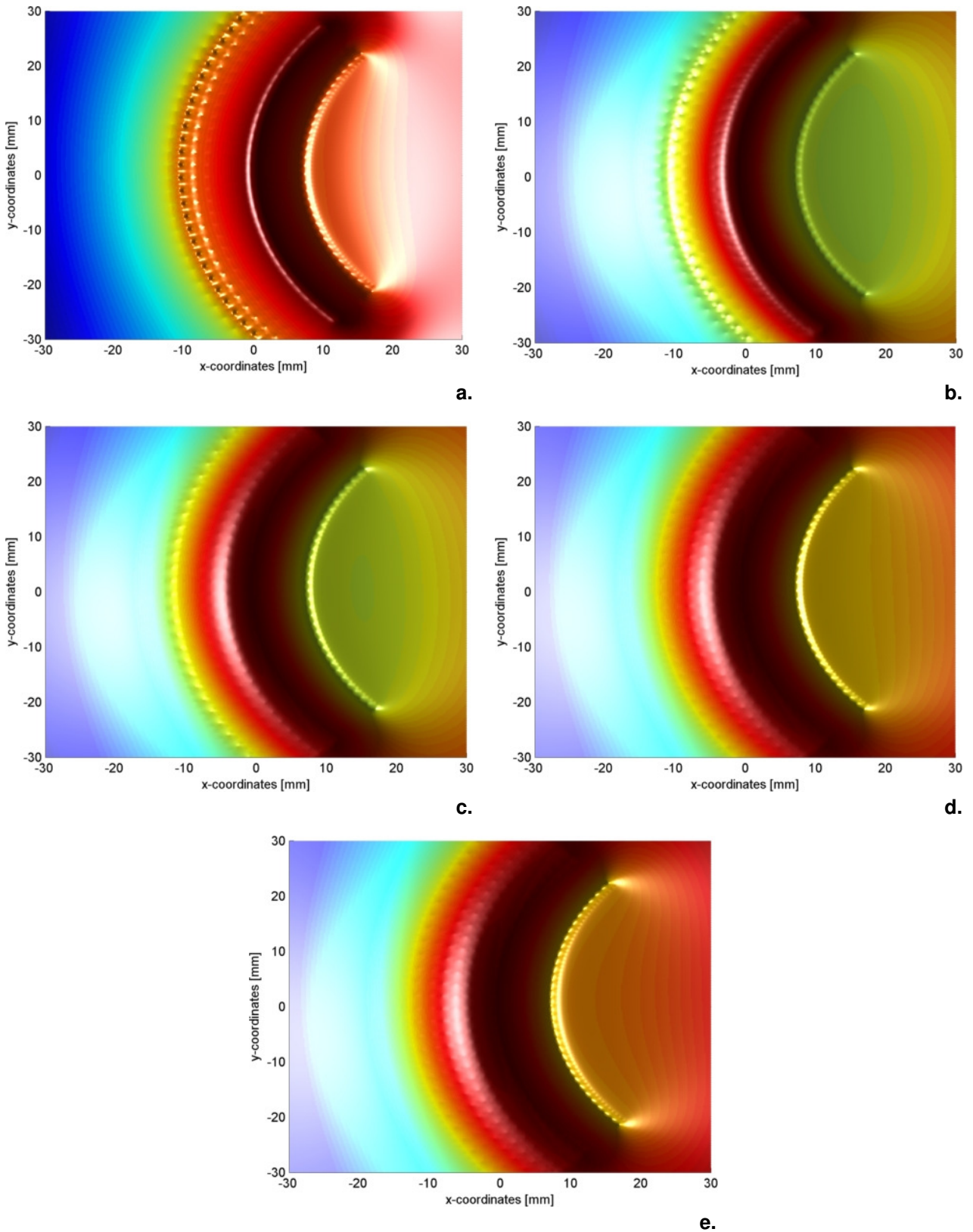


Figure 3-25: Calculation of the distribution of the contact stress, for a coefficient of friction of: (a) $\mu=0.1$, (b) $\mu=0.3$, (c) $\mu=0.5$, (d) $\mu=0.7$, (e) $\mu=0.9$, between the raised face flange and gasket insert immediately after seating

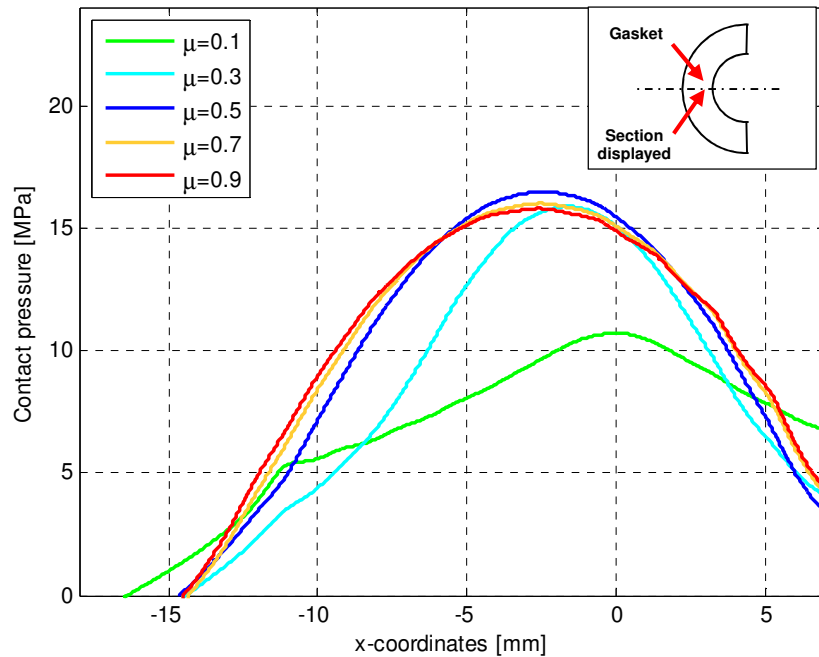


Figure 3-26: Variation in the contact pressure as a function of the coefficient of friction for the raised face flange after a period of 10 minutes

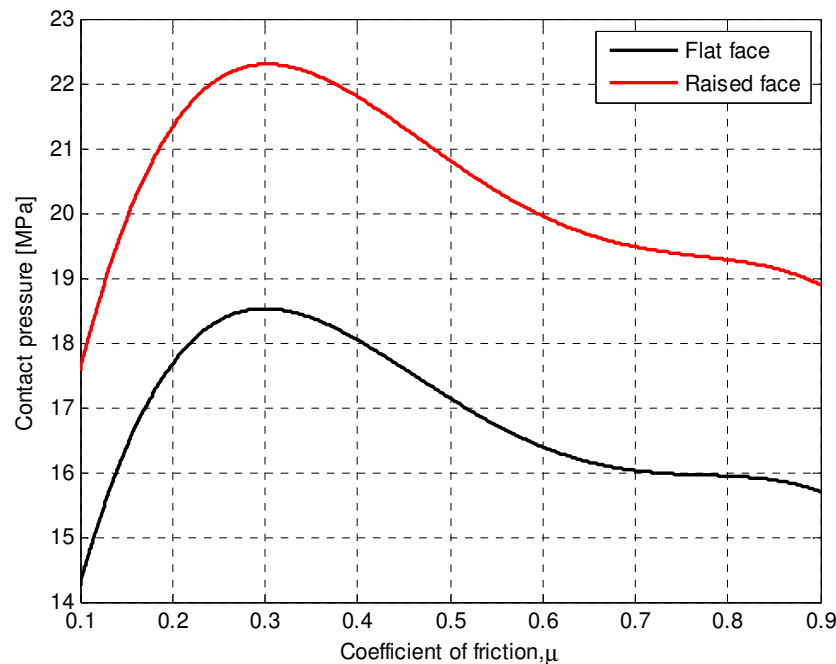


Figure 3-27: Comparison of the maximum contact pressure between the gasket insert and flat face and raised face flange for various coefficients of friction

3.4.3.2. Contact between the O-ring and flanges

As with the contact between the gasket and flanges, the contact between the O-ring and flanges was also assumed to be frictional. However, as before, the coefficient of friction between the surface of the O-ring and flange face was not experimentally determined. Due to this, it was necessary to investigate whether or not the exact coefficient of friction is important and whether or not it will have a significant effect on the results. Two sets of results were of particular importance in this case. Firstly, whether or not the contact pressure between the O-ring and flange faces changed as the value of the coefficient of friction changed and, secondly, whether the O-ring deformed significantly differently when the coefficient of friction was varied. The change in the contact pressure between the surface of the flange and the O-ring was determined for the seating conditions.

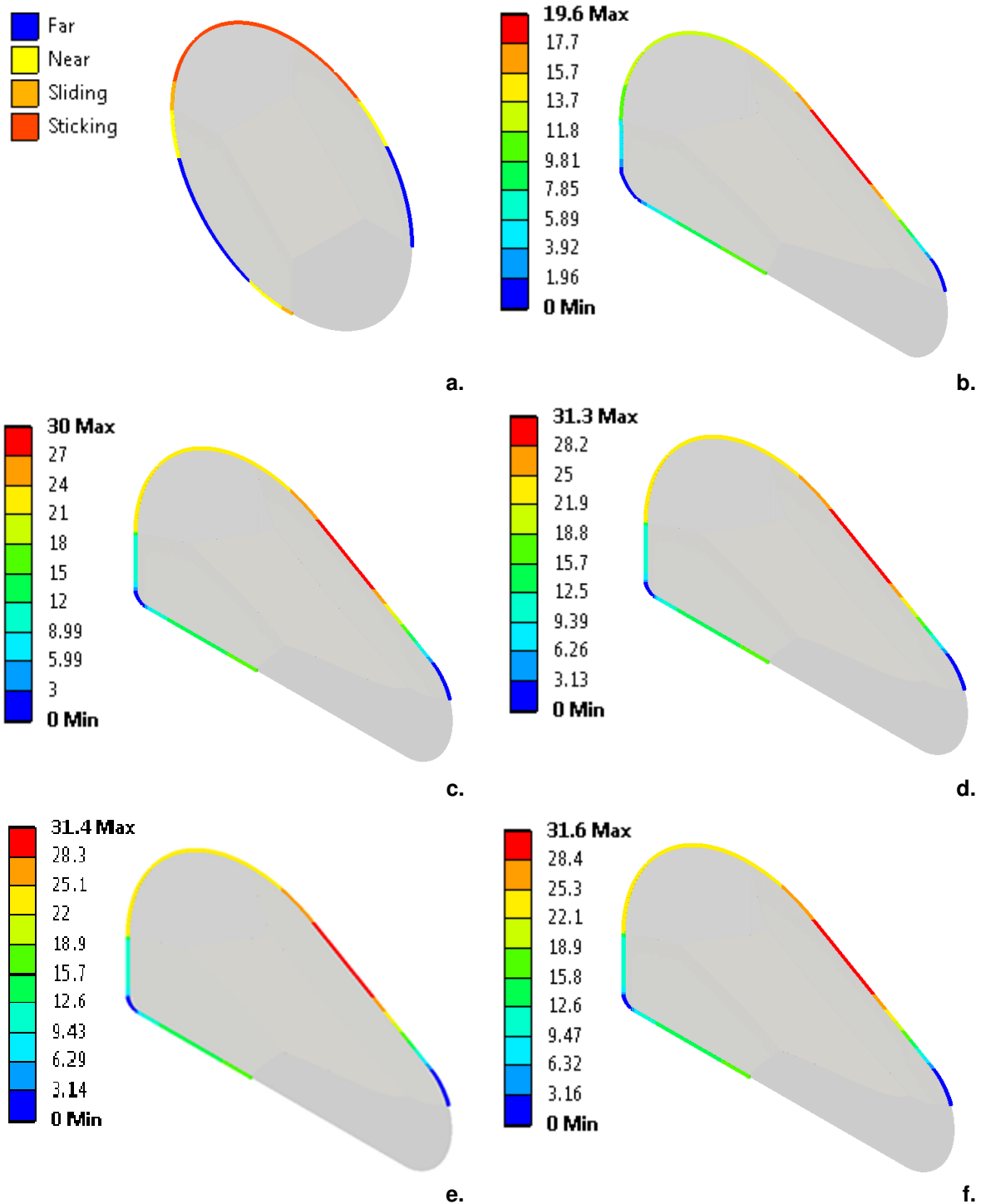


Figure 3-28: Contact pressure between the O-ring and flange face for (a) the underformed O-ring, and for the following coefficients of friction: (b) $\mu=0.1$, (c) $\mu=0.3$, (d) $\mu=0.5$, (e) $\mu=0.7$, (f) $\mu=0.9$

A very similar model to the one used in Section 3.3.2. was used in this instance to investigate the effect which the value of the coefficient of friction had on the deformation of the O-ring. The only significant difference, however, was that the O-ring and O-ring groove dimensions for the experimental setup were used. The dimensions of the O-ring groove are shown in Appendix B, whereas the dimensions of the O-ring are the same as those shown in Table 3-3. As with the material characterisation the model used for this investigation was a 2D axisymmetric model. Only the bottom plate was constrained against

displacement in the axial direction. A prescribed displacement of 1.3 mm was applied to the top plate. This value was chosen since it will result in complete closure, i.e. Body 1 and Body 2 will make contact.

Based on the results shown in Figure 3-28 it was found that the maximum contact pressure only increased by 5.1% when the coefficient of friction was increased from 0.3 to 0.9. At a coefficient of friction of 0.1, however, the difference was 38% when compared to the results at a coefficient of friction of 0.9. From these results it was assumed, for this investigation, that the coefficient of friction had a very small impact on the maximum contact pressure results obtained when the coefficient of friction was greater than 0.3.

For the second part of the investigation the deformation of the O-ring was considered. Shown in Figure 3-29 is a plot of the deformed O-ring, after bolting-up, for various coefficients of friction. From the results it may be observed that the deformation does not vary significantly. The largest variation in deformation existed near the top surface of the bottom flange at the side nearest to the bore.

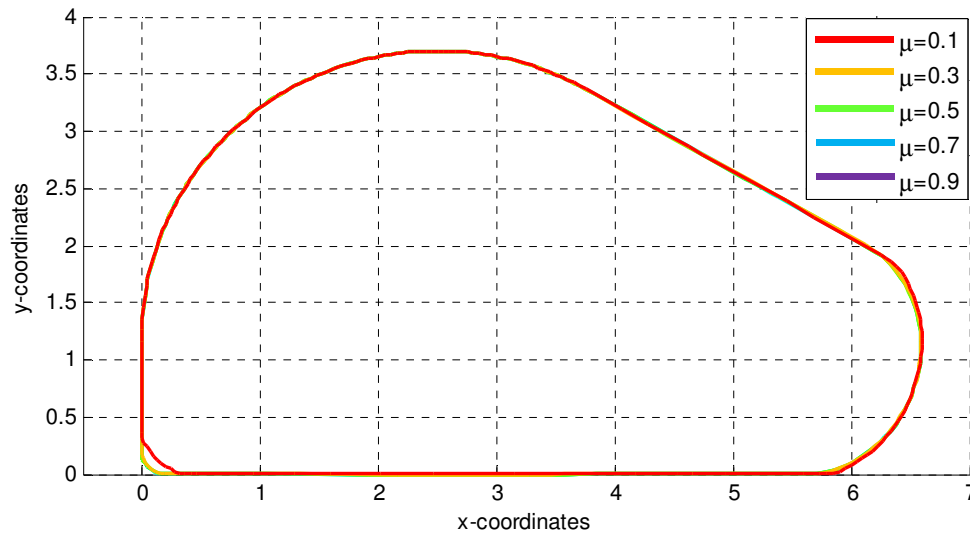


Figure 3-29: Deformation of the O-ring for different coefficient of friction values during seating

3.4.3.3. Assumed contact interfaces for the initial finite element modelling and analysis

Based on the aforementioned findings, the assumed contact interfaces between the various components are given in Table 3-14. In short, it was assumed that the nuts are bonded to the bolts, the fasteners (nut and bolts) are also bonded to the top surfaces of the flanges; and the gasket / O-ring has a frictional contact with the faces of the various flanges.

Table 3-14: Contact table for the finite element analysis of the experimental setup

	Top flange	Bottom flange	Top cap	Bottom cap	Bolts	Nuts	Gasket
Top flange	-	No contact	Bonded	No contact	Bonded	No contact	Frictional
Bottom flange	No contact	-	No contact	Bonded	No contact	Bonded	Frictional
Top cap	Bonded	No contact	-	No contact	No contact	No contact	No contact
Bottom cap	No contact	Bonded	No contact	-	No contact	No contact	No contact
Bolts	Bonded	Bonded	No contact	No contact	-	Bonded	No contact
Nuts	Bonded	Bonded	No contact	No contact	Bonded	-	No contact
Gasket / O-ring	Frictional	Frictional	No contact	No contact	No contact	No contact	-



3.4.4. Assumptions for the boundary conditions

For the finite element model of the experimental setup the boundary conditions were chosen to mimic those of the actual experimental setup. The experimental setup comprised of two flanges, two caps, a gasket / O-ring, fasteners, a top cap, a bottom cap, and a base plate. The bottom cap is mounted to the base plate and the circular bolted flange assembly is in-turn fastened to the bottom cap.

From the literature presented in Chapter 2, as well as from the results presented in Section 3.4.5.1., it was assumed that an axisymmetric model may be used for comparative purposes between the experimental setup and the finite element analysis if the bolt tightening increments are sufficiently large. It will be shown in Chapter 4 that a sufficiently large amount of bolt tightening increments were applied when the experiment was conducted, and an axisymmetric model may therefore, be assumed.

In order to replicate the physical constraint on the base cap as well as to implement an axisymmetric model, three boundary conditions needed to be applied. The first two boundary conditions were zero displacements normal to the axisymmetric surfaces. The third boundary condition which was applied was to fix the bottom cap. This was done by applying a full cylindrical constraint to the bottom cap. A full cylindrical constraint, constrains the selected face from any axial, radial, or tangential displacement. It was, however, desired to further simplify the model. One way was to omit the bottom cap. This, however, meant that the full cylindrical constraint could no longer be applied and an alternative boundary condition would need to be used. A decision was made to omit the bottom cap and replace the cylindrical constraint with a zero displacement on the bottom surface of the flange shell in the axial direction. This change had no effect on the strain values and contact pressures in all three cases. It was, therefore, decided to include this simplification in the finite element model.

3.4.5. Assumptions made for the loads

Two load conditions were applied to the circular bolted flange connections. These two loads were the bolt pretensions and the internal pressure.

3.4.5.1. Assumptions made regarding the bolt pretensions

It was briefly shown in Chapter 2 that the bolt tightening sequence and the number of increments have an effect on the contact pressure between the gasket and flange face as a result of flange rotation. For the initial finite element modelling and analysis it was desired to apply the bolt pretensions in such a way so as to ensure that a uniform load is applied to the flange / gasket. The bolt pretension was applied by making use of a solid bolt model and a pre-tension element as described in Chapter 2.

If the pretensions, which result from the bolt tightening, does not apply an axisymmetric pressure over the surface of the gasket, it will imply that only a full finite element model may be used to which the full tightening technique is applied. This is undesirable from a finite element analysis point of view, since an axisymmetric model which has a single bolt load, solves much faster due to the fact that it is less computationally expensive. It was, therefore, desired to apply all the bolt pretensions at the same time and within a single time increment.

Since this was impossible to mimic in the experimental setup a suitable bolt tightening technique, which was able to mimic this, needed to be found. As stated in Chapter 2, the following procedure should be followed when bolting-up a four bolt PN10 DN50 flange: Each bolt should, firstly, be tightened by hand following the sequence 1→3→2→4 (where bolts 1 through 4 are clockwise adjacent to one another). The next step is that the bolts should be tightened to within 30% of the final torque (following the same sequence). Step 2 is repeated until the bolts are tightened to within 60% of the final torque. For the final step, as with Steps 2 and 3, the bolts are tightened in the same sequence. However, in the final step the bolts are tightened to the final desired torque. This method was investigated with a finite element analysis of the full models of the raised face flange, and flat face flanges. This bolt tightening procedure was mimicked in the finite element analysis. In addition to this the number of increments per bolt were also increased. The number of bolt tightening increments were increased from three, in increments of three, to 24.

For each instance the strains at the locations where the flanges were instrumented (shown in Figure 3-30 and explained in greater detail in Chapter 4) were calculated. In total there were four locations which were instrumented. The strains at these four locations were measured in the radial, tangential, and transposed axial directions. The exact values for this investigation were not important. However, how the values varied was. The strains at each location for a specific bolt fastening procedure (either three increments per bolt, or 6 increments per bolt, etc.) were compared to the strains at the same location for a model where all of the bolts were completely fastened simultaneously. In addition to the comparison of the strain the contact pressure between the gasket and flange faces were also compared. As with the strains the contact pressures were calculated for each bolt tightening procedure and then compared to the case where the bolt loads were applied simultaneously.

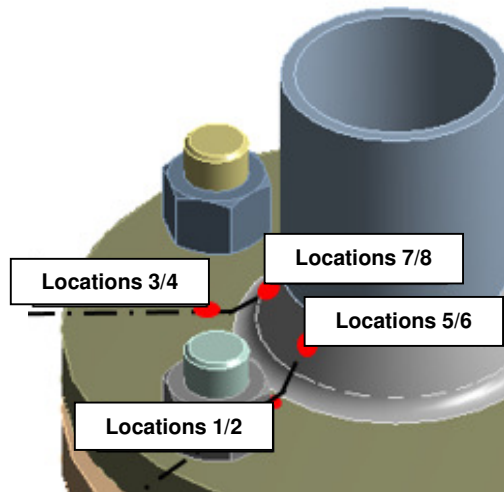


Figure 3-30: Positions of Locations 1 to 4 on the flange ring and hub

Similar results were obtained for the flat and raised face flange. As a result of this only the results for the flat face flange are shown. The first set of results shown is for the calculated strain values at the eight locations on the ring and hub of the flange. All the results lie within 5% when compared to the instance where the bolt load is equally distributed (all the bolt pretensions are applied instantaneously).

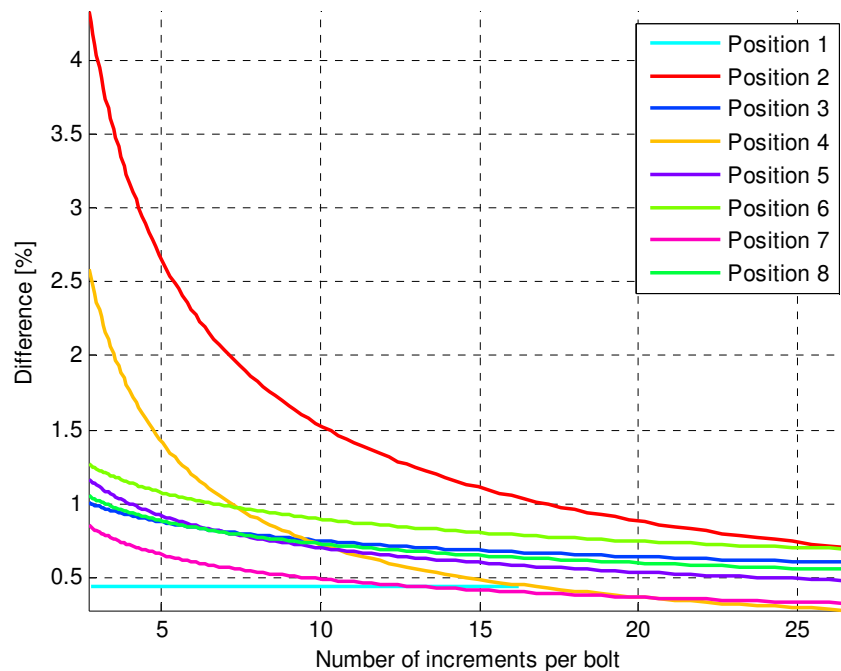


Figure 3-31: Difference in the calculated strain values, at the various strain gauge positions, as a function of the number of bolt tightening increments



The second set of results which were considered, was the difference between the contact pressure, between the flange face and the gasket surface, when an equally distributed load was applied (as is the case when all of the bolt pre-tension is applied at the same time), and when the bolts were individually fastened.

The contact pressure between the surface of the gasket and the flange face was determined at four locations. These four locations are: in-line with Bolt 2 and 3, midway between Bolts 1 and 2, and midway between Bolts 3 and 4. These locations are shown in Figure 3-32 (a). For the instance where an equally distributed load was applied the contact pressure could be assumed to be axisymmetric since all the pressures in-line and in-between the bolts corresponded. When the bolt loads were, however, applied in individual increments the differences in contact pressure between two regions, which corresponded for the case where all of the bolt loads were applied, were compared. The biggest difference in contact pressures between the relevant regions was observed to be at the four aforementioned locations. It was for this reason that these locations were selected.

From the results shown in Figure 3-32 it may be observed that the difference in pressure decreases as the number of increments per bolt increases. A maximum pressure difference of 5.1 MPa exists at Location 2 when three increments per bolt is applied. The minimum pressure difference, when three bolt loads are applied, is 2.8 MPa. When a total of eight tightening increments per bolt is, however, applied three out of the four locations differ by less than 1 MPa when compared to the case where the bolt loads are applied simultaneously. The maximum difference is at Location 2 and is 1.3 MPa. From Figure 3-32(c). to Figure 3-32(f). the following was observed: the pressures at Locations 1 and 2 are higher than the contact pressure which is predicted by the case where the bolt loads are applied simultaneously. The pressure from Locations 3 and 4 are, however, lower. As the number of tightening increments are increased, the contact pressure at Locations 1 and 2 becomes lower, and the contact pressure at Locations 3 and 4 increases.

From both the results of the predicted strains and contact pressures the following may be concluded: As the number of tightening increments per bolt increases the predicted strains and contact pressures tends towards the case where the bolt loads are applied both simultaneously and instantaneously and allows for an axisymmetric approximation of the full model. For this investigation it was assumed that an axisymmetric model may be assumed when a minimum of eight tightening increments per bolt were applied.

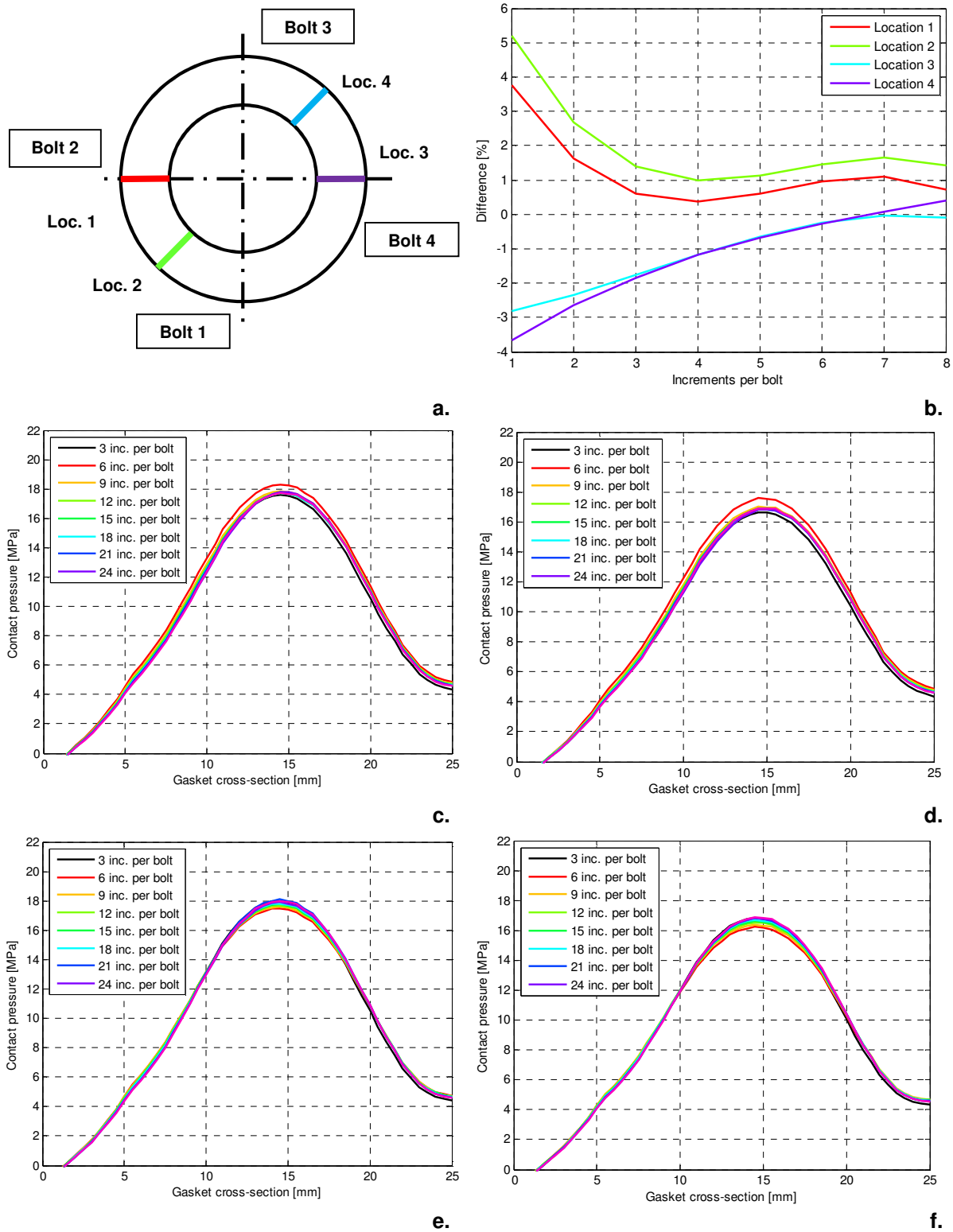


Figure 3-32: (a) Locations of where pressure distributions were compared, (b) reduction in contact pressures at the locations, (c, d, e, f) stress distributions at Locations 1, 2, 3, and 4

3.4.6. Meshing of the finite element models

The finite element models for all three the different circular bolted flange connections were automatically meshed and refined in ANSYS 16.2.

The mesh refinement was based on a convergence study done in ANSYS. The maximum allowable change for the strains in the tangential and radial direction of the flange were limited to 1%. Similarly the change in the maximum contact pressure between the flange face and gasket insert surface, as well

as the change in the maximum axial strain in the modified M16 bolt were also limited to 1%. The mesh refinement was done on the surface of the flange ring and hub as well as on the bolt and gasket. This was done since these were the areas where the strain gauges were instrumented and the contact pressure measurements were taken. The number of elements and nodes applicable to each model, after the convergence was done, is shown in Table 3-15, for different flange connections.

Table 3-15: Number of nodes and elements for the various flange configurations

Flange type	Nodes	Elements
Flat face	131 867	88 063
Raised face	128 260	85 190
Raised face with an O-ring groove	120 186	58 521

3.4.7. Application of the contact interface, loads, and boundary conditions

The way in which the loads and boundary conditions were applied to the finite element model are shown in Figure 3-33. This was applicable to all three the different flange configurations. In addition to this, shown in Figure 3-34 and Figure 3-35, was the application of the contact interfaces with regards to the type of contact, the designation of the target body, and the designation of the contact body. The contact interfaces shown in Figure 3-34 are applicable to both the flat face flange and raised face flange, whilst the contact interfaces shown in Figure 3-35 are applicable to the raised face flange with an O-ring groove.

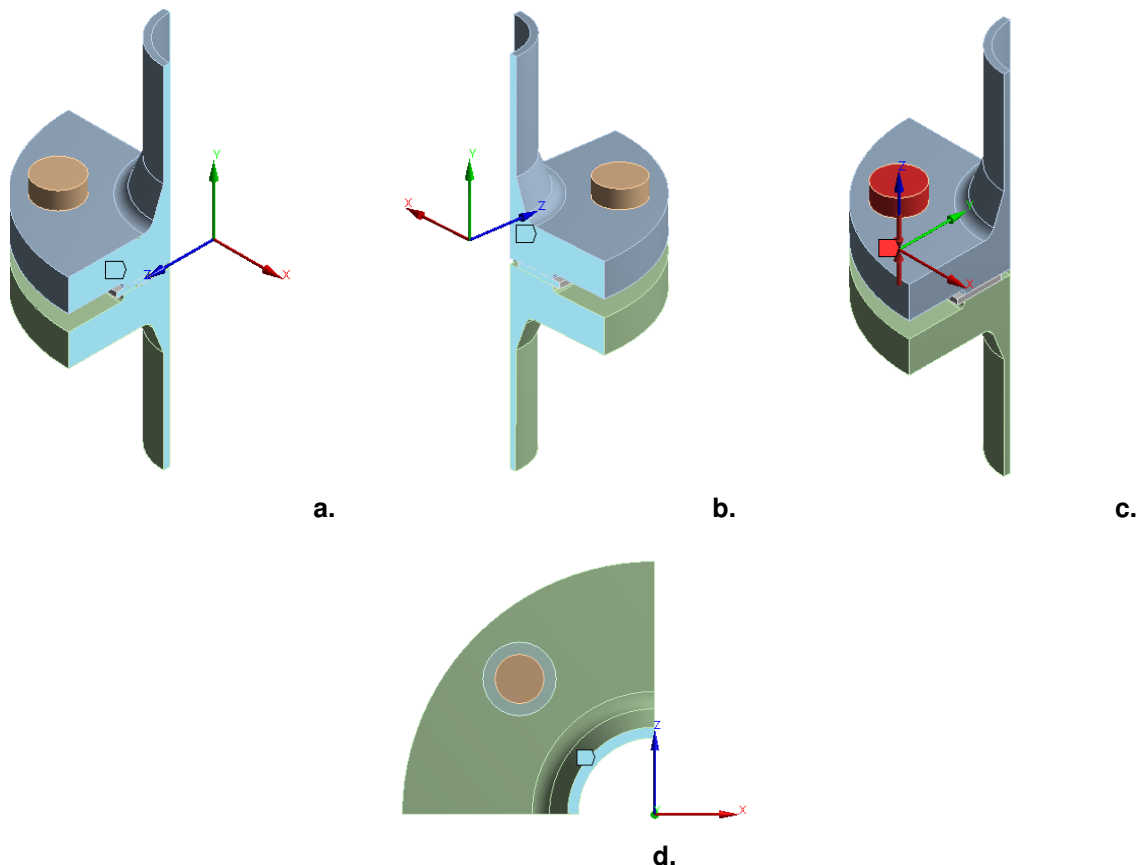


Figure 3-33: (a, b) Application of zero displacement normal to the surface of the flange in the tangential direction, (c) application of bolt pretension, and (d) zero displacement in the axial direction

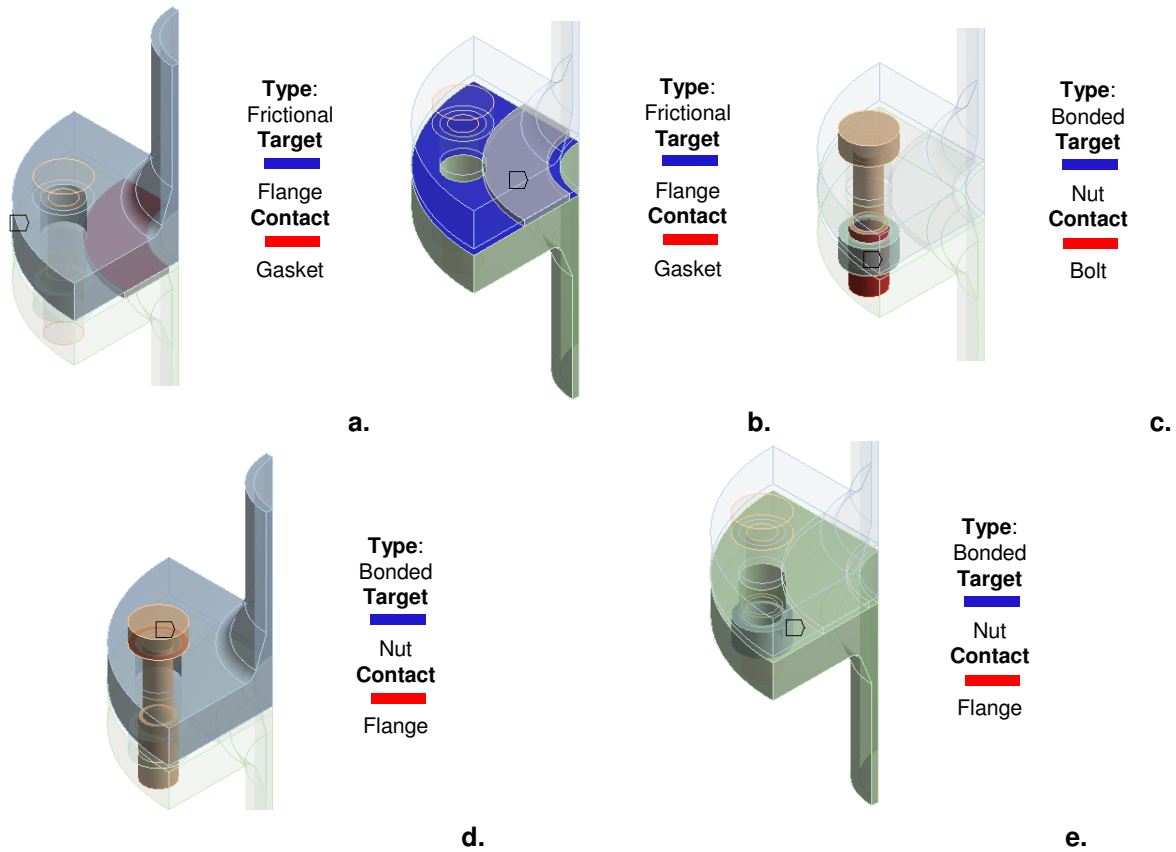


Figure 3-34: Contact interfaces between: (a) gasket and top flange, (b) gasket and bottom flange, (c) nut and bolt, (d) bolt and top flange, and (e) nut and bottom flange for the flat and raised face flanges

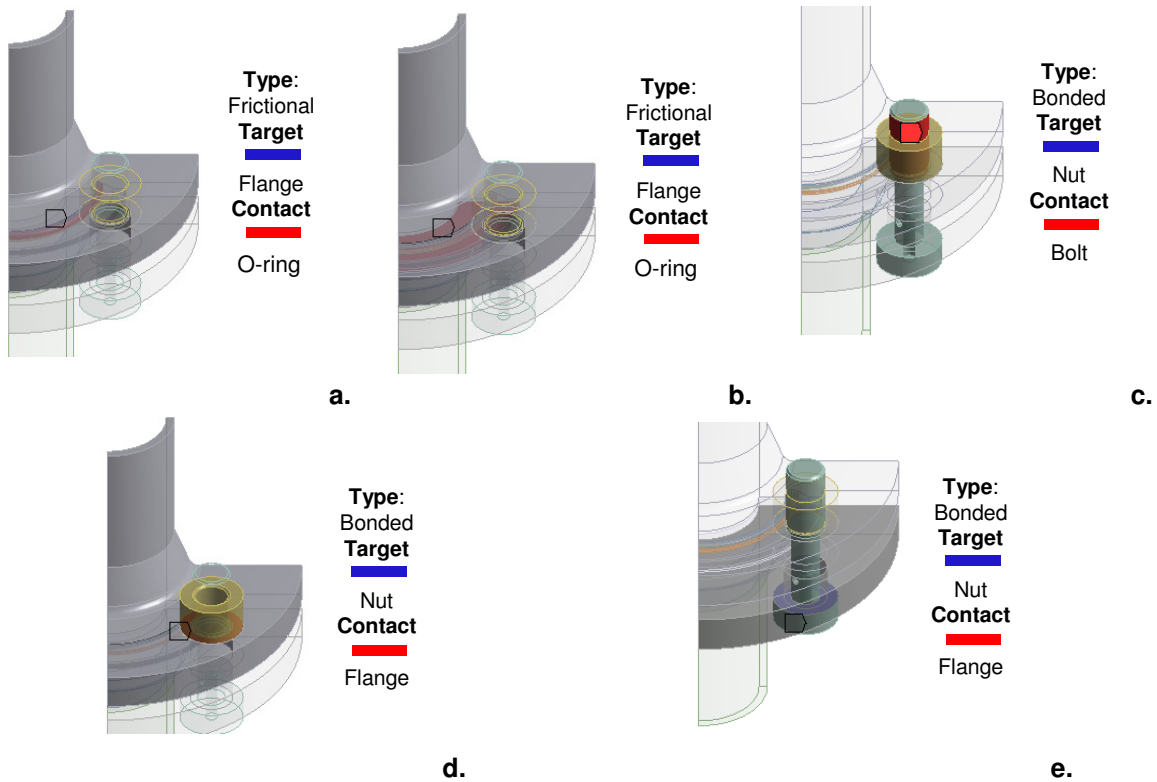


Figure 3-35: Contact interface between: (a) O-ring and top flange, (b) O-ring and bottom flange, (c) nut and bolt, (d) bolt and top flange, and (e) nut and bottom flange for the raised face flange with an O-ring groove

3.5. Results from the initial finite element modelling and analysis

The results from the finite element modelling and analysis are split into two sections. The first section shows all of the calculated strains, for the three flange configurations, at the locations where the flange was instrumented (discussed in Chapter 4). The second section shows the results for the contact pressure between the gasket and flat face flange, and the gasket and the raised face flange.

3.5.1. Results for the initial finite element model and analysis of the flat face flange

Shown in Table 3-16 is a summary of all the predicted strain results.

Table 3-16: Summary of the strains from the finite element analysis for the flat face flange

Strain gauge position	Flat face		Raised face		O-ring
	Strain before creep-relaxation [$\mu\text{m/m}$]	Strain after creep-relaxation [$\mu\text{m/m}$]	Strain before creep-relaxation [$\mu\text{m/m}$]	Strain after creep-relaxation [$\mu\text{m/m}$]	Strain [$\mu\text{m/m}$]
1.	204.62	170.47	201.52	141.31	255.68
2.	85.25	70.42	97.99	71.86	80.57
3.	108.57	84.76	83.35	68.42	108.32
4.	253.20	212.23	261.27	187.89	236.33
5.	71.62	58.58	68.73	53.67	87.09
6.	164.06	132.68	164.06	123.80	140.47
7.	85.95	61.66	116.82	87.55	75.73
8.	165.07	132.62	160.35	120.52	145.28

3.5.2. Results for the predicted contact pressures

This section is split into two subsections, one for the results of the flat face flange and one for the results of the raised face flange.

3.5.2.1. Predicted contact pressure results for the flat face flange

From the results shown in Figure 3-36 it may be observed that a peak contact pressure of 17.5 MPa is obtained. This peak pressure is located along a diameter between the inside and outside diameter of the gasket insert. The contact pressure decreases towards the inside and outside diameters of the gasket insert.

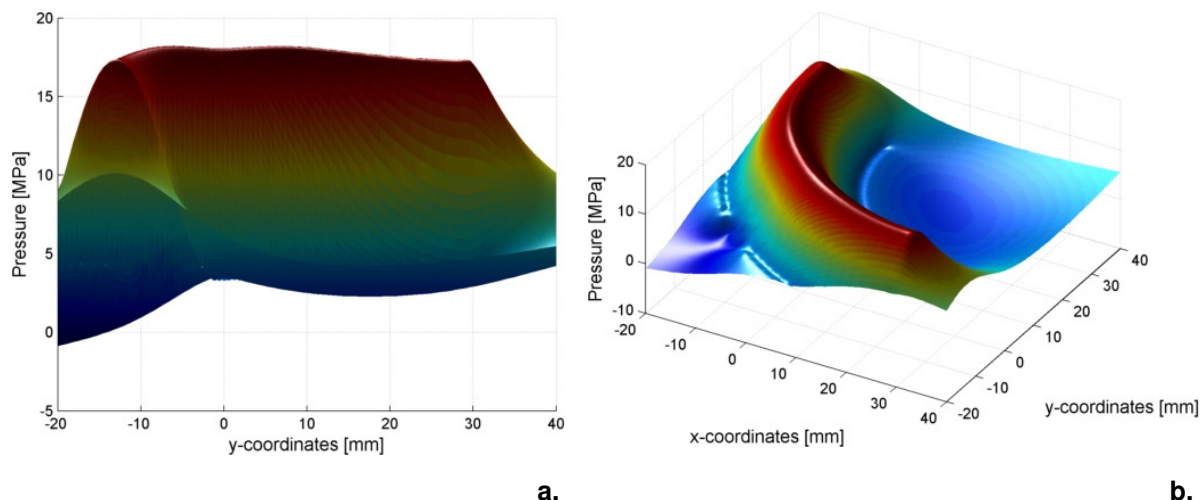


Figure 3-36: The predicted contact stress between the gasket insert and the flat face flange right after bolt tightening for the (a) front and (b) isometric views

Figure 3-37 shows the results for the predicted contact pressure between the flat face flange and the gasket insert after creep-relaxation has taken place. From Figure 3-37 it may be seen that the peak contact pressure is 14.3 MPa. This implies a reduction of 18% in the contact pressure from right after the bolt loads were applied until after the 10 minute period.

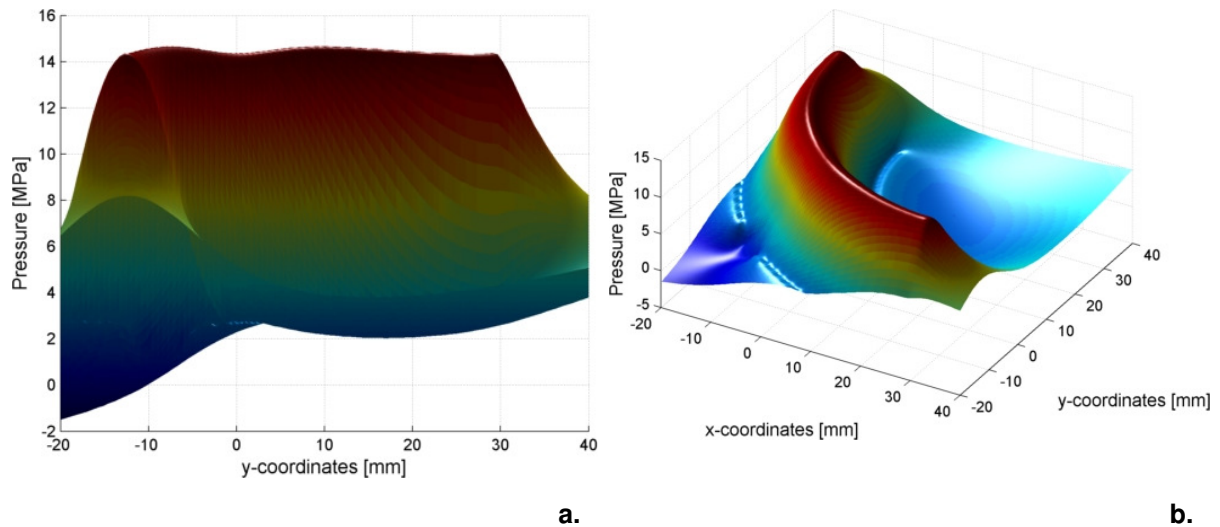


Figure 3-37: The predicted contact stress between the gasket insert and the flat face flange after a period of 10 minutes for the (a) front and (b) isometric views

3.5.2.2. Predicted contact pressure results for the raised face flange

A peak pressure of 22.9 MPa was predicted for the raised face flange, as shown in Figure 3-38. This is 31% higher than the maximum contact pressure calculated for a period of 10 minutes after the bolts had been tightened (Figure 3-39). As before, the peak pressure was between the bolts along diameter between the inner and outer diameter, of the gasket. The general shape of the contact pressure remains the same from immediately after the bolts were tightened until 10 minutes after the bolts were tightened. The only difference is in the magnitude of the contact pressure.

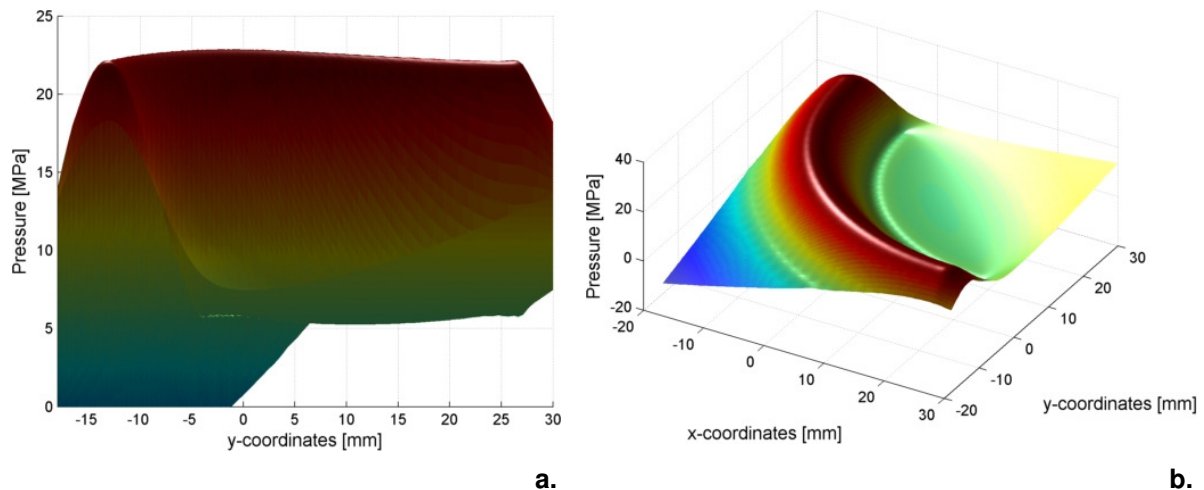


Figure 3-38: The predicted contact stress between the gasket insert and the raised face flange right after bolt tightening for the (a) front and (b) isometric views

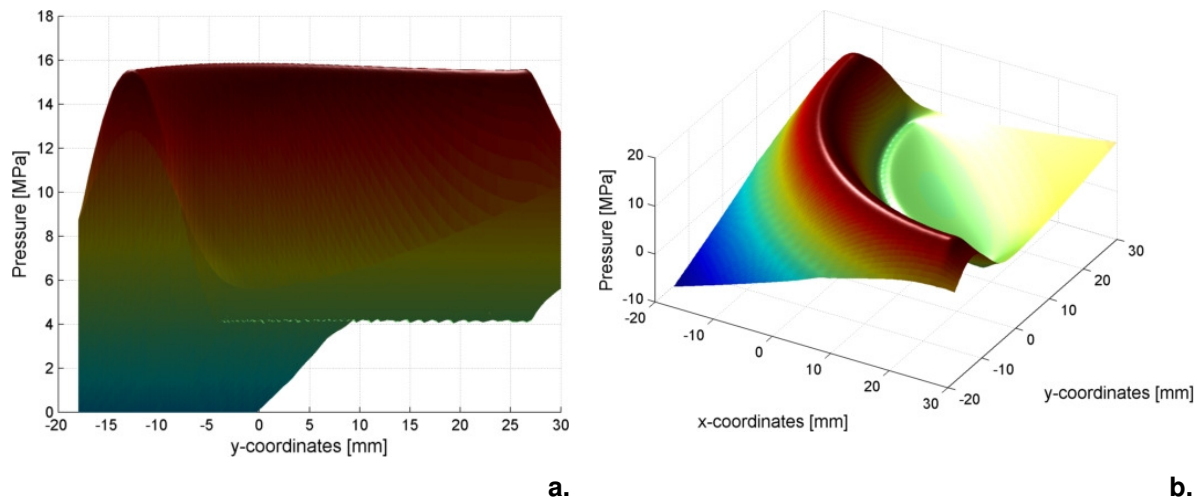


Figure 3-39: The predicted contact stress between the gasket inset and the raised face flange after a period of 10 minutes for the (a) front and (b) isometric views

3.6. Conclusion for the initial finite element modelling and analysis

This conclusion is split into two subsections. The first subsection deals with the strains and contact pressures which were calculated for the various flange designs. The second subsection focuses on the additional investigations done improve the quality of the non-linear finite element models.

3.6.1. Discussion of the calculated strains and contact pressures

3.6.1.1. Flat face flange

From the initial finite element modelling and analysis of the flat face flange the maximum and minimum strains calculated were $253.20 \mu\text{m/m}$ and $71.62 \mu\text{m/m}$, respectively, for the instance immediately after the bolts were tightened, from the predefined locations shown in Figure 3-30. The maximum calculated strain was in the tangential direction on the ring of the flange, in-between the bolts. The minimum calculated strain, on the other hand, was located on the hub of the flange, in-between the bolts, in the transposed axial direction. The strains reduced by between $\sim 17\%$ and $\sim 28\%$ due to creep relaxation.

A maximum contact pressure of 17.5 MPa was calculated for the interface between the surface of the gasket and the face of the flange. This maximum contact pressure was located along a diameter between the inner and outer diameter of the gasket and in-line with the bolt. The maximum pressure reduced by 18% to 14.3 MPa from immediately after the bolts were tightened until a period of 10 minutes afterwards, due to creep-relaxation.

3.6.1.2. Raised face flange

The calculated strain results for the raised face flange are comparable to those of the flat face flange. The maximum and minimum calculated strains were $261.27 \mu\text{m/m}$ and $68.77 \mu\text{m/m}$, respectively. These values were located at the same positions as the maximum and minimum values for the flat face flange. As before, the effect of creep-relaxation reduced the calculated strains. The reductions in strains, for the raised face flange, were marginally higher than for the flat face flange and lay between $\sim 18\%$ and $\sim 30\%$.

The maximum contact pressure for the raised face flange, as for the flat face flange, was located along a diameter between the inner and outer diameters of the gasket, and in-line with the bolt. A maximum contact pressure of 22.9 MPa was calculated for the raised face flange. This is $\sim 24\%$ greater than the maximum contact pressure calculated for the flat face flange. As before, the maximum contact pressure reduced from immediately after the bolts were fastened until a period of 10 minutes had elapsed. The maximum calculated contact pressure reduced to 16 MPa .



3.6.1.3. Raised face flange with an O-ring groove

Only the calculated strain immediately after the bolts had been fastened were considered for the raised face flange with an O-ring groove. The maximum calculated strain was in-line with the bolt, in the axial direction, on the ring of the flange, and was $255.68 \mu\text{m/m}$. The minimum calculated strain on the other hand was, $75.73 \mu\text{m/m}$ and was located in-line with the bolt, on the hub of the flange, and in the transposed axial direction.

3.6.2. ***Discussion of the results of the material modelling, selected coefficients of friction, and the number of bolt increments***

3.6.2.1. Material modelling

It was found, from the material characterisation, that the behaviour of the non-asbestos, compressed fibre gasket with aramid fibre and nitrile binder could be approximated by assuming a non-linear viscoelastic model. The non-linear viscoelastic model was created by using a Neo-Hookean material model and Prony shear relaxation. The use of a non-linear viscoelastic material model allowed for the accurate prediction of the creep-relaxation behaviour of the gasket as well as the contact pressure distribution between the surface of the gasket and face of the flange. A third order Ogden material model, on the other hand, gave suitable results for the behaviour of the nitrile O-ring.

3.6.2.2. Effect of the coefficient of friction between the packing materials and flange faces

From the initial finite element modelling and analysis it was found that the coefficient of friction between the gasket and the flange face plays a significant role in the amount of initial gasket closure (seating condition), and the closure due to creep-relaxation (operating condition). A reduction in the coefficient of friction will result in an increase in both gasket closure during the seating phase, as well as the closure due to creep-relaxation during the operating phase. A reduction in the coefficient of friction, for both the flat and raised face flanges, will result in higher maximum contact pressures. The higher maximum contact pressure will, however, be more localised than the contact pressure for higher coefficients of friction. In addition to this it was also found that the coefficient of friction selected / determined will have a greater effect on the contact pressure of small diameter flanges which operate at high pressures than on large diameter flanges which operate at low pressures.

The coefficient of friction between the O-ring and the face of the flange, however, had a much less significant effect. A slight increase (5%) in the maximum contact pressure was calculated for a coefficient of friction of 0.3 and 0.9. The effect of the coefficient of friction on the total deformation of the O-ring was also assumed to be negligible.

3.6.2.3. Number of bolt increments

For a EN 1092-1 PN 10 DIN 50 flat face flange, raised face flange, and raised face flange with an O-ring groove, it was found that as the difference between the assumption of an ideal model (where the strains and contact pressure are axisymmetric) and real-life scenario decreased as the number of increments per bolt were increased. Suitable results, where the difference is less than 5%, could be obtained by following the standard bolt tightening procedure as prescribed by ASME.

CHAPTER 4: EXPERIMENTAL SETUP AND RESULTS

4.1. Overview of the experimental setup and results

The purpose of this chapter was to present the validation of the results obtained from the initial finite element modelling and analysis. This chapter, therefore, focuses on: the experimental values which needed to be determined for the validation of the finite element modelling and analysis; the experimental setup; the data acquisition systems which were used; the experimental procedure, and the experimental results. In addition to this the experimental results obtained were compared to those calculated by the initial finite element models and analysis.

4.2. Experimental values which were determined for the validation

The experiment included the following, during as well as after bolt tightening / gasket seating:

1. Strain gauge measurements on the flanges.
2. Strain gauge measurements on the fasteners.
3. Contact pressure measurements between the gasket surface and flange faces.

For the strain measurements on the flange, it was decided to follow a similar approach to that of Bouzid *et al.* [30] and Sawa *et al.* [33], as discussed in Chapter 2. The strains, on the flange, were measured both in-line with the fasteners as well as in-between the fasteners. Strains on both the flange ring and flange hub were measured. It is known that there is a significant difference between the actual axial strains in a bolt and those which may be calculated based on the input of a torque wrench. Based on this it was decided to modify and instrument a bolt with strain gauges in such a way so as to obtain the actual axial strains on the bolt. Finally, for a circular bolted flange connection, which makes use of a gasket, the contact pressure between the gasket surfaces and the flange faces were of particular interest. It was, therefore, decided to make use of a TekScan pressure sensor, which was able to measure the contact pressure between the gasket surface and flange face.

4.3. Experimental setup

Three different circular bolted flange connections were considered in this investigation. Although the experimental setup remained essentially the same, three different flange pairs were used. The experimental setup for each of the flange pairs are shown in Figure 4.1 to Figure 4.3.

In all three instances the experimental setup comprised of the following components: a flange pair; four M16 Class 8.8 steel bolts, four M16 nuts, a top cap, a bottom cap, a base plate, four M8 bolts, packing material, and four M8 nuts. The bottom cap was bolted to the base plate by means of the four M8 bolts and nuts. The bottom flange was able to screw onto the bottom cap since the shell of the bottom flange and bottom cap were threaded. The packing material (either the gasket insert or O-ring) was placed between the top and bottom flange faces. The flange pairs were bolted together by means of the four M16 bolts and nuts. Finally, in a similar fashion to the bottom cap, the top cap screwed onto the top flange.

Although the actual axial strains in the bolts were measured by means of strain gauges, a torque wrench was used to fasten the bolts and assemble the circular bolted flange connections. This was done to ensure that the torque was applied in set increments.

In addition to the components of the circular bolted flange connection a TekScan model No. 5051-10 000 psi pressure sensor, and its relevant components were also used in the experimentation. The TekScan equipment was used to determine the contact pressure between the top flange face and the top surface of the gasket insert. The contact pressure measurements were only done for the flat face and raised face flanges and not for the modified raised face flange with an O-ring.

An Edaq Lite data acquisition system was also used. The purpose of the Edaq Lite data acquisition system was to obtain all of the strain measurements from the strain gauges at the various locations on the flange and modified M16 bolt.

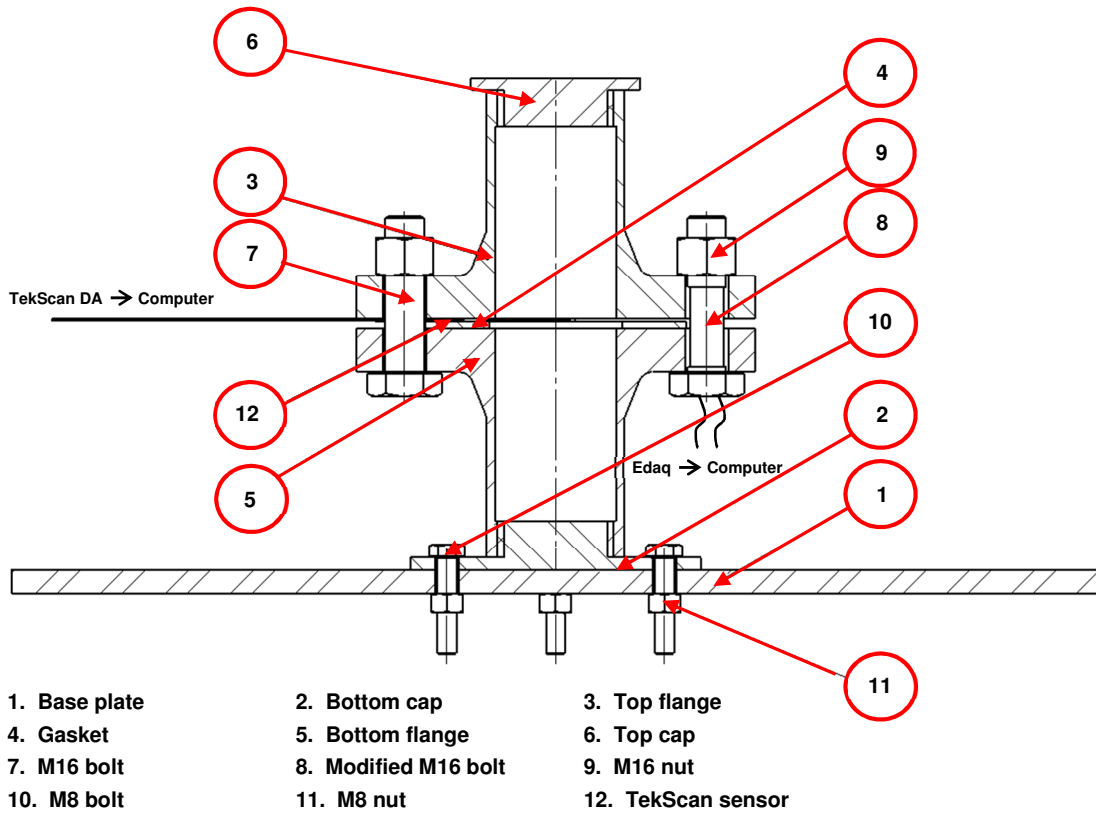


Figure 4-1: Experimental setup for the flat face flange

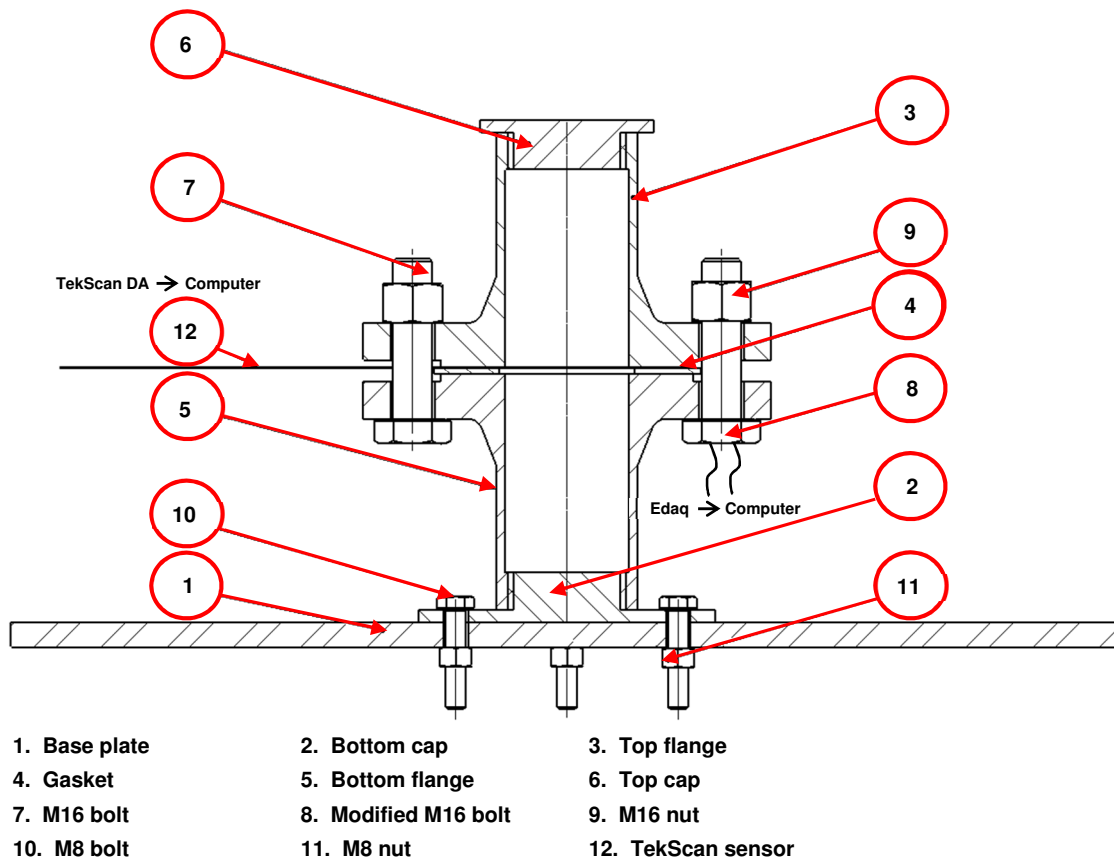


Figure 4-2: Experimental setup for the raised face flange

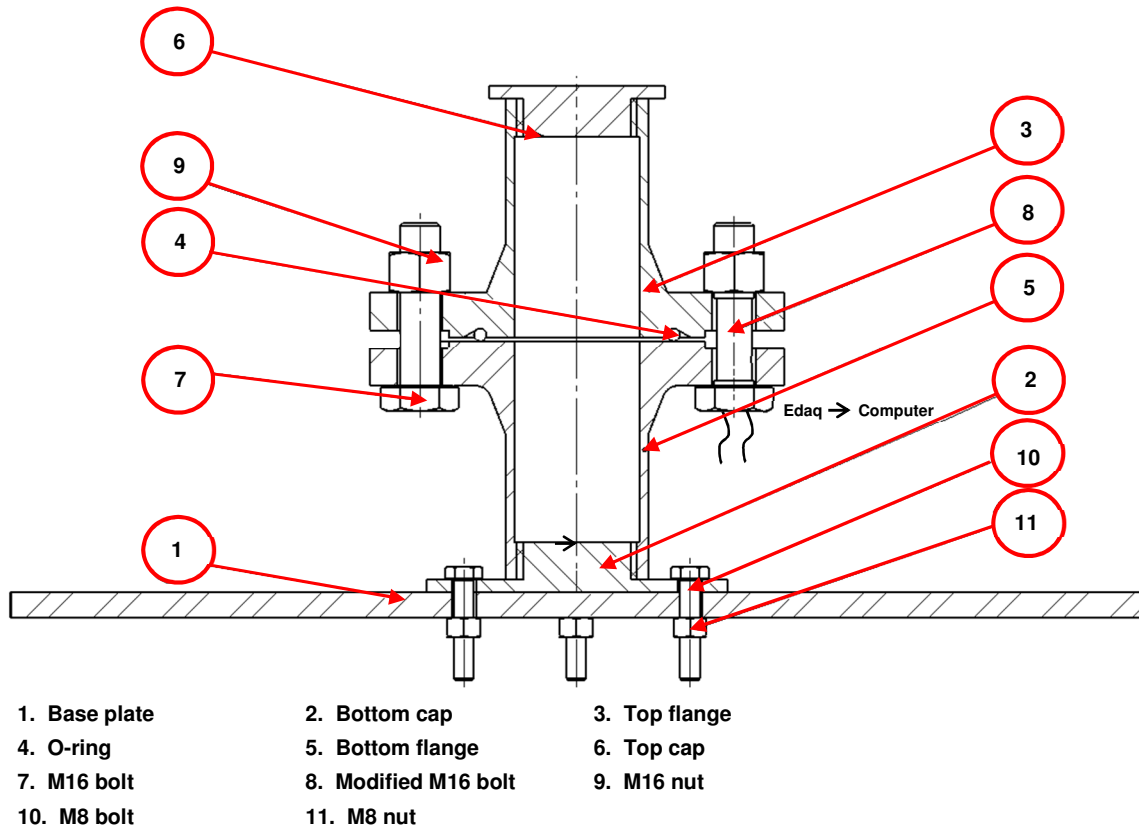


Figure 4-3: Experimental setup for the raised face flange which has been modified to contain an O-ring groove

4.3.1. Design and manufacture of the flanges

The flanges were manufactured from EN 24, tempered steel. The dimensions of the flanges were chosen to match those of an EN 1092-1 PN 10 DIN 50 flange for all three the different face configurations. The dimension for the flat face flange, raised face flange, and raised face flange with an O-ring groove are given in Appendix B.

4.3.2. Modification to fasteners

One of the four M16 bolts was modified so that it could be instrumented with strain gauges. A section of the bolt's shank diameter was reduced to 12 mm. This was done so that two uniaxial strain gauges could be instrumented on the bolt at 180° from one another around the circumference. In addition to this, two holes were drilled in the bolt to allow for the passage of cables. The dimensions of the modified bolt are shown in Figure 4-4. The locations of the strain gauges are discussed and shown in greater detail in the following section.

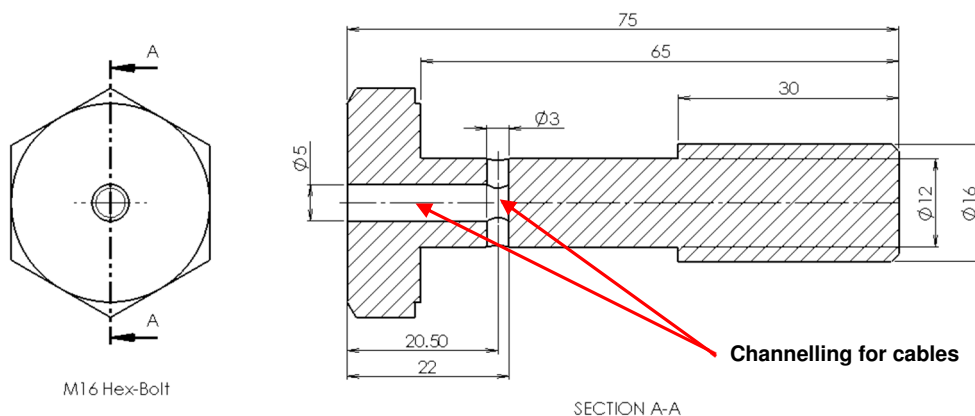


Figure 4-4: Modifications to the standard M16 bolt

4.3.3. Instrumentation of flanges and fasteners

Each of the three types of flanges were instrumented, in a similar fashion, with four strain gauges; two 90° rosettes and two 45° rosettes. The strain gauges were acquired from HBM and had the following product designations for the 90° and 45° rosettes respectively: K-XY31-3/350 and K-RY81-3/350. They were instrumented in such a way so as to measure the strains in the radial, and tangential direction in-line with and in-between the bolts, as well as in the transposed axial direction on the hub.

The hub of the flange, as shown in Figure 4-5, was instrumented with two 45° rosettes. This was initially done so that the stresses at those locations could be determined from the relevant strains. It was, however, decided to only consider the strains when validating the finite element model and analysis. Based on this the number of measurement locations on the hub were reduced from six to four with the 45° gauges being omitted.

Figure 4-5 shows the general positions of all the strain gauges which were instrumented on both the hub and ring of the flange.

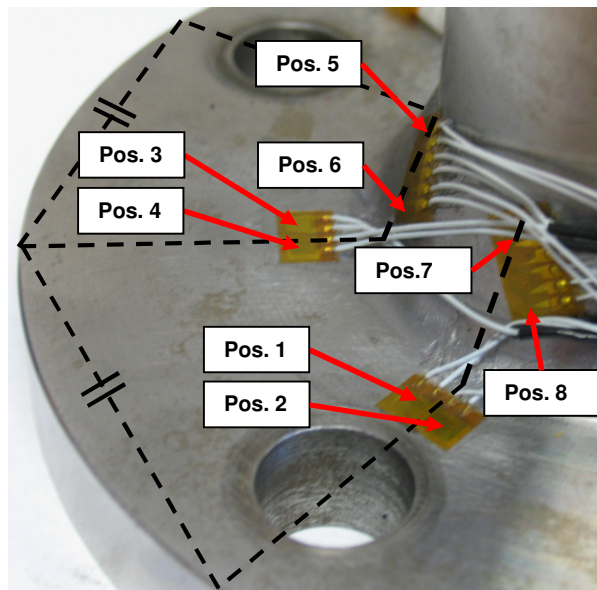


Figure 4-5: General locations of all the strain gauges which were instrumented on the flange

The modified M16, Class 8.8 bolt was instrumented with two uniaxial strain gauges. The purpose of these strain gauges were to measure the axial strains in the bolt. The strain gauges were placed halfway between the two drilled side holes, and at 180° from one another (i.e. on opposite sides of the bolts). In addition to this both strain gauges were placed 22 mm from the washer face of the bolt (as shown in Figure 4-6).

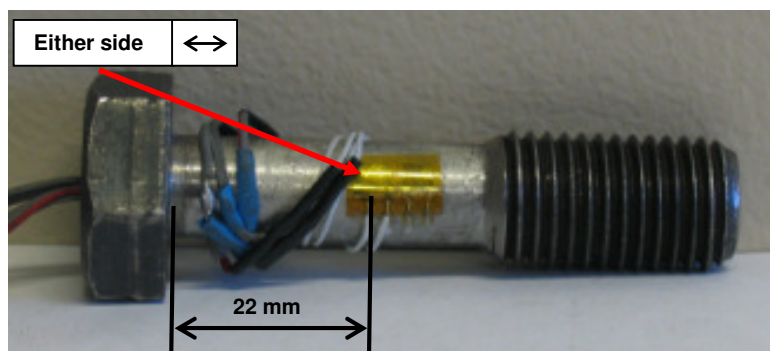


Figure 4-6: Position of the uniaxial strain gauges relative to the washer face on the modified M16 bolt

Shown in Figure 4-7 are the locations of the 90° rosettes on the ring of the flange. These rosettes measured the strain in the radial and tangential direction on the ring of the flange. More specifically, the strain gauge at Position 1 measured the strain in the radial direction of the ring in-line with the bolt; whereas the strain gauge at Position 3 measured the strain in the radial direction between two bolt holes. The strain gauges at Positions 2 and 4 measured the strains in the tangential (or circumferential) direction in-line with the bolt and in-between the bolts, respectively.

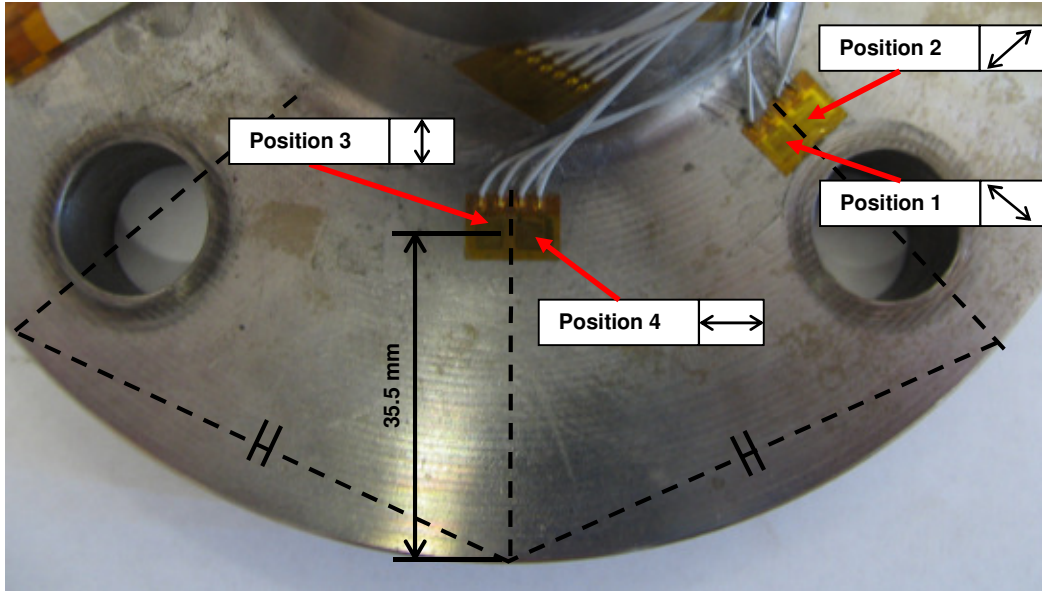


Figure 4-7: Location of the 90° rosettes on the ring of the flange

Finally, the hubs of the flanges were instrumented with two 45° rosettes. As with the 90° strain gauges the 45° strain rosettes were placed in-line with and in-between the bolt holes (as shown in Figure 4-8). The strain gauges at Position 5 and 7 were instrumented to measure in the transposed axial direction. The strain gauges at Positions 6 and 8 measured the strain in the tangential direction of the hub. Both of the 45° rosettes were placed 8 mm below the thin edge of the hub, as shown in Figure 4-8.

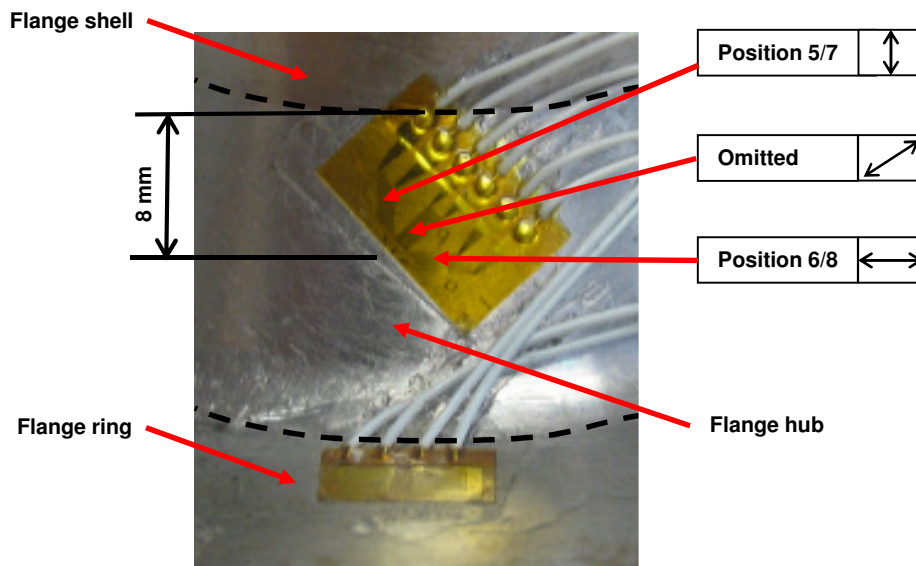


Figure 4-8: Position of the 45° rosettes relative to the ring-hub interface of the flange

Strain measurements were recorded using an Edaq Lite data acquisition system. This system allows for quarter bridge measurements since it is able to internally complete the bridges. All strain gauge

calibrations and corrections were done by means of Somat TCE v3.22.0 build 545 software [39] and the Edaq Lite. Correction for the lead-wire resistances were done.

All of the strain gauges were measured independently with a quarter bridge configuration, which was completed internally by the Edaq Lite data acquisition system, as was mentioned before. Shown, below, in Table 4-1, is the bridge configuration, gauge factor, bridge factor and sampling frequency which was used in the measurements of the strains.

Table 4-1: Bridge configuration, gauge factor, bridge factor, and sampling frequency used for the measurement of the trains

	Bridge configuration	Gauge factor	Bridge factor, B	Sampling frequency [Hz]
Value/Configuration	350 ohm, quarter bridge	2.01	1	10 Hz

4.3.4. Pressure instrumentation and measurement

Two options existed for the measurement of the contact pressure. The first option was to use FujiFilm's pressure sensitive film, whilst the second option was to make use of a TekScan sensor. The big disadvantage of FujiFilm's pressure sensitive film is that it is only able to measure the maximum applied pressure, and cannot, continuously, measure a change in contact pressure. A TekScan sensor, however, is able to do this and was, therefore, used to obtain the contact pressures between the gasket surface and the flange face for the seating condition. The contact pressure between the flange face and gasket surface was determined between bolt holes as shown in Figure 4-9.

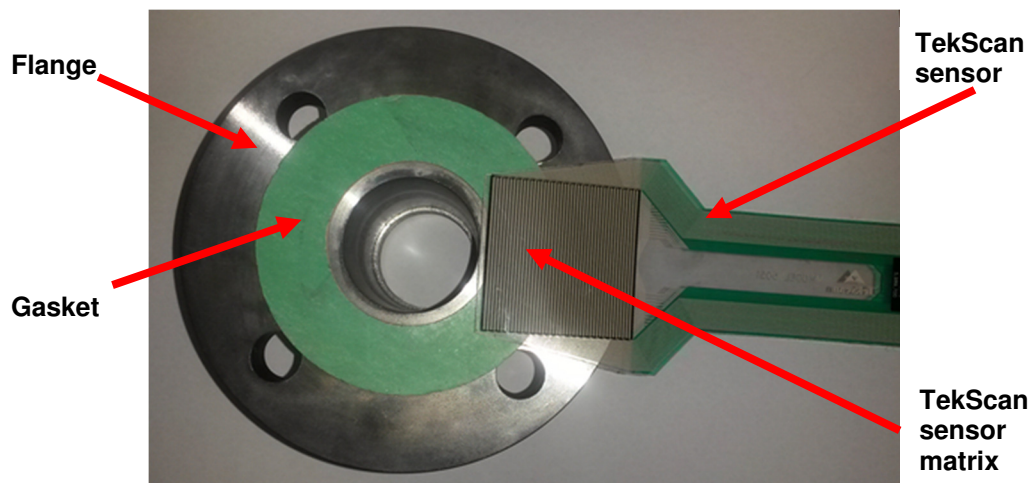


Figure 4-9: TekScan sensor model 5051-10 000 and how it was positioned in the flange assembly for the experimentation

To determine the contact pressure a TekScan model No. 5051-10 000 psi sensor was used. The sensor was conditioned, calibrated and loaded using Lloyd instruments' EZ50 50 kN Universal testing machine. A sensitivity of S-29 was selected on the I-Scan, TekScan software. The sensor was calibrated in eight increments from 3 125 N to 46 875 N. The pressure sensor was calibrated between two smooth, level metal interfaces. The metal plates chosen were regarded to have a high enough stiffness so as to regard any plate deformation as negligible.

4.4. Experimental procedure

The aim of the experiment was to validate the results of the initial finite element modelling and analysis. The experimental procedure was divided into separate parts. The first part was concerned with the measurements of the strains on the bolt, and at the aforementioned strain gauge locations on the flange

during the seating condition. In addition to this the contact pressure was also measured between the flange faces and the gasket. The second step was to measure the reduction in the strain and contact pressure due to creep-relaxation.

The following procedure was followed in order to validate the results of the finite element analysis of the three different types of circular bolted flange connections: Bolt 1 (shown in Figure 4-10) was tightened first, followed by Bolt 3, Bolt 2, and finally Bolt 4.

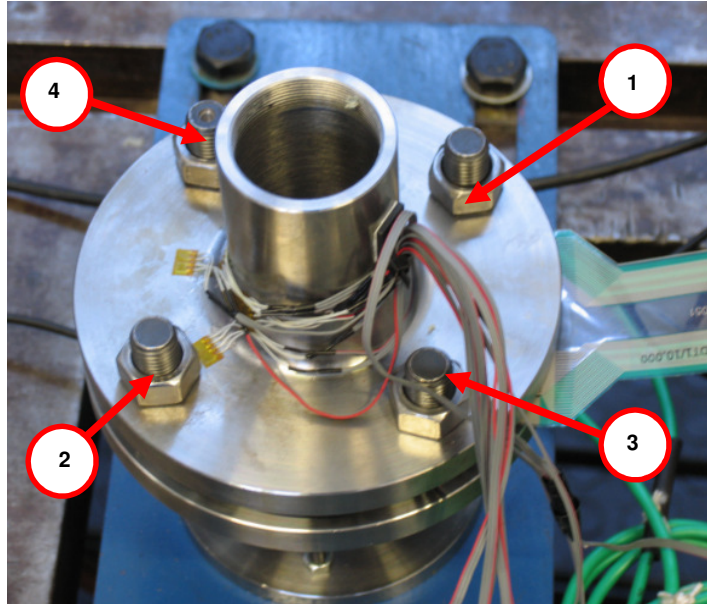


Figure 4-10: Bolt tightening sequence for the experimental setup

The bolts were tightened by means of a torque wrench. The bolts were all initially torqued to 14 N.m (according to the torque wrench), where after they were torqued in increments of 3 N.m to final value of 50 N.m. It was aimed to tighten the bolts in intervals of 10 seconds. Once all of the bolts were torqued the system was left for 10 minutes. This was done to measure the effect of the creep-relaxation on the measured strains and contact pressures for both the flat face flange and the raised face flange. The experiment was repeated six times for each flange configuration. Although only the strain results are given for the instances immediately after the bolts were fastened, and 10 minutes after the bolts were fastened, the strains were continually measured throughout the bolting-up phase.

4.5. Results from the experimentation

The experimental results are given in three sections – one section for each of the three different flange configurations. The first two sections are for the flat face and raised face flanges. These sections are split into two subsections: one for the measured strains and one for the measured contact pressures.

The measured strains on the shaft of the bolt were used to find the actual applied bolt pretensions during the experimentation. This was done as follows: the bolt pretension in the finite element analysis was set slightly higher than anticipated, the bolt strains at various loads were then calculated until the measured bolt strains corresponded to the calculated bolt strains from the finite element analysis. Once the correct load had been determined the finite element analysis was solved again, this time with the exact correct bolt pretension. Since the measured bolt strains matched the calculated bolt strains from the finite element analysis, the results, for comparative purposes, are not shown.

4.5.1. Strain gauge and contact pressure results for the flat face flange

The mean, maximum, and minimum measured strains, from the six experiments, at each of the eight aforementioned locations on the ring and hub of the flat face flange, are shown in Table 4-2, for the instance immediately after the bolts had been tightened. The measured strains, 10 minutes after the bolts had been tightened, are shown in Table 4-3.

Table 4-2: Summary of the strain gauge results, for the experimental setup of the flat face, flange immediately after the bolts had been tightened

Strain gauge position	Mean measured strain [$\mu\text{m/m}$]	Maximum measured strain [$\mu\text{m/m}$]	Minimum measured strain [$\mu\text{m/m}$]
1	204	233	161
2	69	89	39
3	99	109	91
4	254	281	236
5	64	81	47
6	165	180	150
7	83	97	74
8	173	186	155

Table 4-3: Summary of the strain gauge results, for the experimental setup of the flat face flange, 10 minutes after the bolts had been tightened

Strain gauge position	Mean measured strain [$\mu\text{m/m}$]	Maximum measured strain [$\mu\text{m/m}$]	Minimum measured strain [$\mu\text{m/m}$]
1	198	227	153
2	67	88	35
3	97	108	86
4	249	275	230
5	62	79	46
6	160	176	142
7	79	94	71
8	167	181	146

Creep-relaxation resulted in a reduction of the measured strain values (Table 4-2 and Table 4-3). This reduction in measured strain, however, did not exceed $10 \mu\text{m/m}$ for all of the instrumented locations. The minimum and maximum variation, between the minimum and maximum measured strain values, were between $18 \mu\text{m/m}$ and $72 \mu\text{m/m}$ immediately after the bolts were tightened; and $22 \mu\text{m/m}$ and $74 \mu\text{m/m}$ 10 minutes after the bolts had been tightened.

The results for the contact pressure measurements are shown for the instances immediately after the bolts had been tightened (Figure 4-11), and 10 minutes after the bolts had been tightened (Figure 4-12). From the results shown in Figure 4-11 two important aspects may be observed. The first important aspect is the shape of the measured contact pressure. From Figure 4-11 a. and b. it may be observed that the highest pressures were obtained in the middle of the gasket, i.e. along the diameter between the inner and outer diameter. Secondly the values at the edges (where $y=5$ and $y=40$) of the measured area, i.e. the edges nearest to the bolts, are slightly higher than the values in the middle ($y=25$). This shape corresponds to the results of the viscoelastic material presented by Yamaguchi *et al.* [31]. The second aspect which needed to be observed is the magnitude of the measured contact stresses. As shown in Figure 4-11 c. a maximum contact pressure of 25.5 MPa is measured. This maximum value is, however, at a peak and the majority of values which were measured along the diameter between the inner and outer diameter of the gasket were between 20 MPa and 25 MPa. These values decreased towards both the inner and outer diameters of the gasket.

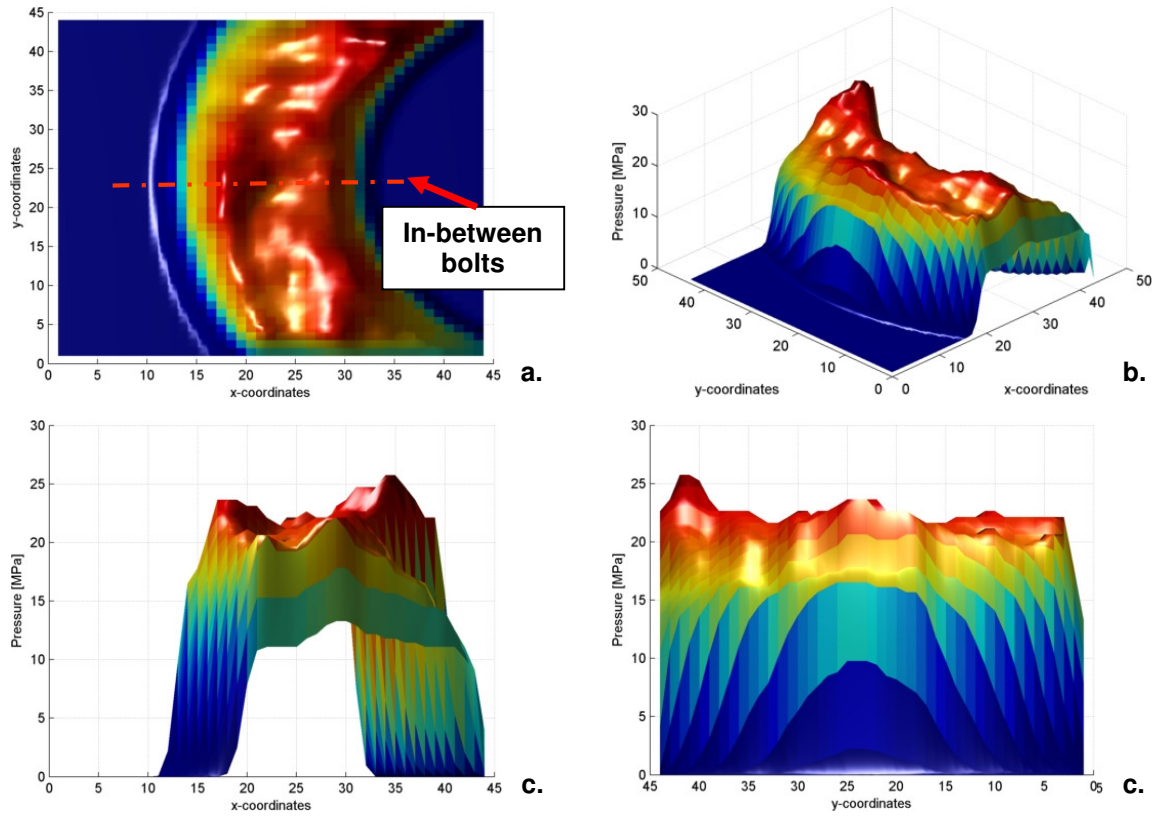


Figure 4-11: (a) Top view, (b) isometric view, (c) front view, and (d) back view of the measured pressure distribution, for the flat face flange, immediately after the bolts had been tightened

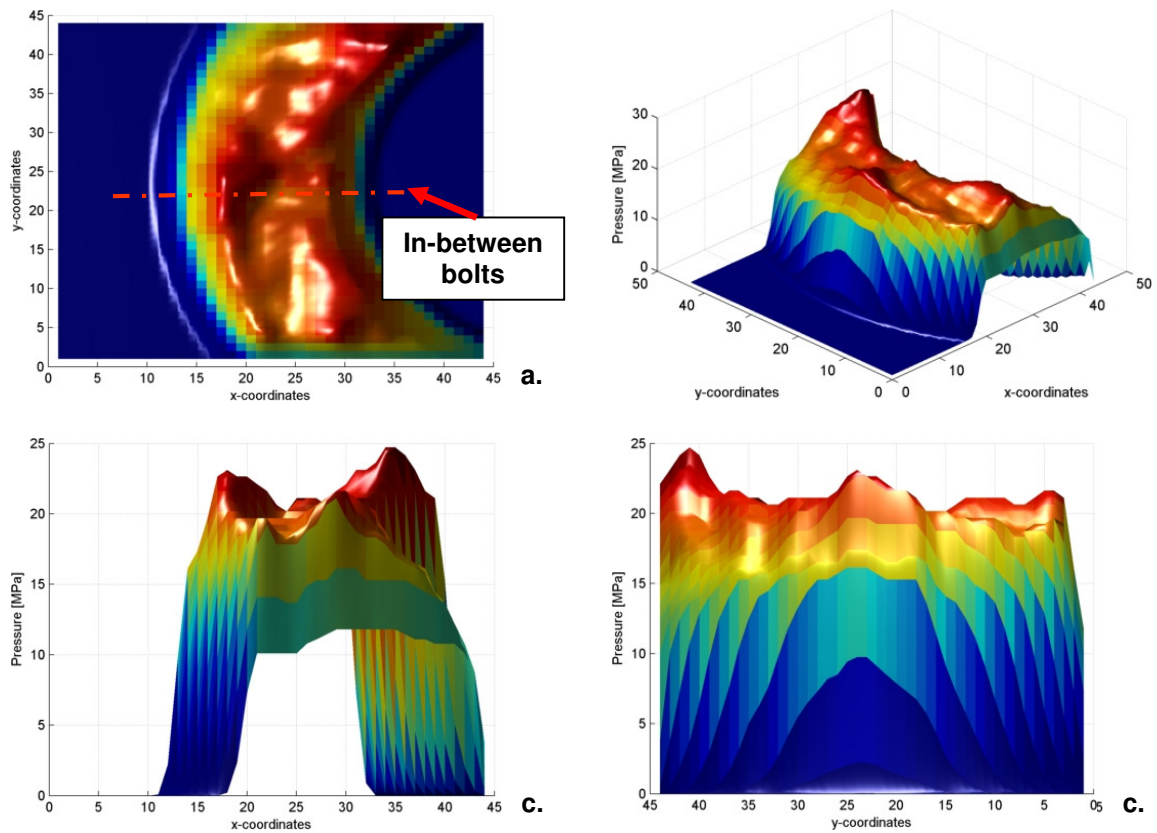


Figure 4-12: (a) Top view, (b) isometric view, (c) front view, and (d) back view of the measured pressure distribution, for the flat face flange, 10 minutes after the bolts had been tightened

A similar shape is obtained for the contact pressure after the 10 minute period. The largest values are again along a diameter which lies between the inner and outer diameter of the gasket insert. Again, the values near bolt holes are slightly larger. There has also been a slight reduction in the magnitude of the measured contact stresses. The peak contact pressure value in this instance was 25 MPa. The majority of the peak values, however, are only slightly greater than 20 MPa.

4.5.2. Strain gauge results for the raised face flange

Shown below are the mean measured strains at each of the eight aforementioned locations on the ring and hub of the raised face flange. Both the mean, maximum, and minimum measured strain values are given for the instances immediately after the bolts had been tightened (Table 4-4) and when the entire assembly was left for 10 minutes (Table 4-5).

From the results shown in Table 4-4 and Table 4-5 it may be seen that the effect of creep-relaxation, again, resulted in a reduction of the measured strains. The reduction in the measured mean strains exceeded $10 \mu\text{m}/\text{m}$ for three out of the eight locations. The remaining locations all had a reduction in the mean strain of less than $10 \mu\text{m}/\text{m}$. None of the mean results, however, reduced by more than $20 \mu\text{m}/\text{m}$. On average the reduction in the measured strain for the raised face flange is 57% higher than the for the flat face flange. The minimum and maximum variation, between the minimum and maximum measured strain values, remained between $16 \mu\text{m}/\text{m}$ and $69 \mu\text{m}/\text{m}$ immediately after the bolts were tightened; and $11 \mu\text{m}/\text{m}$ and $66 \mu\text{m}/\text{m}$ 10 minutes after the bolts had been tightened.

Table 4-4: Summary of the strain gauge results, for the experimental setup of the raised face, flange immediately after the bolts had been tightened

Strain gauge position	Mean measured strain [$\mu\text{m}/\text{m}$]	Maximum measured strain [$\mu\text{m}/\text{m}$]	Minimum measured strain [$\mu\text{m}/\text{m}$]
1	199	222	181
2	96	122	61
3	80	86	71
4	259	295	231
5	74	90	63
6	162	209	140
7	113	129	94
8	161	169	153

Table 4-5: Summary of the strain gauge results, for the experimental setup of the raised face flange, 10 minutes after the bolts had been tightened

Strain gauge position	Mean measured strain, [$\mu\text{m}/\text{m}$]	Maximum measured strain, [$\mu\text{m}/\text{m}$]	Minimum measured strain, [$\mu\text{m}/\text{m}$]
1	189	215	166
2	90	116	57
3	74	79	67
4	243	267	220
5	69	84	59
6	150	195	129
7	104	123	86
8	150	154	143

As before the results for measured contact pressure between the gasket and raised face flange are shown for the instances immediately after the bolts were tightened (Figure 4-13), and after a 10 minute period (Figure 4-14).

As with the flat face flange the raised face flange had its highest contact pressure value located along a diameter between the outer and inner diameter of the gasket insert. Again, as was the case with the flat face flange, the raised face flange had slightly higher values nearer to the bolts than it did midway between the bolts. All of the values reduced closer to the inner and outer diameters of the gasket insert.

The maximum contact pressure of the raised face flange, immediately after the bolts had been tightened was 28 MPa. However, this value was located close to the bolt hole and was an isolated maximum. The majority of peak values, as shown in Figure 4-13, are between 20 MPa and 25 MPa for the instance where the bolts had just been fastened. The maximum contact pressure value for the raised face flange is 2.5 MPa higher than that of the flat face flange. The values along the diameter between the inner and outer diameter are, however, slightly lower for the raised face flange when compared to the flat face flange between the bolt holes. This may be observed in Figure 4-13.

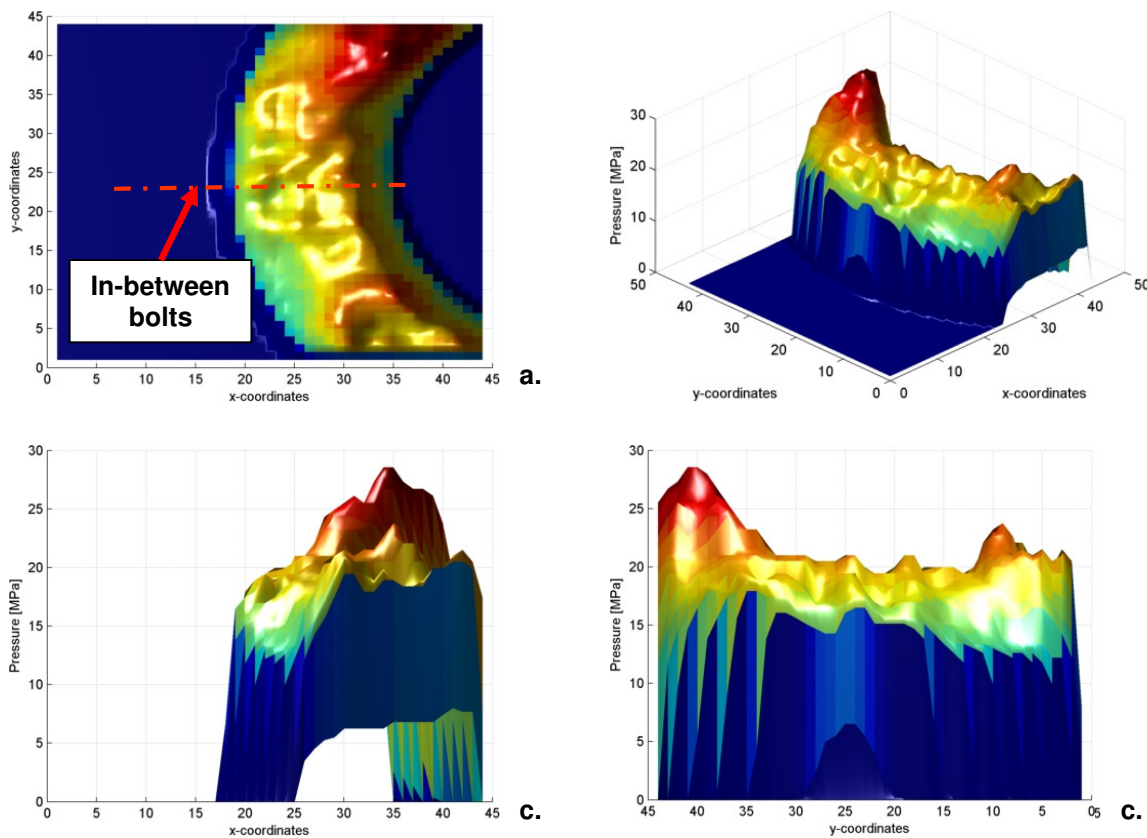


Figure 4-13: (a) Top view, (b) isometric view, (c) front view, and (d) back view of the measured pressure distribution, for the raised face flange, immediately after the bolts had been tightened

Shown in Figure 4-14 are the results for the contact pressure after the 10 minute period. Again, it may be observed that there has been a reduction in the contact stress from right after bolting until the 10 minute period had ended.

The same isolated maximum peak existed close to the bolt hole and had, in this instances, a value of 26 MPa. The values between the bolt holes and along the diameter between the inner and outer diameter of the flange reduced to approximately 20 MPa. It may be observed that creep-relaxation resulted in a greater decrease in contact pressures at the higher peaks than at the lower peaks. This will be discussed in greater detail in the following section.

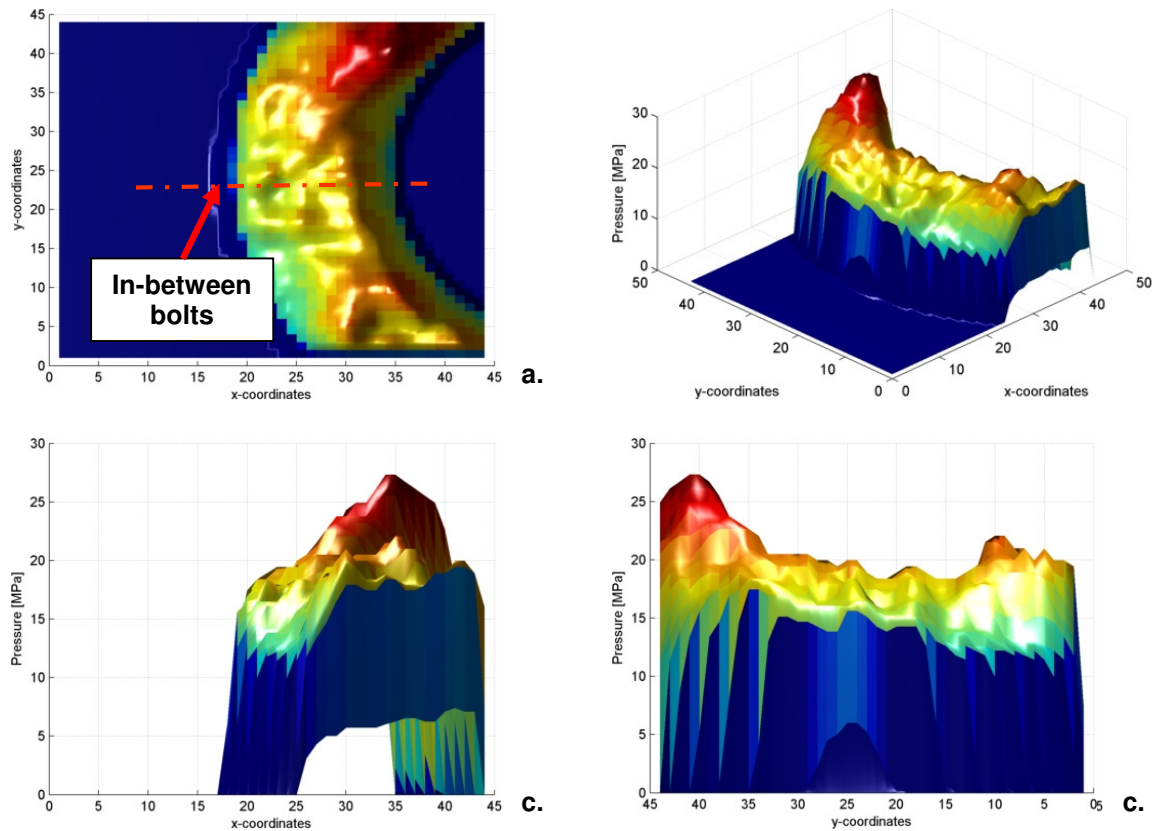


Figure 4-14: (a) Top view, (b) isometric view, (c) front view, and (d) back view of the measured pressure distribution, for the raised face flange, 10 minutes after the bolts had been tightened

4.5.3. Strain gauge results for the raised face flange with an O-ring groove

Unlike before, only the measured strain results for the flange with an O-ring groove were considered. It was found that the creep-relaxation of the O-ring had a negligible effect on the measured strains. As a result only the measured strains right after the bolts had been fastened are shown in Table 4-6.

Table 4-6: Summary of the results for the experimental setup of the raised face flange with an O-ring groove after tightening

Strain gauge position	Mean measured strain [$\mu\text{m}/\text{m}$]	Maximum measured strain [$\mu\text{m}/\text{m}$]	Minimum measured strain [$\mu\text{m}/\text{m}$]
1	257	281	236
2	109	116	102
3	104	114	90
4	235	261	218
5	89	95	83
6	145	159	136
7	75	80	70
8	145	162	136

4.6. Comparison of the experimental results to the finite element analysis results

In this section, the results from the experimentation are compared to the results of the finite element analysis shown in Chapter 3. There are two subsections for the flat and raised face flanges in which the strains and contact pressure are individually compared. There is, however, only one section for the comparison of the results of the raised face flange with an O-ring groove.

4.6.1. Comparison of the experimental and predicted values for the flat face flange

The first set of strain gauge values which were compared are those immediately after the bolts had been tightened. In the finite element model of the flat face flange it was assumed that an axisymmetric model, in which the bolt load is instantaneously applied (i.e. not in increments as in the experiment), is sufficient to accurately predict these experimental values.

The mean experimental values (blue), the maximum and minimum experimental values (black), and the predicted values from the finite element analysis (red) are shown in Figure 4-15. These results are for the instance immediately after all of the bolts had been tightened for both the finite element analysis as well as for the experimental setup.

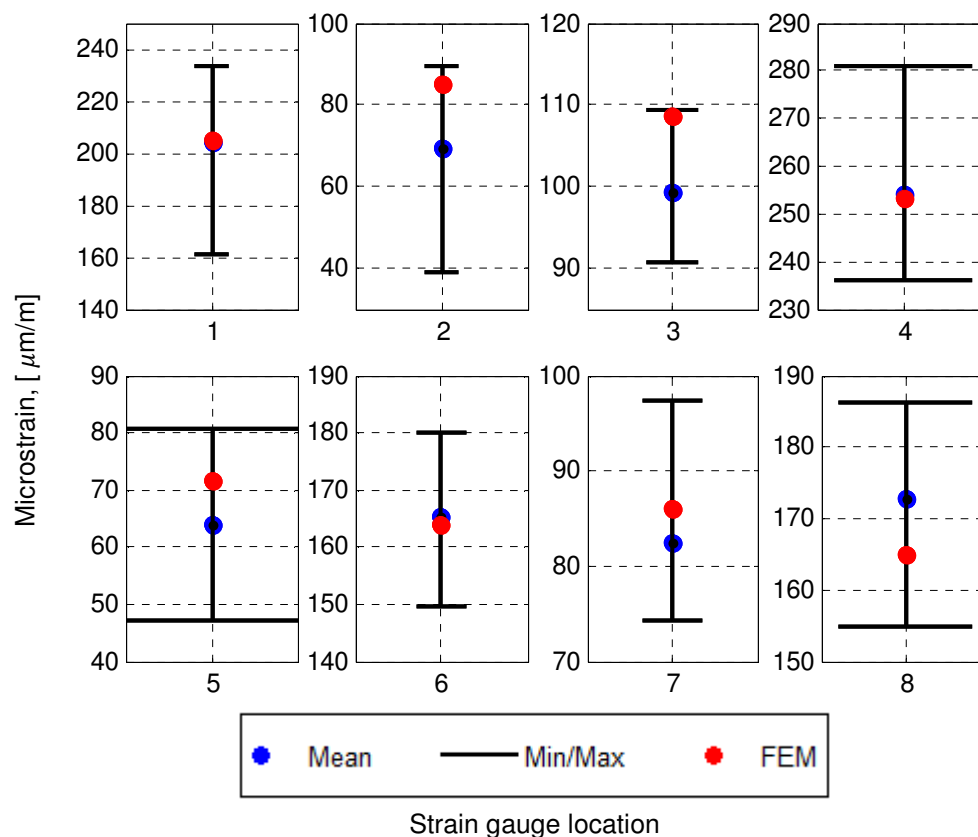


Figure 4-15: Comparison of the measured strains to the calculated strains from the finite element analysis for the flat face flange immediately after the bolts had been tightened

As shown in Figure 4-15 all of the calculated values from the finite element analysis lie between the minimum and maximum boundaries and six out of the eight positions differ by less than 10% when compared to the mean value. The largest difference between the mean experimental strain value and the calculated one was at Position 2 where there was a difference of 23.1%.

The values calculated by the finite element model and analysis were assumed to compare sufficiently well to those of the experimental setup of the flat face flange immediately after tightening. For this particular instance – a flat face flange immediately after bolting-up (before creep-relaxation) – the finite element model and analysis was deemed to be acceptable.

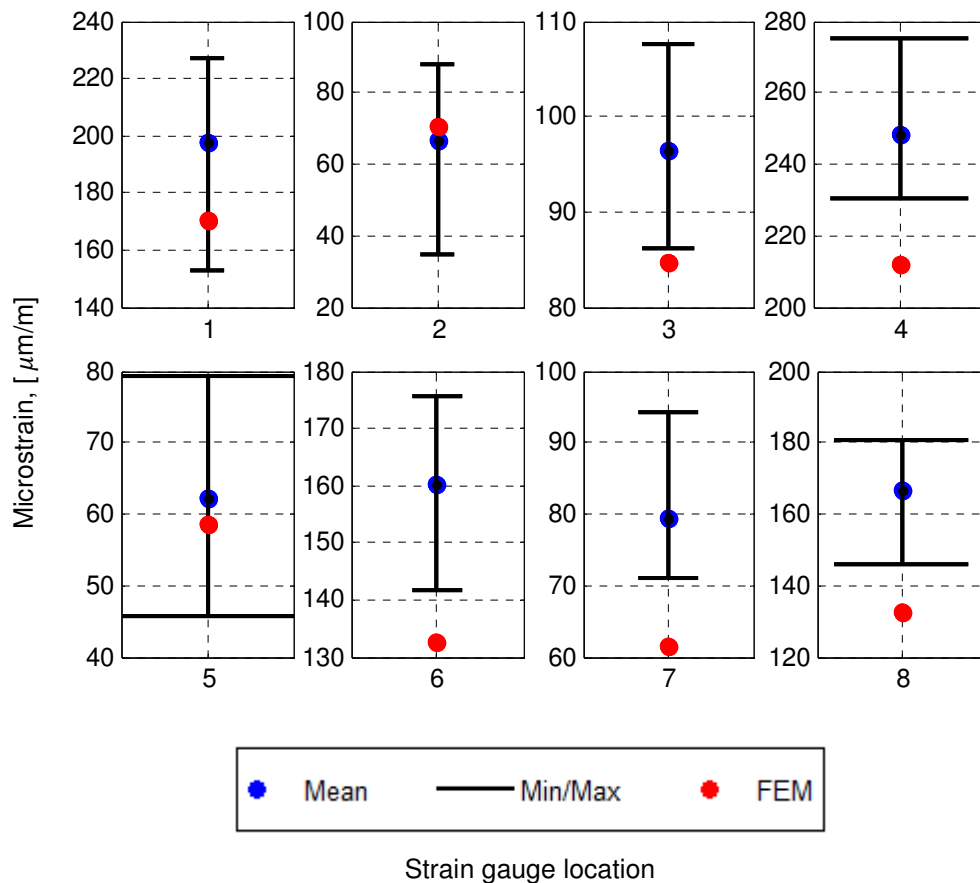


Figure 4-16: Comparison of the measured strains to the calculated strains from the finite element analysis of the flat face flange after a 10 minute period

From the comparison of the values shown in Figure 4-16 the following may be observed: only three of the calculated values from the finite element analysis lay between the maximum and minimum values at each of the eight locations. A comparison of the total reduction in the mean measured and calculated strains, due to creep-relaxation, are shown in Figure 4-17. From these results it may be observed that the values calculated by the finite element analysis exceeded those measured during the experimentation by more than 400% at all of the positions. Another important aspect to observe from Figure 4-17 is that the finite element model predicts a greater reduction in the strains at all eight locations. From these results it may, therefore, be argued that model is significantly more conservative when compared to the behaviour of the flat face flange assembly in the experiment.

At this point it is important to remember that during the experimentation all of the bolts were cross-tightened individually 12 times. This was done in an attempt to ensure that the strains and contact pressures in the flat face flange assembly were axisymmetric. This was the only difference between the finite element analysis and the experimental setup. These results show that the finite element model for the flat face flange, where the total bolt load is applied instantaneously, is unable to predict the strains in the flange correctly after the 10 minute period when creep-relaxation was allowed.

An analysis of the results shown in Figure 4-15 to Figure 4-17 are summarised in Table 4-7. From the results shown in Table 4-7 it may be seen that the calculated strain values, from the finite element analysis, are within 10% of the mean measured values for 6 out of the 8 locations immediately after the bolts had been fastened. Conversely, for the instance where 10 minutes had been allowed for creep-relaxation to occur, only two out of the 8 calculated strains had a difference of less than 10% when compared to the measured values. This reaffirms the prior statement the finite element model, as implemented at the end of Chapter 3, is suitable to predict the behaviour of the flat face flange assembly during bolt up. It is, however, not suitable to predict the behaviour of the bolted flange connection, in the experiment, when the total bolt pretension is not applied simultaneously. It, therefore, appears that

time and the subsequent number of bolt tightening increments play a significant role in the effect which the creep-relaxation behaviour has on the bolted flange assembly.

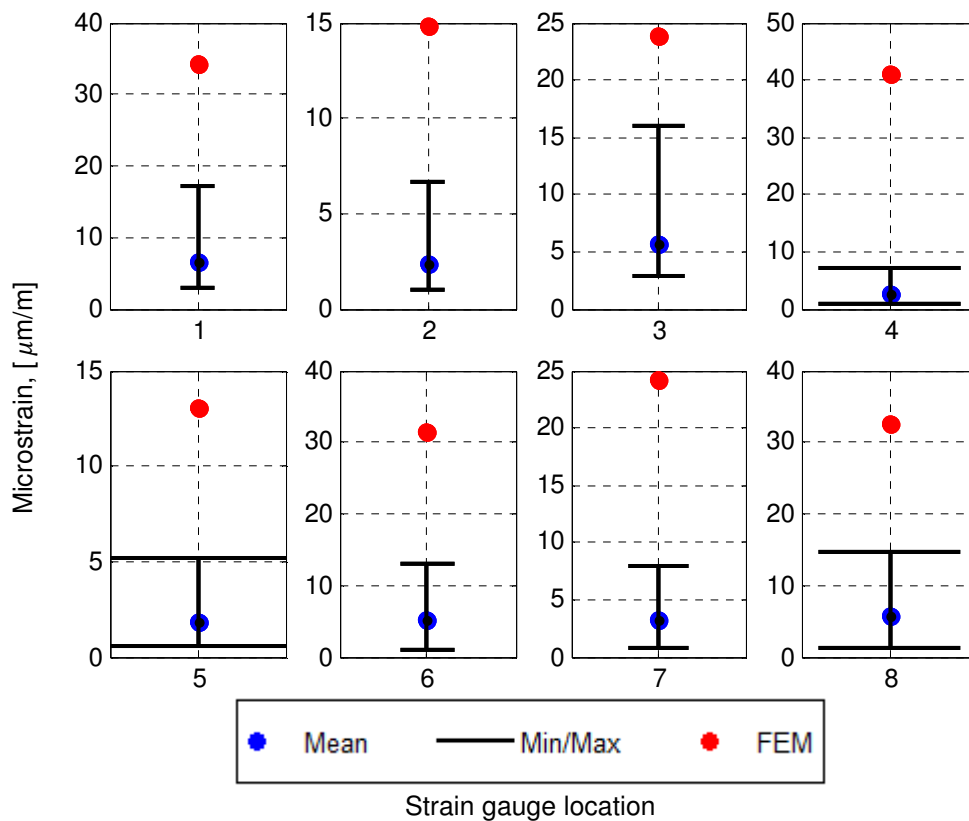


Figure 4-17: Comparison of the reduction in the measured strains to the reduction in the calculated strains from the finite element analysis of the flat face flange

Table 4-7: Summary of the results of the comparison between the measured and calculated strains for the flat face flange

Strain gauge position	Difference between the experimental and finite element results for the flat face flange		
	Immediately after the bolts were tightened [%]	10 minutes after the bolts were tightened [%]	Reduction in strain due to creep-relaxation [%]
1	0.31	13.87	416.93
2	23.09	5.19	541.24
3	9.30	12.22	318.27
4	0.41	14.62	1 375.70
5	11.79	5.93	626.72
6	0.84	17.24	511.66
7	4.12	22.27	652.61
8	4.45	20.58	463.55

In an attempt to explain the model's inability to accurately predict the strains in the flange 10 minutes after the bolts had been tightened the following was done: Instead of using an axisymmetric model where the entire bolt load was applied in a single step it was decided to mimic the experiment in all aspects. A full model was used. In addition to this the exact tightening procedure was followed. The

bolts were tightened in exactly the same procedure as given in Section 4.5. Each bolt was tightened twelve times. Between each tightening increment the model was left for 10 seconds (as in the experiment) before a pretension was applied to the next bolt. The strain results at the 8 locations, for this analysis is shown in Figure 4-18 (green dots). A summary of the analysis of the results is given in Table 4-8.

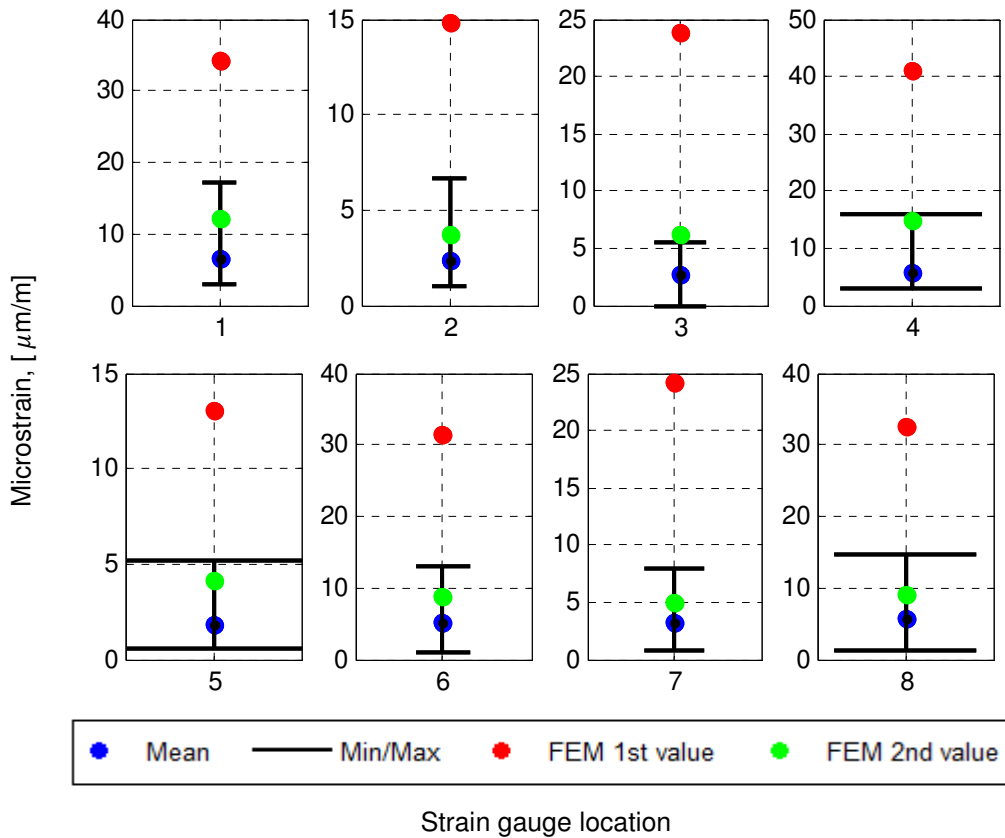


Figure 4-18: Comparison of the reduction in the measured strains to the reduction in the predicted strains from the second finite element analysis of the flat face flange

Table 4-8: Comparison of the strain reduction results calculated by the initial and modified finite element analysis to the measured strain reduction results for the flat face flange

Strain gauge position	Difference between the experimental and finite element results for the flat face flange	
	For the first FEM [%]	For the second FEM [%]
1	416.93	86.19
2	541.24	63.01
3	318.27	122.2
4	1 375.70	163.50
5	626.72	132.40
6	511.66	69.39
7	652.61	54.30
8	463.55	56.47

From Figure 4-18 and Table 4-8 it may be observed that the calculated values from the second finite element analysis is significantly closer to the mean measured strain values at all eight locations. The calculated results remained higher than the mean measured strains at all eight locations. However, all of the predicted results lay within the maximum and minimum measured values. Based on this the model was assumed to be acceptable.

The measured contact pressure from the experiment was compared to the calculated one from the finite element analysis: The final contact pressure was subtracted from the contact pressure right after the bolts had been tightened to give the reduction in contact pressure which resulted from creep-relaxation. The results for the calculated and measured reduction in contact pressure are given separately in Figure 4-19 and Figure 4-20, respectively.

The first set of results considered are those from the finite element analysis. From Figure 4-19 it may be observed that the greatest reduction in the contact stress, as a result of creep-relaxation, lies on a diameter between the inside and outside diameter of the gasket (as was the case with the maximum contact pressures). It has a maximum reduction of 4.2 MPa, which lies in-line with the bolt.

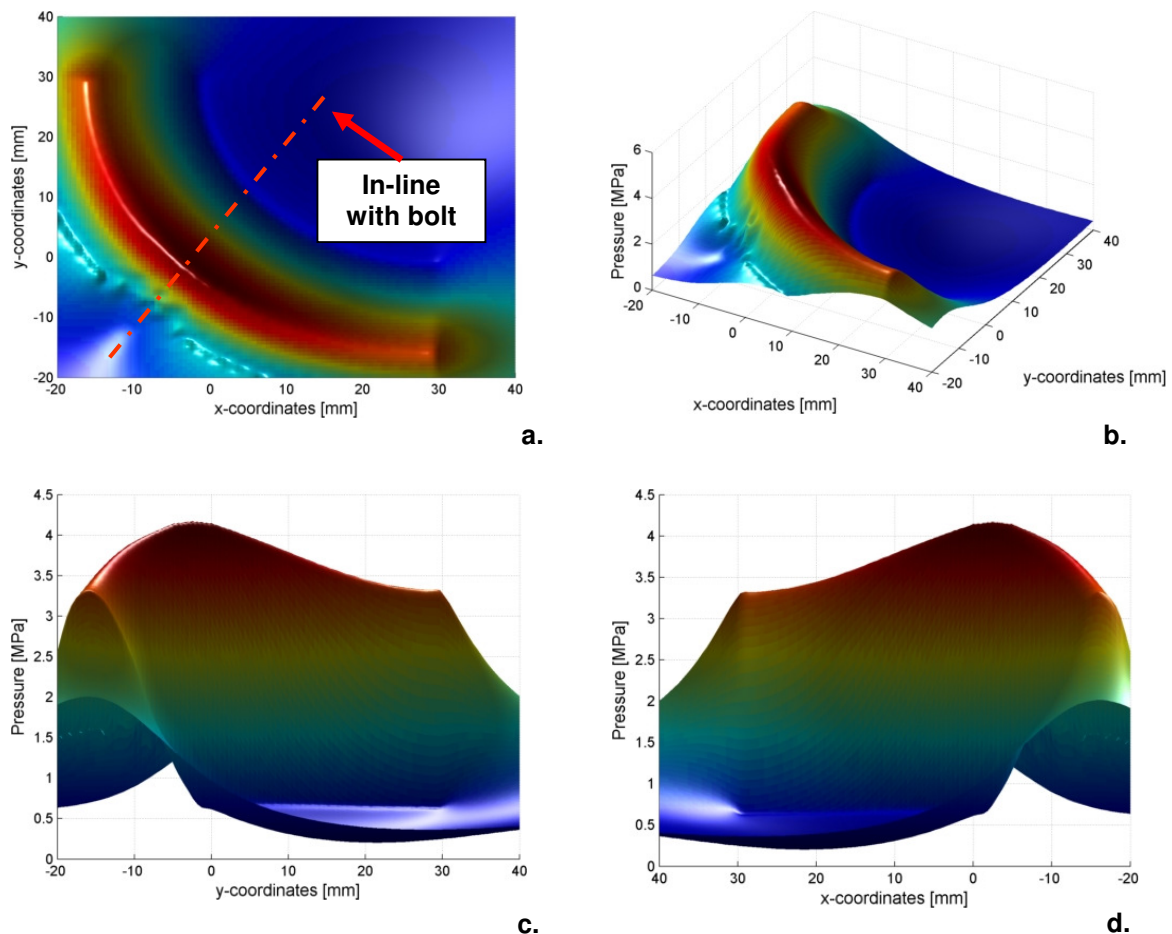


Figure 4-19: (a) Top view, (b) isometric view, (c) front view, and (d) back view of the calculated reduction in contact stress between the gasket insert and the flat face flange

The second set of results are those which were measured. From Figure 4-20 it may be observed that the general shape of the contact pressure reduction plot does not match the one predicted by the finite element analysis (Figure 4-19). Instead it has a large number of peaks and dips. These peaks and dips may be attributed to 'pixilation' due to the resolution of the measured results from the TekScan sensor. The magnitudes, with reference the 'pixilated' peaks and dips, may be explained by considering the behaviour of the gasket insert. As previously stated the gasket material is not entirely homogenous. As a result of this the stiffness in the gasket varies. However, the maximum peaks in the measured results lie in approximately the same region as those calculated, namely, along a diameter between the inner

and outer diameters of the gasket insert. In addition to this it may be observed that the maximum peak lies close to the bolt hole, as is the case with the calculated values. The maximum reduction in the measured contact stress was 1.9 MPa. This was, however, an isolated peak and the majority of the peak reductions lay between 1.4 MPa and 1.6 MPa. This is approximately three times less than those predicted by the finite element analysis of the flat face flange. As before the reason for this is that the model, as applied in Chapter 3, is unable to accurately predicted the behaviour of the flange assembly after all the bolts had been tightened. Again the reason for the difference may be attributed to the way in which the bolt pretensions were applied as previously discussed.

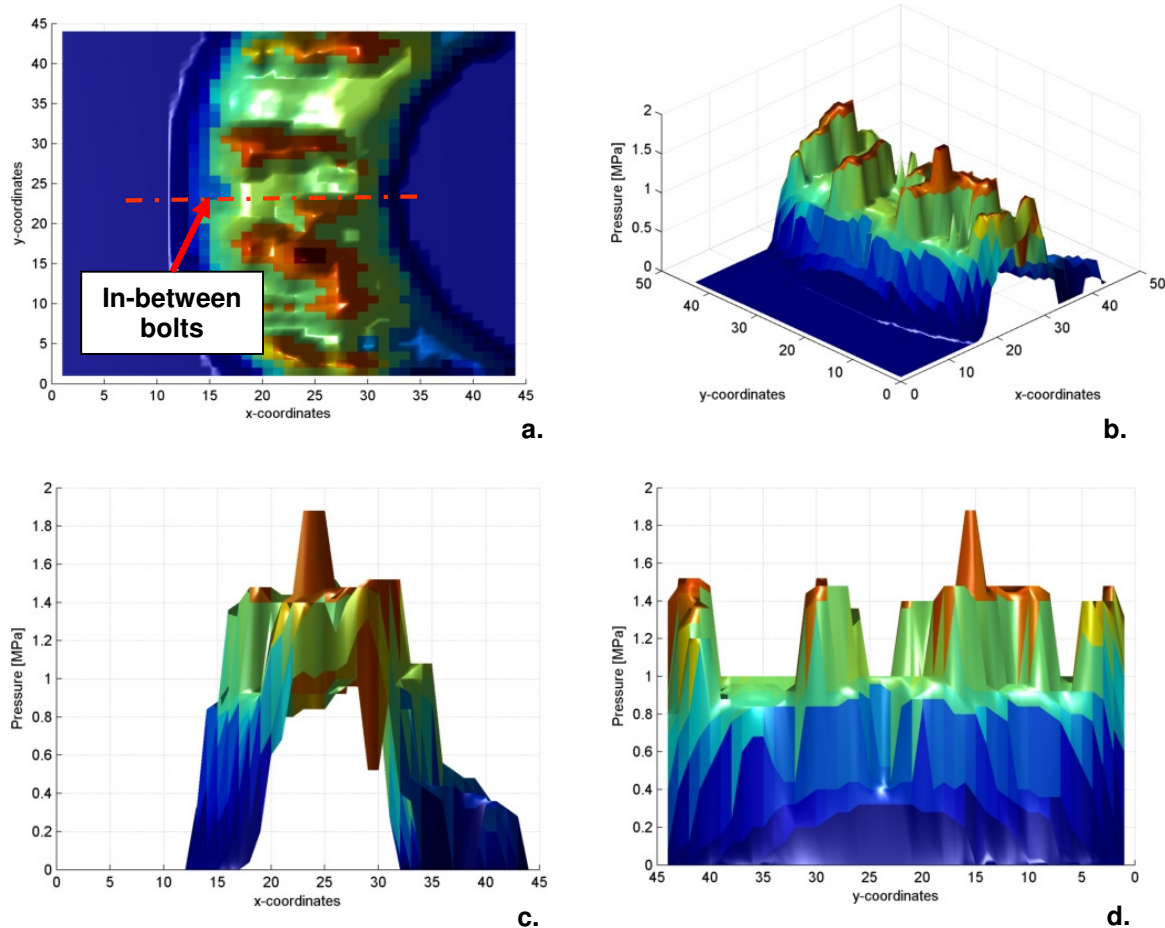


Figure 4-20: (a) Top view, (b) isometric view, (c) front view, and (d) back view of the measured reduction in the contact pressure between the flat face flange and gasket insert

In an attempt to validate the results obtained from the experimental setup a similar procedure as used in the previous section was implemented. Instead of an axisymmetric model, a full model was used. Each of the bolts were tightened using exactly the same procedure as was used in the experiment. A time of 10 seconds was allowed for between each bolt tightening increments.

The results for the modified finite element model and analysis are given in Figure 4-21. From the results it may be observed that the shape of the reduction in the contact pressure match the one given in Figure 4-19 for the unmodified finite element model and analysis. The major difference between Figure 4-19 and Figure 4-21, however, is the magnitude of the reduction of the contact pressure due to creep-relaxation of the gasket insert. A maximum reduction of 1.16 MPa occurs in-line with the bolt. This almost four times less than the value calculated in Figure 4-19. This value is also much closer to the one measured. When the maximum value from the predicted reduction in contact pressure is compared to the maximum peak values (with the omission of the peak at 1.9 MPa) of the measured contact pressure the difference lies between 3% and 17%. This difference was deemed to be acceptable.

As with the calculated strains after the bolts were tightened, the calculated contact pressure, by means of the finite element model depicted in Chapter 3, may be said to be conservative. The contact pressures calculated exceeds those measured. This is due to the fact that in reality the gasket is allowed to exhibit creep-relaxation behaviour, which influences the contact pressure, during the bolting-up stage.

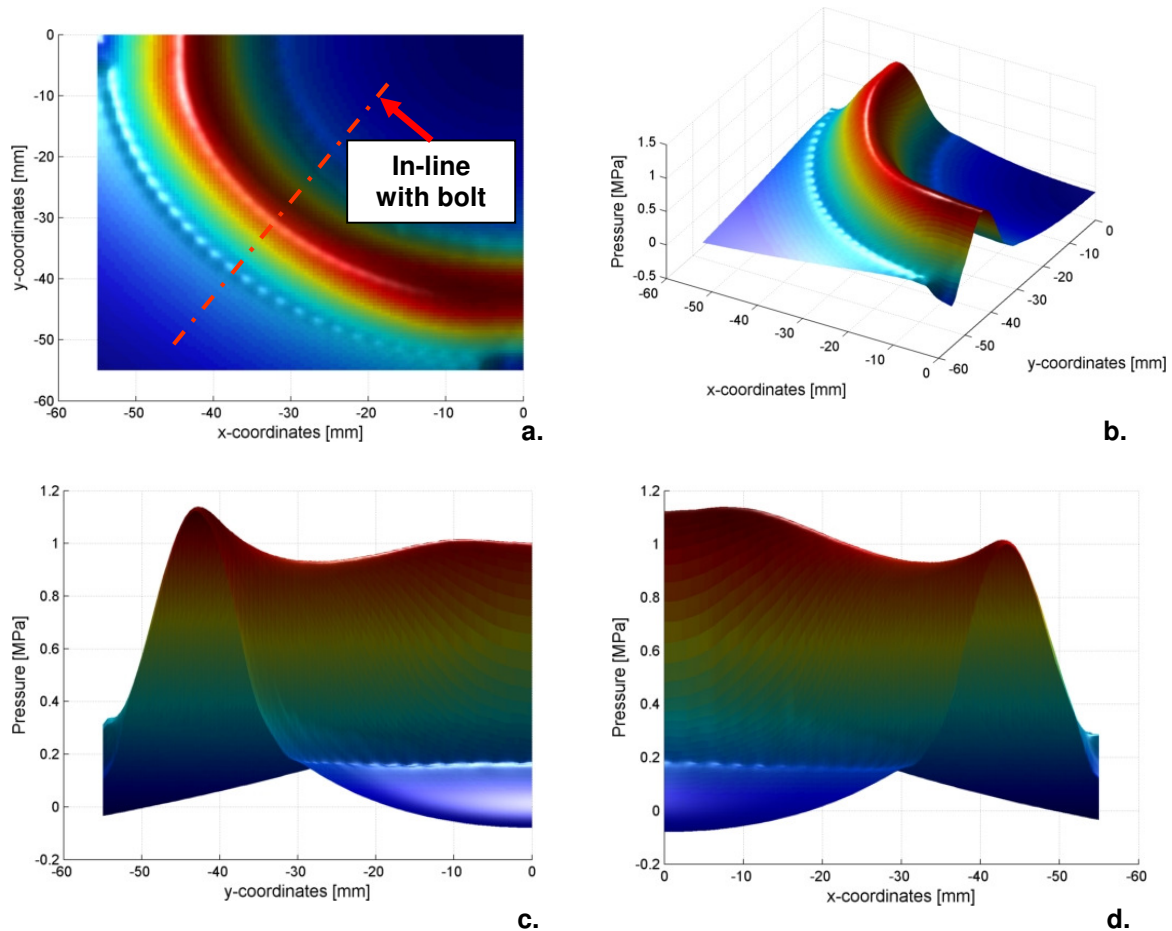


Figure 4-21: (a) Top view, (b) isometric view, (c) front view, and (d) back view of the calculated contact pressure between the gasket insert and the flat face flange based on the modified finite element model and analysis

From the the aforementioned discussion as well as on the results shown in Chapter 3 regarding the bolt tightening increments the following statement may be made: the effect which creep-relaxation has on the contact stress between the flange face and the gasket surface is greatly influence by both the amount of time between bolt tightening increments as well as the number of bolt tightening increments.

Based on this statement it was decided to investigate to what extent the number of bolt tightening increments as well as the amount of time between bolt tightening increments had on the contact pressure. For this investigation a full model of the flat face flange assembly was used. The two variables which were changed in this investigation were the number of bolt increments as well as the time between the bolt increments. For simplicity it was decided to limit both the time and the number of bolt increments. In total 24 analysis were completed. The time between each bolt tightening increment was varied from 10 seconds to 60 second. The number of bolt tightening increments, in total, was increased from 12 to 48 in increments of 12 (i.e. 3 increments per bolt). For each of the aforementioned 24 analysis the contact pressure right after all the bolts were tightened, as well as after a period of 10 minutes were calculated. From this percentage difference between the two instances was determined in attempt to quantify the effect which creep relaxation had.

A radial basis function was used to plot the results as a surface. This was done to give an idea of how the percentage difference increases / decreases with an increase / decrease in the time between the increments and the number of increments. The results are shown in Figure 4-22.

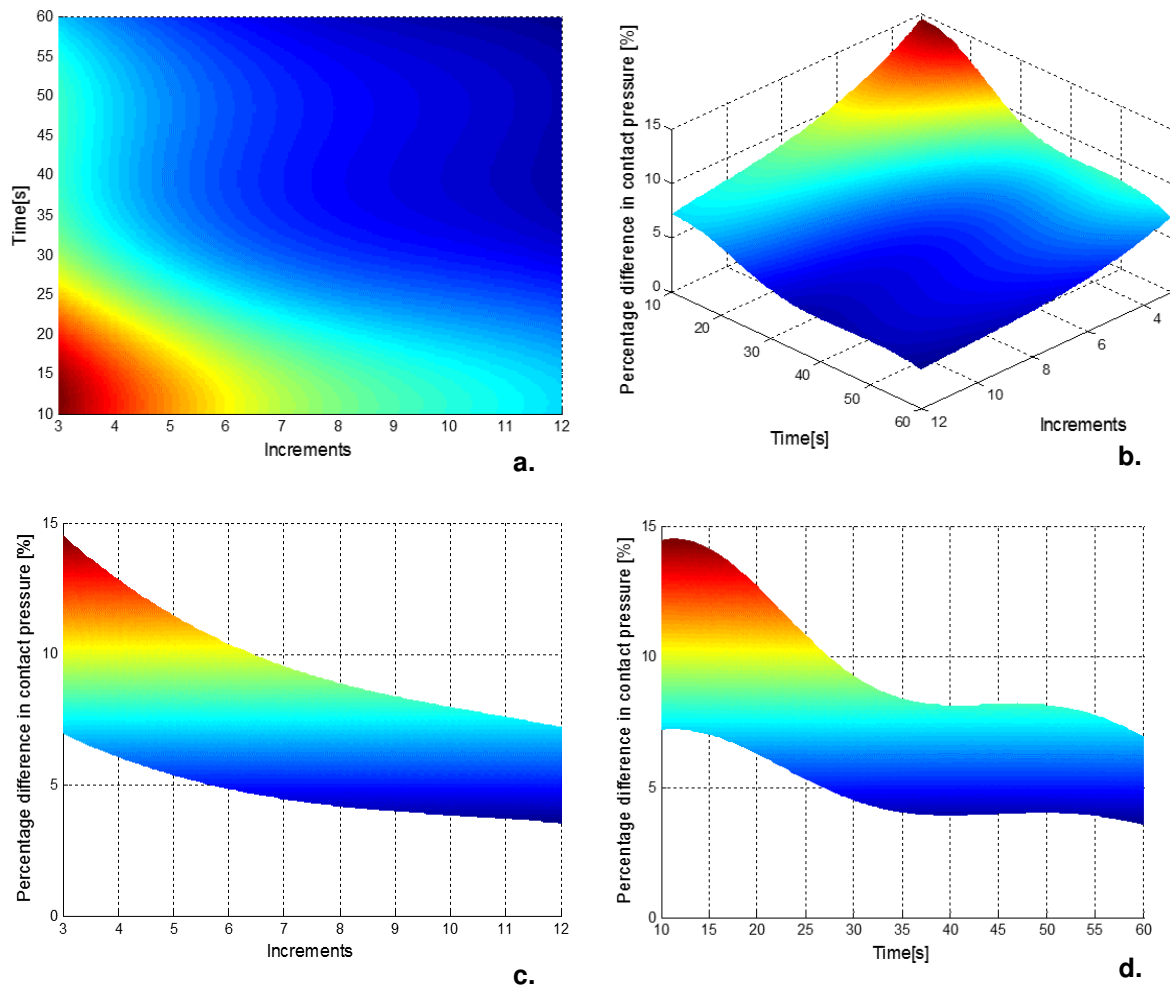


Figure 4-22: (a) Top view, (b) isometric view, (c) front view, and (d) back view of the percentage difference in the contact pressure as a function of the number of bolt tightening increments and time between the bolt tightening increments for the flat face flange

From the results shown in Figure 4-22 it may be seen that the greatest percentage difference between the contact pressure immediately after the bolts had been fastened and 10 minutes after the bolts had been fastened occurred when only three increments per bolt were used, and a maximum time of 10 seconds were allowed between each increment. On the other hand, when 12 increments per bolt were applied with a time of 60 seconds between each bolt tightening increment the minimum percentage difference in the contact pressure was obtained. The maximum difference in the contact pressure was 14.5%, while the minimum difference was 3.5%. This shows that an increase in either the number of bolt increments or the amount of time between each bolt increment may significantly reduce the effect which creep-relaxation has on the contact pressure and, subsequently, difference between the contact pressure immediately after the bolts had been tightened and when the circular bolted flange connection is in operation.

When the time between the bolt increments was limited to 10 seconds and the number of increments were increased to 12 the difference in the contact pressure was 7.2%. Conversely, when the number of increments was limited to three and the time between the bolt increments was increased to 60 seconds the difference in the contact pressure was 6.9%. This shows that one is able to optimise for either the amount of time between each bolt increment or for the number of bolt increments or both in an attempt to decrease the effect which creep-relaxation has on the contact pressure between the surface of the gasket and the flange face.

4.6.2. Comparison of the experimental and predicted values for the raised face flange

The calculated strains for the raised face flange, as with the flat face flange, compared well to the experimentally determined values for the instance immediately after the bolts were tightened. These results are shown in Figure 4-23. The finite element model and analysis of the raised face flange, which made use of a single bolt pretension applied instantaneously, also lacked the ability to accurately predict the strain values, at the various locations, after a period of 10 minutes. These results are shown in Figure 4-24.

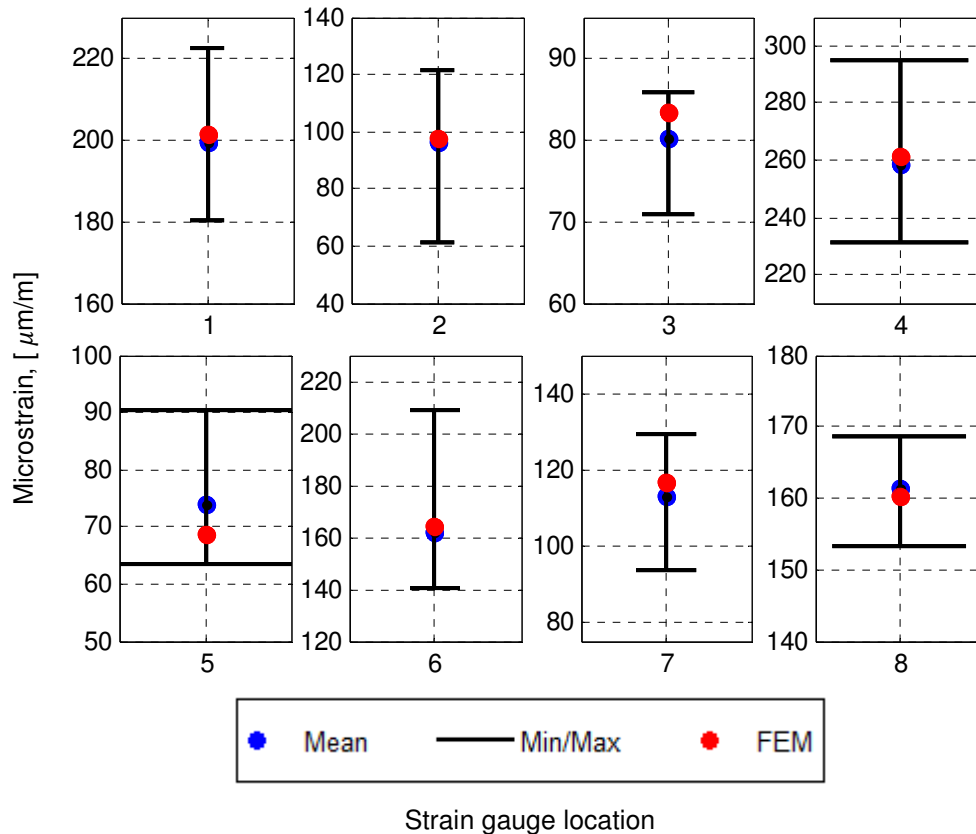


Figure 4-23: Comparison of the measured strains to the calculated strains from the finite element analysis for the raised face flange immediately after the bolts had been tightened

From Figure 4-23 and Table 4-9 the following was observed and calculated: For the seating phase of the raised face flange the calculated strains lay within the boundaries of the maximum and minimum measured strain values at all eight locations. In fact, the greatest percentage difference between the calculated and measured strains was 7.1%. The remaining seven positions showed a difference of less than 5%. The initial finite element model as was shown in Chapter 3 was, therefore, assumed to be acceptable for predicting the correct strains during the seating phase of the raised face flange.

The strains calculated by the finite element model and analysis after a period of 10 minutes differed from the measured values by more than 10% for seven out of the eight locations when compared to the mean measured value. The calculated values, for half of the locations, lay outside the bounds of the maximum and minimum measured strain values. As with the flat face flange, the finite element model of the raised face flange was unable to accurately predict the strains in the flange 10 minutes after the bolts had been fastened.

From Table 4-9 it may be seen that the difference in the measured and calculated strains, as a result of creep-relaxation, was in excess of 140% in all instances. These results were not regarded to be acceptable for the validation of the finite element model. As with the strain values calculated by the finite element model and analysis of the flat face flange so the calculated values of the raised face flange exceeded those measured at all of locations. Hence, the finite element model overestimated the effect which the creep-relaxation had on the flange assembly.

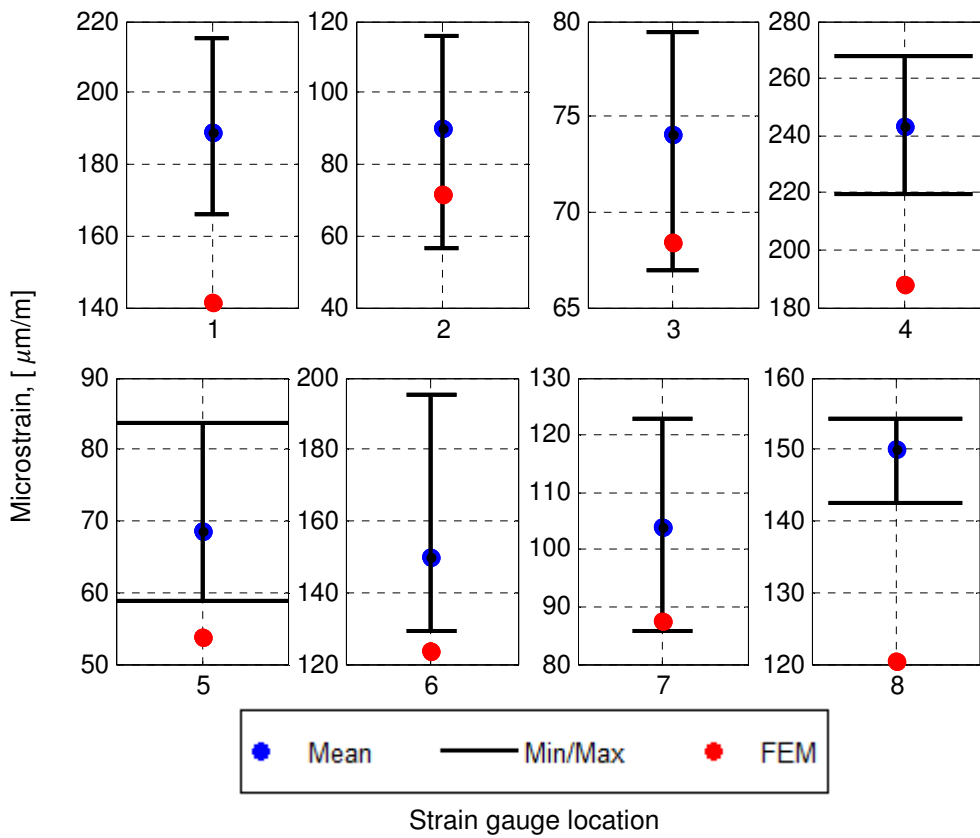


Figure 4-24: Comparison of the measured strains to the calculated strains from the finite element analysis of the raised face flange after a 10 minute period

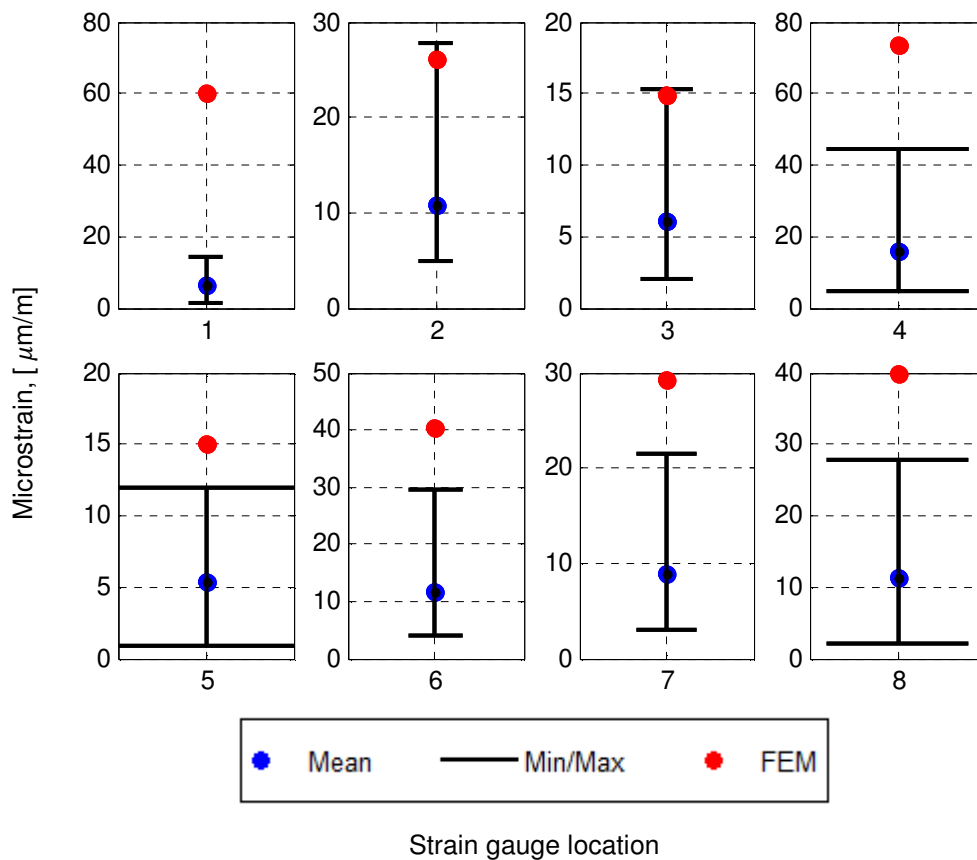


Figure 4-25: Comparison of the reduction in the measured strains to the reduction in the calculated strains from the finite element analysis of the raised face flange

Table 4-9: Summary of the results of the comparison between the measured and calculated strain for the raised face flange

Strain gauge position	Difference between the experimental and finite element results for the flat face flange		
	Immediately after the bolts were tightened [%]	10 minutes after the bolts were tightened [%]	Reduction in strain due to creep-relaxation [%]
1	1.0	25.1	872.5
2	1.9	20.2	142.1
3	4.0	7.6	145.8
4	1.1	22.8	359.4
5	7.1	21.7	177.5
6	1.5	17.3	241.0
7	3.6	15.7	225.6
8	0.6	19.7	253.1

The results of the of the raised face flange were validated for a period of 10 minutes after bolt tightening by following the same procedure as in the preceding section. A full model instead of an axisymmetric model was used and the bolt loads were applied by following exactly the same procedure as in the experiment. The results for this investigation are shown in Figure 4-26.

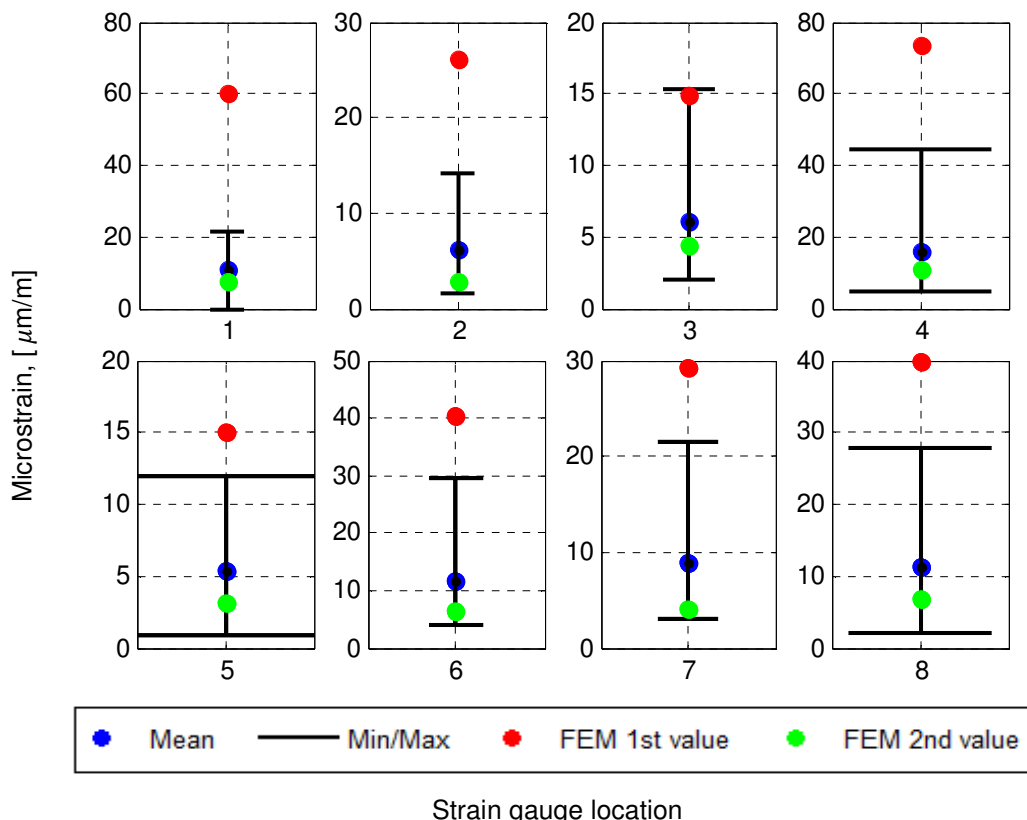


Figure 4-26: Comparison of the reduction in the measured strains to the reduction in the predicted strains from the second finite element analysis of the raised face flange

From Figure 4-26 it may be observed that the calculated values of the modified finite element model and analysis lies between the maximum and minimum measured values at all eight locations. The maximum difference between the calculated and measured mean values was 54.8%.

Table 4-10: Summary of the results of the comparison between the measured and calculated strain for the raised face flange

Strain gauge position	Difference between the experimental and finite element results for the raised face flange	
	For the first FEM [%]	For the second FEM [%]
1	872.5	32.3
2	142.1	53.5
3	145.8	27.2
4	359.4	30.5
5	177.5	41.4
6	241.0	44.5
7	225.6	54.8
8	253.1	38.8

The contact pressure from the finite element model and analysis of Chapter 3 was compared to the measured contact pressure from the experiment. Shown in Figure 4-27 and Figure 4-28 are the results obtained for the reduction in the contact pressure from both the experiment and initial finite element modelling and analysis.

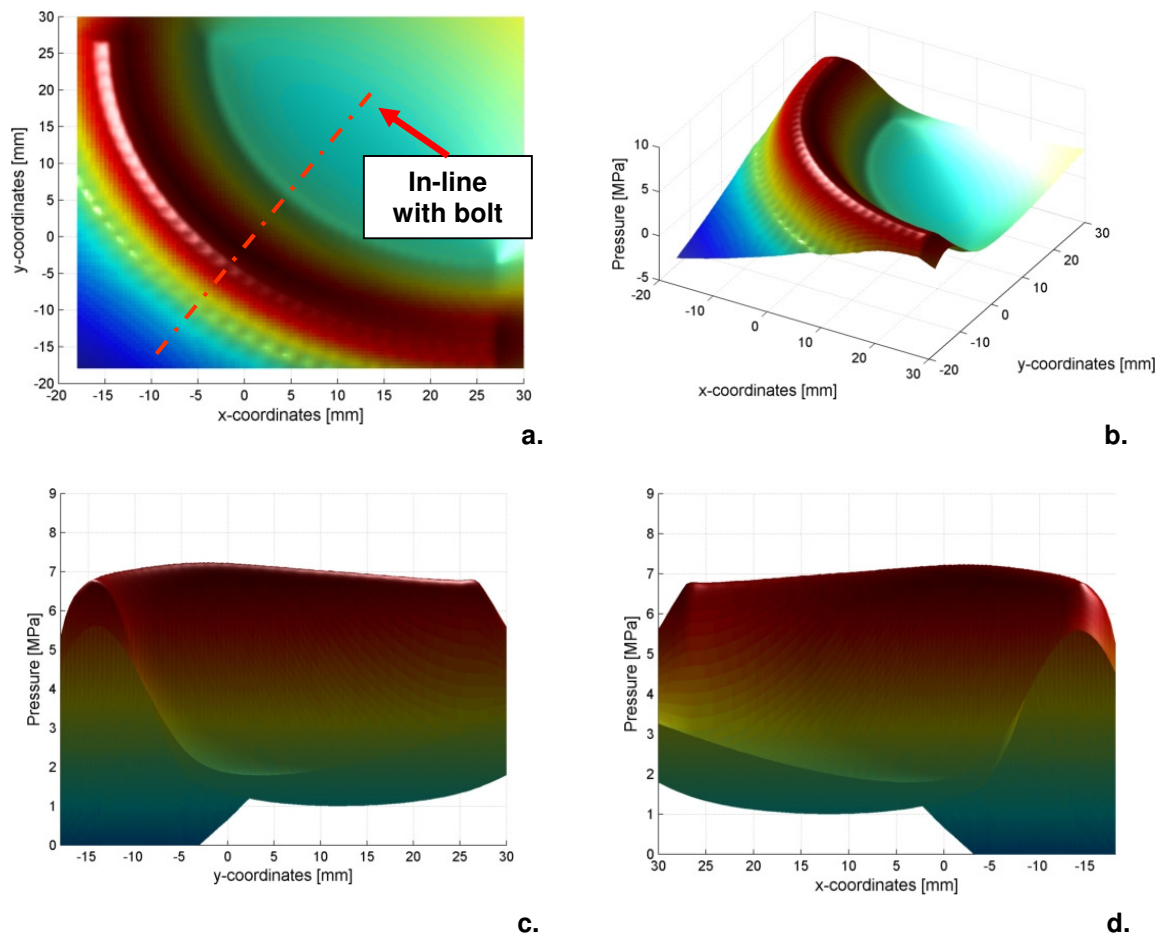


Figure 4-27: (a) Top view, (b) isometric view, (c) front view, and (d) back view of the calculated contact stress between the gasket inset and the raised flange after a period of 10 minutes

As expected, based on the strain results, the reduction in the contact pressure calculated by the finite element analysis was higher than that measured. A peak reduction of 7.1 MPa in the contact pressure was calculated by the finite element analysis. In contrast to this the maximum measured reduction in contact pressure was 1.7 MPa. As before, this value is approximately four times smaller.

As for the flat face flange, it was decided to use a full model with bolt increments which mimicked those of the experiment in order to determine whether or not this discrepancy could be explained. The bolt loads, as in the preceding section, were applied in the same manner. When this finite element analysis was run the results obtained for the contact pressure reduced significantly, although the general shape of the contact pressure remained the same. The peak contact pressure for this finite element analysis was 1.2 MPa and was located in-line with the bolt on a diameter between the inside and outside diameter of the gasket insert. These results are shown in Figure 4-28.

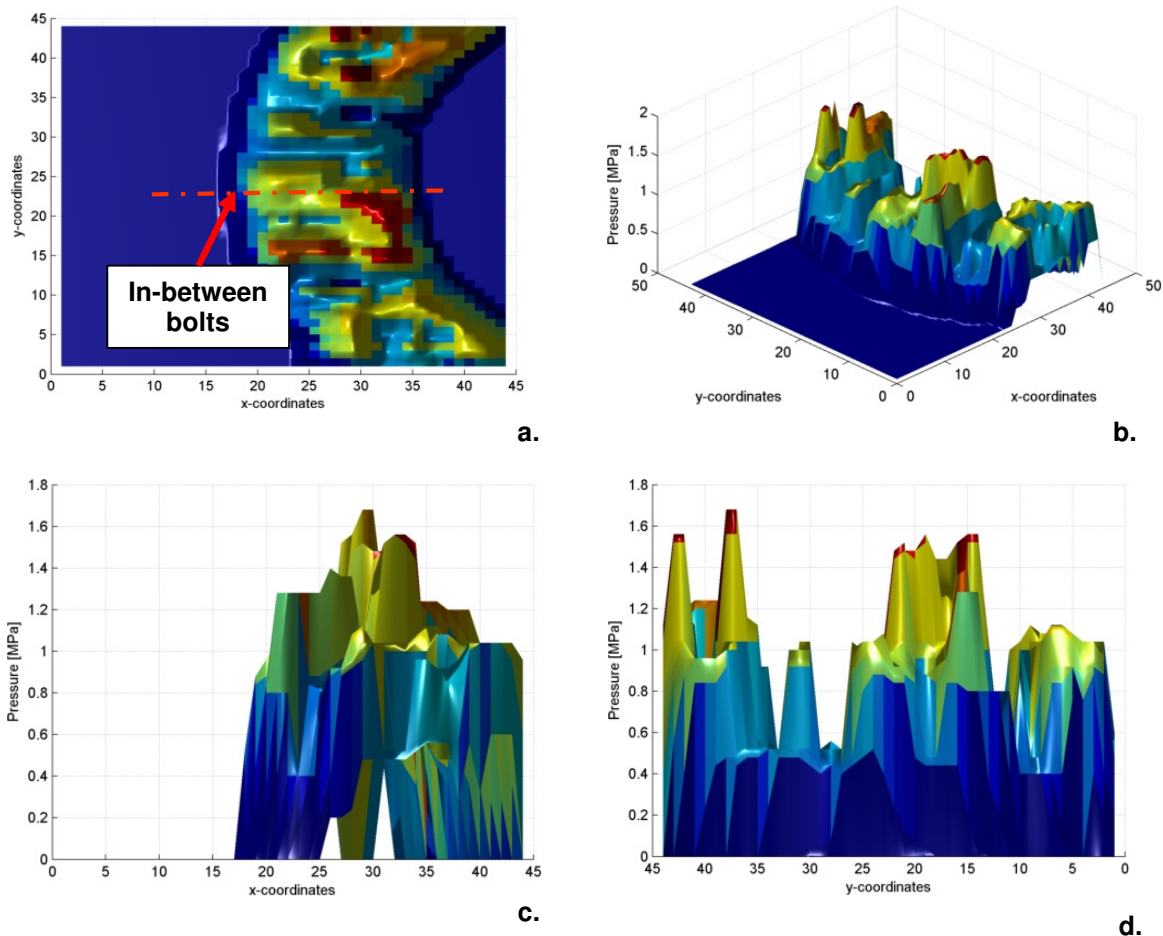


Figure 4-28: (a) Top view, (b) isometric view, (c) front view, and (d) back view of the measured reduction in the contact pressure between the raised face flange and gasket insert

From Figure 4-28 it may be seen that the measured reduction in contact pressure again has multiple maximum peaks and does not have the smooth reduction in contact pressure from the diameter between the inner and outer diameter of the gasket to the outside edges. However, despite this the calculated value of 1.2 MPa was assumed to be much more comparable to the measured reduction which had a maximum peak of 1.7 MPa. This proves, as previously shown, that the number of bolt tightening increments as well as the time between the bolt tightening increments play a significant role in the reduction of the contact pressure due to the creep-relaxation behaviour. It also shows that when the initial finite element model is expanded to a full model the calculated values correspond well to the experimental results. Furthermore, it may be concluded that the initial finite element model is conservative in its prediction of the reduction in contact pressure due to creep-relaxation.

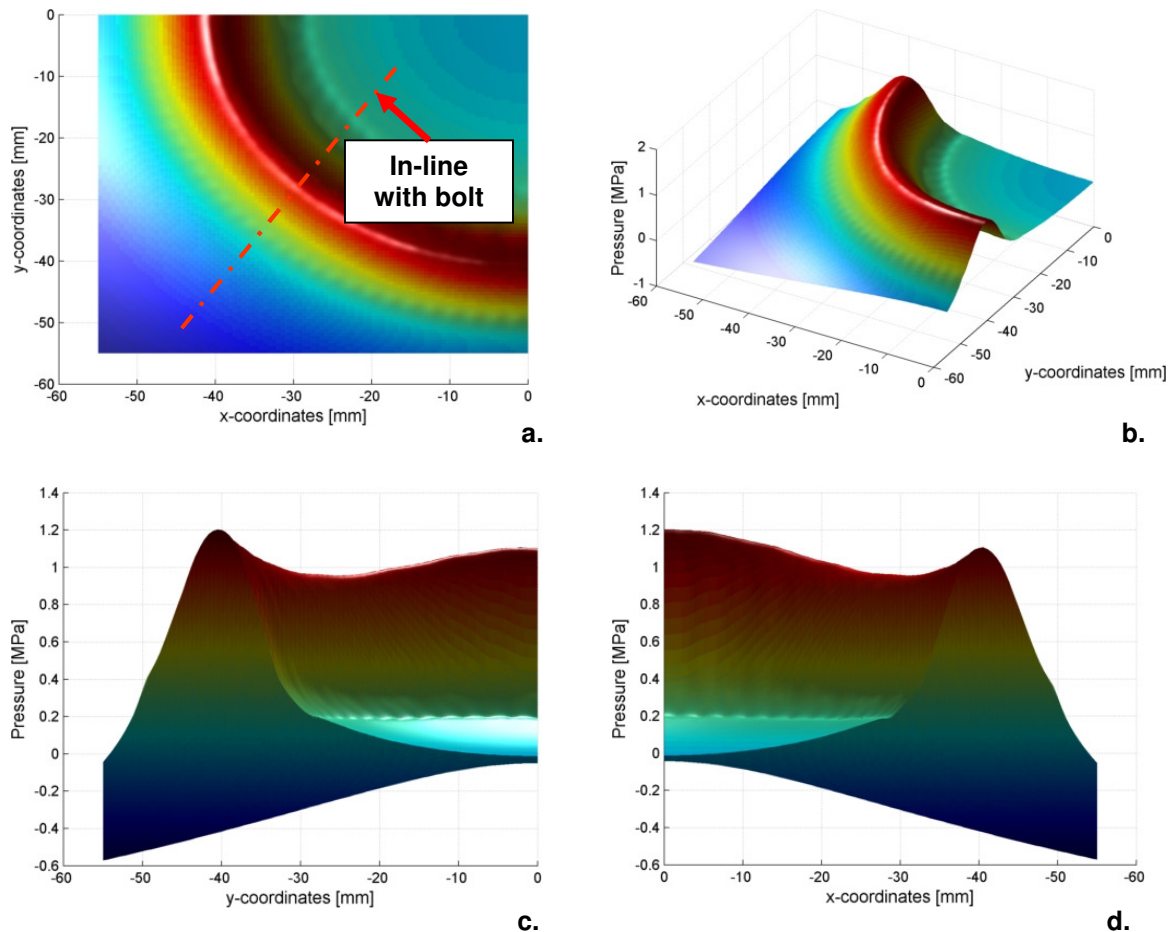


Figure 4-21: (a) Top view, (b) isometric view, (c) front view, and (d) back view of the predicted contact stress between the gasket insert and the raised face flange after a period of 10 minutes based on the modified finite element model and analysis

As before, a brief investigation was done to determine the effect which both the bolt tightening increments and the time between the bolt tightening increments had on the reduction of the contact pressure due to the creep-relaxation of the gasket insert. The exact same procedure as for the flat face flange was used and the results for this investigation are shown in Figure 4-29.

From Figure 4-29 it may be seen that the greatest percentage difference between the contact pressure, immediately after the bolts had been fastened and 10 min. after the bolts had been fastened, occurred when only three increments per bolt were used, and a maximum time of 10 s were allowed between each increment. The smallest reduction in contact pressure was obtained when 12 increments per bolt were applied with a time of 60 s between each bolt tightening increment. The maximum difference in the contact pressure was 14.42%, while the minimum difference was 3.29%. This shows that an increase in either the number of bolt increments or the amount of time between each bolt increment may significantly reduce the difference between the contact pressure right after the bolts had been tightened and when the circular bolted flange connection is in operation.

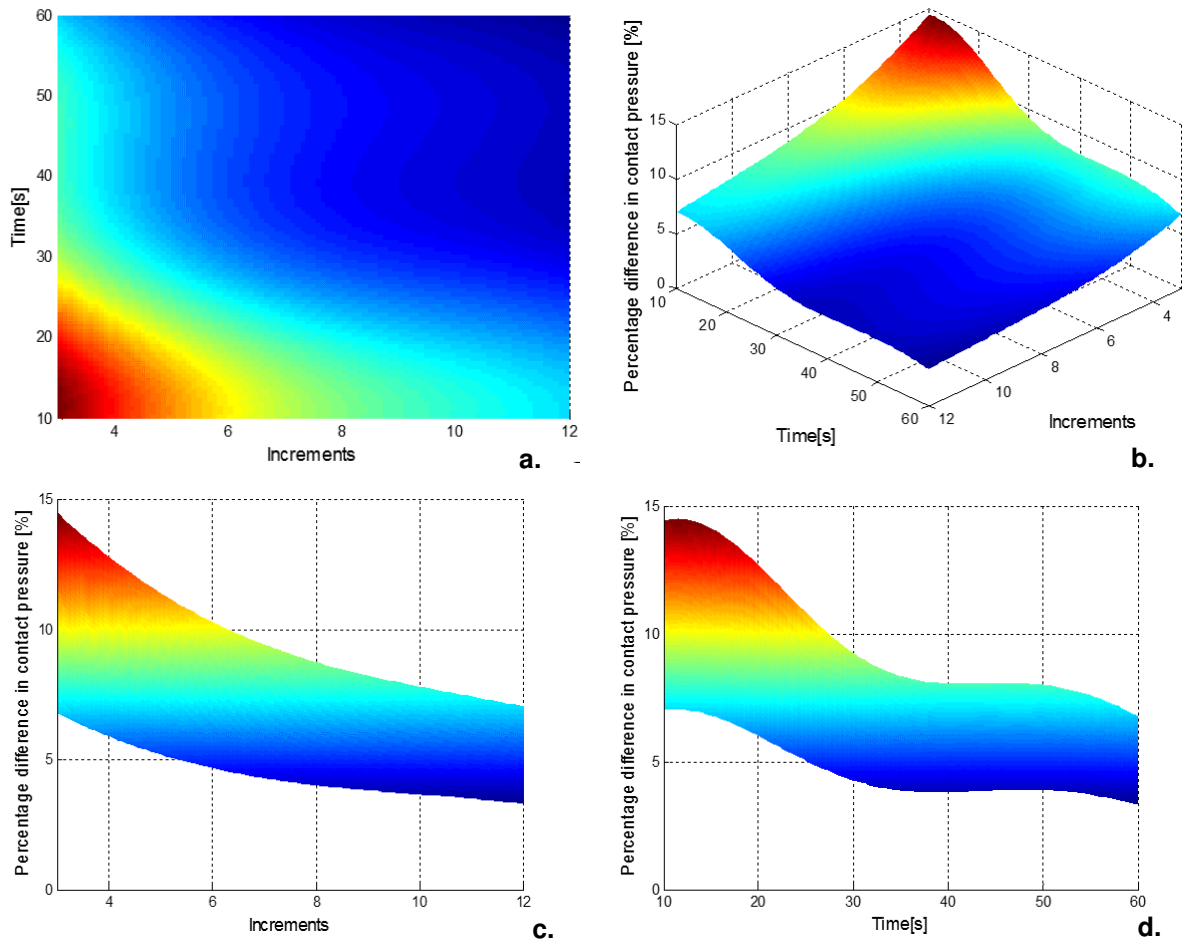


Figure 4-29: (a) Top view, (b) isometric view, (c) front view, and (d) back view of the percentage difference in the contact pressure as a function of the number of bolt tightening increments and time between the bolt tightening increments for the raised face flange

4.6.3. Comparison of the experimental and predicted values for the raised face flange with an O-ring groove

As previously stated only strain measurements were recorded on the flange for the raised face flange with an O-ring groove. It was also observed that the creep-relaxation of the O-ring had a negligible effect on the measured strains. As a result of this the only values which were compared are the predicted strain values, at the various locations on the flange, to the measured strain value immediately after bolting-up. A comparison of these results are shown in Figure 4-30 Table 4-11.

Table 4-11: Summary of the results of the comparison between the measured and calculated strains for the raised face flange with an O-ring groove

Strain gauge position	Difference [%]
1	0.58
2	35.12
3	3.53
4	0.46
5	2.05
6	3.76
7	0.16
8	0.21

From Figure 4-30 it may be observed that the predicted value of the finite element analysis lies between the maximum and minimum measured values for seven out of the eight locations. It is only lies outside these limits at Position 2, which was the tangential measurement in-line with the bolt. The predicted results differed by no more than 4% when compared to the experimental results, with the exception of the strain at Position 2 which differed by 35.1%. Despite the large difference at Position 2, the initial finite element model for the raised face flange with an O-ring groove was regarded to have suitable accuracy from which the large diameter flanges could be designed and optimised.

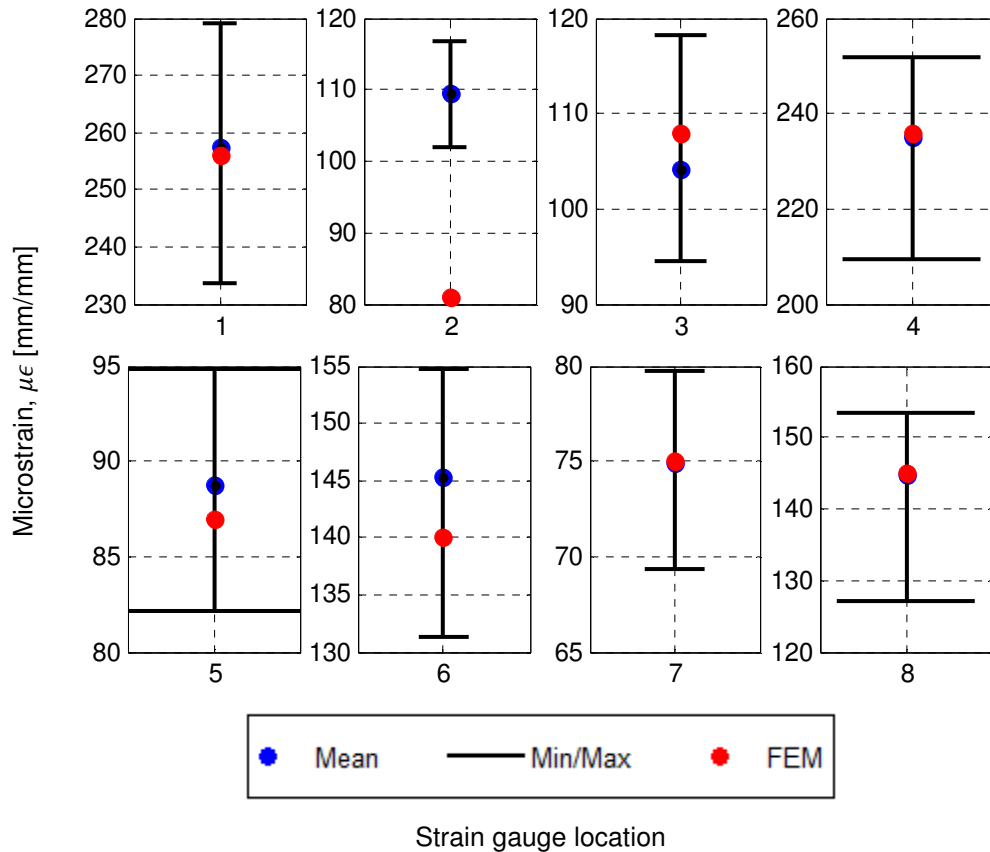


Figure 4-30: Comparison of the measured strains to the calculated strains for the finite element analysis of the raised face flange with an O-ring groove

4.7. Conclusion of the experimental setup and results

The purpose of this chapter was to validate the results of the initial finite element and analysis. A discussion of the experimental results obtained, and the comparison thereof to the calculated results of Chapter 3, is discussed below for the three different flange designs.

4.7.1. Discussion of the validation of the flat face flange

The first set of results which were compared were for the flat face flange. It was found that the initial finite element model and analysis (as described in Chapter 3) had a difference of less than 10% for six out of the eight positions when compared to the mean experimental values. The position with the largest difference, when compared the mean experimental value, was the tangential strain on the ring of the flange, in-line with the bolt and it had a difference of 23.1%. All of the calculated strains, from the finite element analysis, lay between the maximum and minimum measured strains. Based on this it was decided that the initial finite element model for the flat face flange was acceptable for the bolting-up phase. When the strain results measured 10 minutes after bolting-up were compared to the calculated strains of the flat face flange model the following was noticed: none of the predicted strains lay within the maximum and minimum boundaries of the measured strains at the various positions; the reduction in strains calculated by the finite element model and analysis exceeded that which was measured at all

of the positions; and none of the calculated reduction in strains had a difference of smaller than 400% when compared to the mean measured strains at the various positions. Based on this it was deemed that the initial finite element model and analysis for the flat face flange, as described in Chapter 3, is not suitable for predicting the behaviour of the flange assembly during the experiment. In an attempt to find the cause of this discrepancy a full finite element model, instead of an axisymmetric model, was used. In addition to this the bolt loads were applied in exactly the same manner in which they were applied in the experiment with regards to both the sequence as well as the average time between bolt tightening. This change in the finite element model and analysis resulted in all of the predicted values being between the minimum and maximum measured strains. It also resulted in a more than 330% reduction in the difference. From these results it may be concluded that the bolt sequence and time between bolting-up has a significant effect on the reduction in strains caused by the creep-relaxation behaviour of the gasket insert. From a design point of view the axisymmetric model, for the flat face flange, is still deemed to be suitable since it can accurately predict the value for the bolting-up phase and overestimate the value thereafter which will result in a slightly more robust design. However, if a model is required to predict the behaviour of a flange, after the bolting-up phase, a full model (based on the axisymmetric model) which includes both the bolt sequence and the time between bolt increments may be used.

A similar trend was observed when the calculated and measured contact pressures were compared to one another for the flat face flange and gasket insert. The reduction in the contact pressure between the gasket insert and the flat face flange was calculated by the axisymmetric model to be 4.1 MPa. The measured reduction in the contact pressure had a single maximum peak at 1.9 MPa, although the majority of the maximum peaks lay between 1.4 MPa and 1.6 MPa. The calculated reduction in the contact pressure by the initial finite element model was, therefore, two to three times larger. As with the discrepancy between the measured strains and those predicted by the axisymmetric model a full model with the exact bolting-up sequence and time between bolt increments was used to find a probable answer. The results of this finite element model and analysis showed a reduction in the contact pressure of 1.15 MPa which is much comparable to values between 1.4 MPa and 1.6 MPa. This, again, highlighted, two important aspects. Firstly the axisymmetric model is conservative in the way it models the effect of the creep-relaxation on the contact pressure. It overestimates the reduction in contact pressure and may, therefore, be deemed to be acceptable from a design point of view. Secondly, that the bolt sequence and time between the bolting increments has a significant impact the overall effect of the creep-relaxation behaviour of the gasket insert.

4.7.2. Discussion of the validation of the raised face flange

A comparison of the results for the raised face flange showed the following: for the seating phase the calculated strains of the initial finite element model and analysis differed by less than 10% when compared to the mean experimental values. In addition to this all of the calculated values lay between the maximum and minimum measured values. From these results the initial finite element model and analysis was considered to be suitable for predicting the strains during the seating phase. The calculated strain values of the finite element model of the raised face flange exceeded the measured experimental values for a period of 10 minutes after bolting-up. Seven out of the eight calculated values lay outside the minimum and maximum measured strain values. As before a full finite element model of the raised face flange, with the experimental sequence given in Section 4.5., was used to investigate this difference. When this model was applied it was found that all of the calculated strains lay between the maximum and minimum measured values. The calculated values also differed by less than 55% when compared to the mean measured values at all of the positions. Again the effect which the bolt sequence and time between bolt tightening increments has on the values obtained was emphasised.

As expected the calculated contact pressure, as predicted by the initial finite element model, was more than four times greater than that which was measured for the raised face flange. It is known that bolt sequence and time between bolt increments has an effect on the reduction in contact pressure as a result of creep-relaxation. Because of this it was decided to again implement the previously described full model. The results from the full model predicted a maximum reduction in contact stress of 1.2MPa

which differs by only 25% when compared to the measured results and is significantly lower than the original 80%.

As stated the time between the bolt increments as well as the number of bolt increments has an effect on the reduction of the contact stress due to creep-relaxation. This effect was briefly investigated by varying both the time between bolt increments as well as the number of bolt increments. It was found that reduction in contact pressure, for both the flat face and raised face flange, could be minimised by increasing the time, increasing the number of increments, or increasing both. Depending on the desired contact pressure this knowledge may be used to optimise bolt tightening techniques.

4.7.3. Discussion of the validation of the raised face flange with an O-ring groove

The final set of results which were presented was that of the raised face flange with an O-ring groove. Since the creep-relaxation of the O-ring had a negligible effect on the measured strains only the results during the seating condition were considered. The predicted strains for all the locations, except one, differed by less than 5% when compared the measured strains. Based on this the model was deemed to have acceptable accuracy for the design of large diameter flanges and the relevant optimisation thereof.



CHAPTER 5: APPLICATION OF METHOD TO LARGE DIAMETER FLANGES

5.1. Background relating to the design of large diameter flanges

ASME VIII's inability to accurately predict stress values, in large diameter flanges which operate at high pressures, results in two undesirable consequences. The first consequence is that flanges are often overdesigned; and the second is that, despite being overdesigned, the flanges tend to leak as a result of insufficient contact pressure between the packing material and the flange faces [18]. Leakage, generally, occurs as a result of: excessive flange rotation, gasket creep-relaxation, or insufficient bolt pre-tension. ASME VIII attempts to correct for the flange rotation, however, no design rules are suggested for determining the effect which creep-relaxation has on the contact pressure between the packing materials and the flange faces [20].

In Chapter 3 finite element models were suggested for the three types of flanges used by Rand Water, namely: a flat face flange, a raised face flange, and a raised face flange with an O-ring groove. The finite element models accounted for the effects of creep-relaxation (with reference to the flat and raised face flanges), and flange rotation. The results of the initial finite element modelling and analysis, for the three types of flanges, were validated by means of small-scale experimentation. The results for the experimentation and the comparison thereof to the results of the initial finite element analysis were shown and discussed in Chapter 4. These validated finite element models for the flat face flange, the raised face flange, and the raised face flange with an O-ring groove were used as the basis for the design of large diameter flanges which operate at pressures between 1 500 kPa and 8 000 kPa. Apart from simply using these models as the basis for the design of large diameter flanges, it was also shown that they could be used for the optimisation thereof.

5.2. Design methodology and assumptions

For the design of large diameter flanges, which are required to operate at both low and high pressures, a number of assumptions were made. These assumptions are discussed below. It should, however, be remembered that the values presented in this section are based on the aforementioned material assumptions (specifically for the packing materials). If the material properties of the packing materials (both the gasket insert and the O-ring) change drastically then the design values discussed below will no longer be true. The purpose of this chapter is to merely illustrate the capability of the model as opposed to expanding the existing flange tables by giving 'ready-to-use' design values.

5.2.1. General assumptions made for the design of large diameter flanges

The assumptions made were: although the models had not been validated for the operating conditions it was assumed that internal pressure, which is known to play a significant role, may be applied in order to obtain initial values for the operating condition from the finite element analysis. The effects of thermal expansion, external loads, and bending moments have not been included in the finite element modelling and analysis of the large diameter flanges, as was discussed in Chapter 1. Finally, it was shown in Chapter 3 that the method of bolt tightening had a significant effect on both the seating and operating contact pressures. For the design of the large diameter flanges it was assumed that the recommendations made in Chapter 3, regarding the number of bolt tightening increments, had been correctly applied and that the load applied to the surface of the gasket was evenly distributed across the bolted flange connection. This assumption, as stated in Chapter 3, allowed for the use of an axisymmetric model.

5.2.2. Design methodology

The design of the large diameter flanges was split into three steps. The first step was to use ASME VIII Division 1's design-by-rule approach to obtain an estimate of the initial dimensions. As previously stated, ASME VIII (Division 1) does not necessarily have the ability to guarantee a leak tight design where all the stresses are accurately predicted for large diameter flanges which operate at high pressures. Based on this the finite element models, which were developed in Chapter 3 and validated in Chapter 4, were used to check that the circular bolted flange assemblies met the following criteria:

1. The maximum equivalent Von Mises stresses in the flanges and fasteners did not exceed their respective allowable stresses for both the seating and operating conditions.
2. There was sufficient contact pressure between the faces of the flanges and their respective packing materials during the operating conditions.
3. The maximum equivalent Von Mises stress in the gasket did not exceed the maximum tensile strength given by the manufacturer – i.e. no 'blow-out'.

The third, and final step, was to optimise the designed and checked flanges. The flanges were optimised for a number of criteria, which is discussed in Section 5.5.

5.3. Design of large diameter flanges by means of ASME VIII, Division 1

The large diameter flanges were designed by means of the ASME VIII, Division 1, with the aid of Iysoft's Pipmill software [40]. For illustrative purposes the circular bolted flange connections were designed with a nominal bore of 4 m. This was done in order to show that the method which was developed may be applied to the maximum desired nominal bore values for the expansion of the flange tables for all three types of circular bolted flange connections. Shown in Figure 5-1 are some of the principal flange dimensions which needed to be specified in the design of the large diameter flanges in accordance with the ASME VIII, Division 1's design methodology.

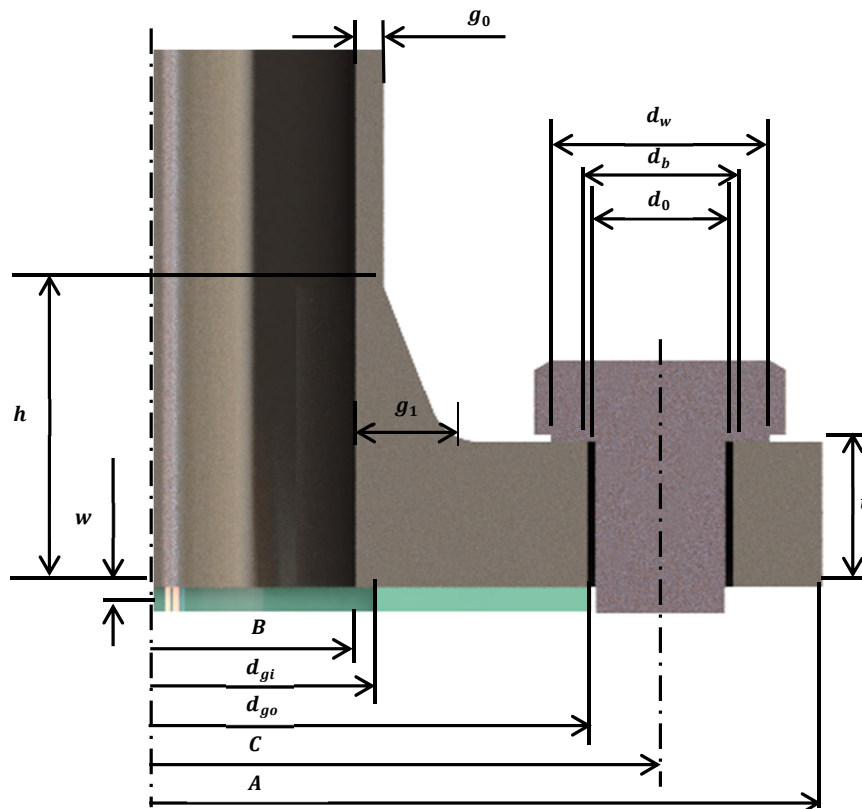


Figure 5-1: Principal dimensions of a circular bolted flange connection

Both the flat and raised face flanges were designed by means of the ASME VIII, Division 1's code for test pressures of 1 500 kPa, and 3 500 kPa, respectively. Since the design of the O-ring groove is not prescribed by ASME VIII, Division 1, the dimensions for the raised face flange was used as an initial guess.

5.3.1. Design of the large diameter flat and raised face flanges by means of ASME VIII, Division 1

For the design of the flat and raised faces flanges, by means of the ASME VIII, Division 1 code, a gasket factor and a value for the seating stress needed to be assigned to the gasket material, as was discussed in Chapter 2. The gasket insert which was used and characterised was a Klinger C 4400 non-asbestos

compressed fibre gasket with aramid and a nitrile rubber binder. The gasket factor, m , which was assigned by the manufacturer was 3.90. The value for the required seating stress, y , was given as 20 MPa [41]. These two values were assumed for the design of both the large diameter flat face flange and the large diameter raised face flange.

The design process for the flat face flange is shown below. A similar procedure was followed for the raised face flange. The design values, for the flat and raised face flanges, are summarised in Appendix D, and the principal flange dimensions are given in Table 5-2.

The first step in the design process, from Section 2 of Chapter 2, was to establish:

1. The temperatures for both the seating and operating conditions.
2. The operating pressure.
3. The flange material.
4. The bolting material.

As previously discussed, the flanges will be used to connect large pipes which are responsible for the supply of water to households. Based on this it was assumed that both the seating and operating conditions will be at an ambient temperature of 25°C. The operating pressures will be assumed to be equal to the test pressures for the initial design and finite element analysis of the large diameter flanges. The flat face flange will, therefore, be subjected to an internal pressure of 1 500 kPa, whilst the raised face flange will have an internal pressure of 3 500 kPa. The choice of the material for both the flanges and fasteners was arbitrary since the purpose of this chapter was merely to illustrate the suggested design method. It was assumed that the flange material was ASTM A-350; and the bolts were Class 8.8 fasteners.

5.3.2. Calculation of the allowable flange and bolt stresses

The next step in the design of the large diameter flanges was the calculation of the maximum allowable flange and bolt stresses. The maximum allowable flange and fastener stresses were taken as the smaller of the two values calculated by Equations 2.4. and 2.5. The flange and bolt materials have yield strengths of 250 MPa and 640 MPa, respectively, at an ambient temperature of 25°C. The tensile strengths for the flange and fastener materials, at 25°C, are 485 MPa and 830 MPa, respectively [42] [43]. Therefore from Equations 2.4. and 2.5. for the flange material:

$$\begin{aligned} S_{fo} &= \min \left\{ \left(\frac{250}{1.5} \right), \left(\frac{485}{2.4} \right) \right\} \\ &= \min \{167, 202\} \\ &= 167 \text{ MPa} \end{aligned}$$

and for the bolts:

$$\begin{aligned} S_b &= \min \left\{ \left(\frac{660}{1.5} \right), \left(\frac{830}{2.4} \right) \right\} \\ &= \min \{440, 346\} \\ &= 346 \text{ MPa} \end{aligned}$$

5.3.3. Calculation of the root area of the bolts

Once the allowable stresses for the flanges and fasteners had been calculated the root area, R_a , of the bolts could be calculated. This calculation was done by substituting Equations 2.7. to 2.11. into Equation 2.6. This resulted in the following:

$$\begin{aligned} R_a &= \frac{\max \left(\frac{b\pi G y}{S_a}; \frac{\frac{G^2 \pi P}{4} + 2b\pi G m P}{S_b} \right)}{n} \\ &= \frac{\max \left(\frac{(11.26) \cdot \pi \cdot (4077.46) \cdot y}{167}; \frac{\frac{(4077.46)^2 \cdot \pi \cdot (1.5000)}{4} + 2 \cdot (11.26) \cdot (11.26) \cdot 3.9 \cdot 1500}{346} \right)}{68} \end{aligned}$$

$$= \frac{\max(17\,274; 341\,805)}{68}$$

$$= 40 \text{ mm}$$

It may be observed that either the number of bolts or root area of the bolts could have been changed. An increase in the number of bolts will result in a decrease in the required root area of the bolts, and conversely a decrease in the number of bolts would have resulted in an increase in the root area of the bolts. For this part of the chapter the number of bolts was fixed at 68 and the root area of the bolts was determined. At a later stage it may be possible to optimise the design in order to find the ideal desired relationship between the number of bolts and the root area of the bolts.

5.3.4. Calculation of the total bolt load

The total bolt load was determined from the total bolt area by means of Equation 2.12. When 68 bolts are used:

$$W = \frac{(403\,326)(346)}{2}$$

$$= 6.977 \times 10^7 \text{ N}$$

5.3.5. Calculation of the assumed principal forces and their moments

The next step was the calculation of the assumed principal forces and their associated moments. From Equations 2.13. to 2.24. the loads, lever arms and moments were calculated for the operating conditions of the flange.

$$H_D = \frac{\pi B^2 P}{4}$$

$$= 1.88 \times 10^7 \text{ N}$$

$$H_G = W_{m1} - H$$

$$= H + H_p$$

$$= \frac{G^2 \pi P}{4} + 2b\pi GmP$$

$$= 1.67 \times 10^6 \text{ N}$$

$$H_T = H - H_D$$

$$= \frac{G^2 \pi P}{4} - H_D$$

$$= 1.96 \times 10^7 - 1.88 \times 10^7$$

$$= 7.37 \times 10^5 \text{ N}$$

$$h_D = R + 0.5g_1$$

$$= 196 \text{ mm}$$

$$h_G = \frac{C - G}{2}$$

$$= 257 \text{ mm}$$

$$h_T = \frac{R + g_1 + h_G}{2}$$

$$= 277 \text{ mm}$$

$$\begin{aligned} M_D &= H_D h_D \\ &= 3.69 \times 10^9 \text{ N.mm} \end{aligned}$$

$$\begin{aligned} M_G &= H_G h_G \\ &= 4.35 \times 10^8 \text{ N.mm} \end{aligned}$$

$$\begin{aligned} M_T &= H_T h_T \\ &= 2.04 \times 10^8 \text{ N.mm} \end{aligned}$$

The maximum operating moment is the sum of the moments in all the directions, therefore:

$$\begin{aligned} M_O &= M_D + M_G + M_T \\ &= 3.68 \times 10^9 + 4.36 \times 10^8 + 2.04 \times 10^8 \\ &= 4.33 \times 10^9 \text{ N.mm} \end{aligned}$$

From this the moment for the seating condition may be calculated as follows:

$$\begin{aligned} M_O' &= H_G h_G \\ &= 1.80 \times 10^{10} \text{ N.mm} \end{aligned}$$

5.3.6. Ratios and shape factors

Once the principal loads and moments had been determined, the shape factors were determined. The shape factors include the following variables: K , T , Z , Y , U , V , F , and f . These factors were read off from a series of plots given in ASME VIII, Division 1.

$$\begin{aligned} K &= \frac{A}{B} \\ &= 1.19 \end{aligned}$$

The shape factors which were read off from the plots are given in Table 5-1.

Table 5-1: Shape factors for the design of the large diameter flat face flange

Symbol	Value
F	0.84
f	1.00
T	1.84
U	12.49
V	0.28
Y	11.36
Z	5.86

$$\begin{aligned} d &= \frac{U}{V} h_o g_o^2 \\ &= 4.42 \times 10^8 \text{ mm}^3 \end{aligned}$$

$$\begin{aligned} h_o &= \sqrt{B g_o} \\ &= 692.82 \text{ mm} \end{aligned}$$

$$\begin{aligned} e &= \frac{F}{h_o} \\ &= 1.21 \times 10^{-3} \text{ mm}^{-1} \end{aligned}$$

5.3.7. Stress formula factors

The values obtained for the shape factors were then used to calculate the stress formula factors. The following stress factors were calculated:

$$\begin{aligned}\beta &= \frac{4}{3} \cdot te + 1 \\ &= \frac{4}{3} \cdot (250) \cdot 1.25 \times 10^{-3} + 1 \\ &= 1.41\end{aligned}$$

$$\begin{aligned}\lambda &= \gamma + \delta \\ &= \frac{\alpha}{T} + \frac{t^3}{d} \\ &= \frac{(te + 1)}{T} + \frac{t^3}{d} \\ &= 0.74\end{aligned}$$

$$\begin{aligned}m_o &= \frac{M_o}{B} \\ &= 1.08 \times 10^6 N\end{aligned}$$

$$\begin{aligned}m_G &= \frac{M_o'}{B} \\ &= 4.50 \times 10^6 N\end{aligned}$$

5.3.8. Stress calculations

The final step in the design method was the calculation of the operating and seating stresses in the axial, radial, and tangential direction. For the operating axial, radial, and tangential stress Equation 2.39. to 2.41. were applicable:

$$\begin{aligned}S_H &= \frac{f m_o}{\lambda g_1^2} \\ &= 36 MPa\end{aligned}$$

$$\begin{aligned}S_R &= \frac{\beta m_o}{\lambda t^2} \\ &= 33 MPa\end{aligned}$$

$$\begin{aligned}S_T &= \frac{m_o Y}{t^2} - Z S_R \\ &= 5 MPa\end{aligned}$$

For the seating axial, radial, and tangential stress Equations 2.36. to 2.41. were applicable:

$$\begin{aligned}S_H &= \frac{f m_G}{\lambda t^2} \\ &= 151 MPa\end{aligned}$$

$$\begin{aligned}S_R &= \frac{\beta m_G}{\lambda t^2} \\ &= 136 MPa\end{aligned}$$

$$\begin{aligned}S_T &= \frac{m_G Y}{t^2} - Z S_R \\ &= 19 MPa\end{aligned}$$

The complete design of the large diameter flat and raised face flanges – in accordance with ASME VIII, Division 1 – is shown in Appendix D. However, shown in Table 5-2 is a summary of principal dimensions of the designed large diameter flat and raised face flanges. .

Table 5-2: Initial values for the dimension of the flat and raised face flanges

Parameter	Symbol	Dimensions for the flat face flange [mm]	Dimensions for the raised face [mm]
Hub length	h	330	330
Hub thickness – large	g_1	200	190
Hub thickness – small	g_0	120	97
Flange thickness	t	250	200
Flange inner diameter	B	4 000	4 000
Flange outer diameter	A	4 752	4 790
Bolt hole diameter	d_h	90	90
Pitch circle diameter	C	4 592	4 590
Bolt diameter	d_b	80	80
Number of bolts	N	68	68
Gasket inner diameter	d_{gi}	4 020	4020
Gasket outer diameter	d_{go}	4 481	4 481
Raised face	rf	N.A.	10

Shown in Table 5-3 are the predicted axial, radial, and tangential stresses for both the seating and operating conditions for the flat and raised face flanges. In both instances the lowest predicted stresses were in the tangential direction.

Table 5-3: Predicted axial stress, radial stress, and tangential stress for the design of the large diameter flat and raised face flanges in accordance with ASME VIII, Division 1,

	Flat face flange			Raised face flange		
	Axial stress [MPa]	Radial stress [MPa]	Tangential stress [MPa]	Axial stress [MPa]	Radial stress [MPa]	Tangential stress [MPa]
Seating	151.1	135.9	19.2	91.2	103.3	12.6
Operating	36.5	32.8	4.6	120.7	136.8	16.7

5.4. Finite element modelling for the large diameter flanges

In this section the relevant material models, geometry, contact interfaces, loads, and boundary conditions for the finite element modelling and analysis of the three types of large diameter flanges will be discussed.

5.4.1. Relevant material models for the large diameter flanges

The material for both the flanges and fasteners were assumed to be linear-isotropic with a modulus of elasticity, E , of 207 GPa and a Poisson's Ratio 0.3.

It was assumed that the same type of gasket, as previously discussed, is used in the design of the large diameter flat and raised face flanges. The same material model as characterised in Chapter 3 was, therefore, used. It should be noted, however, that the contact pressures to which the gasket was subjected were much greater for the large diameter flanges than for the experimental instance. The subsequent effect was that the amount of creep, as shown in Chapter 3, was overestimated. This, therefore, lead to a more conservative approximation of the contact pressure between the gasket surface and the flange faces. For the O-ring, a third order Ogden material model was assumed with the same material coefficients as shown in Table 3-4.

5.4.2. Geometry

For the geometry of the finite element models of the flat and raised face flanges it was assumed that axisymmetric models may be used. The initial dimensions, for the finite element models of the flat and raised face flanges, were calculated from the ASME VIII, Division 1 code. The same initial dimensions as for the raised face flange (shown in column two of Table 5-2) were assumed for the raised face flange with an O-ring groove. The only difference in design between the two was the addition of the O-ring groove in the latter case. In this instance three different sized O-rings were considered, and subsequently three different groove sizes were implemented. Three different O-ring sizes were considered in order to determine the effect which the O-ring size has on the maximum equivalent Von Mises stress in the flange, and the contact pressure between the flange face and O-ring. The three different O-ring groove sizes, which were implemented, are given in Figure 5-2.

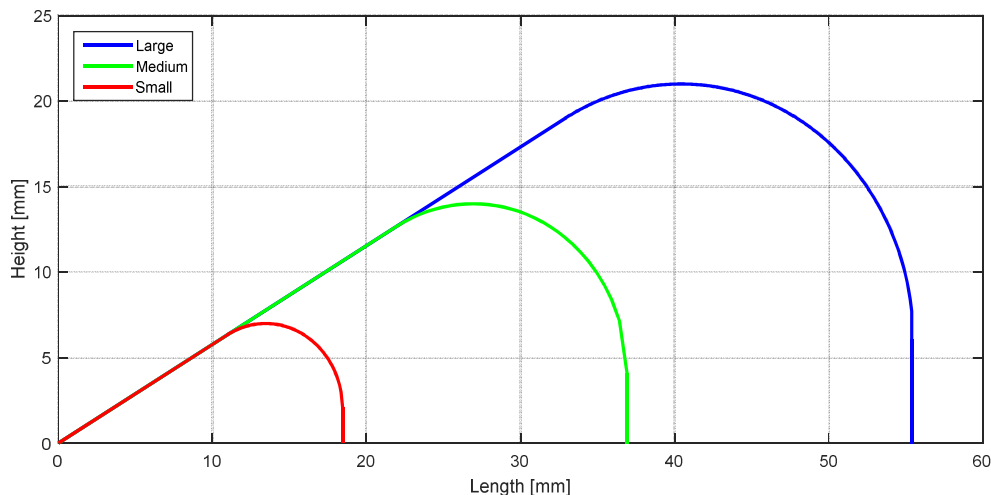


Figure 5-2: Cross-sectional dimensions of the three investigated O-ring grooves

For the finite element modelling and analysis of the large diameter flat and raised flanges it was desired to reduce the number of elements and subsequently the solving time. This was achieved by assuming a symmetrical plane midway through the gasket thickness as discussed and shown in Chapter 2, Section 2.3. Unlike the flat and raised face flanges, a simplified axisymmetric model could not be assumed for the raised face flange with an O-ring groove since the circular bolted flange connection was not symmetrical about the plane created by the packing material. This is because a raised face flange and a raised face flange with an O-ring groove were used.

5.4.3. Contact interfaces

The contact interfaces were applied in the same manner as was discussed in Chapter 3, Section 3.4.7. In short, the fasteners were bonded to the faces of the flanges, the bolts and nuts were bonded, and the interfaces between the packing materials and the flange faces were specified to be frictional. The coefficient of friction between the gasket and flange face, and O-ring and flange face were assumed to be 0.3 and 0.9, respectively.

5.4.4. Loads and boundary conditions

The loads and boundary conditions were applied to the finite elements models as was specified in Chapter 3. For the axisymmetric models the faces in the circumferential direction were normally

constrained against translation. In addition to this, for the flat and raised face flanges, the symmetry plane was constrained against any axial translation (Figure 5-3 a.). The bottom face of the bottom flange was constrained against any axial translation for the circular bolted flange connection which made use of a raised face flange with an O-ring groove (Figure 5-3 b.).

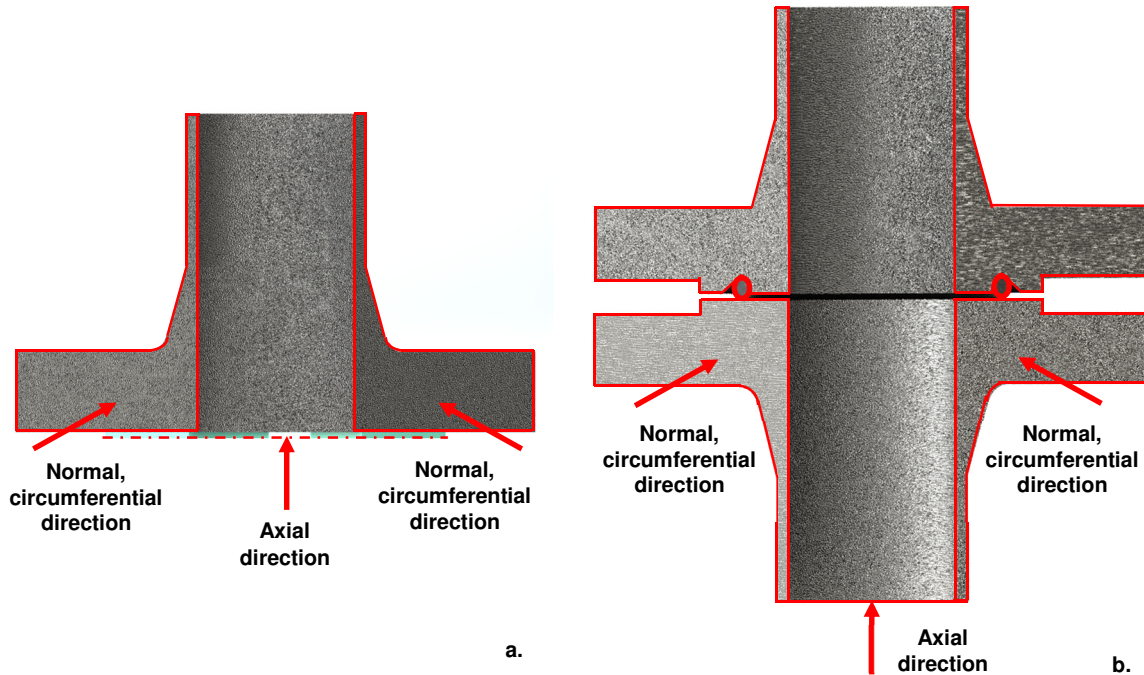


Figure 5-3: Application of the boundary conditions to the non-linear finite element models of (a) the flat and raised face flanges, and (b) the raised face flange with an O-ring groove

Two loads were applied to the finite element model (Figure 5-4). The first load was the bolt pre-tension. This was done in the same way as discussed in Chapter 3. In addition to the bolt pre-tension a pressure load was also applied.

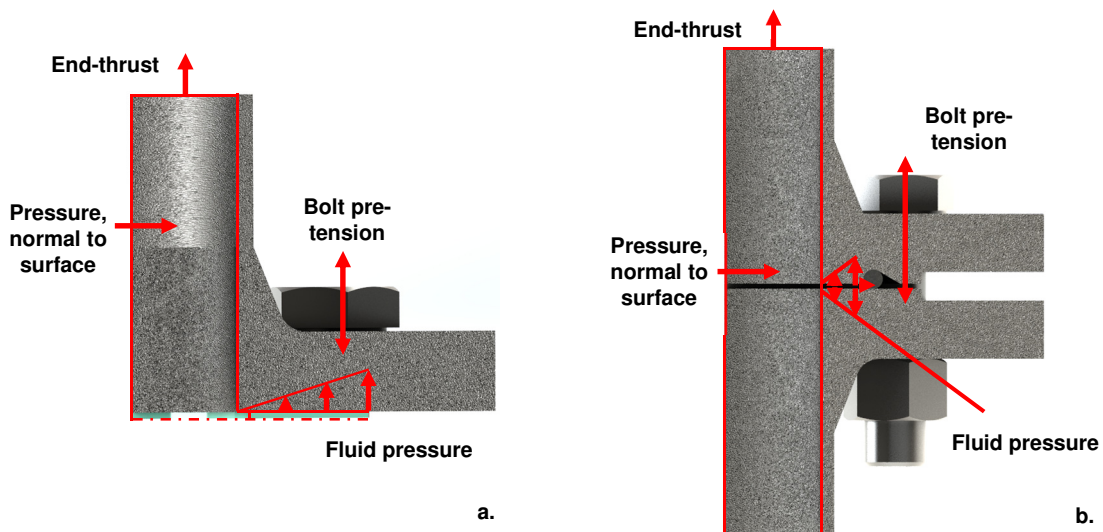


Figure 5-4: Application of the loads to the non-linear finite element models of (a) the flat and raised face flanges, and (b) the raised face flange with an O-ring groove

The application of the pressure load was slightly more complex than that of the bolt pre-tension. It should be noted that the initial finite element models were not validated for the pressurised condition. The pressure was applied to the inside surfaces of the flange. However, in addition to this, the gap created as a result of flange rotation also needed to be accounted for. The bolt loads as prescribed by ASME VIII, Division 1, were applied to the circular bolted flat and raised face flanges. An individual bolt load of 5×10^5 N was, however, applied to the raised face flange with an O-ring groove.

At this point it is important to explain the timeline associated with the application of the loads for the flat and raised face flanges. At time Step 1, which is within the first second, the bolt pre-tension was applied. The bolt pre-tension resulted in flange rotation which created a gap between the surface of the gasket and the faces of the flanges. Subsequently this resulted in localisation of the contact pressure where the gasket becomes pinched. Time Step 2 was from 1 second to 4 000 seconds. This time step mimicked an instance where 4 000 seconds was allowed to pass from the gasket seating phase to the operating phase. During the 4 000 seconds the gasket experienced creep-relaxation which resulted in a reduction in contact pressure. The final time step, Step 3, was from 4 000 to 4 001 seconds and represents the operational phase. During this time step the specified internal pressure was applied. The pressure was applied to the inside surfaces of the flanges, and the gasket. In addition to this an end thrust, which resulted from the internal pressure, was also applied to the top surface of the top flange. However, as previously stated, pressure should also be applied to the gap created between the gasket surface and the flange face which resulted from flange rotation during the seating phase. This was achieved through the application of 'fluid pressure' in ANSYS 16.2.

The timeline associated with the raised face flange with an O-ring groove is slightly different. At time Step 1 a prescribed displacement was applied at the interface between the washer face of the bolt and the top surface of the flange. This prescribed displacement was equal to the gap between the raised face flange and the raised face flange with the O-ring groove. A bolt adjustment equal to the same value was also applied during Step 1. Once the flange faces made contact the bolt pretension was applied. The final step, Step 3, was when the pressure was applied. As before, pressure was applied to the internal faces of the flange as well as between the flange faces and the O-ring (fluid pressure). In addition to this the end thrust was also applied.

5.4.5. Assumption for the failure criteria

The finite element models and analysis needed to predict whether or not the flange design is both safe and leak tight. A flange design was regarded to be leak tight when there was sufficient contact pressure between the surface of the gasket and the faces of the flange during the operational phase. A circular bolted flange connection, on the other hand, will be assumed to be safe when the allowable stress criteria given in Table 5-4 have been met:

Table 5-4: Assumed failure criteria for the design of the large diameter flanges

Parameter	Requirement	Value [MPa]
Allowable flange stress	Smaller than	167
Allowable bolt stress	Smaller than	346
Maximum tensile strength of gasket	Smaller than	15
Minimum contact pressure	Larger than	5

5.4.6. Results from the finite element analysis of the large diameter flat face flange

This section is subdivided into two subsections. The first subsection shows the results obtained for: the contact pressure between the gasket surface and the flat face flange, the maximum axial stress, the maximum tangential stress, and the maximum radial stress. These results are then compared to the minimum values for an acceptable safe and leak tight design. In the second subsection the maximum

axial, radial and tangential stresses calculated by the finite element analysis were compared to the predicted values as calculated by the ASME VIII, Division 1 code.

5.4.6.1. Results for the finite element analysis of the large diameter flat face flange

A summary of the results shown in and Figure 5-5 and Figure 5-6 is given in Table 5-5. There was a 19.2% reduction in the contact pressure from the seating condition to the operating condition. Approximately half of the contact area had a contact pressure greater than 0 MPa. The final contact pressure was sufficient to ensure a leak-tight connection. The axial, radial and tangential stresses reduced by 7.9%, 5.7% and 19.8%, respectively from the seating to the operating condition. The maximum equivalent Von Mises stress for the flange exceeded the failure criterion for both the seating and operating conditions. The maximum equivalent Von Mises stress for the bolt, during the seating condition exceeded, the failure criteria. The maximum equivalent Von Mises stress for the gasket, on the other hand, remained below the maximum value of 15 MPa.

Table 5-5: Results from the finite element analysis of the flat face flange

Parameter	Symbol	Seating condition [MPa]	Operating condition [MPa]
Maximum contact pressure	P_{cont}	75	60.6
Maximum axial stress	S_H	74.6	68.7
Maximum radial stress	S_R	70.2	66.2
Maximum tangential stress	S_T	167.4	134.2

Table 5-6: Comparison of the results from the finite element analysis to the failure criteria for the flat face flange

Parameter	Seating condition [MPa]	Operating condition [MPa]
Maximum equivalent Von Mises: Flange	190.8	172.6
Maximum equivalent Von Mises: Bolt	386.8	343.7
Maximum equivalent Von Mises: Gasket	14.9	9.7
Maximum contact pressure	46.2	31.1

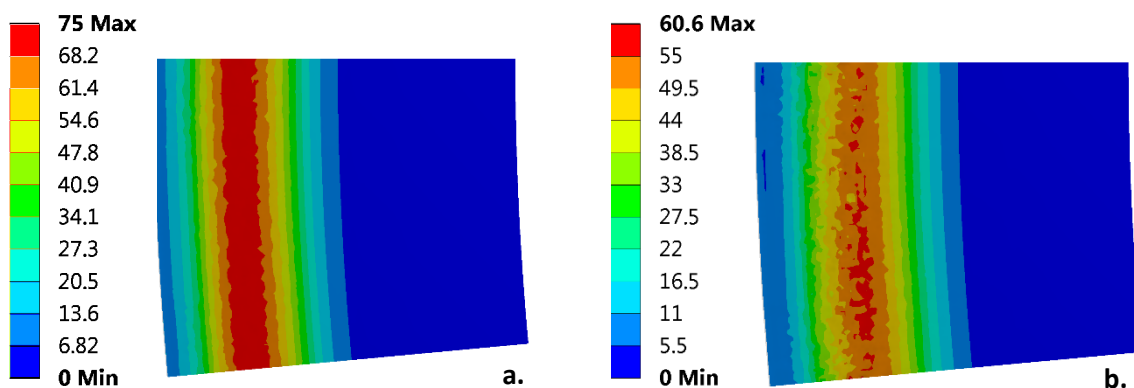


Figure 5-5: Contact pressure between the surface of the gasket and the flat face flange for the (a) seating and (b) operating conditions

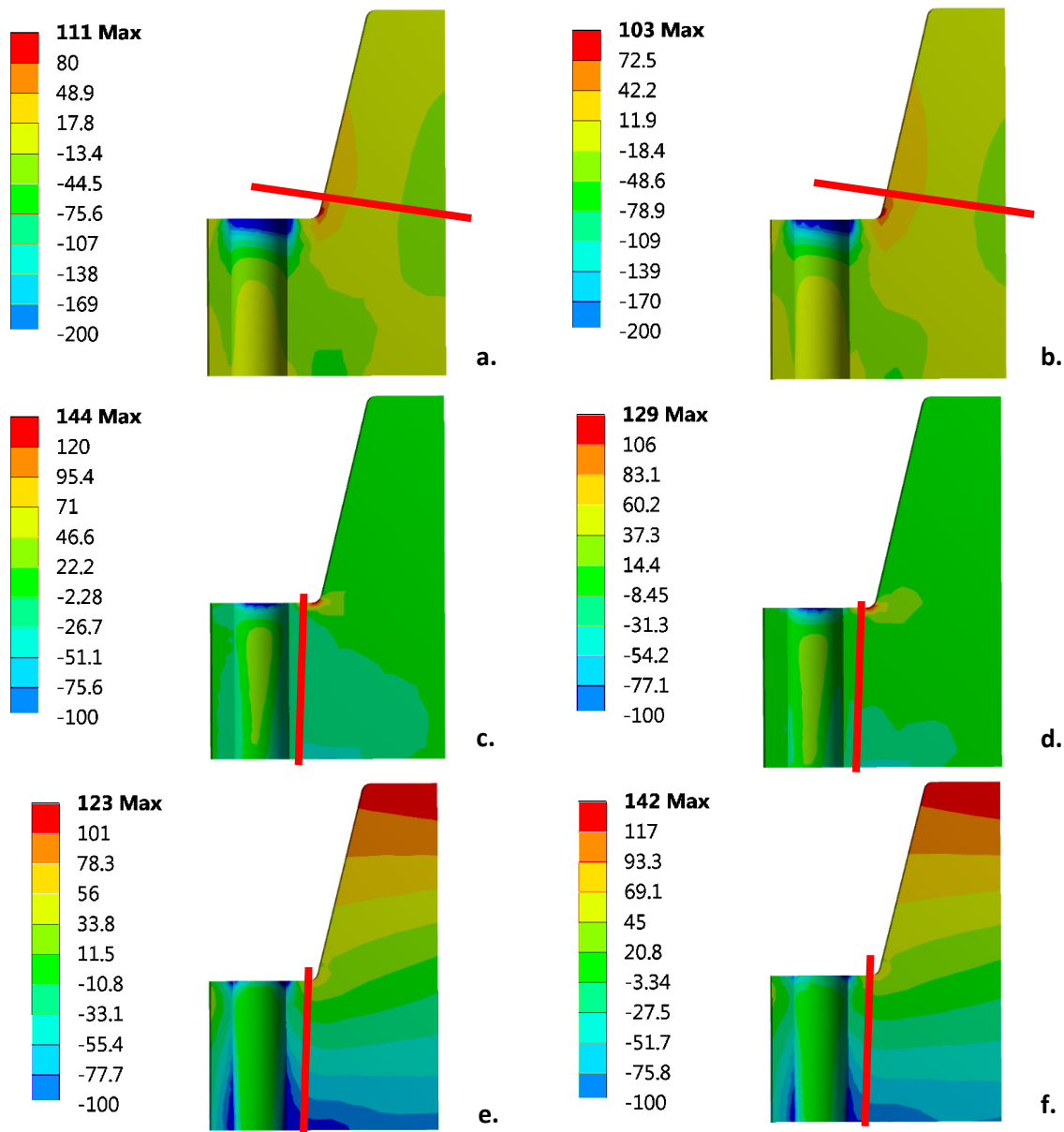


Figure 5-6: (a, b) Axial, (c, d) radial, and (e, f) tangential stress for the seating and operating conditions of the large diameter flat face flange

5.4.6.2. Comparison of the results for the flat face flange as calculated by ASME to the finite element analysis

The predicted values, as calculated from ASME VIII, Division 1, were compared to the calculated values from the finite element analysis. From the results shown in Table 5-7 it may be observed that the stress value predicted by ASME for the axial stress during the seating condition is 2.02 times greater than the stress value calculated by the finite element analysis. ASME also predicted that the maximum axial stress value decreased by 76% from the seating to the operating condition. This is significantly greater than the 8% reduction calculated by the finite element analysis. The predicted axial stress value was approximately half that of the calculated stress value for the operating condition due to the 76% reduction. For the maximum predicted and calculated radial stress, a similar trend was observed. For the seating condition the predicted radial stress value exceeded the calculated stress value by a factor 1.94. There was, again, a 76% reduction in the predicted stress from the seating to the operating conditions, whilst there was only a 6% reduction in the calculated stress. The calculated stresses in the tangential direction far exceeded those predicted by ASME – 9 and 33 times for the seating and operating conditions, respectively. If the finite element model is assumed to be correct, then the results

in Table 5-7 show that ASME VIII does not have the ability to accurately predict stresses for large diameter flat face flanges.

When the calculated results for the flat face flange were compared to the results obtained by Nagata & Sawa [18], the following conclusion was drawn: The stress distributions shown in Figure 5-6 compared well to those shown in Section 2.2.4. In addition to this Nagata & Sawa [18] found that the calculated tangential stress exceeds the predicted tangential stress, whereas the predicted radial and axial stresses exceed those calculated by the finite element analysis. Although the flange sizes and operating conditions differ, the comparison of the finite element analysis results to those of Nagata & Sawa [18] confirms the statement that the ASME VIII design-by-rule approach lacks the ability to accurately predict stresses in large diameter flanges.

Table 5-7: Comparison of the maximum axial, radial, and tangential stresses calculated by the finite element analysis and predicted by ASME VIII, Division 1 for the flat face flange

Parameter	Seating condition			Operating condition		
	Value from FEA [MPa]	Value from ASME [MPa]	Ratio of ASME/FEA	Value from FEA [MPa]	Value from ASME [MPa]	Ratio of ASME/FEA
Maximum axial stress	74.6	151.1	2.02	68.7	36.5	0.53
Maximum radial stress	70.2	135.9	1.94	66.2	32.8	0.50
Maximum tangential stress	167.4	19.2	0.11	134.2	4.6	0.03

5.4.7. Results for the large diameter raised face flange

The results for the raised face flange are split into two subsections. The first subsection presents the results from the finite element modelling and analysis, whilst the second subsection compares the results to those predicted by ASME.

5.4.7.1. Results from the finite element analysis of the large diameter flat face flange

The contact pressure between the surface of the gasket and the raised face flange decreased by 29.6%. As before, the flange stresses in the axial, radial, and tangential directions also decreased from the seating to the operating condition. The highest stress value was in the tangential direction and the lowest stress value in the radial direction.

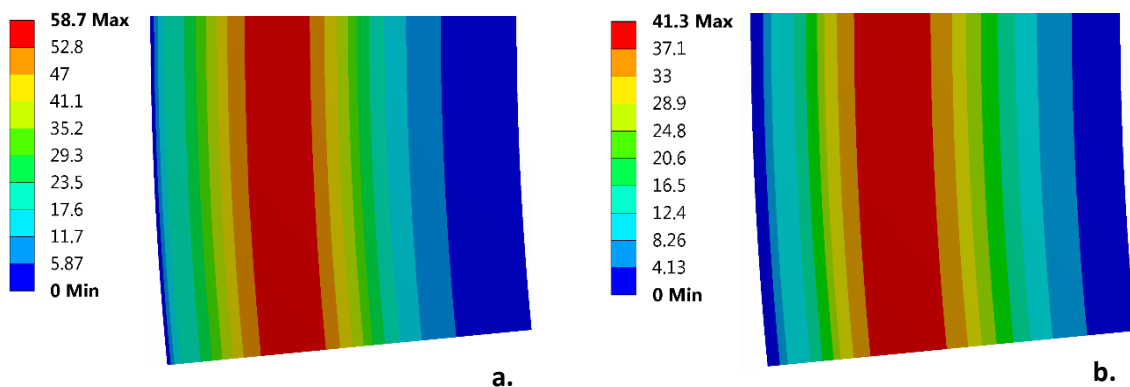


Figure 5-7: Contact pressure between the surface of the gasket and the raised face flange for the (a) seating and (b) operating conditions

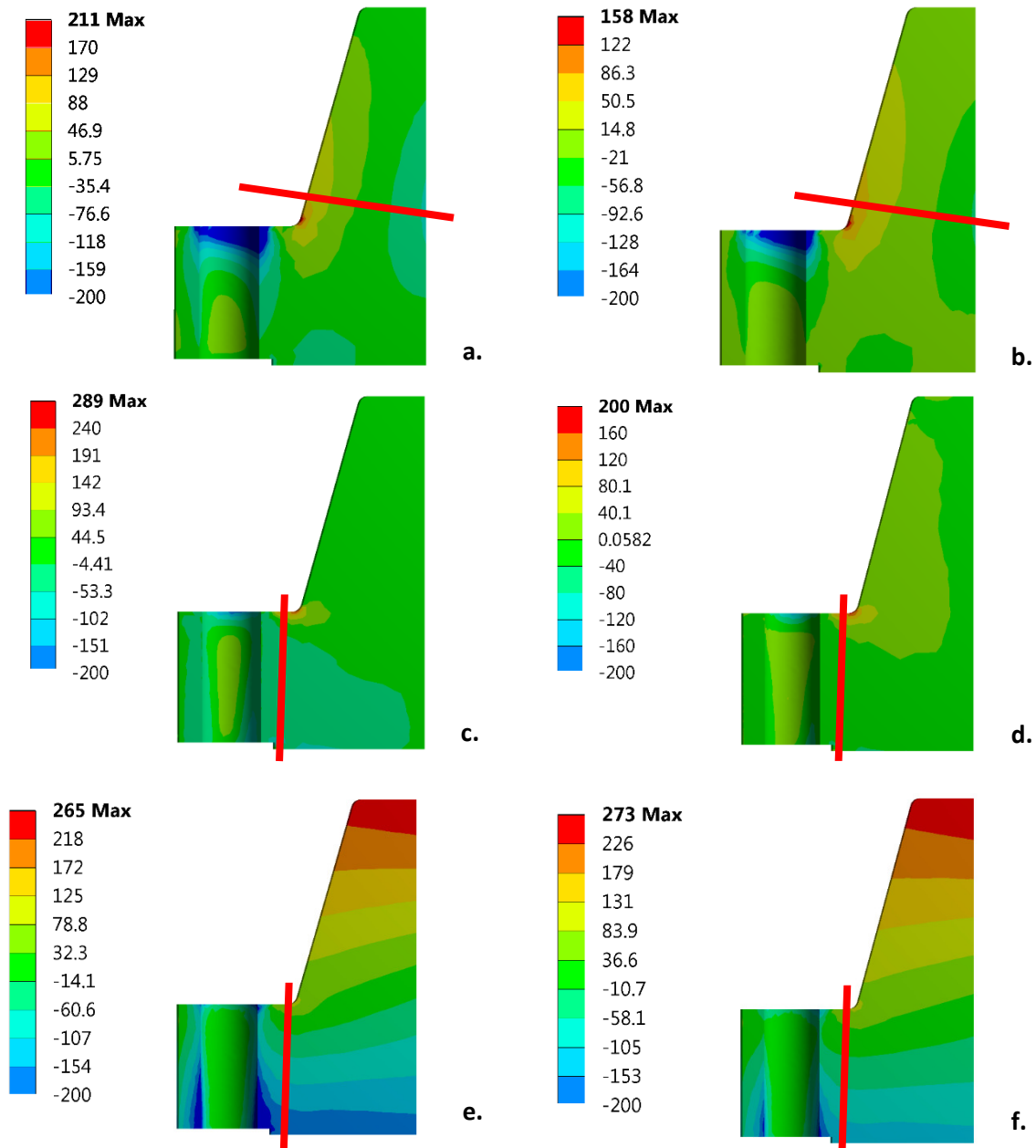


Figure 5-8: (a, b) Axial, (c,d) radial, and (e,f) tangential stress for the seating and operating conditions of the large diameter raised face flange

Table 5-8: Results from the finite element analysis of the flat face flange

Parameter	Symbol	Seating condition [MPa]	Operating condition [MPa]
Maximum contact pressure	P_{cont}	58.7	36.4
Maximum axial stress	S_H	135.7	99.1
Maximum radial stress	S_R	70.8	45.1
Maximum tangential stress	S_T	235.3	173.5

Table 5-9: Comparison of the results from the finite element analysis to the failure criteria for the raised face flange

Parameter	Seating condition [MPa]	Operating condition [MPa]
Maximum equivalent Von Mises: Flange	190.8	172.6
Maximum equivalent Von Mises: Bolt	386.8	343.7
Maximum equivalent Von Mises: Gasket	14.9	9.7
Maximum contact pressure	46.2	31.1

5.4.7.2. Comparison of the results for the raised face flange as calculated by ASME to the finite element analysis

As for the flat face flange, the predicted values (calculated from ASME) were compared to the calculated values from the finite element analysis for the raised face flange. The results for this comparison are shown in Table 5-10. The calculated tangential stress values, for both the seating and operating conditions, were significantly higher than those predicted by ASME. Conversely, the calculated radial stress values were lower than the predicted values for both the seating and operating condition.

The results for the raised face flange, like those for the flat face flange, compared well to the trends which were identified by Nagata & Sawa [18]. This again reaffirms the statement that the ASME design-by-rule does not have the ability to accurately predict the stresses for large diameter flanges.

Table 5-10: Comparison of the maximum axial, radial, and tangential stresses calculated by the finite element analysis and predicted by ASME VIII, Division 1 for the raised face flange

Parameter	Seating condition			Operating condition		
	Value from FEA [MPa]	Value from ASME [MPa]	Ratio of ASME/FEA	Value from FEA [MPa]	Value from ASME [MPa]	Ratio of ASME/FEA
Maximum Axial stress	135.7	91.2	0.67	99.1	120.7	1.22
Maximum radial stress	70.8	103.3	1.46	45.1	136.8	3.03
Maximum tangential stress	235.3	12.6	0.05	173.5	16.7	0.10

5.4.8. Results for the large diameter raised face flange with an O-ring groove

The raised face flange with an O-ring groove – as required by Rand Water – cannot be compared to ASME. The reason for this is that ASME does not follow the same design with regards to the groove. The most important aspects, with regards to the design, however, is that the bolted flange connection be safe and leak tight. Because of this emphasis was placed on determining the contact pressure between the O-ring and flange faces and the maximum equivalent Von Mises stress in the flange during both the seating and operating conditions.

From Table 5-11 it may be seen that an increase in the O-ring size results in an increase in the maximum equivalent Von Mises stress. In addition to this it may be concluded that the maximum equivalent Von Mises stress more than doubles from the seating to the operating condition, for this specific flange design, regardless of the O-ring size.

Table 5-11: Maximum equivalent Von Mises stress, for the seating and operating conditions, when either the small, medium and large O-ring is used

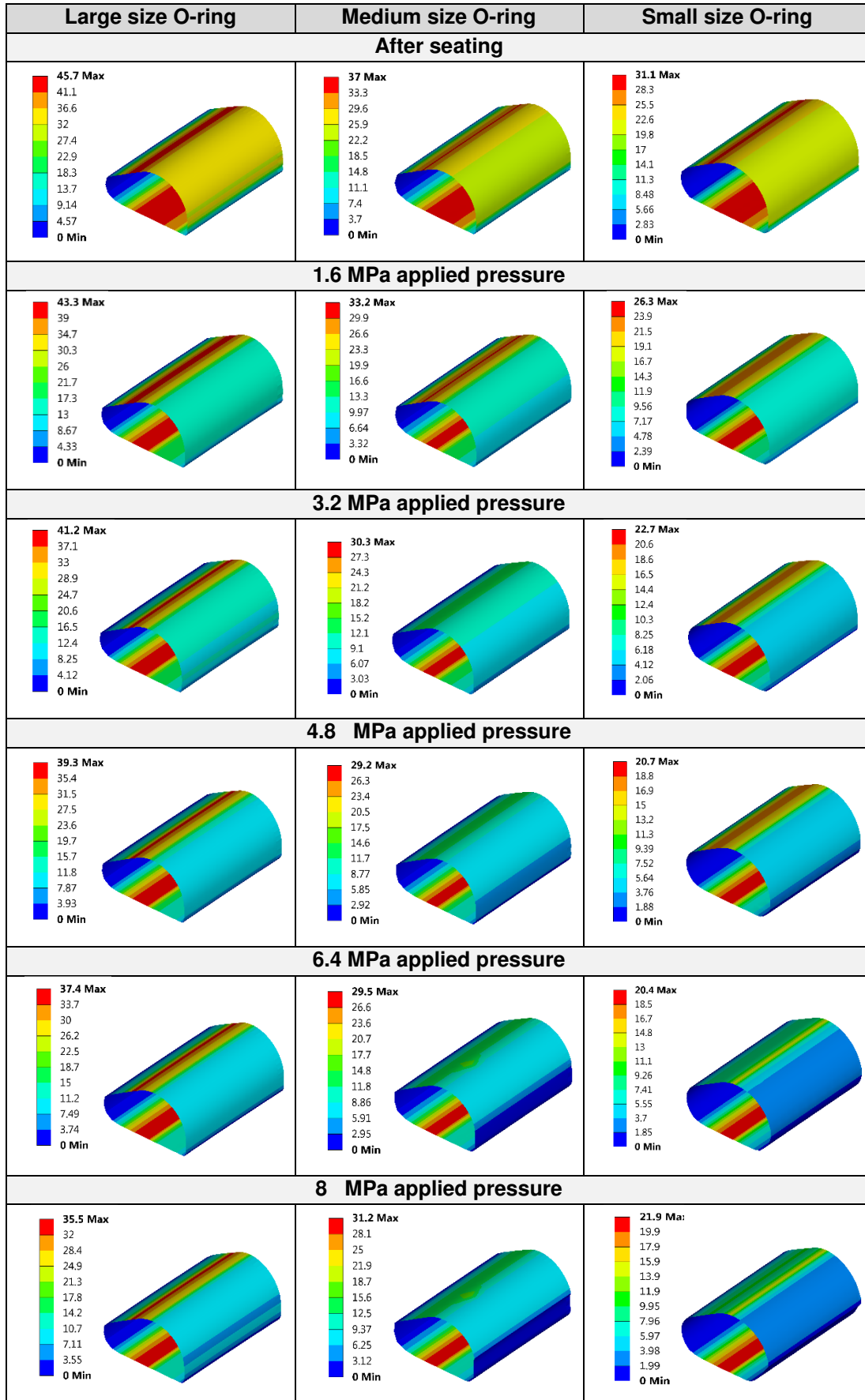
O-ring size	Maximum flange equivalent Von Mises stress		
	Seating [MPa]	Operating [MPa]	Ratio Operating/Seating
Large	94.32	207.18	2.20
Medium	91.22	196.46	2.15
Small	69.04	170.69	2.47

When the results shown in Table 5-11 are compared to the failure criteria, it may be seen that although the flange does not yield, its maximum equivalent Von Mises stress is above the allowable limit. The design, which makes use of the dimensions as prescribed for the raised face flange, is therefore not acceptable.

Shown in Table 5-12 are the results for the contact pressure between the flange faces and the O-ring for the three, aforementioned, sizes. The contact pressure between the faces of the flange and O-ring are given, in all three instances, immediately after seating and as the internal pressure is increased from 0 MPa to 8 MPa. The highest contact pressure, for both the seating and operating conditions, was obtained for the large diameter O-ring. As the size of the O-ring decreased so the maximum contact pressure decreased (Table 5-12). In all three instances the contact pressure between the O-ring and the top flange, and the O-ring and the bottom flange remained higher than 10 MPa for the seating and operating conditions. The maximum contact pressure between the top flange and the O-ring decreased by more than 40% for both the medium and small O-rings. The contact pressure for the large O-ring, however, decreased by less than 25%. Visible deformation of the small O-ring may be observed when the 8 MPa internal pressure was applied. Despite this, and the fact that the inside diameter of the small O-ring lost contact with the face of the flange when 8 MPa internal pressure was applied, the bolted flange connection remained leak-tight for all three O-ring sizes.

Despite being leak-tight, the maximum equivalent Von Mises stress in the flange exceeded the allowable limit and the circular bolted flange connection needed to be redesigned. It was also desired to design the flange to be as light as possible. As a result of this an optimisation for the design of a raised face flange with an O-ring groove was done and is shown in the next section. For this optimisation it was assumed that the medium O-ring provided suitable results and was therefore selected. It should be noted that all three O-ring sizes gave suitable results and a selection of any one of them at this point would have been acceptable.

Table 5-12: Contact pressure distributions, during operation, for the large, medium, and small O-rings



5.5. Optimisation of large diameter flanges

The optimisation of the large diameter flanges was split into three subsections, namely: the initial parameterisation, the response surface generation, and the response surface optimisation.

The section regarding the parameterisation includes the initial variable assumptions as well as a parameter correlation. The second subsection focuses on the generation of a suitable response surface. A brief overview of the various types of response surfaces are given as well as the final response surface type which was selected. The final part of the optimisation process was the optimisation from the response surface. The first step in response surface optimisation was the selection and definition of the objective and constraint functions. Once the objective and constraint functions had been defined a suitable optimisation technique was selected and implemented.

5.5.1. Parameterisation of the large diameter finite element models

The model parameterisation was limited to the dimensions shown in red in Figure 5-9. In addition to these dimensions the number of bolts used in the circular bolted flange connection was also varied. This was done in an attempt to draw a conclusion as to whether or not a large number of smaller bolts are more suitable than a small number of large bolts. This was done by either increasing or decreasing the sector size with relation to the bolt diameter. For the flat and raised face flanges the gasket area was kept constant. As a result of this neither the inner nor the outer diameter of the gasket were parameterised. For the raised face flange with an O-ring groove, on the other hand, the O-ring size, groove size, and groove diameter were kept constant. For all three flange designs, the bolt pitch circle was kept constant.

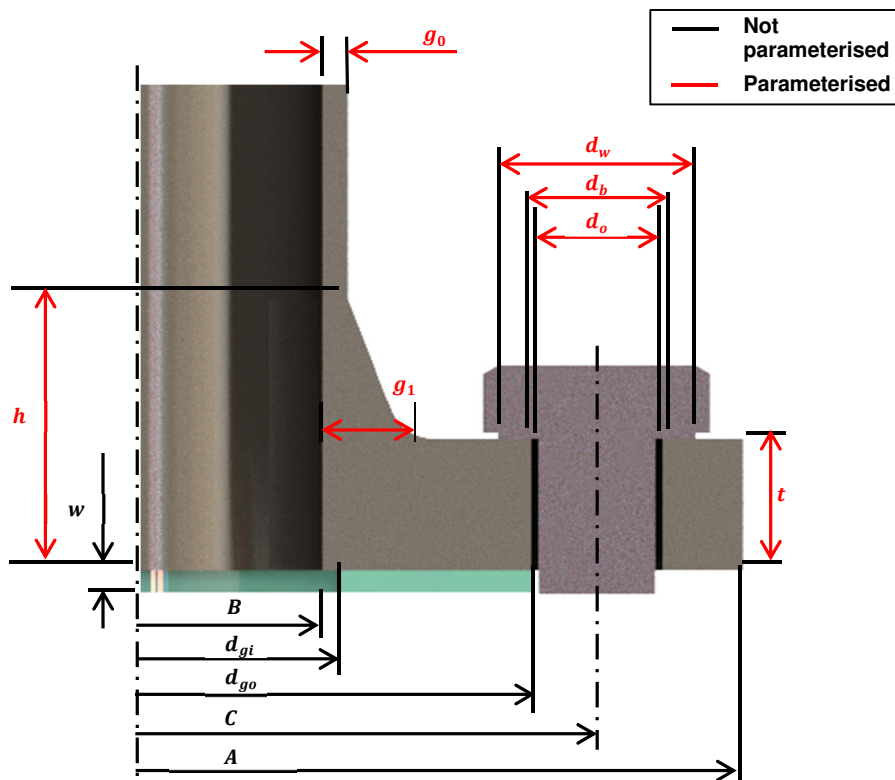


Figure 5-9: Flange dimensions that were parameterised

For the parameterisation only the dimensions for the flange thickness (t), the bolt diameter (d_b), the large hub thickness (g_1), the small hub thickness (g_0), and the length of the hub (h) were varied. The washer face diameter of the bolt (d_w), the size of the hole (d_o), and the number of bolts were all assumed to be dependent on the diameter of the bolt.

5.5.1.1. Assumption for the relationship between the bolt diameter and bolt hole size, and bolt diameter and washer face diameter

For the relationship between the bolt diameter and the bolt hole size, and the bolt diameter and the washer face diameter, it was assumed that the bolts used are as prescribed by the British BS 4190:2001 standard for metric black hexagon bolts, screw and nuts [44]. The design and optimisation was limited to the range of bolts between M60 and M90. Shown in Table 5-13 are the applicable bolt hole and washer face diameters for each bolt diameter. It is important to note that these bolt sizes were used as 'manufactural values' in ANSYS 16.2 and were, therefore, incremented as shown in Table 5-13. In short, no values such as 56.10 mm for the nominal size of the bolt were used in the optimisation. The values placed between brackets are undesired bolt sizes. As shown in the preceding section, unnecessary high contact pressures, as a result of excessive bolt pretensions, exist between the flange face and packing materials. As a result of this the bolt pretension was also allowed to be varied. An increase in the bolt pretension, for a specific design, will effectively result in an increase in both the maximum equivalent Von Mises stress in the flange and the maximum calculated contact pressure.

Table 5-13: Number of bolts, hole diameter, and washer face diameter for the respective nominal bolt sizes.

Configuration	Nominal size of bolt	Number of bolts	Hole diameter for coarse thread [mm]	Washer face diameter of bolt [mm]
1	(M60)	120	70	90
2	M64	108	74	95
3	(M68)	92	78	100
4	M72	84	82	105
5	(M76)	76	86	110
6	M80	68	91	115
7	(M85)	60	96	120
8	M90	52	101	130

For the parameterisation of the washer face and bolt hole size as functions of nominal bolt size, in ANSYS 16.2, fixed relationships were required. This was achieved by plotting the values for the washer face and bolt hole diameter as functions of the nominal bolt size. The results are indicated by the black circles in Figure 5-10 and Figure 5-11. In each case the results were fitted with a linear curve. For the fit of the hole diameter as a function of the nominal bolt size the following relationship was obtained (where all dimensions are in mm):

$$d_o = 1.0419d_b + 7.3792 \quad (5.1)$$

This fit had a root mean square error and a mean maximum error of 2.02, and 1.67, respectively. The fit of the washer diameter as function of the nominal bolt size had a root mean square error, and a mean maximum error of 3.21, and 2.15., respectively. This fit had the following relationship:

$$d_w = 1.3451d_b + 8.4507 \quad (5.2)$$

In both instances the fit was deemed to be acceptable and the relationships between the nominal bolt size and the hole diameter, and the nominal bolt size and the washer face diameter were used in the optimisation.

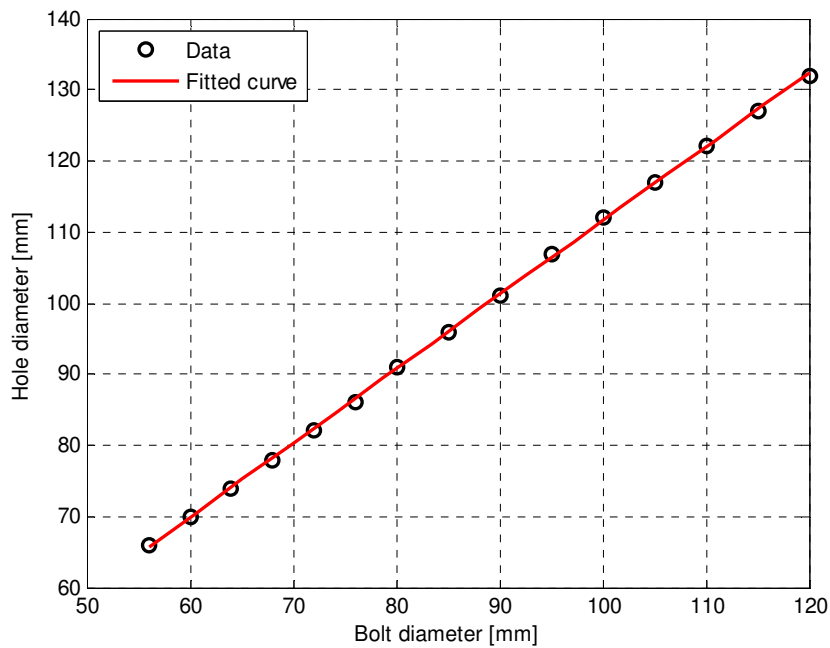


Figure 5-10: Data and fitted data for the hole diameter as a function of the bolt diameter

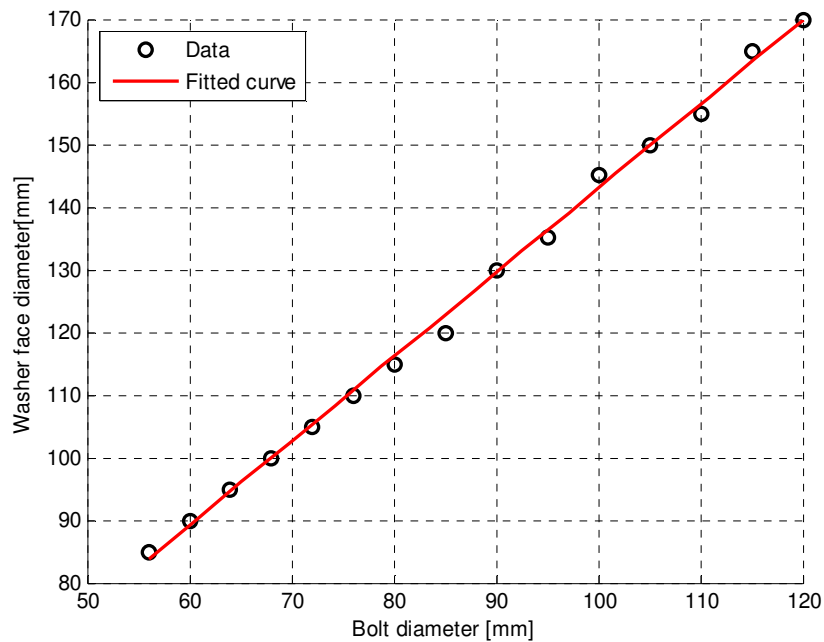


Figure 5-11: Data and fitted data for the washer face diameter as a function of the bolt diameter

5.5.1.2. Assumed upper and lower bounds for the flange dimensions and bolt loads

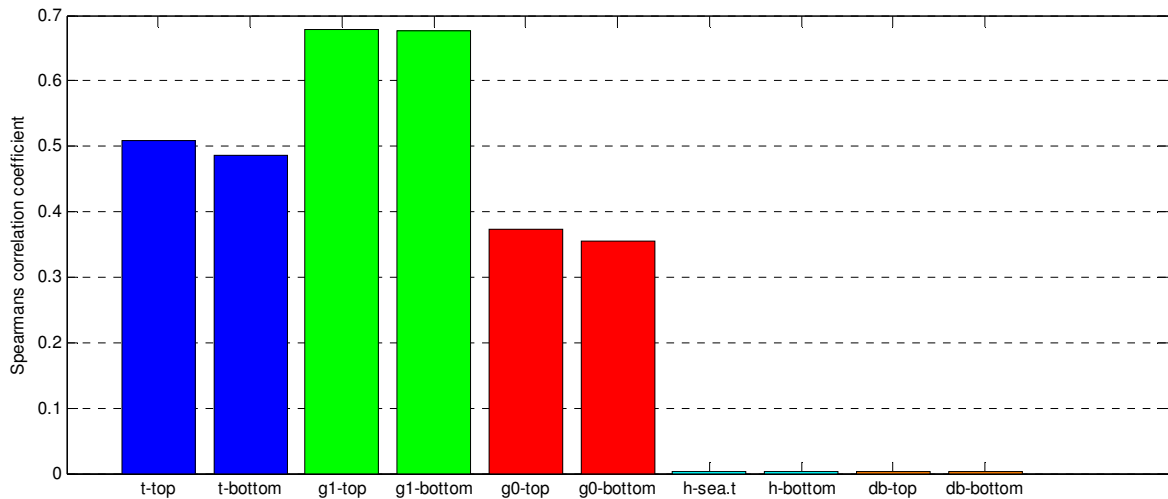
Only the flange thickness, large hub thickness, small hub thickness, bolt diameter, hub length, and individual bolt loads were changed during the optimisation process. The parameter ranges for the dimensions and bolt pretensions, as shown in Table 5-14, were used for the flat face flange, raised face flange, and the raised face flange with an O-ring groove. A Latin hypercube sampling design, making use of Table 5-14, was used as a basis from which to create the response surface. A total of 50 sampling points were considered for the three types of flanges.

Table 5-14: Parameter ranges for the optimisation of the flat face flange, raised face flange, and raised face with an O-ring groove flange

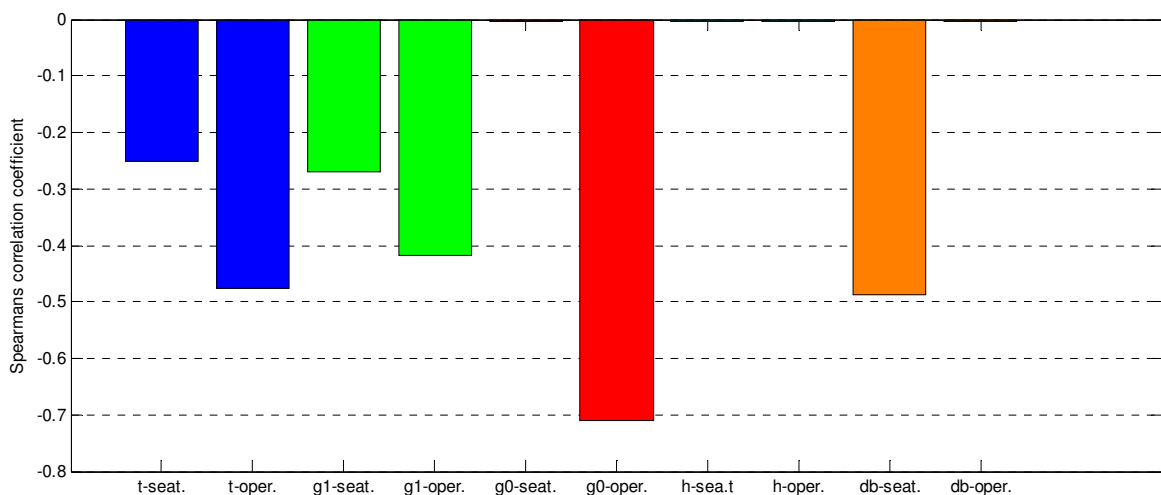
Parameter	Flange bounds	
	Lower	Upper
Flange thickness, t [mm]	150	350
Large hub thickness, g_1 [mm]	110	210
Small hub thickness, g_0 [mm]	80	160
Bolt diameter, d_B [mm]	56	90
Hub length, h [mm]	250	410
Individual bolt load, [$\times 10^5$ N]	3	10

5.5.1.3. Results for the parameter correlation

Shown in Figure 5-12, Figure 5-13, and Figure 5-14 are the results for the parameter correlation of the raised face flange with an O-ring groove, the flat face flange, and the raised face flange.



a.



b.

Figure 5-12: Parameter correlation between the dimensions of the raised face flange with an O-ring groove and the (a) maximum contact pressure, and (b) flange equivalent Von Mises stress

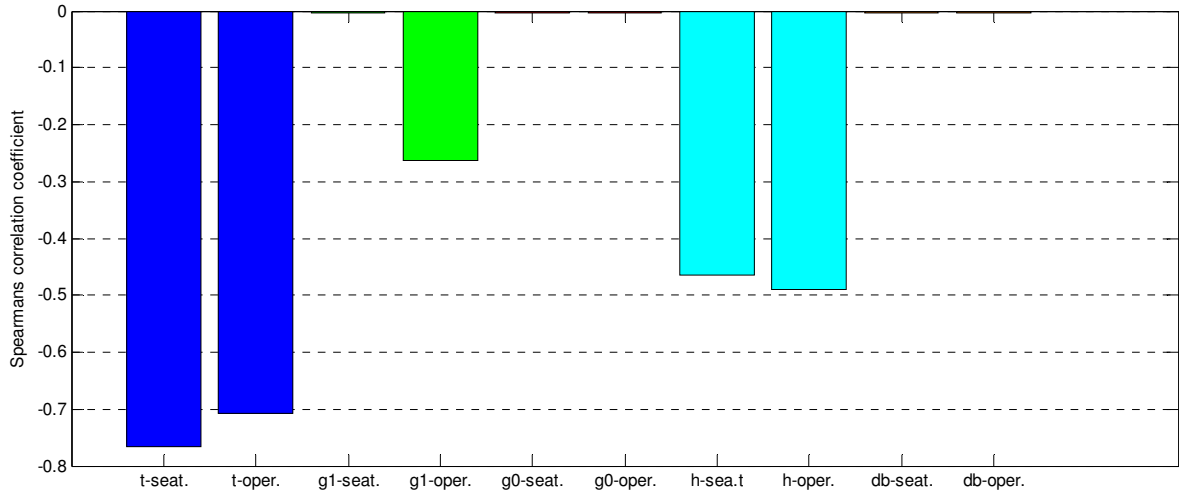


The parameter correlation was limited to three parameters during the seating and operating conditions, for the flat and raised face flanges, namely: the maximum contact pressure between the surface of the gasket and the face of the flange; the maximum equivalent Von Mises stress in the flange; and the maximum flange rotation. The correlation between these parameters and the flange thickness, large hub thickness, small hub thickness, length of the hub, and the bolt diameter were determined. Only the maximum contact pressure during operation and the maximum equivalent Von Mises stress, during the seating and operating conditions, were considered for the raised face flange with an O-ring groove.

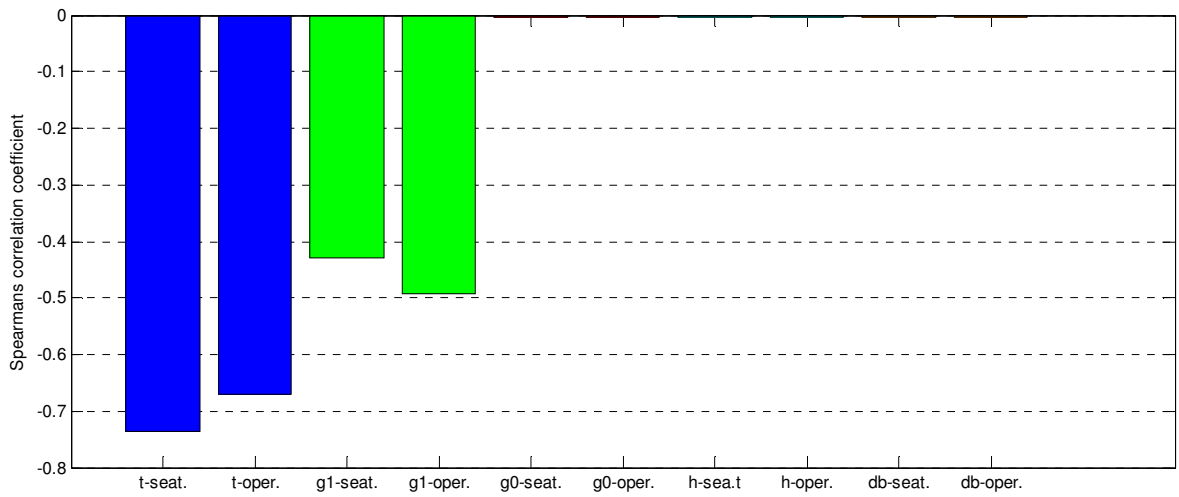
For the parameter correlation of the flat face flange, the flange thickness had a Spearman correlation coefficient of between 0.65 and 0.80 when compared to the maximum contact pressure, equivalent Von Mises stress, and flange rotation, for the seating and operating conditions (Figure 5-13). This implied that, for both the seating and operating conditions, a decrease in the flange thickness was likely to result in an increase in the maximum contact pressure, equivalent Von Mises stress, and flange rotation. This may be explained as follows: a reduction in flange thickness results in a reduction in stiffness which increases the rotation experienced by the flange. During flange rotation the gasket becomes pinched. This means that the maximum contact pressure increases, although the contact area decreases. This behaviour was shown in Chapter 2, Section 2.4.2. The large hub length, on the other hand, had a correlation of between -0.40 and -0.50 with the maximum equivalent Von Mises stress, and a correlation of between -0.20 and -0.30 for the maximum flange rotation for both the seating and operating conditions. The correlation between the large hub thickness and the maximum equivalent Von Mises stress shows that as the large hub thickness decreases the maximum equivalent Von Mises stress increases. This is due to the fact that a smaller large hub thickness results in a reduction in the flange stiffness and a subsequent increase in the flange stresses. The correlation between the large hub thickness and the maximum flange rotation is not very large, which implies that an increase in the large hub thickness will have a minor effect on the decrease of the flange rotation due to a slight increase in the relevant stiffness. From Figure 5-13, it may be observed that there is no correlation between the large hub thickness and the maximum contact pressure during seating, however, there is a correlation of -0.25 during the operating condition. A possible explanation for this may be that flange rotation increases from the seating to the operating condition. As a result of this the large hub thickness begins to play a minor role in limiting the flange rotation. An increase in the large hub thickness will, therefore, begin to limit the flange rotation and the pinching effect it has on the gasket resulting in a decrease in the maximum contact pressure and an increase in the area of the gasket in contact with the flange. In all three instances the correlation between the small hub thickness and the bolt diameter, and the maximum contact pressure, equivalent Von Mises stress, and flange rotation is 0. This shows that for this particular selection it does not matter whether there are many smaller bolts or fewer larger bolts which have to the same total bolt area and apply the same load to the circular bolted flange connection.

As for the flat face flange, the correlation of the raised face flange was limited to the maximum contact pressure between the surface of the gasket and the face of the flange, the maximum equivalent Von Mises stress in the flange, and the maximum flange rotation. A Spearman correlation coefficient between -0.65 and -0.75 was calculated for the flange thickness and the maximum contact pressure, equivalent Von Mises stress, and flange rotation for both the seating and operating conditions (Figure 5-14). The reason for this large correlation and the implication thereof remains the same as for the flat face flange.

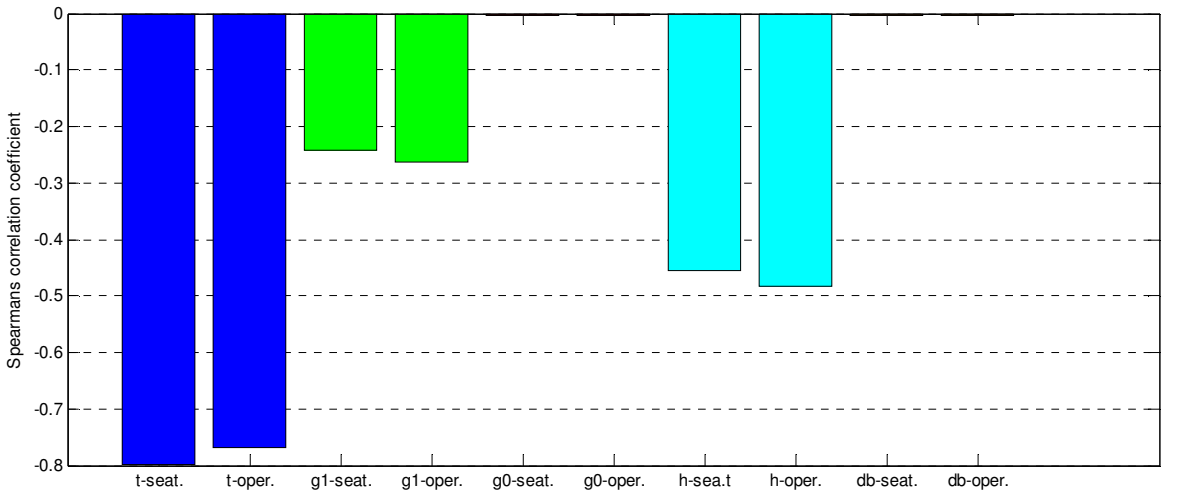
Finally, from Figure 5-12 it may be seen that a reduction in either the flange thickness, bolt diameter or the large hub thickness, during the seating and operating conditions, will result in an increase in the maximum equivalent Von Mises stress of the raised face flange with an O-ring groove. During the operating condition a decrease in the small hub thickness will have the largest impact on an increase in the maximum equivalent Von Mises stress. An increase in the flange thickness, large hub thickness, and small hub thickness will have a significant influence on the contact pressure during both the seating and operating conditions. This may be due to the following reason: a reduction in any of these dimensions will result in a reduction of the flange stiffness. This, in-turn, will lead to greater local flange rotation, due to the metal-on-metal contact, which will, subsequently reduce the maximum obtainable contact pressure.



a.

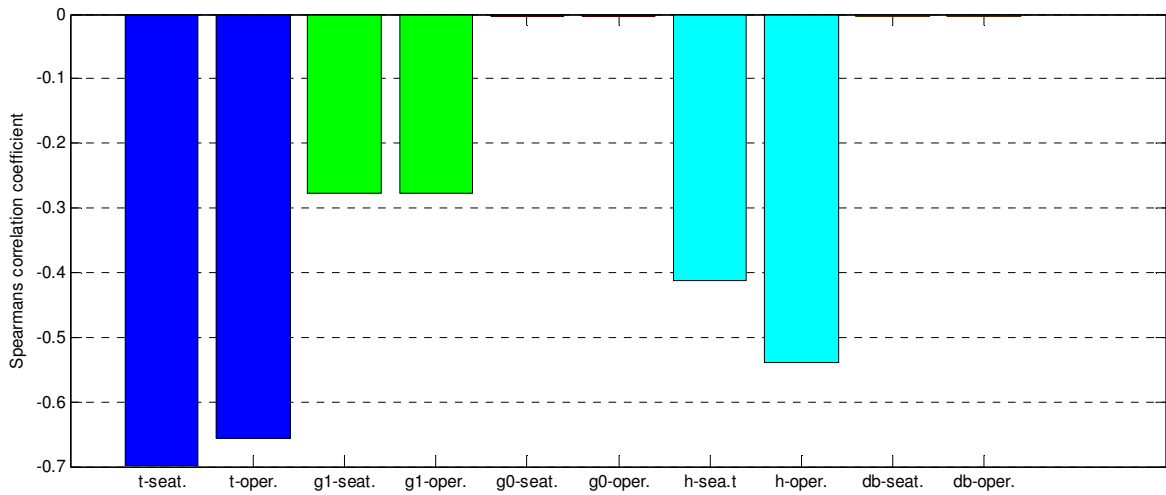


b.

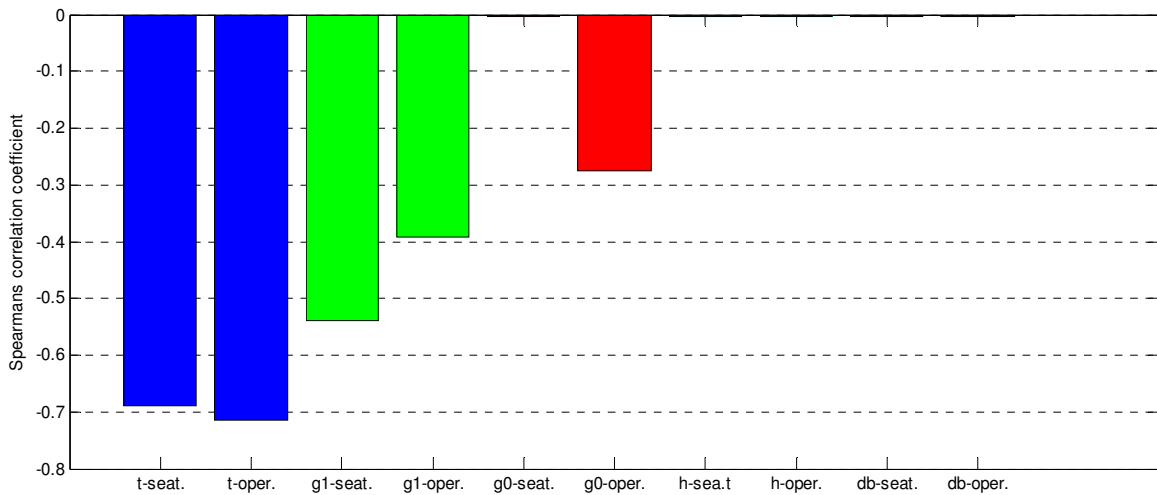


c.

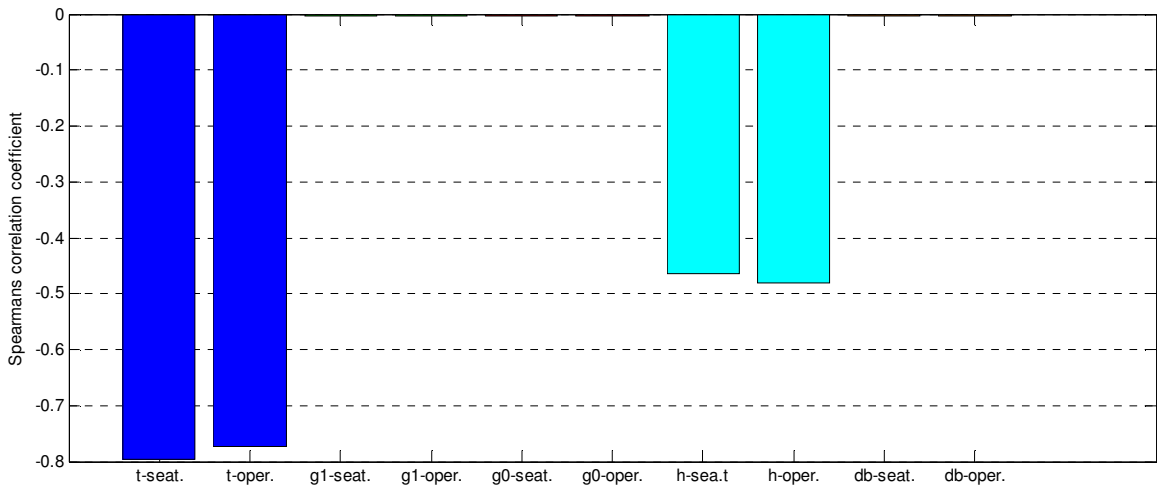
Figure 5-13: Parameter correlation between the dimensions of the flat face flange and the (a) maximum contact pressure, (b) flange equivalent Von Mises stress and (c) flange rotation



a.



b.



c.

Figure 5-14: Parameter correlation between the dimensions of the raised face flange and the (a) maximum contact pressure, (b) flange equivalent Von Mises stress and (c) flange rotation

5.5.2. Response surface generation and optimisation

ANSYS 16.2 provides four different types of response surfaces. An overview of each of the different types of response surfaces is given in Appendix F. The response surfaces are: standard second order polynomial response surface, Kriging, non-parametric regression, and sparse grid.

The goal of the optimisation of the flanges was not to find the optimal solution. It was merely desired to show the possibilities of the finite element model with regards to optimisation and to show that it is possible to design safe and leak-tight large diameter flanges which are significantly lighter than would be permissible by the ASME VIII, Division 1, design code. As a result of this, and the information given in Appendix F, it was decided to make use of the Kriging method for the response surface generation. Since only an optimised solution was sought after, the accuracy of the Kriging method was regarded to be less crucial since all of the candidate points which were selected were validated. The response surface optimisation was done by making use of the multi-objective genetic algorithm (MOGA) in ANSYS 16.2. This method was used instead of the other three methods (Shifted-Hammersly, non-linear programming by quadratic Lagrangian, and mixed integral sequential quadratic programming method) since it is able to handle multiple objectives; provides an accurate solution, and identifies both the global and local minima (as discussed in Appendix F).

5.5.2.1. Objective and constraint functions

A summary of the objectives and constraints for the optimisation of all the flange designs is given in Table 5-15.

Table 5-15: Objectives and constraint functions for the optimisation

Parameter	Objective	Applicable flange design	Constraint	
			Type	Value [MPa]
Flange – Max. equivalent Von Mises stress, seating	Minimise	- Flat face / - Raised face / - Raised face with an O-ring groove	Smaller than-	167
Flange – Max. equivalent Von Mises stress, operating	Minimise	- Flat face / - Raised face / - Raised face with an O-ring groove	Smaller than	167
Bolt – Max. equivalent Von Mises stress, seating	Minimise	- Flat face / - Raised face / - Raised face with an O-ring groove	Smaller than-	346
Bolt – Max. equivalent Von Mises stress, operating	Minimise	- Flat face / - Raised face / - Raised face with an O-ring groove	Smaller than	346
Gasket – Max. equivalent Von Mises stress, seating	Minimise	- Flat face / - Raised face /	Smaller than-	15
Gasket – Max. equivalent Von Mises stress, operating	Minimise	- Flat face / - Raised face /	Smaller than	15
Max. contact pressure, operating	No objective	- Flat face / - Raised face / - Raised face with an O-ring groove	Greater than	5
Total mass of flange	Minimise	- Flat face / - Raised face / - Raised face with an O-ring groove	-	-



5.5.2.2. Results from the optimisation of the flat and raised face flanges

The purpose of the optimisation was twofold: firstly to show that optimisation may be used to reduce the mass of the original design while maintaining a safe and leak tight connection; and secondly to show that the code calculation, in some instances, gives over conservative results (this phenomenon was also highlighted by Nagata & Sawa [18]).

From the response surface optimisation six candidate points were selected for both the flat and raised face flanges. The candidate points and their applicable dimensions are shown in Table 5-16 and Table 5-18 for the flat and raised faces flanges, respectively. In each instance the maximum equivalent Von Mises stress, for both the seating and operating conditions, for the flange, gasket, and bolts was calculated. In addition to this, the operating contact pressure between the surface of the gasket and face of the flange was also calculated.

Of the six candidate designs for the flat face flange only two would have adhered to the design-by-rule as laid out in ASME VIII, Division 1 (shown in Figure 5-15). The remaining four candidate designs would have been rejected due to an overestimate of the axial and radial stresses. The actual axial, radial, and tangential stresses are all below the allowable stresses as dictated by ASME VIII, Division 1. All of the designs, also pass when the failure criteria, as given in Table 5-4, are accepted. By adding the optimisation process and adopting the failure criteria given in Table 5-4, a reduction in mass of more than 25% is possible. As shown in Table 5-17 four of the candidate design points of the flat face flange had a reduction in mass of more than 25%, whilst two points had a reduction in mass greater than 30%.

For the raised face flange, all six candidate design points would have been rejected by ASME VIII, Division 1 (Table 5-18). As with the flat face flange, the raised face flange would have been rejected, by ASME VIII, Division 1, due to an overestimation of the axial and radial stresses. For all six instances, however, the calculated axial, radial, and tangential stresses, from the finite element analysis, were below the allowable limits. As before, all the designs pass when the failure criteria as given in Table 5-4, are accepted. From Table 5-19 it may be seen that the optimisation enables a mass reduction of up to 25% when compared to the initial design.

5.5.2.3. Results from the optimisation of the raised face flange with an O-ring groove

From the results shown in Table 5-20 and Table 5-21 it may be seen that all six candidate designs for the raised face flange with an O-ring groove adhere to the failure criteria given in Table 5-4 since the maximum equivalent stresses calculated in the flanges and bolts are below 167 MPa and 346 MPa, respectively. The contact pressure between the O-ring and top flange, and the O-ring and bottom flange was also calculated to be in excess of 10 MPa during the operating phase. The total flange mass varied between 16 370 kg and 19 043 kg for the six candidate designs.

These results prove that the suggested method of design, by making use of ASME VIII, Division 1 as an initial guess, non-linear finite element modelling, and an optimisation scheme is able to design large diameter raised face flanges with O-ring grooves which are both safe and leak-tight.

Table 5-17: Results from the optimisation of the flat face flange

Design point	Total mass [kg]	Mass reduction [%]	Operating contact pressure [MPa]	Max. seat. flange stress [MPa]	Max. oper. flange stress [MPa]	Max. seat. bolt stress [MPa]	Max. oper. bolt stress [MPa]	Max. seat. gasket stress [MPa]	Max. oper. gasket stress [MPa]
1	10 794	27	12.9	105.5	109.6	214.2	191.1	7.6	4.2
2	9 456	36	11.4	102.9	114.9	258.2	236.1	7.1	3.9
3	10 567	28	11.4	104.8	103.7	230.8	209.3	6.9	3.8
4	10 869	26	14.9	118.7	121.7	231.2	206.2	8.3	4.8
5	9 608	35	14.8	113.7	125.1	248.3	221.9	8.5	4.8
6	10 688	27	15.2	123.8	127.7	263.4	234.1	8.6	4.9

Table 5-16: Dimension of the candidate flat face designs

Design point	Flange thickness, t [mm]	Hub thickness large, g_1 [mm]	Hub thickness small, g_0 [mm]	Hub length, h [mm]	Bolt diameter, d_B [mm]	Pretension per bolt [$\times 10^5$ N]
1	194.1	133.1	118.2	279.8	72	3.61
2	168.1	145.2	83.3	273.1	90	4.99
3	179.1	163.6	112.0	275.9	85	4.60
4	205.3	125.9	98.9	283.9	72	3.94
5	163.3	135.8	93.9	303.8	68	3.40
6	210.1	130.6	91.0	253.2	85	5.53

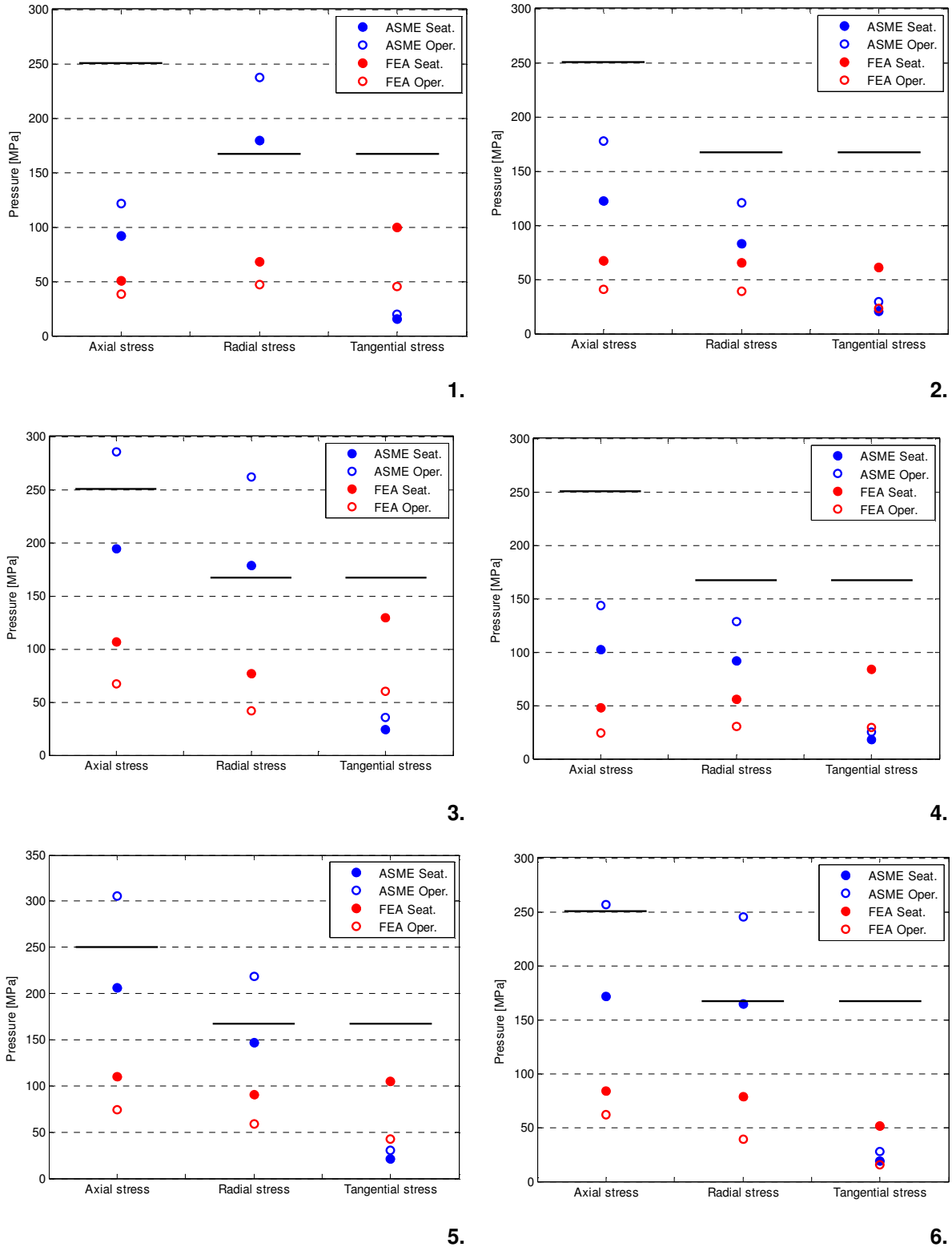


Figure 5-15: Comparison of the axial, radial, and tangential stresses calculated by the finite element analysis with the predicted values by ASME for the six flat face flange candidates

Table 5-19: Results from the optimisation of the raised face flange

Design point	Total mass [kg]	Mass reduction [%]	Operating contact pressure [MPa]	Max. seat. flange stress [MPa]	Max. oper. flange stress [MPa]	Max. seat. bolt stress [MPa]	Max. oper. bolt stress [MPa]	Max. seat. gasket stress [MPa]	Max. oper. gasket stress [MPa]
1	10 865	13	5.7	111.2	128.0	232.3	187.2	6.1	2.5
2	12 497	0	7.3	115.8	139.1	217.5	151.5	6.5	2.9
3	9 574	24	9.9	179.0	176.6	339.2	264.6	9.0	4.1
4	12 373	1	9.3	129.1	151.3	219.7	160.6	7.8	3.7
5	11 000	12	7.4	171.1	132.2	226.9	178.8	6.8	3.1
6	11 258	10	5.4	140.2	115.7	215.7	165.8	5.4	2.3

Table 5-18: Dimension of the candidate raised face designs

Design point	Flange thickness, t [mm]	Hub thickness large, g_1 [mm]	Hub thickness small, g_0 [mm]	Hub length, h [mm]	Bolt diameter, d_B [mm]	Pretension per bolt [$\times 10^5$ N]
1	152.3	191.3	136.3	294.9	72	3.15
2	218.5	151.7	86.4	337.6	90	5.84
3	152.5	128.8	91.9	326.9	76	4.69
4	209.5	168.1	82.1	341.5	68	3.74
5	167.7	124.8	120.2	362.7	76	4.13
6	156.9	136.6	125.5	385.8	90	4.98

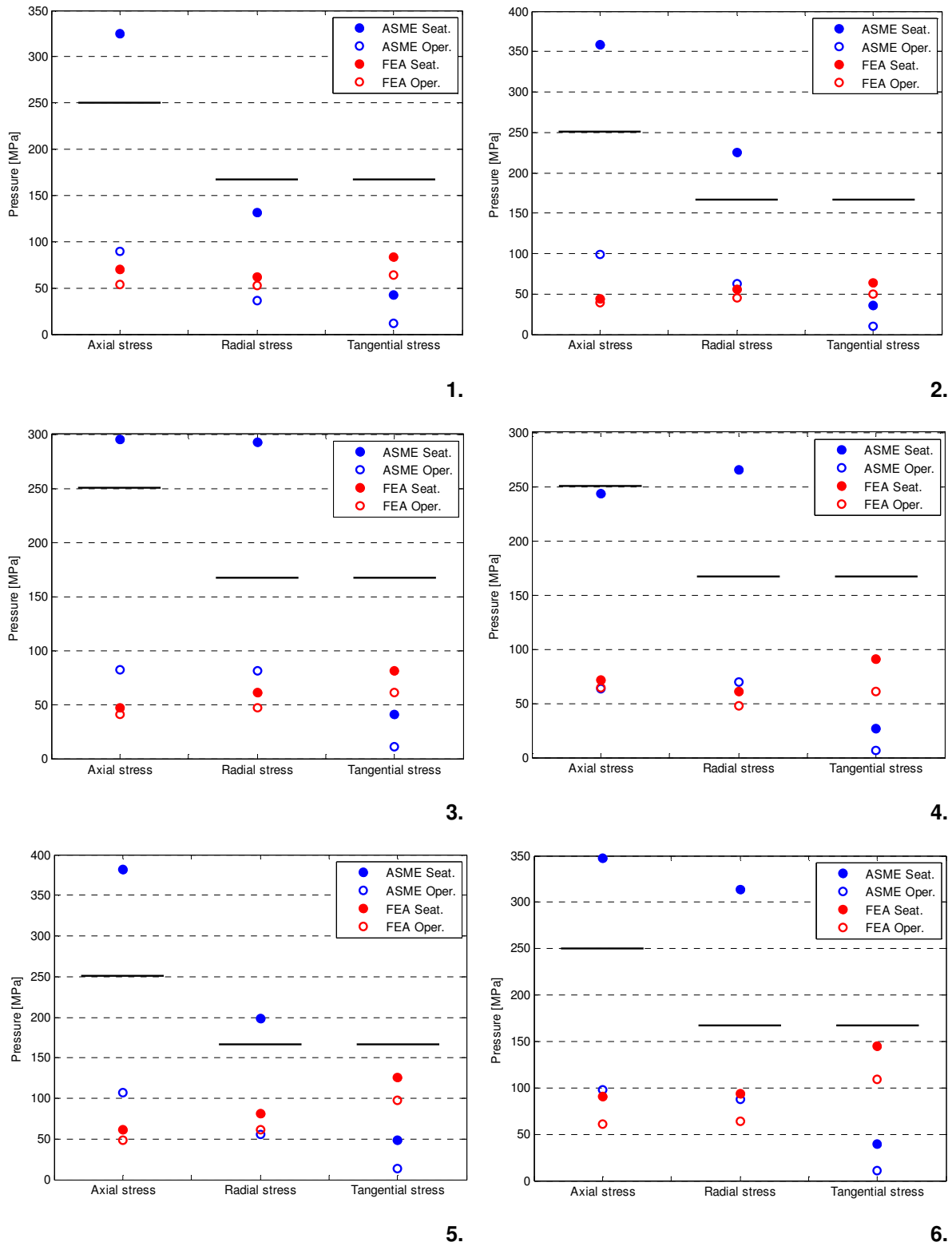


Figure 5-16: Comparison of the axial, radial, and tangential stresses calculated by the finite element analysis with the predicted values by ASME for the six raised face flange candidates

Table 5-21: Results from the optimisation of the raised face flange with an O-ring groove

Design point	Operating contact pressure top [MPa]	Operating contact pressure bottom [MPa]	Max. seating flange stress [MPa]	Max. operating flange stress [MPa]	Max. seating bolt stress [MPa]	Max. operating bolt stress [MPa]
1	29.7	27.7	52.1	146.6	106.8	153.9
2	29.3	27.3	58.0	157.0	115.1	152.6
3	28.8	26.6	61.6	163.0	107.3	140.5
4	33.9	39.3	66.3	149.2	134.1	128.6
5	34.6	32.7	61.4	154.3	124.9	141.5
6	36.2	34.7	61.4	144.3	128.9	133.7

Table 5-20: Dimensions of the candidate raised face flange designs with O-ring grooves

Design point	Flange thickness, t [mm]	Hub thickness large, g_1 [mm]	Hub thickness small, g_0 [mm]	Hub length, h [mm]	Bolt diameter, d_B [mm]	Pretension per bolt [$\times 10^5$ N]
1	257.6	210.0	160.0	385.8	85	3.0
2	241.1	196.0	142.9	403.7	85	3.7
3	259.3	188.2	135.9	372.5	80	3.3
4	306.6	173.0	158.0	400.0	80	4.4
5	279.2	200.3	152.9	380.6	68	3.3
6	312.5	198.2	159.2	372.2	72	3.9



5.6. Conclusion of the application of the non-linear finite element models to the design of large diameter flanges

The procedure for the design of large diameter flanges was divided into three steps. The first step was to design the required flange by means of ASME VIII, Division 1. This was done to get an initial estimate of the dimensions. The second step was to use these dimensions in a non-linear finite element model and analysis and compare the results to the specified failure criteria. The final step was optimisation. This was done to design a safe, leak tight, and light flange.

Large diameter flat face and raised face flanges were, initially, designed by means of ASME VIII, Division 1. The prescribed dimensions, bolt pretensions, and internal pressures from ASME were replicated in the non-linear finite element models, and the relevant analyses were completed. From the results, of both the flat and raised face flanges, it was found that there was a large discrepancy between the axial, radial, and tangential stress values predicted by ASME and those calculated by the finite element analysis. If the results of the finite element are assumed to be correct then it may be argued that the design-by-rule methodology suggested by ASME VIII, Division 1, does not have the ability to accurately predict flange stresses. This conclusion matches the one made by Nagata & Sawa [18], who also brought into question ASME's ability to accurately predict flange stresses. It was also found that the bolt pre-tension prescribed by ASME is unnecessarily high due to the fact that, for both the flat and raised face flanges, the operating contact pressure is ten times greater than the internal pressure.

For circular bolted flange connections, which made use of a raised face flange with an O-ring groove, the effect which O-ring size has on the maximum equivalent Von Mises stress in the flange, as well as the contact pressure between the O-ring and flange faces was investigated. It was found that an increase in O-ring size resulted in an increase in both the contact pressure as well as in the flange's maximum equivalent Von Mises stress.

The optimisation processes were subdivided into three subsections. The first subsection was the parameterisation and parameter correlation of the various flange designs. It was found that a reduction in either the flange thickness, large hub thickness, or hub length, for the flat and raised face flanges, resulted in an increase in the flange rotation, maximum equivalent Von Mises stress of the flange, and in the maximum contact pressure between the gasket and flange faces. For the raised face flange with an O-ring groove an increase in either the flange thickness, large hub thickness, or small hub thickness resulted in an increase in the maximum contact pressure between the O-ring and flange face, and a decrease in the maximum flange equivalent Von Mises stress.

The flange designs were optimised by using the allowable stresses in the bolts and fasteners, and the minimum contact pressures as constraints. For the optimisation the maximum equivalent Von Mises stresses in the flanges and fasteners were compared to the maximum allowable stresses. The maximum operating contact pressure, between the packing materials and the flange faces, was compared to the minimum allowable contact pressure. For each of the three different types of flanges six candidate designs were selected. The candidate design points for the flat and raised face flanges were compared to ASME. It was found that the majority of candidate designs, for both the flat and raised face flanges, were rejected by ASME due to an inaccurate prediction of the flange stresses. It was finally found that light, safe and leak tight flanges could be accurately designed by using the suggested non-linear finite element models and applying the prescribed design methodology.



CHAPTER 6: RECOMMENDATIONS FOR FUTURE WORK AND CONCLUSION

6.1. Recommendations for future work

The primary objective of this investigation was to propose a suitable non-linear finite element model for the expansion of Rand Water's existing flange tables. Although this was achieved, various possibilities for improving both the model and the applicability of the model exists. These possibilities include, and are explained in greater detail below:

1. Improving the material models of the packing materials and increasing the number of packing materials considered.
2. Determining the coefficients of friction between various packing materials and flange faces.
3. Investigating and finding a method for the ideal bolt tightening sequence by making use of finite element analysis.
4. Determining, including, and evaluating the effect which external forces and bending moments have on the results of the finite element modelling and analysis of large diameter flanges.
5. Completing large scale experimentation in order to validate the finite element models which were used for the design of the large diameter flanges.

6.1.1. Material modelling

Material models were assigned to the two types of packing materials in Chapter 3. A non-linear viscoelastic material model was assigned to the non-asbestos compressed fibre gasket by means of Neo-Hookean and Prony shear relaxation models. A third order Ogden material model, on the other hand, was assigned to the nitrile O-ring. With regards to the material characterisation of the packing materials there are a large number of models. This investigation only considered a single type of gasket from the many currently in use. ASME VIII currently assigns m and y factors to different types of gaskets and, therefore, only accounts for the through thickness deformation [32]. In reality, however, gasket deformation is a three dimensional problem due to gasket deformation. As a result of this, this method has been widely criticised.

In an attempt to improve upon this it may be possible to group gaskets together – which exhibit similar material properties – and assign a suitable single material model. It is known that there is significant variation in the behaviour and material properties exhibited by gaskets. The challenge, therefore, will be to find the most suitable material model, for a specific group of gaskets, which is conservative enough to account for the variation, but not overly conservative so as to result in an overdesigned flange joint.

6.1.2. Friction

It was shown in Chapter 3 that the value for the coefficient of friction between the packing material and flange face has an impact on the deformation and subsequent contact pressure. It is, therefore, recommended for future work that the frictional behaviour, between the flange face and packing material, as a whole be looked at. It is recommended that values for the coefficient of friction be individually determined for different flange-gasket configurations. It is also suggested that an in-depth study be done to determine the effect which stick-slip conditions have on the contact pressure during bolting-up and operation.

6.1.3. Bolt tightening techniques

The sequence in which bolts are tightened, the number of bolt tightening increments, and the time between each tightening increment all have an effect on the final contact pressure between the packing material and flange faces.

The three aforementioned factors influence the pressure distribution across the face of the gasket, which is in contact with the flange faces, as well as the effect which creep-relaxation has on the contact pressure. It was shown that an increase in the number of bolt tightening increments and the time between the increments reduce the effect which creep-relaxation has. It also ensures that the contact pressure is uniformly distributed along the circumference of the gasket. It is, however, not always possible to increase both the time between the increments and the increments itself. A possible topic

for future research may, therefore, be to investigate an optimisation scheme which calculates the optimal number of bolt tightening increments and time between the bolt tightening increments for a specific flange. The two constraints in this optimisation scheme may be: the desired difference in the distribution of the contact pressure; and the allowable reduction in contact pressure due to creep-relaxation. It may also minimise the total tightening time by reducing the number of bolt tightening increments and time between each increment.

6.1.4. Determination and implementation of external loads and moments

Bolted flange connections are often subjected to external loads and bending moments. The external bending moments and loads may result in a reduction in the contact pressure and subsequent leakage. In this investigation, however, the effect which external bending moments and loads has on the circular bolted flange connection was omitted. The reason it was omitted is because the exact application of these large diameter flanges are yet unknown. However, once this is known it is paramount to include these loads in the finite element models in order to determine the suitability of a specific design.

According to Mathan *et al.* [32] ASME accounts for these external loads by calculating an equivalent internal pressure which replaces the bending moment and axial force. This method, however, does not take into consideration the gasket characteristics. As a result of this a number of additional methods have been developed to improve upon ASME. These methods as cited by Mathan *et al.* [32] include, but are not limited to: using a correction factor based on an energy method; using a superposition approach to estimate load capacities on the flange joints; and replacing the bending moment by an equivalent axial force which is distributed as a sine wave in the circumferential direction. It is, therefore, recommended that in addition to simply including the external loads and bending moments in the finite element models one should also investigate the suitability, and ultimate accuracy, of the various suggested numerical implementations.

6.1.5. Large scale experimentation

The finite element models, for the three types of flanges, were validated by means of small scale experiments. These finite element models were then used to predict the behaviour of large diameter flanges which operate at both low and high pressures. It is suggested that the suitability of the finite element models for large diameter flange operating at both high and low pressures be experimentally validated by means of flanges which have similar diameters and operate at similar pressures.

6.2. Conclusion

The primary aim of this investigation was to propose a methodology, based on non-linear finite element analysis, which could be used to expand the current flange tables of Rand Water to accommodate pipes which have nominal bores of up to 4 m and test pressures of up to 8 000 kPa.

Finite element models for a flat face flange, raised face flange, and raised face flange with an O-ring were developed. For each of these models a material characterisation of the applicable packing material was done. A non-asbestos, compressed fibre gasket which had aramid and nitrile binding, was used as packing material for the flat and raised face flanges. This material was modelled as a non-linear viscoelastic material based on Prony shear relaxation and a Neo-Hookean model. This assumption, regarding the material model, allowed for the accurate prediction of the effect of creep-relaxation as well as the deformation of the gasket during the seating condition. A nitrile O-ring was used as packing material for the raised face flange with an O-ring groove. The nitrile O-ring was successfully modelled with a third order Ogden material model. During the material characterisation it was observed that the coefficient of friction between the gasket and flange face played a significant role in the amount of closure during the seating condition, as well as in the amount of closure caused by creep-relaxation.

The finite element models, for each of the three flange types, were validated by means of small scale experiments. During the validation process it was found that the number of bolt tightening increments as well as the time between the bolt tightening increments had a significant impact on the effect which creep-relaxation had once the circular bolted flange connection was placed in operation. It was found that an increase in either the number of bolting increments or the time between the bolting increments will reduce the effect which creep-relaxation has during operation.



Finally, the validated non-linear finite element models were used to design large diameter flanges. A design procedure, consisting of three steps, was proposed for the design of the large diameter flanges. The first step in the procedure was to design the desired flange by making use of ASME VIII, Division 1. Once the flange was designed the dimensions could be placed into a parameterised non-linear finite element model of the relevant flange and solved. The final step was to use the allowable stress limits, as well as the desired contact stress, to optimise the design. It was found that significantly lighter flanges, which remained both leak tight and safe, could be designed by following this procedure.

The results of the proposed non-linear finite element models were also compared to the predicted results of the ASME VIII, Division 1, design methodology. From the comparison it was found that the ASME VIII, Division 1 design methodology lacked the ability to accurately predict the stresses in the flat and raised face flanges. In both instances the radial and axial stresses were overestimated, whilst the tangential stress was underestimated. This meant that designs, which adhere to the failure criteria, are often rejected by following the ASME VIII, Division 1 design method.

The proposed design methodology, based on non-linear finite element modelling, allows for the accurate prediction of both the stresses in the circular bolted flange connections as well as the contact pressure between the flange faces and packing materials. This in-turn allows for the design of lighter flanges which remain safe and leak tight through an optimisation process.



REFERENECEES

- [1] J. T. Campbell, "Johannesburg, South Africa," *Britannica*. 2013.
- [2] South African Census Bureau, "Statistical release (Revised) Census 2011." p. 78, 2012.
- [3] L. E. Brownell and E. H. Young, *Process Equipment and Design*. New York: John Wiley & Sons, Inc., 1959.
- [4] ASME, "2007 ASME Boiler & Pressure Vessel Code, Section VIII, Division I, Rules for the construction of pressure vessels." The American Society of Mechanical Engineers, New York.
- [5] ASME, "2007 ASME Boiler & Pressure Vessel Code, Section VIII, Division II, Alternative rules, Rules for the construction of pressure vessels." The American Society of Mechanical Engineers, New York, 2007.
- [6] N. W. Murray and D. G. Stuart, "Behaviour of large taper hub flanges," in *Proceedings of the Symposium on Pressure Vessel Research Towards Better Design*, 1961.
- [7] L. Prinsloo, "A critical evaluation of the design of removable cover-plate header boxes for air-cooled heat exchangers," University of Pretoria, 2011.
- [8] E. O. Waters, D. B. Westrom, D. B. Rossheim, and F. S. G. Williams, "Formulas for stresses in bolted flange connections." *Trans American Society of Mechanical Engineers*, p. FSP-59-4, 1937.
- [9] E. O. Waters, D. B. Westrom, D. B. Rossheim, and F. S. G. Williams, "Development of general formulas for bolted flanges." Taylor Forge and Pipe Works, Chicago, 1949.
- [10] E. O. Waters and J. H. Taylor, "The strength of pipe flanges," *Mech. Eng.*, vol. 49, pp. 531-542, 1927.
- [11] R. Huston and H. Josephs, *Practical Stress Analysis in Engineering Design*, 3rd ed. Northwest Florida: CRC Press, 2009.
- [12] E. O. Waters and J. H. Taylor, "Methods of Determining the Strength of Pipe Flanges," *Mech. Eng.*, vol. 49, pp. 1340-1347, 1927.
- [13] D. H. Nash, "UK rules for unfired pressure vessels," in *The Companion Guide to ASME Boiler and Pressure Vessel Code*, 2001.
- [14] Taylor Forge & Pipe Works, "Modern Flange Design, Bulletin 502 - Fifth Edition." Chigaco, Illinois, 1964.
- [15] ANSYS, "Pressure Vessel Design Manual (Fourth Edition)." ANSYS, pp. 139-183, 2012.
- [16] G. F. Lake and G. Boyd, "Design of bolted, flanged joints of pressure vessels," *Proc. Instn Mech. Engrs, L.*, vol. 171, p. 843, 1957.



- [17] D. B. Wesstrom and S. E. Bergh, "Effect of internal pressure on stresses and strains in bolted-flanged connections," *Trans. Amer. Soc. Mech. Eng.*, vol. 73, p. 553, 1951.
- [18] S. Nagata and T. Sawa, "Comparison of flange stress calculated by ASME design code and finite element analysis," in *PVP 2007: 2007 ASME Pressure Vessels and Piping Division Conference*, 2007, pp. 245–252.
- [19] University of Strathclyde, "Pressurised Systems," *16426 Pressurised Systems*, 1999. [Online]. Available: <http://homepages.strath.ac.uk/~clas16/16426P76-93.pdf>. [Accessed: 15-Apr-2015].
- [20] M. Murali Krishna, M. S. Shunmugam, and N. Siva Prasad, "A study on the sealing performance of bolted flange joints with gaskets using finite element analysis," *Int. J. Press. Vessel. Pip.*, vol. 84, no. 6, pp. 349–357, 2007.
- [21] D. Y. Hwang and J. M. Stallings, "Finite element analysis of bolted flange connections," *Comput. Struct.*, vol. 51, no. 5, pp. 521–533, 1994.
- [22] J. Kim, J. Yoon, and B. Kang, "Finite element analysis and modeling of structure with bolted joints," *Appl. Math. Model.*, vol. 31, no. 5, pp. 895–911, 2007.
- [23] J. Montgomery, "Methods for modeling bolts in the bolted joint," *ANSYS User's Conference*, 2002. [Online]. Available: <http://www.ansys.com/Resource+Library/Conference+Papers/Methods+for+Modeling+Bolts+in+the+Bolted+Joint>. [Accessed: 29-Nov-2015].
- [24] ANSYS, "ANSYS 16.2, Mechanical Help, Interface Elements." ANSYS.
- [25] ASME, "Guidelines for pressure boundary bolted flange joint assembly." The American Society of Mechanical Engineers, New York, 2000.
- [26] D. H. Nash and M. Abid, "Combined external load tests for standard and compact flanges," *Int. J. Press. Vessel. Pip.*, vol. 77, no. 13, pp. 799–806, 2000.
- [27] A. A. Alkelani, B. A. Housari, and S. A. Nassar, "A proposed model for creep relaxation of soft gaskets in bolted joints at room temperature," *J. Press. Vessel Technol.*, vol. 130, pp. 1–6, 2008.
- [28] R. Kauer and K. Strohmeier, "Finite element simulation of non-linear, time, and temperature dependent effects of flange gasket materials," *ASME Pip. Press. Vessel.*, vol. 414, no. 2, pp. 59–63, 2000.
- [29] A. Bazergui, "Short term creep and relaxation behaviour of gaskets," *Weld. Res. Council. Bull.*, vol. 294, pp. 9–22, 1984.
- [30] A. Bouzid, A. Chaaban, and A. Bazergui, "The effect of gasket creep-relaxation on the leakage tightness of bolted flange joints," *J. Press. Vessel Technol.*, vol. 117, no. 1, pp. 71–78, 1995.
- [31] A. Yamaguchi, H. Tsuji, and T. Honda, "Simulation of creep/relaxation behavior in bolted flange joints based on 3-D viscoelasticity model of gasket," in *Proceedings of the ASME 2009 Pressure*



- Vessels and Piping Division Conference*, 2009, pp. 185–191.
- [32] G. Mathan and N. Siva Prasad, “Studies on gasketed flange joints under bending with anisotropic Hill plasticity model for gasket,” *Int. J. Press. Vessel. Pip.*, vol. 88, no. 11–12, pp. 495–500, 2011.
- [33] T. Sawa, N. Higurashi, and H. Akagawa, “A stress analysis of pipe flange connections,” *J. Press. Vessel Technol.*, vol. 113, no. November, pp. 497–503, 1991.
- [34] H. Singh and P. Kumar, “Mathematical models of tool life and surface roughness for turning operation through response surface methodology,” vol. 66, pp. 220–226, 2007.
- [35] H. Wang and L. J. Zeng, “Seal evaluation using ANSYS WorkBench,” in *Automotive simulation world congress*, 2012.
- [36] “Nonlinear finite element analysis of elastomers - technical paper.” MSC Software Corporation, 2000.
- [37] I. Green and C. English, “Analysis of elastomeric O-ring seals in compression using the finite element method,” *Tribol. Trans.*, vol. 35, no. 1, pp. 83–88, 1992.
- [38] J. Drago, “Initial gasket compression is key to safe , reliable flange joints,” *Seal. Technol.*, pp. 10–12, 2013.
- [39] “SOMAT TCE Ver. 3.22.0.” HBM [Computer Software].
- [40] “Pipemill.” Ivysoft Ltd. [Computer Software].
- [41] “ASME gasket factors for non-metallic Klinger Mzansi gaskets,” 2015. [Online]. Available: <http://www.klinger.co.za/technical-data/gaskets/docs/Gasket-Factors-ASME.pdf>.
- [42] Abbey Forged Products, “ASTM A350 LF2 - Carbon Steel,” 2015. [Online]. Available: <http://www.abbeyforgedproducts.co.uk/images/downloads/PDF/ASTM-A350-LF2.pdf>. [Accessed: 25-Nov-2015].
- [43] Bolt Depot, “Bolt grade markings and strength chart,” 2015. [Online]. Available: <https://www.boltdepot.com/fastener-information/materials-and-grades/bolt-grade-chart.aspx>. [Accessed: 25-Nov-2015].
- [44] British Standards Institute, “BS 4190:2001 ISO metric black hexagon bolts, screw and nuts - Specification.” 2001.
- [45] R. T. Rose, “The stress analysis of pressure vessels and pressure vessel components,” S. S. Gill, Ed. Oxford: Pergamon Press, 1970, pp. 267–315.
- [46] ANSYS, “Introduction to ANSYS DesignXplorer: Lecture 4, Response Surface.” ANSYS.

APPENDIX A: DIN 2505 METHOD

Apart from the design methodology suggested by Waters, Wesstrom, Rossheim, & Williams [9], a design methodology which emphasised the importance of mutual dependence between the flanges, the fasteners, and the gaskets was suggested by Schwaigerer in 1960 [45]. This method became the basis for the German DIN 2505 standard which was first published as a pre-standard in 1968 and then as a final standard in 1990. This method is, with regards to most aspects, different from those which developed from the research of Waters *et al.* [9] and has the following notable differences: the bolt has its own tolerance; the bolt load changes as a load is applied; and the gasket is analysed in detail. The German DIN 2505 standard was replaced by the European EN 1591 standard and was published with the purpose of supplying the EN 13445 standard with an alternative design method for bolted flange connections. This alternative method was widely accepted and the alternative method of the European EN 1591 standard, which was based on the German DIN 2505 standard, was integrated into the European EN 13445 standard as Annexure G. This method is based on the work of Schwaigerer and has formed the basis of the German standard DIN 2505. It is claimed by Rose [45] that this method has been successfully implemented for flanges up to 2 m in diameter.

The DIN 2505 standard gives values for the initial seating force; the sealing force; maximum permissible loads under assembly conditions for a large variety of gasket materials. The major difference between the DIN 2505 method and the Taylor-Forge and Lake & Boyden method is the importance the mutual dependence of the flanges, the fasteners, and the gaskets. This method makes use of a diagram which is very similar to the one shown in Figure A-1. The DIN 2505 method takes the following three factors into account: the difference in the flexibility of the flange under assembly and pressure conditions as a result of the change in the moment arm; the reduction in the bolt and flange stiffness as a result of the decrease in the modulus of elasticity at increased temperatures; and the creep of the gasket. This method, however, does not account for the pressure inflation effect. Another difference between the DIN 2505 method and the Taylor-Forge and Lake & Boyden method is that emphasis is placed on the plastic collapse moment and not on the stresses. In this method it is assumed that the loading is an external moment applied to the flange ring and all other pressure effects are neglected. The moment is calculated in the same way as the Taylor-Forge method with the exception that the pressure end load is assumed to act at the mid-thickness of the shell rather than through the mid-thickness of the hub at its connection point with the flange [45].

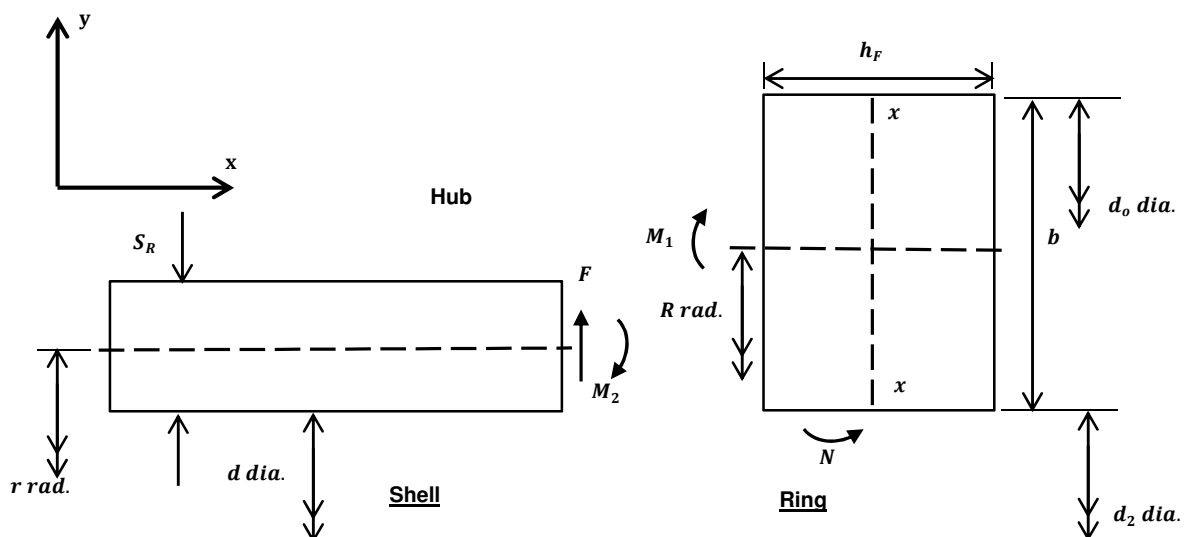


Figure A-1: Analysis of the forces and moments by means of the DIN 2505 method [45]

For the calculations of the forces and moments by means of the DIN 2505 method it is assumed that the ring and shell are both fully plastic. Where the ring experiences tangential stress and the shell experiences axial stress. The sum of the resistances of the ring and shell make up the plastic collapse moment [45].

When the ring is considered (with no cross-sectional deformation) the following bending moment may be calculated:

$$RM_1 = \frac{bh_F^2\sigma_0}{4} \quad (A.1)$$

Where:

- b Flange width [m]
 h_F Thickness of the ring [m]
 RM_1 Bending moment around the x-x axis [N.m]

From this it may, therefore be concluded that the contribution to the total resisting moment is:

$$2\pi RM_1 = \frac{\pi bh_F^2\sigma_0}{2} \quad (A.2)$$

The external collapse moment M_2 per unit length of arc of the mean radius r is:

$$M_2 = \frac{(S_R^2 - S_1^2)\sigma_0}{4} \quad (A.3)$$

Where:

$$S_1 = \frac{P_R}{\pi(d + S_R)\sigma_0} \quad (A.4)$$

Where:

- d Inside diameter of the shell [m]
 P_R End load [N]
 S_1 Thickness [m]
 S_R Thickness of the shell [m]

The contribution to the total moment is, therefore:

$$2\pi r M_2 = \frac{\pi r (S_R^2 - S_1^2)\sigma_0}{2} \quad (A.5)$$

The total moment carried by the flange and shell assembly at collapse is therefore:

$$\frac{\pi}{2} (bh_F^2 + r(S_R^2 - S_1^2))\sigma_0 \quad (A.6)$$

Finally the flange width is reduced to account for the bolt holes. If the flange diameter exceeds 500 mm the reduction is taken as 1.5 times the diameter of the bolt hole. Therefore for the flange:

$$b = \frac{d_0 - d_2 - 2d'_L}{2} \quad (A.7)$$

Where:

- d_0 Outside diameter of the flange [m]
 d_2 Inside diameter of the flange [m]
 d'_L Bolt hole reduction [m]

Similarly for the radius of the shell:

$$r = \frac{d + S_R}{2} \quad (A.8.)$$

From Equations A.1. to A.9. design plastic section modulus (W) of the flange may be calculated by making use of the following equation:

$$W = \frac{\pi}{4} [(d_0 - d_2 - 2d'_L)h_F^2 + (d + S_R)(S_R^2 - S_1^2)] \quad (A.9.)$$

The DIN 2505 method, which has now be included in the European EN-13445 has the following advantages [45]:

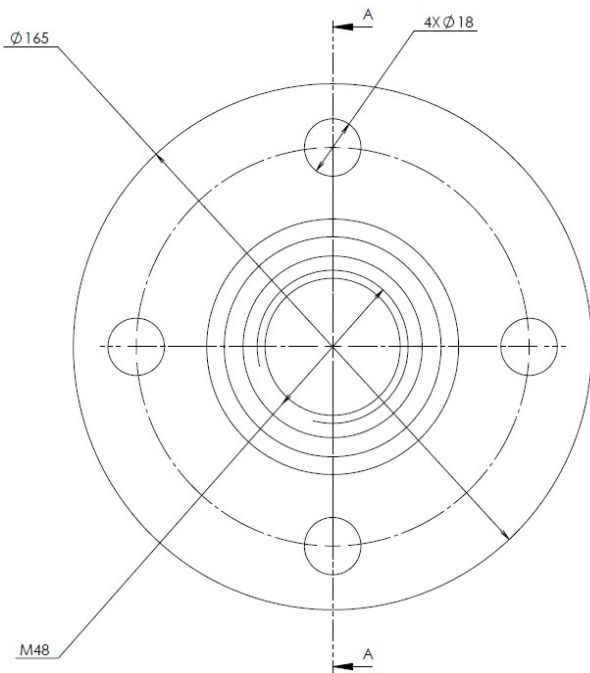
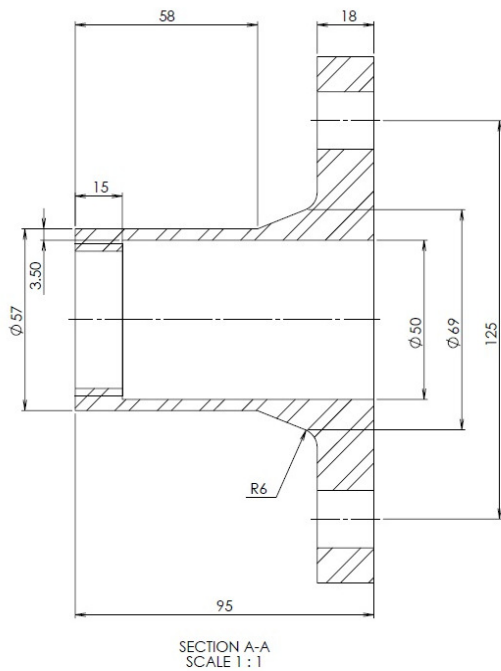
1. It in many cases gives an economical solution.
2. Ensures that the joint is leak free and has the correct leak tightness.
3. Includes the effect of thermal expansion effects due to a difference in temperature of the materials.
4. External loading effects are included.
5. The minimum torque is calculated based upon the bolt selection method.
6. The non-linear elastic behaviour of the gasket is considered.
7. The influence of the number of mounting cycles on the gasket are considered.
8. The range of the allowable bolt forces for the installation may be determined.
9. The fluctuation of the bolt forces are determined based upon the bolting-up method.

It is for these advantage that the DIN 2505 method has been included in the European EN 13445-1 standard as an alternative method for designing flanges. It is also strongly contesting the generally accepted method which stem from the Taylor-Forge method. The biggest drawback, however, is that has not been in use for as long as the Taylor-Forge method and as a result is not as widely used.

APPENDIX B: FLANGE AND MODIFIED BOLT DIMENSIONS

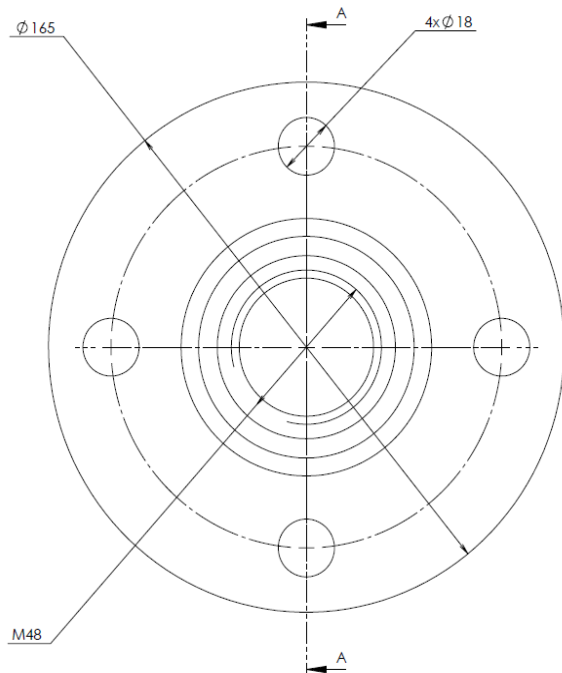
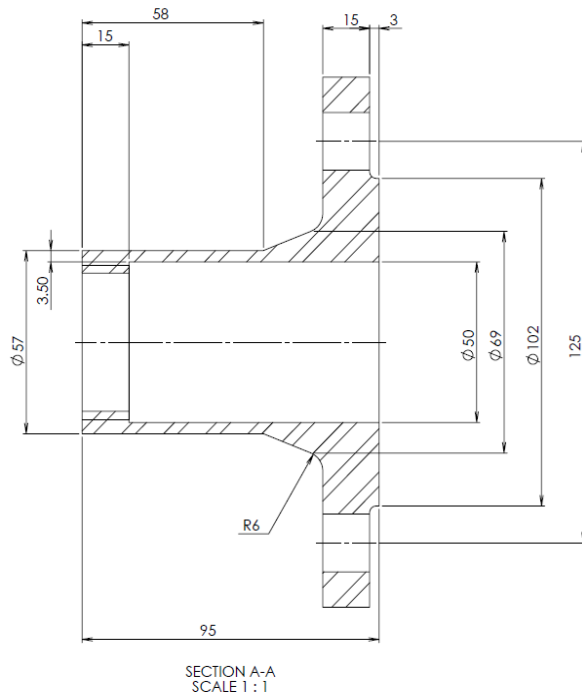
B.1. Dimensions of the flat face flange

Surface finish for flange face: $\frac{6.3}{\sqrt{C}}$ Turning

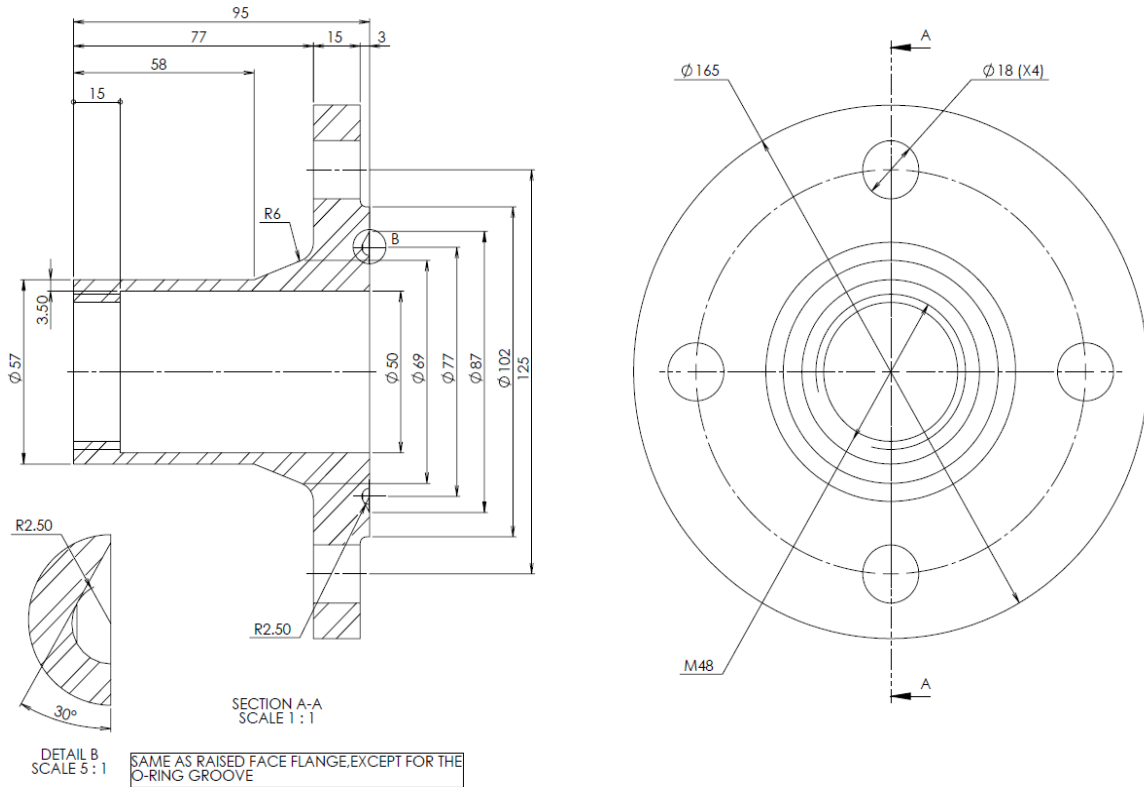


B.2. Dimensions of the raised face flange

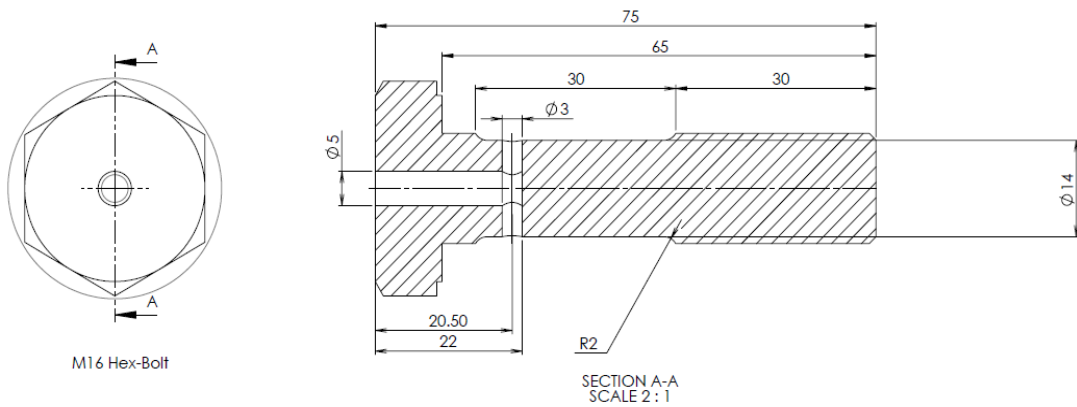
Surface finish for flange face: $\frac{6.3}{\sqrt{C}}$ Turning



B.1. Dimensions of the raised face flange with an O-ring groove



B.1. Dimensions of the modified M16 bolt



APPENDIX C: RESULTS FOR THE INITIAL FINITE ELEMENT MODELLING AND ANALYSIS

C.1. Results for the finite element analysis and modelling of the flat face flange

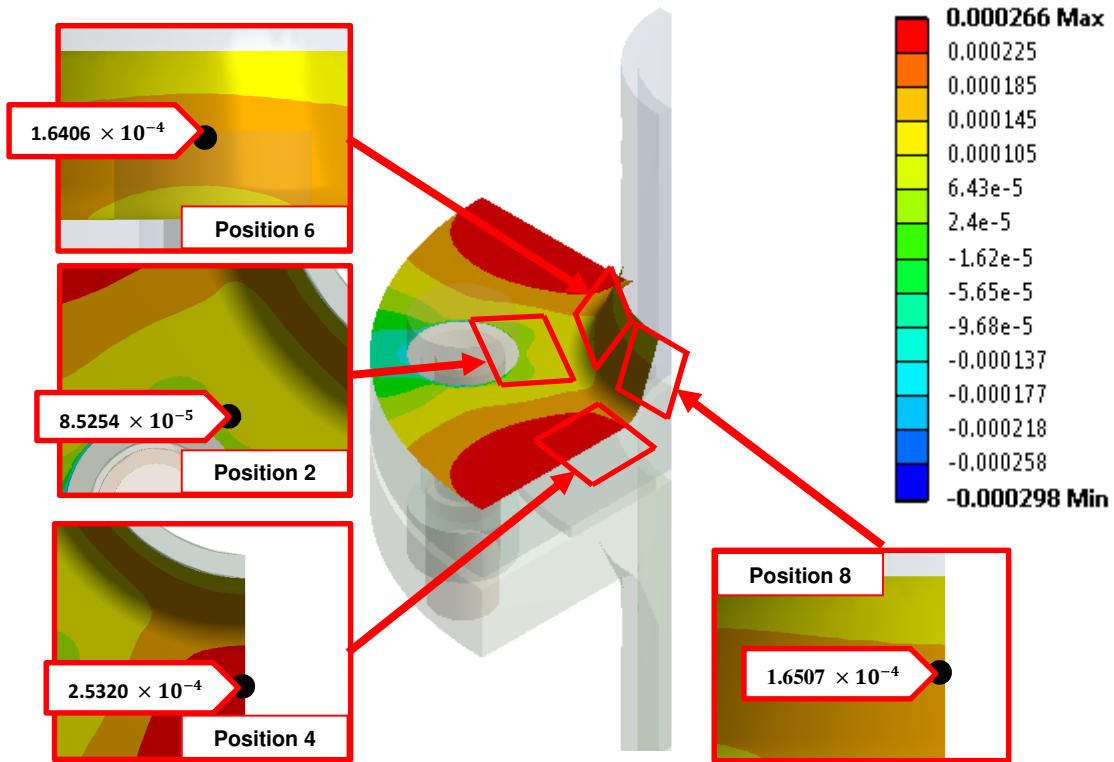


Figure C-1: Strains in the tangential direction on the ring and hub of the flat face flange before creep relaxation

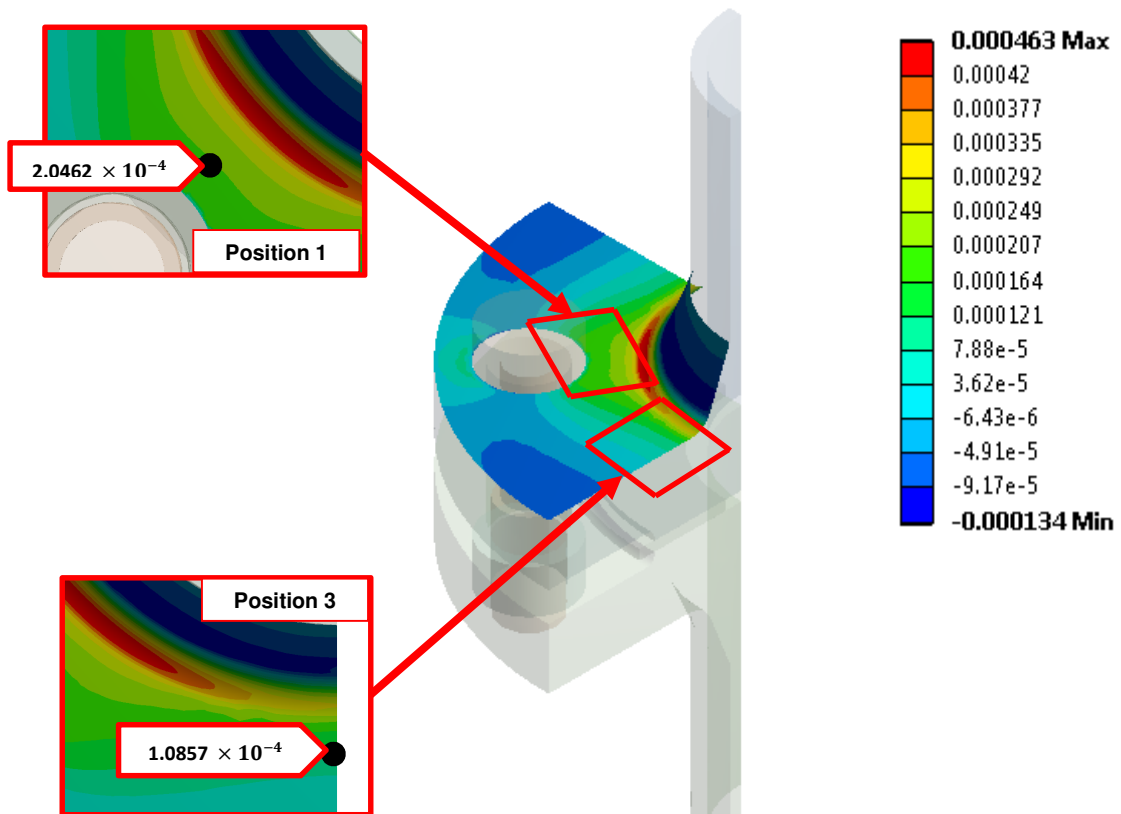


Figure C-2: Strains in the radial direction on the ring of the flat face flange before creep-relaxation

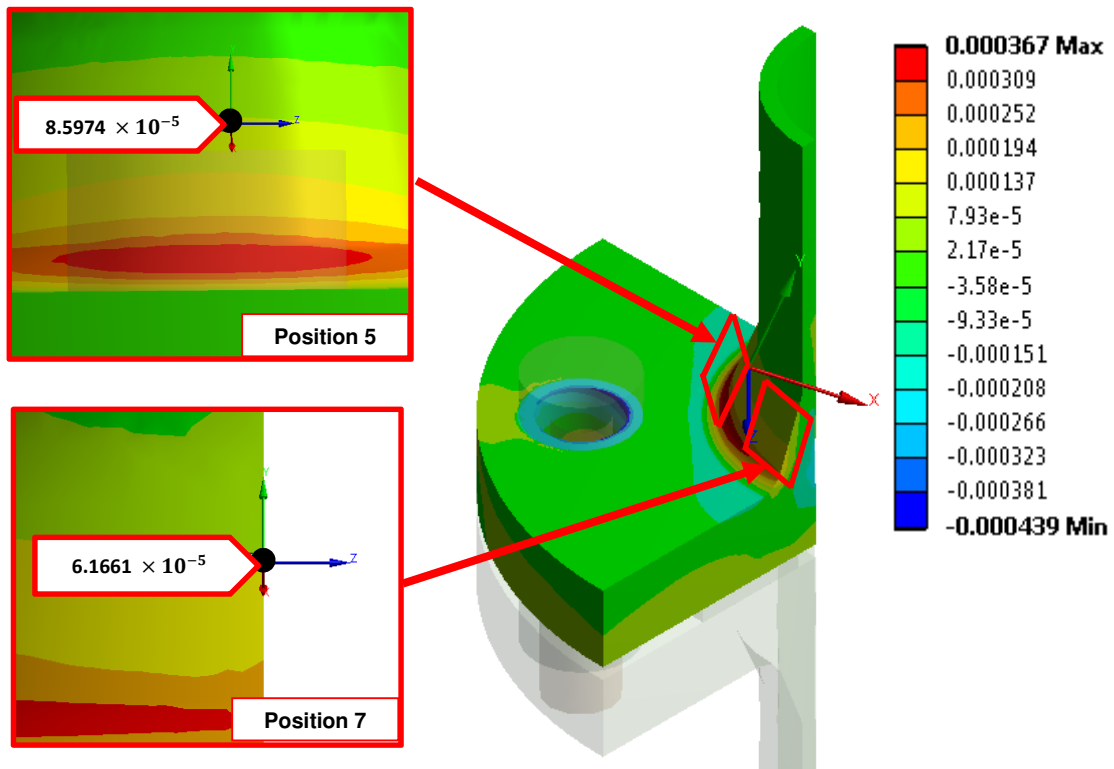


Figure C-3: Strains in the transposed axial direction on the hub of the flat face flange before creep relaxation

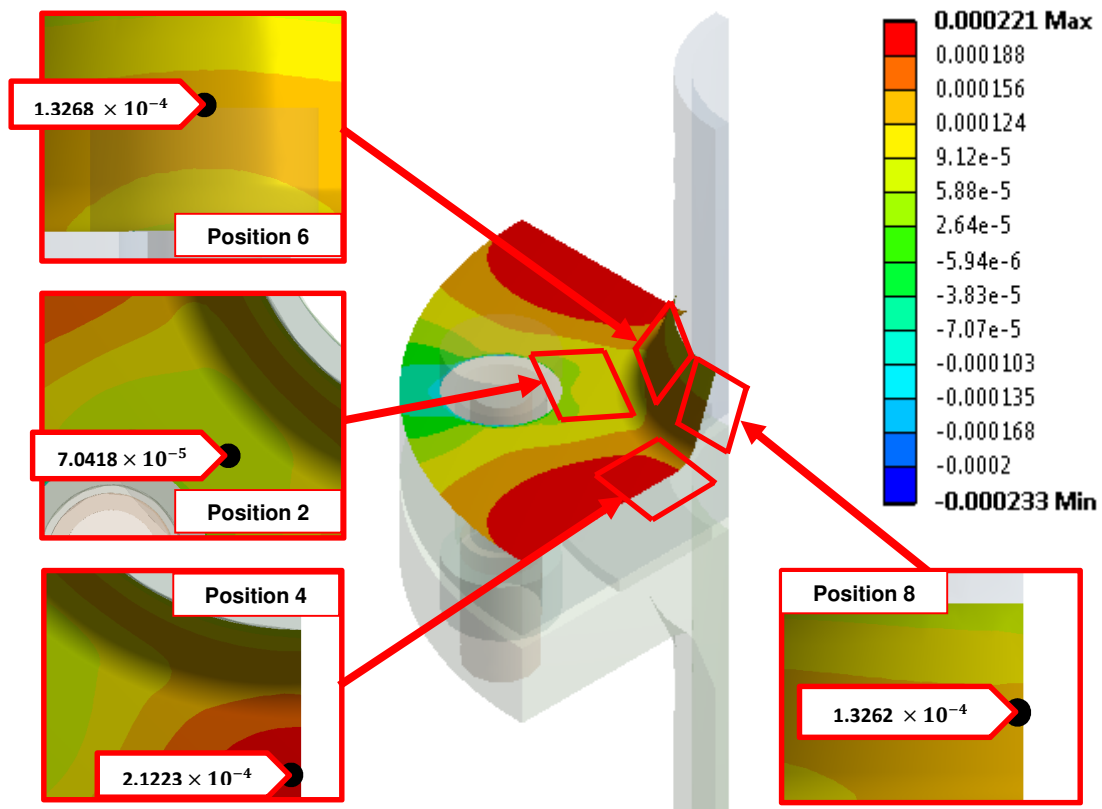


Figure C-4: Strains in the tangential direction on the ring and hub of the flat face flange after creep-relaxation

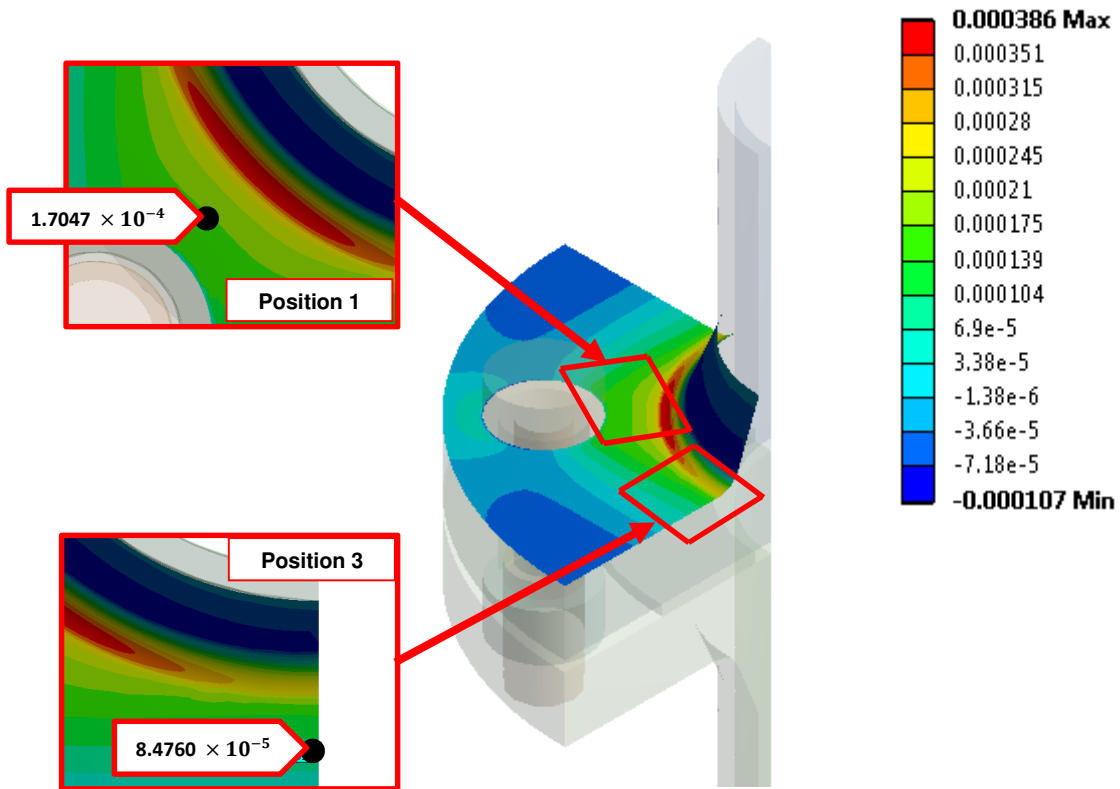


Figure C-5: Strains in the radial direction on the ring of the flat face flange after creep relaxation

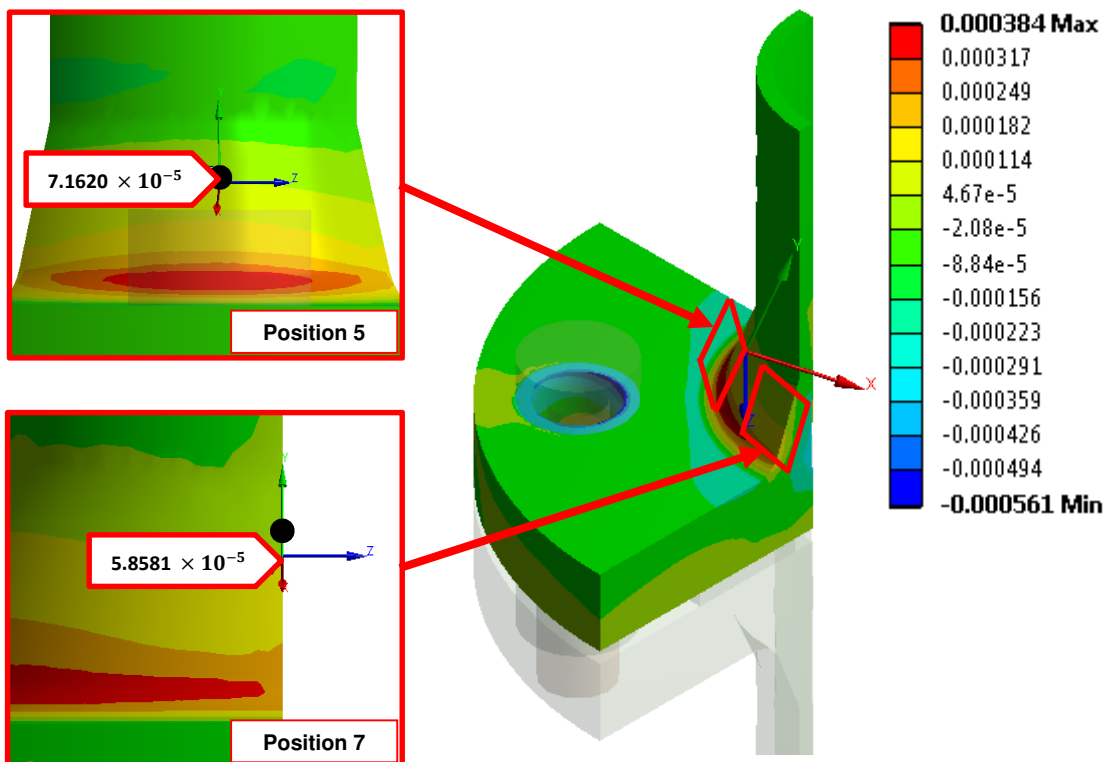


Figure C-6: Strains in the transposed axial direction on the hub of the flat face flange after creep relaxation

C.2. Results for the finite element analysis and modelling of the raised face flange

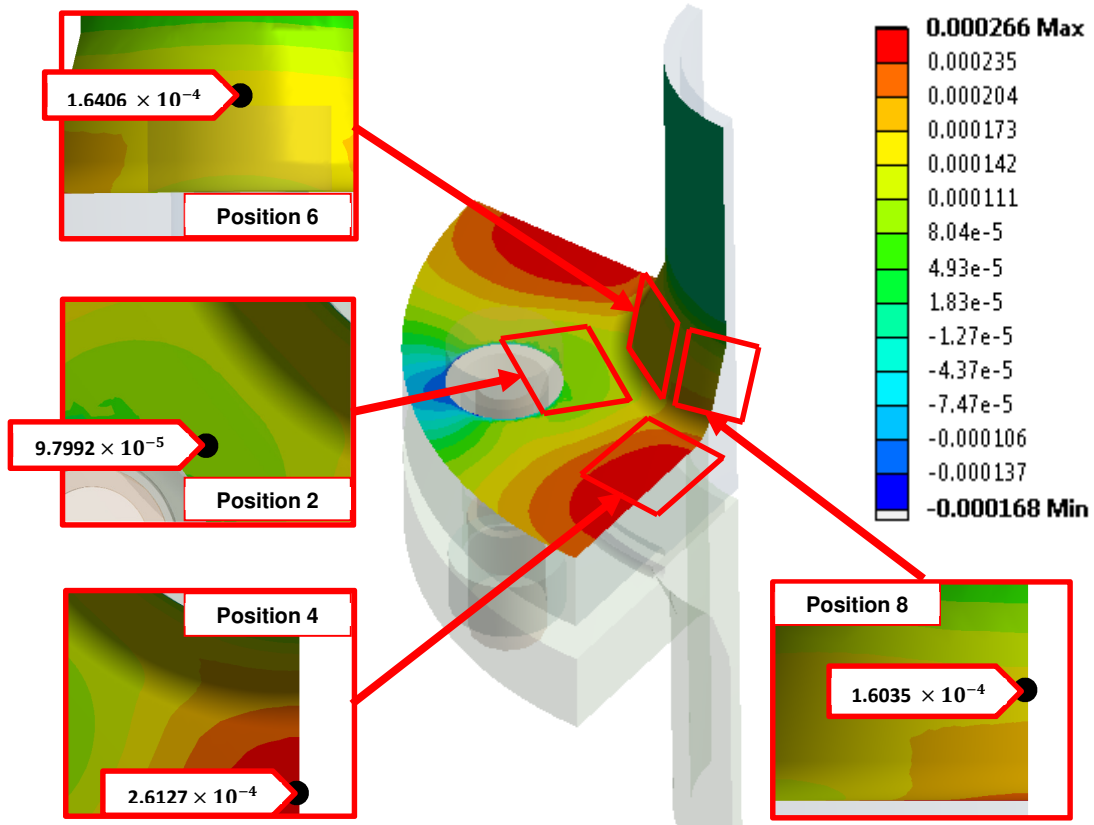


Figure C-7: Strains in the tangential direction on the ring and hub of the raised flange before creep relaxation

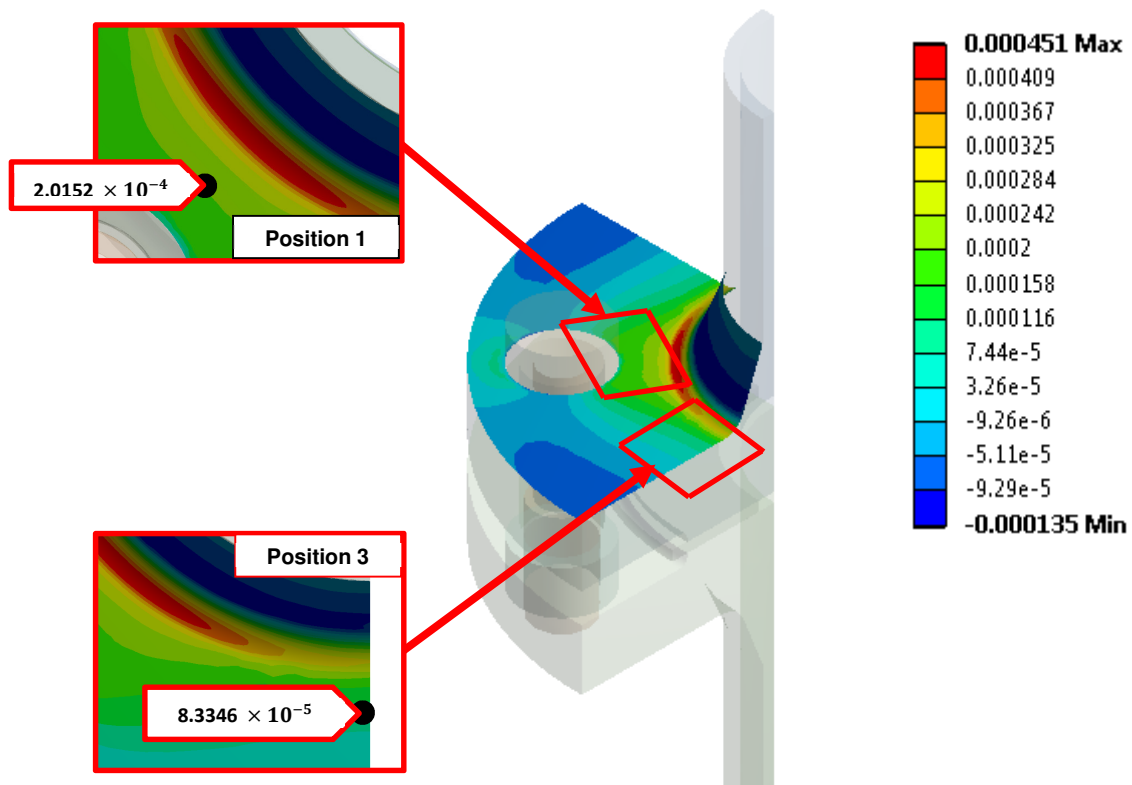


Figure C-8: Strains in the radial and tangential direction on the ring and hub of the raised face flange before creep-relaxation

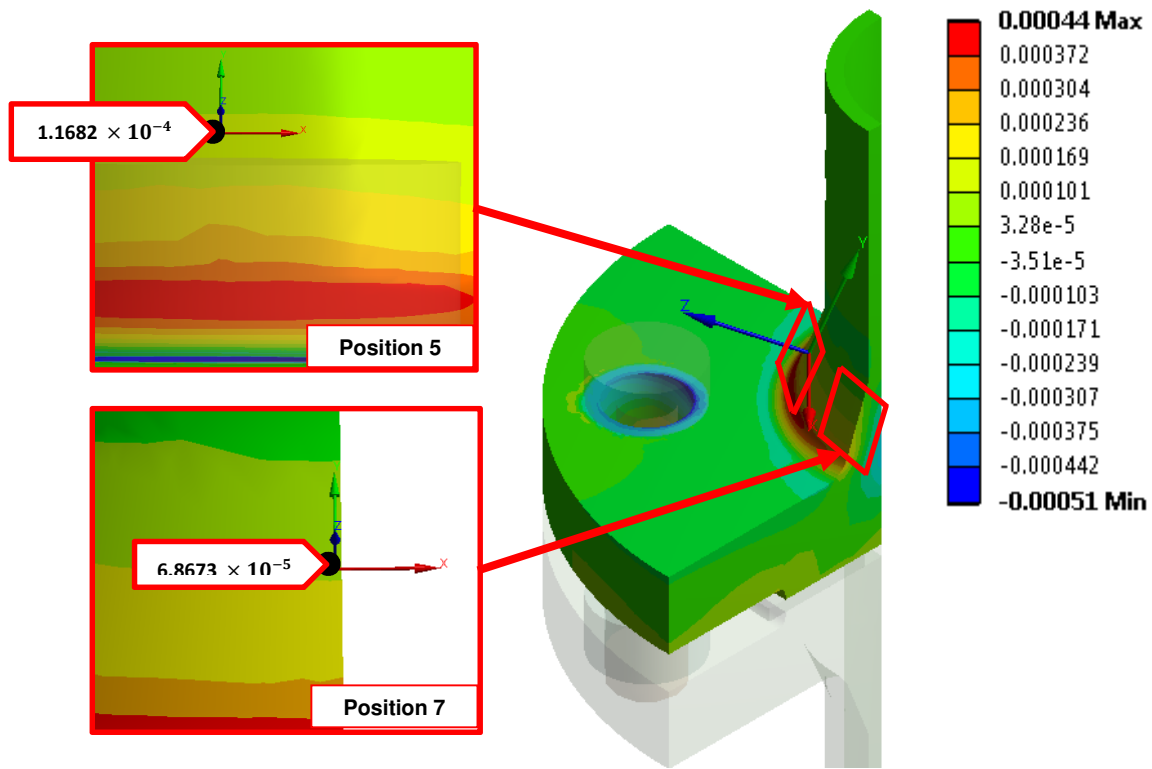


Figure C-9: Strains in the transposed axial direction on the hub of the raised face flange before creep relaxation

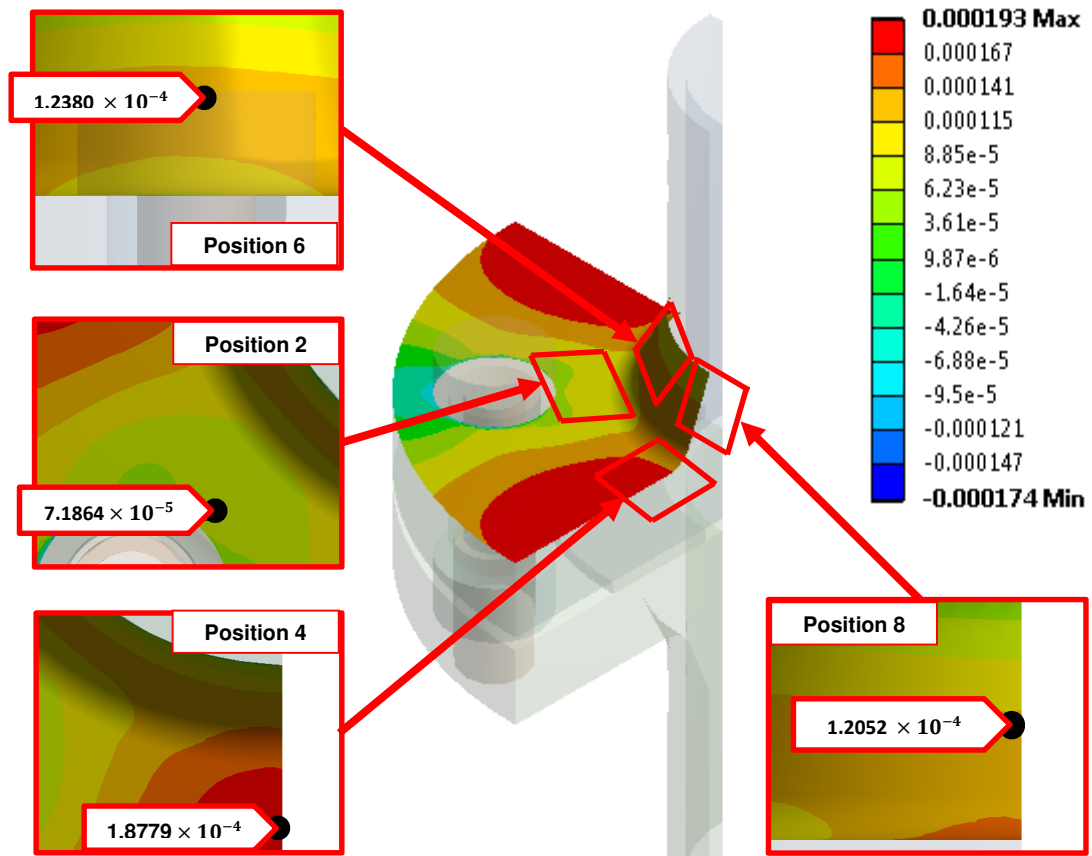


Figure C-10: Strains in the tangential direction on the ring and hub of the raised face flange after creep-relaxation

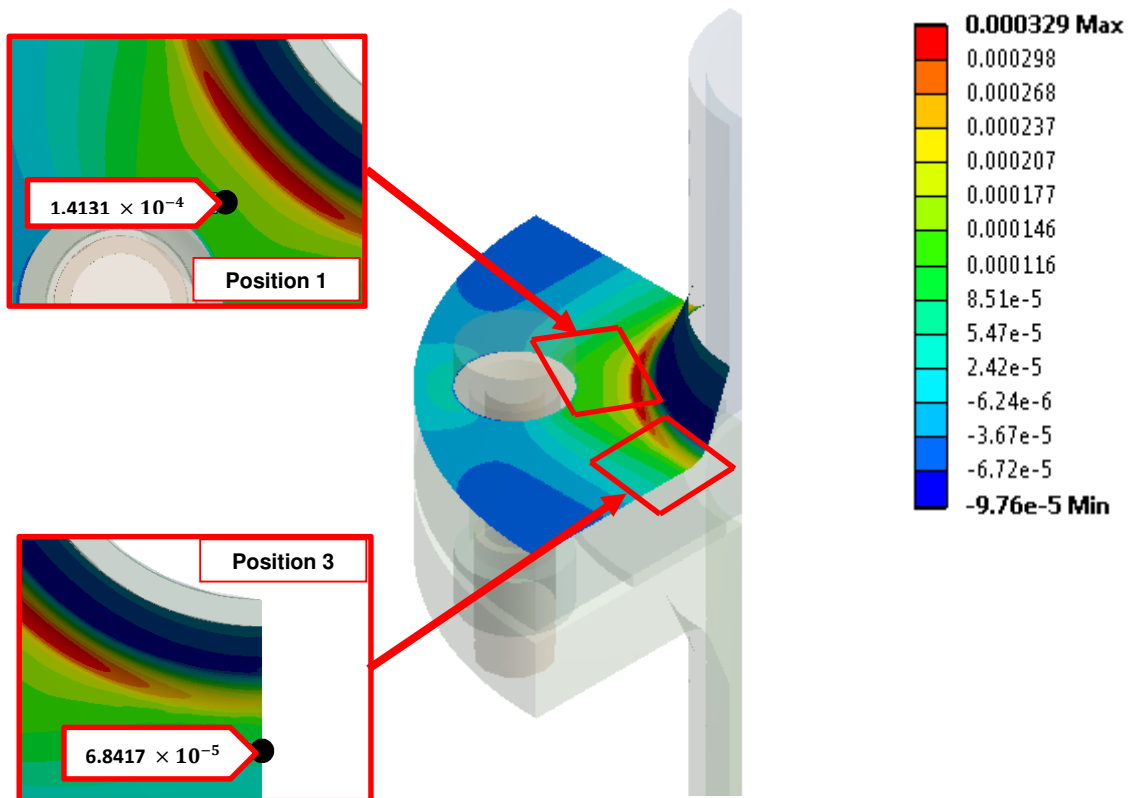


Figure C-11: Strains in the radial direction on the ring and hub of the raised face flange after creep-relaxation

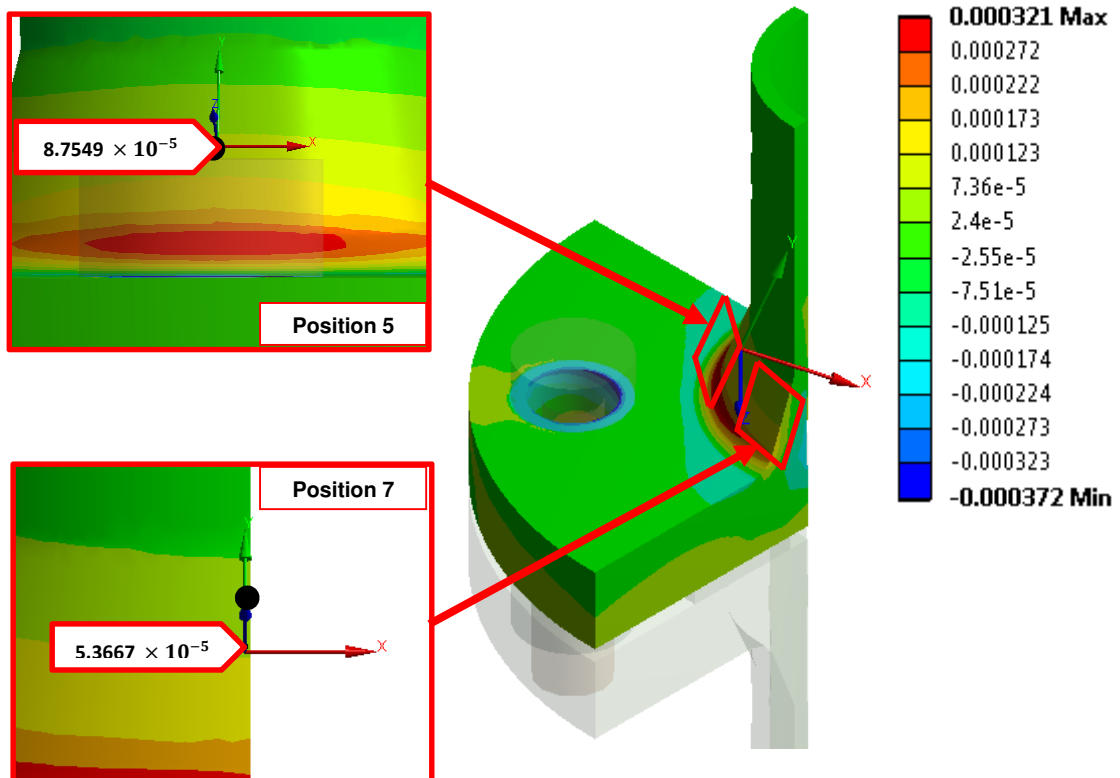


Figure C-12: Strains in the transposed axial direction on the ring and hub of the raised face flange after creep-relaxation

C.3. Results for the finite element analysis and modelling of the modified raised face flange with an O-ring groove

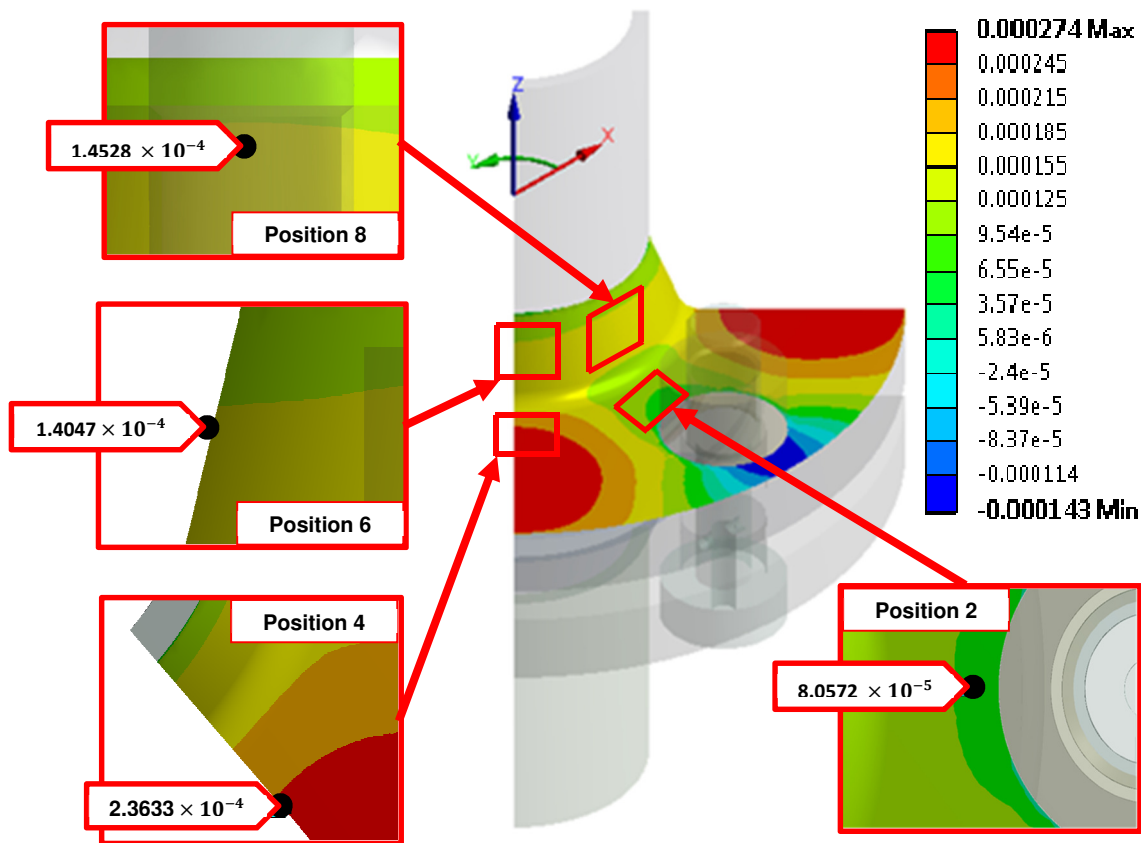


Figure C-13: Strains in the tangential direction on the ring and hub of the raised face flange which has been modified to contain an O-ring

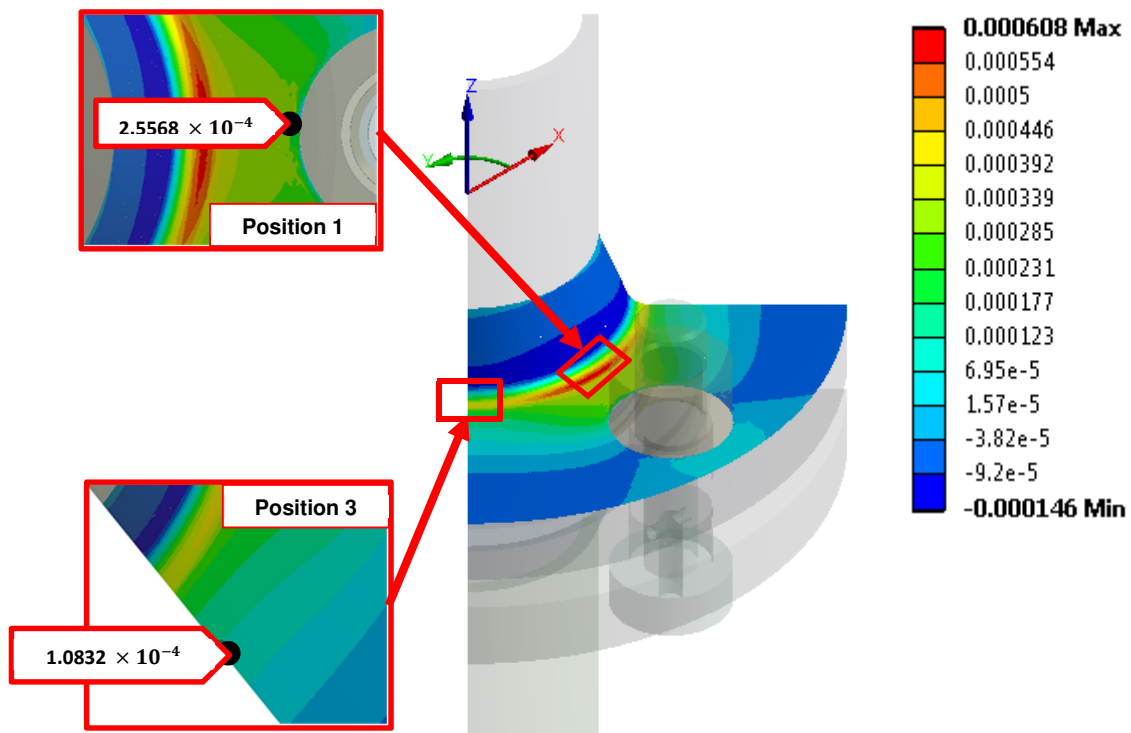


Figure C-14: Strains in the radial and tangential direction on the ring and hub of the raised face flange which has been modified to contain an O-ring

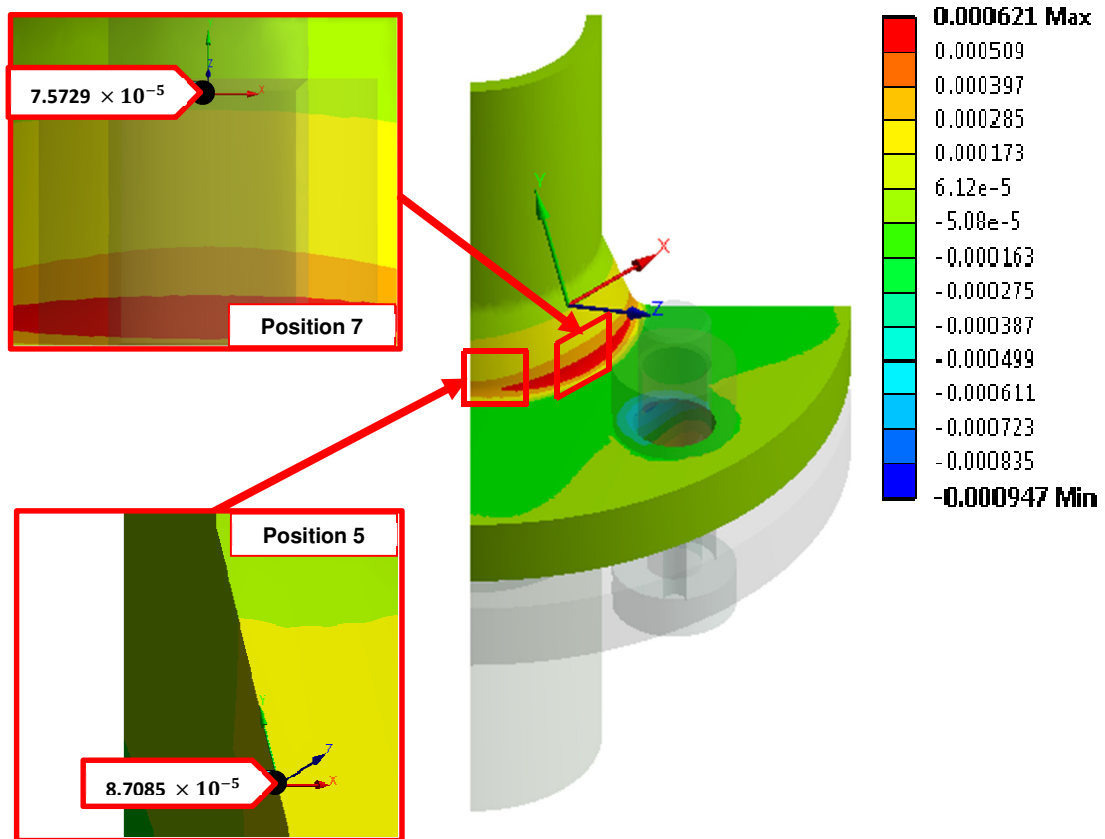


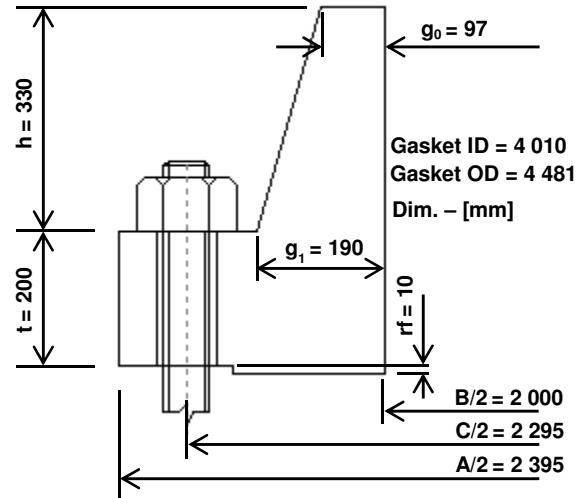
Figure C-15: Strains in the transposed axial direction on the hub of the raised face flange which has been modified to contain an O-ring

APPENDIX D: RESULTS FOR THE INITIAL FINITE ELEMENT MODELLING AND ANALYSIS
D.1. Design of flat face flange by means of ASME VIII, Division 1

1. DESIGN CONDITIONS					
Design pressure, P	1 500 kPa		Allowable stresses		
Design temperature	25°C		Flange		Bolting
Flange material	ASTM A-105	Design, temp., S_{fo}	167 MPa	Design, temp., S_b	346 MPa
Bolting material	ASTM A-193 B7	Atm. Temp., S_{fa}	167 MPa	Atm. Temp., S_a	346 MPa
2. GASKET AND FACING DETAILS					
Gasket	Compressed, non-asbestos		Facing		
3. TABLES 2-3 AND 2-4			4. LOAD AND BOLT CALCULATIONS		
N	68	$W_{m2} = b\pi Gy$	$2.88703 \times 10^6 N$	A_m greater of: $\frac{W_{m2}}{S_a}$ or $\frac{W_{m1}}{S_h}$	$61\,490\text{ mm}^2$
b	11.27 mm	$H_p = 2b\pi GmP$	$1.68891 \times 10^6 N$	A_b	$341\,836\text{ mm}^2$
G	4 077.46 mm	$H = \frac{G^2\pi P}{4}$	$1.95857 \times 10^7 N$	$W = \frac{(A_m + A_b)S_a}{2}$	$6.97721 \times 10^7 N$
y	20 MPa	$W_{m1} = H_p + H$	$2.12746 \times 10^7 N$	m	3.90
5. MOMENT CALCULATIONS					
Operating					
$H_D = \frac{\pi B^2 P}{4}$	$1.885 \times 10^7 N$	$h_D = R + 0.5g_1$	196 mm	$M_D = H_D h_D$	$3.69 \times 10^9 N \cdot mm$
$H_G = W_{m1} - H$	$1.689 \times 10^6 N$	$h_G = \frac{C - G}{2}$	257.27 mm	$M_G = H_G h_G$	$4.35 \times 10^8 N \cdot mm$
$H_T = H - H_D$	$7.371 \times 10^5 N$	$h_T = \frac{R + g_1 + h_g}{2}$	276.63 mm	$M_T = H_T h_T$	$2.04 \times 10^8 N \cdot mm$
				M_O	$4.33 \times 10^9 N \cdot mm$
Seating					
$H_G = W$	$6.9772 \times 10^7 N$	$h_G = \frac{C - G}{2}$	257.27 mm	M_O'	$1.549 \times 10^{10} N \cdot mm$
6. K AND HUB FACTORS					
$K = \frac{A}{B}$	1.188	h/h_o	0.476		
T	1.844	F	0.843		
Z	5.862	V	0.282		
Y	11.362	f	1.000		
U	12.485	$e = \frac{F}{h_o}$	1.216×10^{-3}		
$\frac{g_1}{g_o}$	1.667	$d = \frac{U}{V} h_o g_o^2$	4.416×10^8		
$h = \sqrt{B g_o}$	692.82				
7. STRESS FORMULA FACTORS					
$\beta = \frac{4}{3}te + 1$					1.405
$\lambda = \gamma + \delta$					0.743
8. STRESS CALCULATIONS					
Allowable	Operating		Allowable	Seating	
$1.5S_{fo}$	Axial hub, $S_H = \frac{f m_o}{\lambda g_1^2}$	36 MPa	$1.5S_{fa}$	Axial hub, $S_H = \frac{f m_G}{\lambda g_1^2}$	151 MPa
S_{fo}	Radial flange, $S_R = \frac{\beta m_o}{\lambda t^2}$	33 MPa	S_{fa}	Radial flange, $S_R = \frac{\beta m_G}{\lambda t^2}$	136 MPa
S_{fo}	Tangential flange, $S_T = \frac{m_o Y}{t^2} - Z S_H$	5 MPa	S_{fa}	Tangential flange, $S_T = \frac{m_G Y}{t^2} - Z S_H$	19 MPa
S_{fo}	Greater of: $\frac{(S_H + S_R)}{2}$ or $\frac{S_H + S_T}{2}$	35 MPa	S_{fa}	Greater of: $\frac{(S_H + S_R)}{2}$ or $\frac{S_H + S_T}{2}$	144 MPa
9. Rigidity					
$J_{seating}$	0.14		$J_{operating}$	0.57	≤ 1 Acceptable

D.2. Design of raised face flange by means of ASME VIII, Division 1

1. DESIGN CONDITIONS					
Design pressure, P	3 500 kPa	Allowable stresses			
Design temperature	25°C	Flange		Bolting	
Flange material	ASTM A-105	Design, temp., S_{fo}	167 MPa	Design, temp., S_b	346 MPa
Bolting material	ASTM A-193 B7	Atm. Temp., S_{fa}	167 MPa	Atm. Temp., S_a	346 MPa
2. GASKET AND FACING DETAILS					
Gasket	Compressed, non-asbestos		Facing		
3. TABLES 2-3 AND 2-4			4. LOAD AND BOLT CALCULATIONS		
N	68	$W_{m2} = b\pi Gy$	$7.21905 \times 10^6 N$	A_m greater of: $\frac{W_{m2}}{S_a}$ or $\frac{W_{m1}}{S_p}$	182 134.52 mm ²
b	26.13 mm	$H_p = 2b\pi GmP$	$9.85401 \times 10^6 N$	A_b	341 836 mm ²
G	4 397.55 mm	$H = \frac{G^2\pi P}{4}$	$5.31615 \times 10^7 N$	$W = \frac{(A_m + A_b)S_a}{2}$	$9.06425 \times 10^7 N$
y	20 MPa	$W_{m1} = H_p + H$	$6.30155 \times 10^7 N$	m	3.90
5. MOMENT CALCULATIONS					
Operating					
$H_D = \frac{\pi B^2 P}{4}$	$4.398 \times 10^7 N$	$h_D = R + 0.5g_1$	200 mm	$M_D = H_D h_D$	$8.80 \times 10^9 N \cdot mm$
$H_G = W_{m1} - H$	$9.854 \times 10^6 N$	$h_G = \frac{C - G}{2}$	96.13 mm	$M_G = H_G h_G$	$9.47 \times 10^8 N \cdot mm$
$H_T = H - H_D$	$9.181 \times 10^5 N$	$h_T = \frac{R + g_1 + h_g}{2}$	195.56 mm	$M_T = H_T h_T$	$1.80 \times 10^8 N \cdot mm$
				M_O	$1.15 \times 10^9 N \cdot mm$
Seating					
$H_G = W$	$9.06425 \times 10^7 N$	$h_G = \frac{C - G}{2}$	257.27 mm	M_O'	$8.7132 \times 10^9 N \cdot mm$
6. K AND HUB FACTORS					
$K = \frac{A}{B}$	1.198	h/h_o	0.530		
T	1.840	F	0.820		
Z	5.608	V	0.224		
Y	10.871	f	1.076		
U	11.946	$e = \frac{F}{h_o}$	1.317×10^{-3}		
$\frac{g_1}{g_o}$	1.959	$d = \frac{U}{V} h_o g_o^2$	3.121×10^8		
$h = \sqrt{B g_o}$	622.896				
7. STRESS FORMULA FACTORS					
$\beta = \frac{4}{3}te + 1$			1.351		
$\lambda = \gamma + \delta$			0.712		
8. STRESS CALCULATIONS					
Allowable	Operating		Allowable	Seating	
$1.5S_{fo}$	Axial hub, $S_H = \frac{f m_o}{\lambda g_1^2}$	121 MPa	$1.5S_{fa}$	Axial hub, $S_H = \frac{f m_G}{\lambda g_1^2}$	91 MPa
S_{fo}	Radial flange, $S_R = \frac{\beta m_o}{\lambda t^2}$	137 MPa	S_{fa}	Radial flange, $S_R = \frac{\beta m_G}{\lambda t^2}$	103 MPa
S_{fo}	Tangential flange, $S_T = \frac{m_o Y}{t^2} - Z S_H$	17 MPa	S_{fa}	Tangential flange, $S_T = \frac{m_G Y}{t^2} - Z S_H$	13 MPa
S_{fo}	Greater of: $\frac{(S_H + S_R)}{2}$ or $\frac{S_H + S_T}{2}$	129 MPa	S_{fa}	Greater of: $\frac{(S_H + S_R)}{2}$ or $\frac{S_H + S_T}{2}$	97 MPa
9. Rigidity					
$J_{seating}$	0.393	$J_{operating}$	0.521	≤ 1	Acceptable



APPENDIX E: MANUFACTURED AND INSTRUMENTED FLANGES

E.1. Instrumented flat face flange

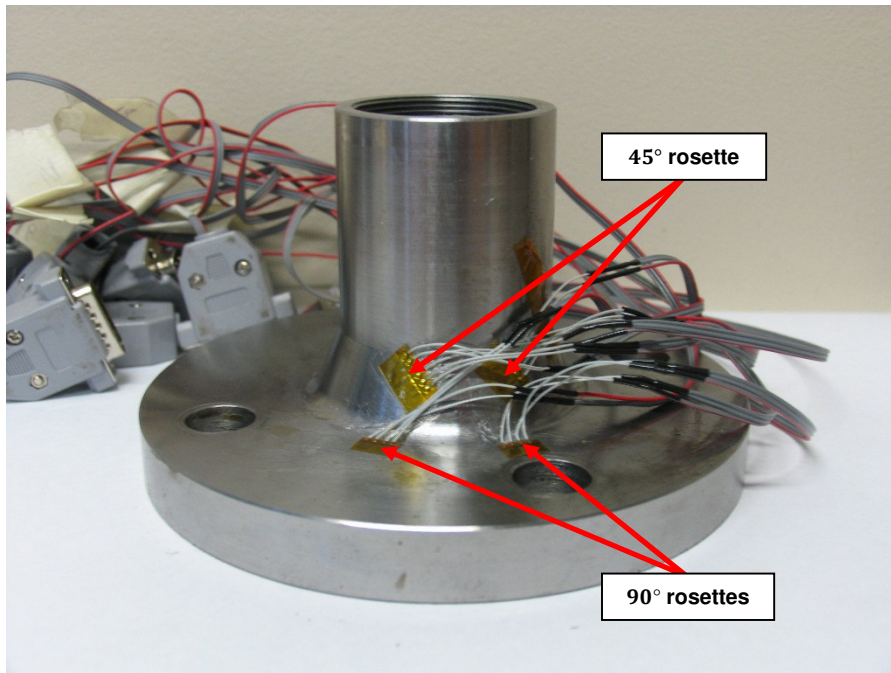


Figure E-1: Photograph of the instrumented flat face flange

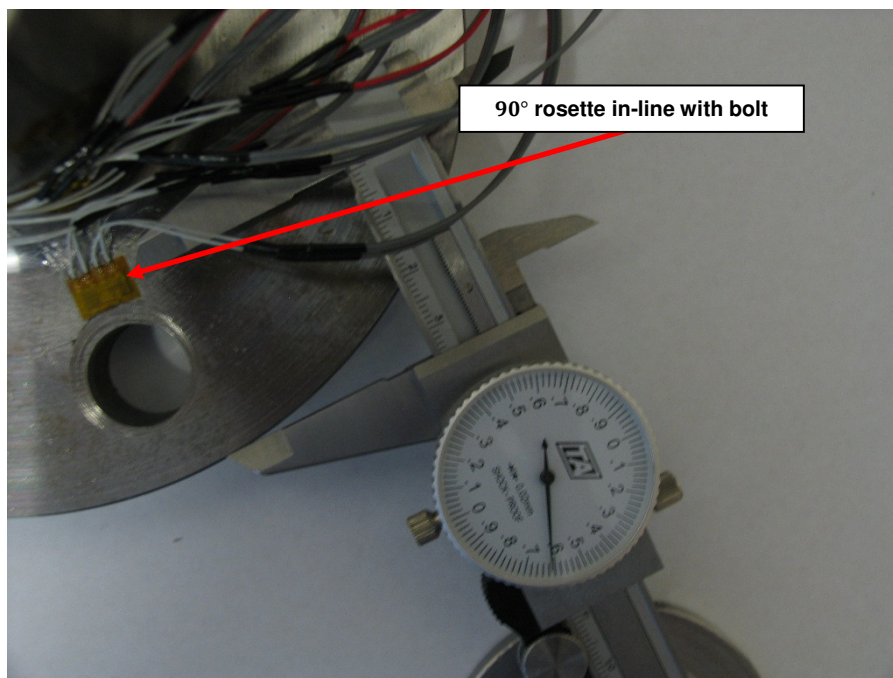


Figure E-2: Photograph of the position of the 90° rosette which is in-line with the bolt on the ring of the flat face flange

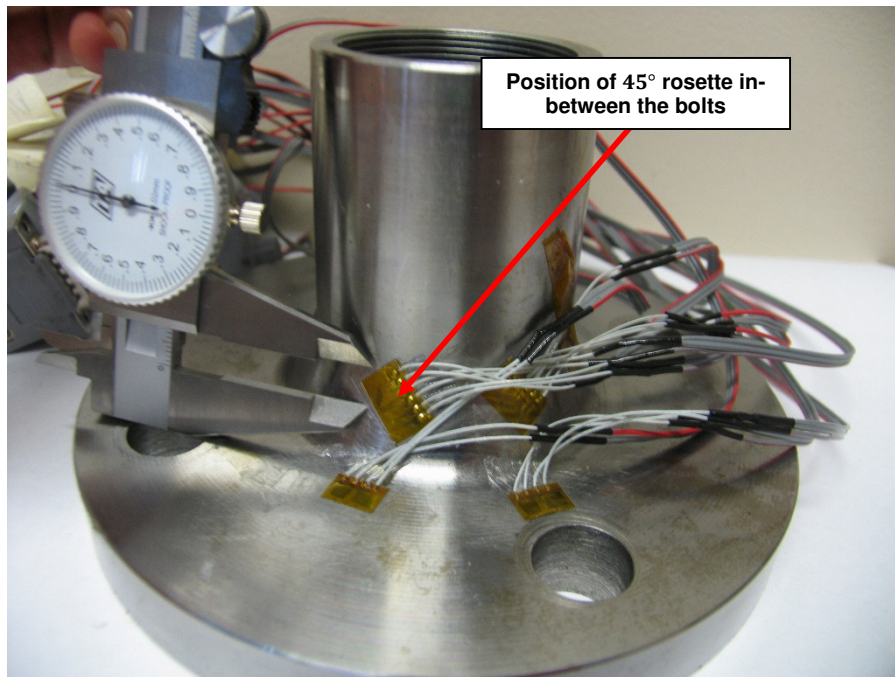


Figure E-3: Photograph of the position of the 45° rosette in-between the bolts on the hub of the flat face flange

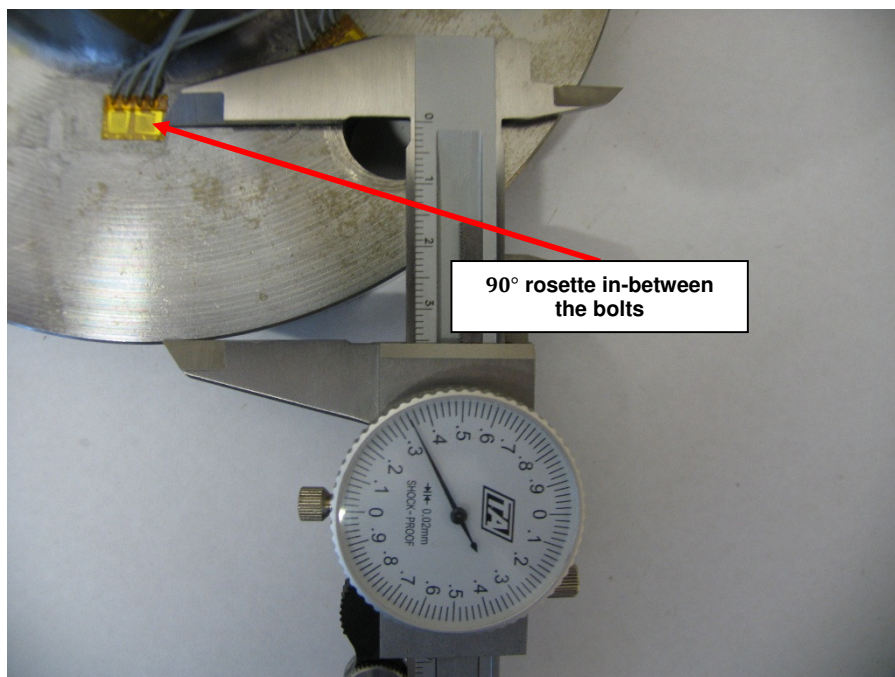


Figure E-4: Position, with the perpendicular distance from the edge of the flange, of the 90° rosette in-between the bolts on the ring of the flat face flange

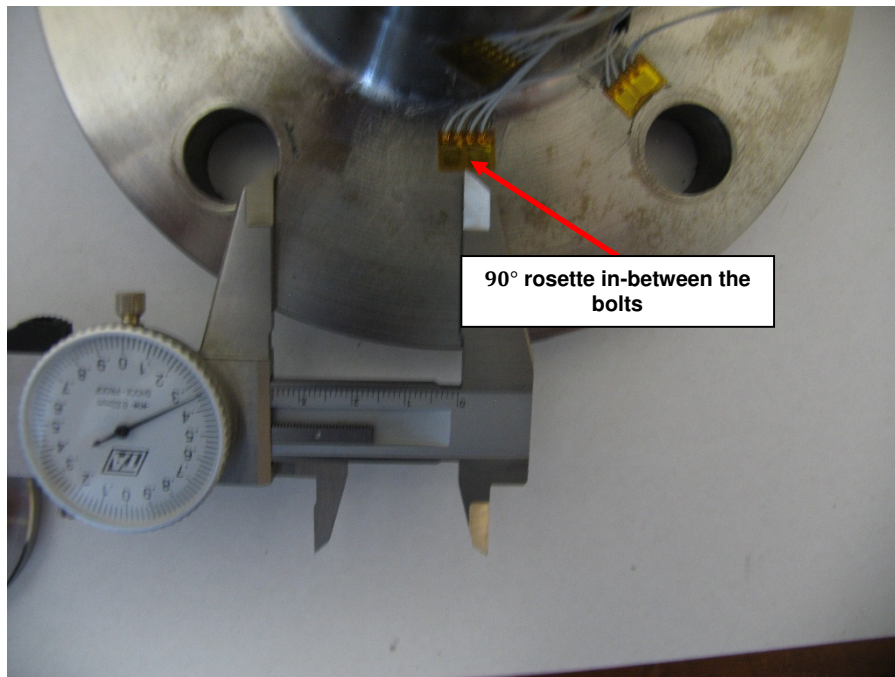


Figure E-5: Position, with the perpendicular distance from the edge of the bolt hole, of the 90° rosette in-between the bolts on the ring of the flat face flange

E.2. Instrumented raised face flange

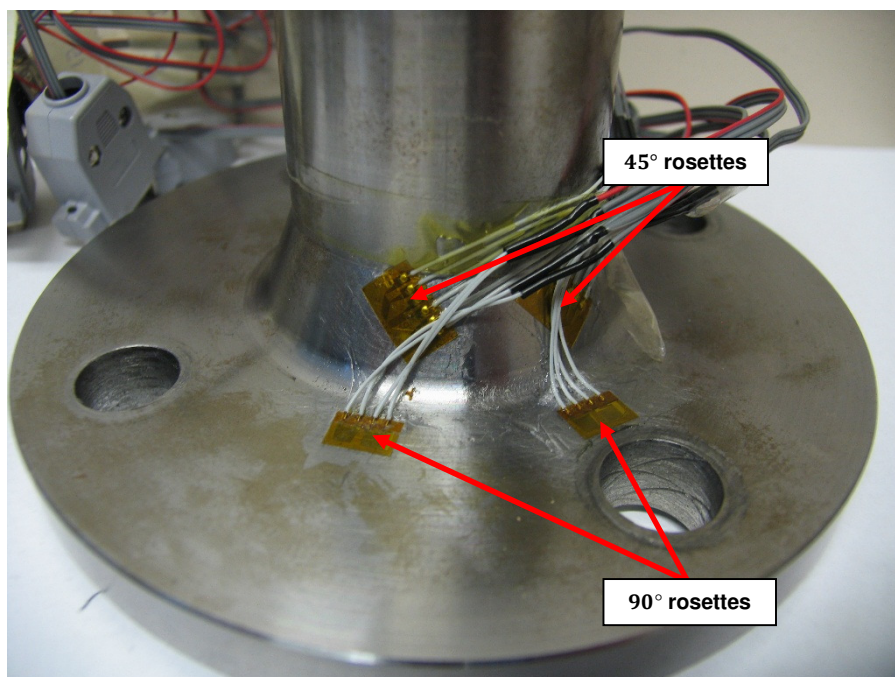


Figure E-6: Photograph of the instrumented raised face flange

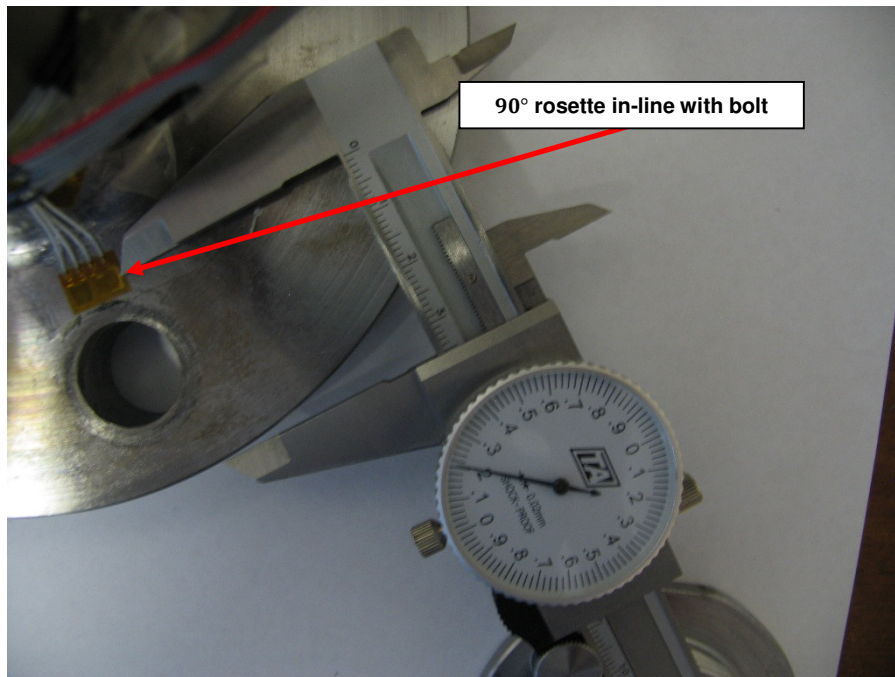


Figure E-7: Photograph of the position of the 90° rosette which is in-line with the bolt on the ring of the raised face flange

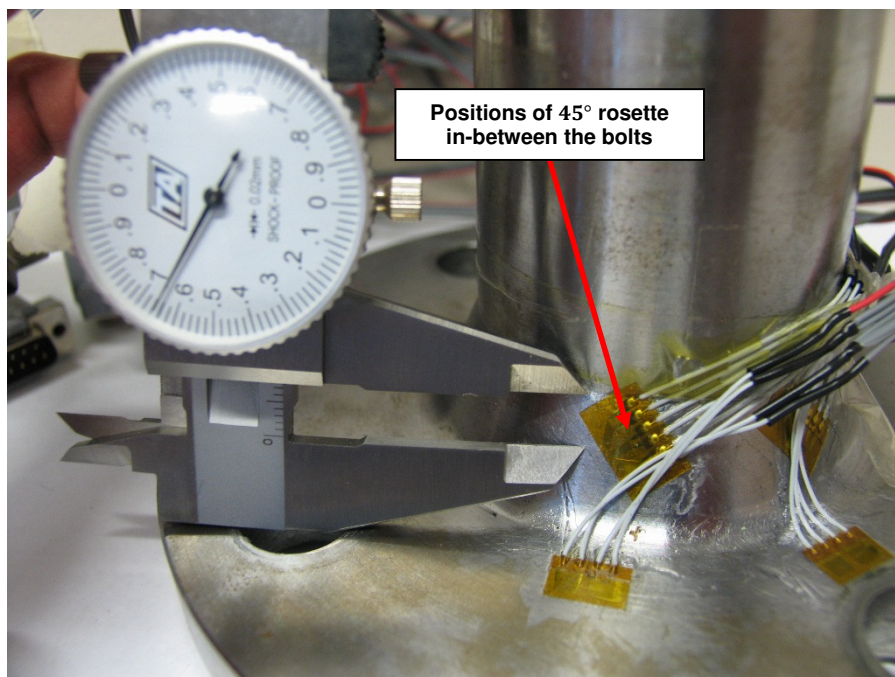


Figure E-8: Photograph of the position of the 45° rosette in-between the bolts on the hub of the raised face flange

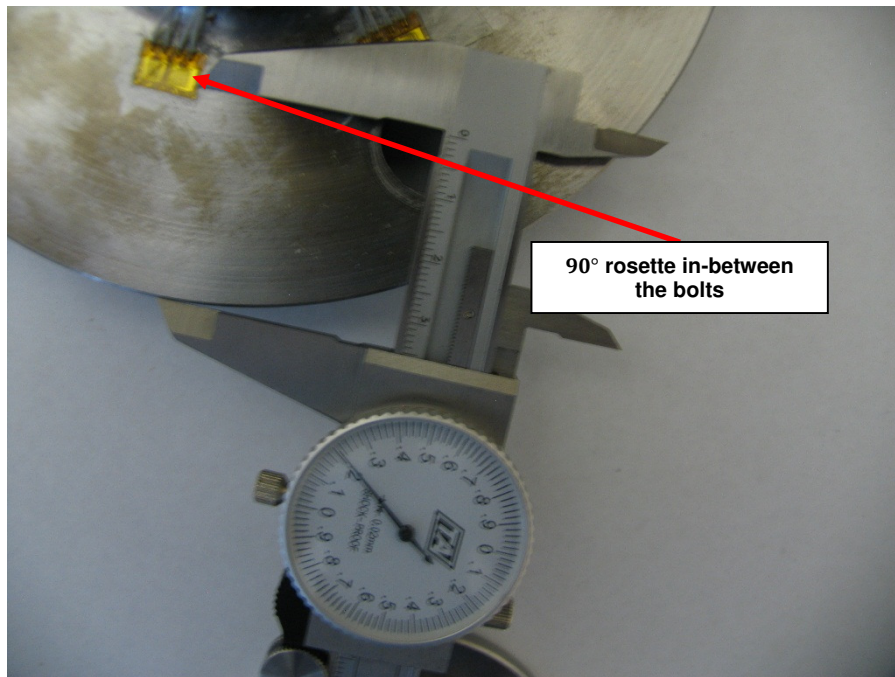


Figure E-9: Position, with the perpendicular distance from the edge of the flange, of the 90° rosette in-between the bolts on the ring of the raised face flange

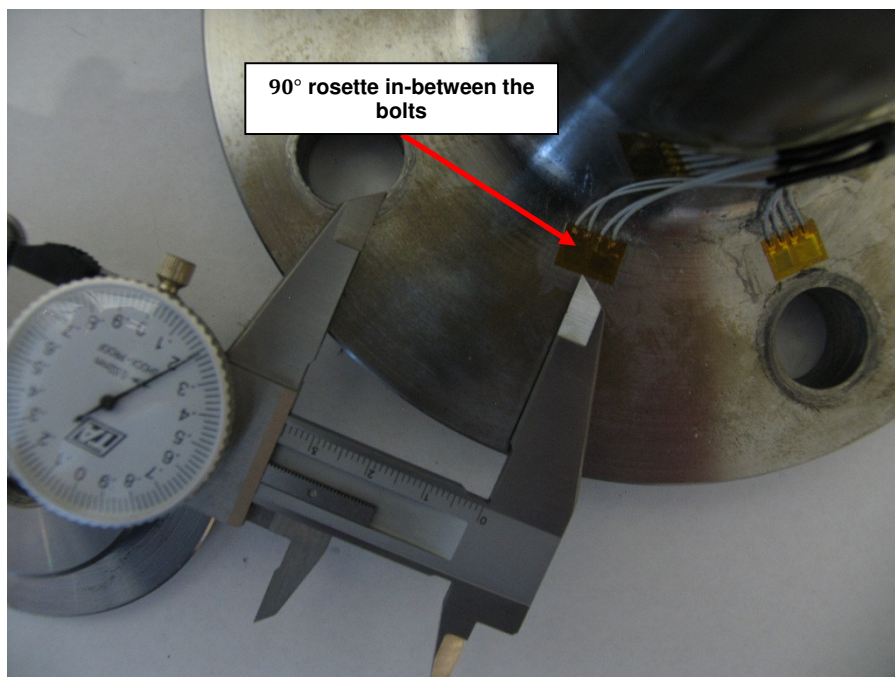


Figure E-10: Position, with the perpendicular distance from the edge of the bolt hole, of the 90° rosette in-between the bolts on the ring of the raised face flange

E.3. Instrumented modified raised face flange with an O-ring groove

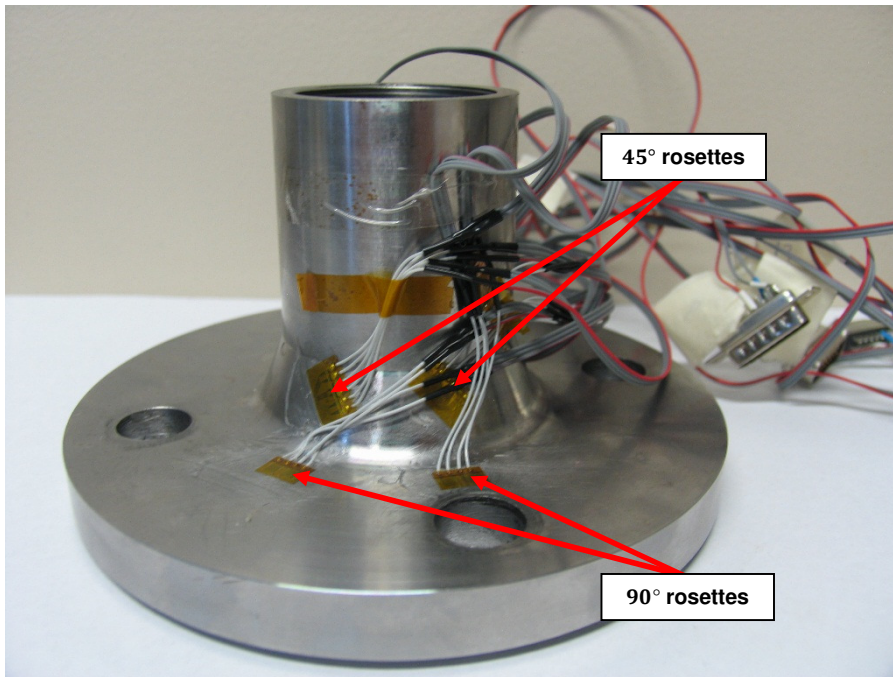


Figure E-11: Photograph of the instrumented raised face flange with an O-ring groove

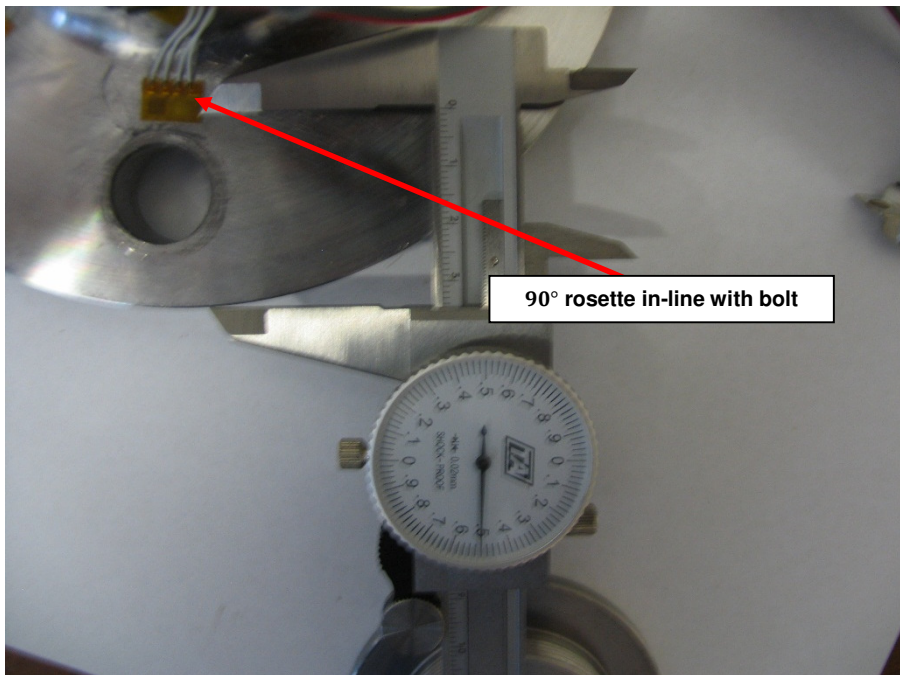


Figure E-12: Photograph of the position of the 90° rosette which is in-line with the bolt on the ring of the raised face flange with an O-ring groove

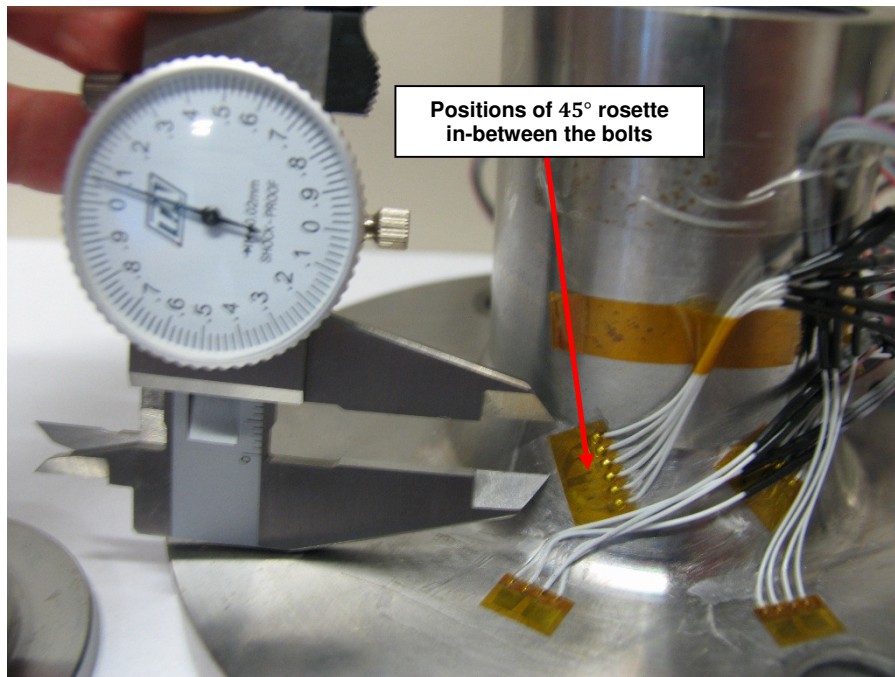


Figure E-13: Photograph of the position of the 45° rosette in-between the bolts on the hub of the raised face flange with an O-ring groove

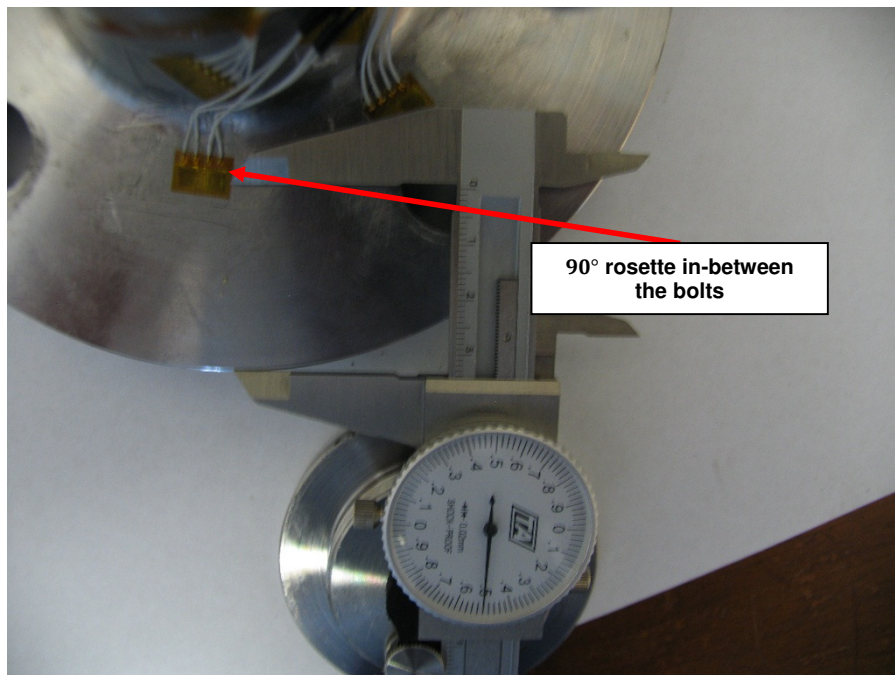


Figure E-14: Position, with the perpendicular distance from the edge of the flange, of the 90° rosette in-between the bolts on the ring of the raised face flange with an O-ring groove

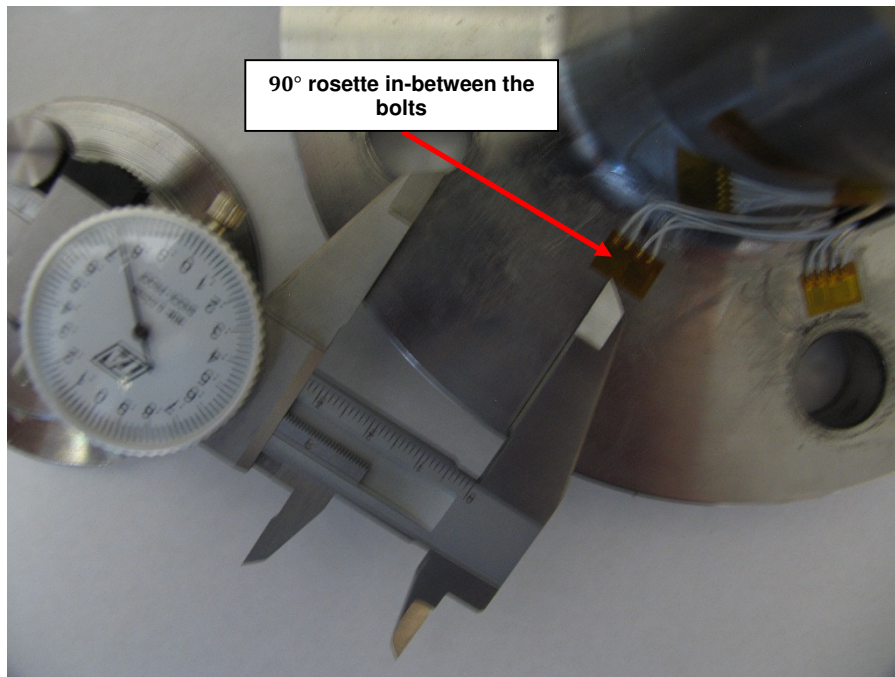


Figure E-15: Position, with the perpendicular distance from the edge of the bolt hole, of the 90° rosette in-between the bolts on the ring of the raised face flange with an O-ring groove

APPENDIX F: RESPONSE SURFACE GENERATION AND OPTIMISATION IN ANSYS

ANSYS [46] provides four different types of response surfaces. A brief overview of each of the different types of response surfaces is given below. The four different types of response surfaces which are:

1. Standard second order polynomial response surface
2. Kriging
3. Non-parametric regression
4. Sparse grid

According to ANSYS [46] the default response surface is a good starting point and is based on a modified quadratic formulation where the output is a second order polynomial function of the inputs. It is also stated that the standard second order polynomial response surface will provide satisfactory results when the variation of the output parameter is fairly smooth.

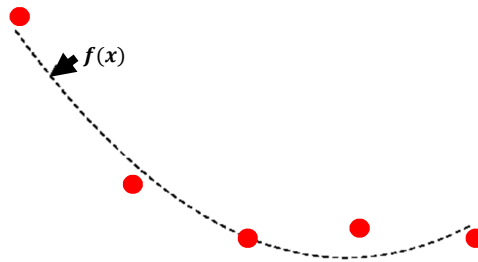


Figure F-1: Example of a 2D response surface approximation by means of a standard second order polynomial

Kriging, on the other hand, is a commonly used method of interpolation for spatial data. According to ANSYS [46] the Kriging method's interpolation is multidimensional and combines a global model of the design space as well as local deviations. The output is, therefore, the sum of a second order polynomial (global behaviour of the model) and a perturbation term (local behaviour of the model). The 'goodness-of-fit' metric for the Kriging method will also be good since it fits the response surface through all of the designed points. The Kriging method is said to give better results than the standard second order polynomial response surface when the variations in the output parameters are non-linear. Two drawbacks with the Kriging method is that it cannot be accurately used when the results are noisy; also, because the Kriging method interpolates between the design points oscillations may appear on the response surface. Due to this it is often necessary to increase the accuracy through refinement. The refinement may be done in ANSYS in one of two ways. The first way is to manually specify additional design points. The second way is to allow the Kriging algorithm to automatically run additional design points which are based on its internal error prediction.

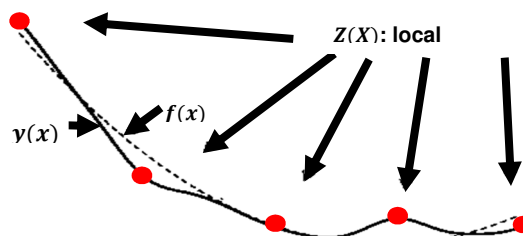


Figure F-2: Example of a 2D response surface approximation by means of Kriging

The next type of response surface is non-parametric regression. This method makes use of a tolerance epsilon (ϵ) which creates a narrow envelope around the true output surface. For this method it is required that the majority of the sample points lie inside the predefined envelope. This method is, generally, used when the response is non-linear or the results are noisy. This method is, however, slow to compute and it is suggested that it only be used when the 'goodness-of-fit' metrics from the quadratic response surface model is unsatisfactory.

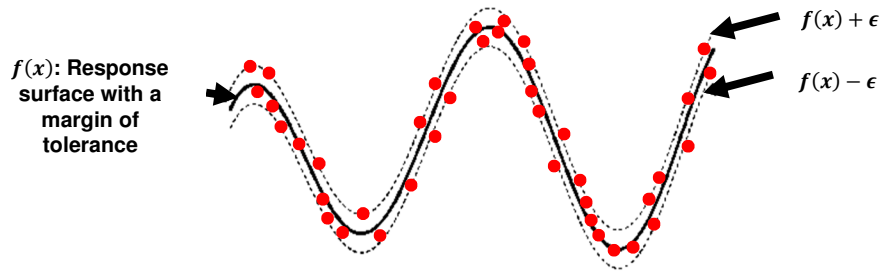


Figure F-3: Example of a 2D response surface approximation by means of non-parametric regression

The sparse grid method is an adaptive response surface which refines itself automatically. The big drawback with this method is that it requires a large number of samples. Due to this it is recommended that this method only be used when the individual design points solve quickly. The sparse grid method only refines in the direction necessary. This results in the same quality response surface with fewer design points.

In ANSYS DesignXplorer there exists four methods for surface response optimisation. These four methods are:

1. Screening (Shifted Hammersley).
2. MOGA (Multi-objective genetic algorithm).
3. NLPQL (Non-linear programming by quadratic Lagrangian).
4. MISQP (Mixed integer sequential quadratic programming method).

The screening method is usually used in preliminary designs. The screening method works by generating a large number of samples from the response surface and sorting them according to the constraints, weightings and objective functions. The screening method has the following advantages:

1. Provides a global overview of the design space.
2. Identifies local and global minima.
3. Available for both continuous and discrete input parameters.

The MOGA method is an iterative multi-objective genetic algorithm which provides a more refined approach than screening. The MOGA method works by going through several iterations and retaining the best samples. This allows for the best Pareto front to be found. The MOGA method has the following advantages:

1. Is able to handle multiple objectives.
2. Provides an accurate solution.
3. Help identify both the global and local minima.

The NLPQL method is a gradient based single objective optimiser which is based on quasi-Newton methods. It is accurate and fast, however, it does not handle multiple objectives, and is available for continuous input parameter only.

The final method which is applicable to response surface optimisation is the MISQP method. The MISQP method solves mixed integer non-linear programming problems by means of modified sequential quadratic programming method. This method has two primary advantages in that it is able to solve quickly and accurately, and has the ability to solve for both discrete and continuous input parameters. Like the NLPQL method it is unable to solve for multiple objectives and provides only a single solution.